The role of the calcineurin/NFAT signaling pathway and its regulation in muscle diseases

Manal Al Zein

A Thesis
In The Department
of
Chemistry and Biochemistry

Presented in Partial Fulfillment of the Requirements
for the Degree of
Doctor of Philosophy (Chemistry) at
Concordia University
Montreal, Quebec, Canada

September 2013

CONCORDIA UNIVERSITY

SCHOOL OF GRADUATE STUDIES

This is to certify that the thesis prepared

By: **Manal Al Zein**

Entitled: **The Role of the Calcineurin/NFAT Signaling Pathway and its Regulation in Muscle Diseases**

and submitted in partial fulfillment of the requirements for the degree of

DOCTOR OF PHILOSOPHY (Chemistry)

complies with the regulations of the University and meets the accepted standards with respect to originality and quality.

Signed by the final examining committee:

Dr. G. Brown	Chair
Dr. K.E.M. Hastings	External Examiner
Dr. A. Piekny	External to Program
Dr. P. Joyce	Examiner
Dr. J. Powlowski	Examiner
Dr. A. Bergdahl	Examiner
Dr. H. Muchall	Administrative Supervisor

Approved by _____
Dr. H. Muchall, Graduate Program Director

August 19, 2013 _____
Interim Dean J. Locke, Faculty of Arts and Science

Abstract

The role of the calcineurin/NFAT signaling pathway and its regulation in muscle diseases

Manal Al Zein, PhD
Concordia University, 2013

Elevations in intracellular calcium activate the phosphatase Calcineurin (Cn) and its downstream target the Nuclear Factor of Activated T cells (NFAT), leading to the expression of genes involved in skeletal muscle growth and cardiac remodeling. In this thesis, we set out to investigate the role of the Cn/NFAT signaling pathway in the progression of two muscle diseases: Duchenne Muscular Dystrophy (DMD), which is characterized by the loss of the functional protein dystrophin, and cardiac hypertrophy. First, to understand the roles of Cn and Cn regulators in DMD, we used *mdx* mice crossed with mice expressing transgenes that manipulate the Cn/NFAT pathway. For instance, the expression of the transgene Parvalbumin (PV) in *mdx* mice leads to attenuation of Cn activity and reduction in the expression of utrophin, a protein that compensates for the loss of dystrophin. Our results show that strategies promoting Ca^{2+}/Cn signaling are considered an effective countermeasure in the treatment of DMD and that Cn regulators might have a critical role in the progression of the disease. Secondly, the role of the NFATc2 transcription factor in Cn-dependent cardiac hypertrophy is emphasized using adult *NFATc2* knockout mice in the presence and absence of biochemical stress. Here we show a cardio-protective role for NFATc2 in normotensive hearts, but not in hearts exposed to stress. Together, the results of this thesis provide a better understanding of the role of the Cn/NFAT pathway in the regulation of various muscle diseases.

Acknowledgements

At the very beginning, I would like to thank GOD for being with me and watching my steps during this journey.

I am very grateful to my committee members especially Dr. Andreas Bergdahl who provided his guidance and advice with no hesitation. His expertise improved my research skills and prepared me for future challenges. My thanks are extended to Drs. Paul Joyce, Justin Powlowski and Alisa Piekny who supported my ambition and encouraged me to work hard.

I would like to express the deepest appreciation to the Chemistry Graduate Program Director, Dr. Heidi Muchall who never hesitated to help me out in spite of her busy schedule. I am greatly indebted to some hidden soldiers at Concordia University who helped me in more than a situation namely, Dr. Joanne Turnbull, Maria Ciaramella, Suzanne Digneault, Jude Lashley and Ronda Rowat, as well as the Faculty of Arts and Science (including all professors and staff), Department of Chemistry and the School of Graduate Studies. A special debt to Drs. Sean Taylor and Marc Champagne who offered technical support whenever needed, and Aileen Murray for her help in animal care.

I also want to thank Dr. Robin Michel for choosing the topic and giving me the chance to join his lab, as well as the past and current lab members to whom I feel grateful and rich especially; Ewa, Patrick, Mathieu, Sarah and Mohammad. Many thanks to my best friends ever; Rasha, Samar, Joanne, Avid and Sima.

Special feelings of gratitude to my lovely parents, brother and sisters who were always next to me in my loneliness abroad. I lovingly dedicate this work to my late parents-in-law (I wish they were here at this moment), my sister-in-law Rima and my adorable family; Mahdi, Faris and Tala for their incredible patience and for supporting me each step of the way. Without you all, I would never accomplish this work.

Finally, special dedication to all those who are suffering form muscle diseases all over the world. I just wish I was able to do more to stop their pain.

Contribution of Authors

In this thesis, I performed all presented experiments with exceptions of:

Chapter 4:

1- Patrick Sin-Chan has generated Figures 1-4 (which have been added to Appendix IV). In Figure 4a, I added data to Patrick's results and performed the calculations and analyses, as well as One Way Analysis of Variance (Anova) test for Figures 4d-4f. Patrick has also interpreted the results coming form the mentioned Figures, which are part of his MSc thesis.

2- Dr. Mathieu St-Louis carried out NFATc1 immunofluorescence experiments in the 14 day Angiotensin II stimulated hearts. I performed the calculations and the corresponding graphs. He also helped in extracting gelatin-stimulated hearts.

3- Dr. Robin N. Michel performed the Angiotensin II implantation with my assistance, and I exchanged the pumps after 14 days.

Note: Dr. Bernard Jasmine (an author in the first manuscript: Chapter 2), works in collaboration with Dr. Robin Michel and they both share funding.

Table of contents

List of Figures

List of Tables

List of Abbreviations

$[Ca^{2+}]_i$	intracellular Calcium
Ach	Acetylcholine
AchR	Acetylcholine Receptor
Ang II	Angiotensin II
ANP	Atrial Natriuretic Peptide
ATF	Activating Transcription Factor
ATP	Adenosine Triphosphate
AU	Arbitrary Units
AVN	Atrioventricular Node
BMD	Becker Muscular Dystrophy
BNP	Brain Natriuretic Peptide
BSA	Bovine Serum Albumin
CAIN	Calcineurin Inhibitor
Calsarcins	Calcineurin-Interacting proteins
CaM	Calmodulin
CaMBP	Calmodulin-Binding Protein
CaMK	Calmodulin-dependent protein Kinase
CK	Casein Kinase
Cn	Calcineurin
CnA	Calcineurin A
CnA*	Activated from of Calcineurin
$CnA\beta_1$	β_1 isoform of CnA subunit
CnB	Calcineurin B
CSA	Cross Sectional Area
CsA	Cyclosporine A
CSRP3	Cysteine Rich Protein3
CTD	C-Terminal Domain
DAB	Diaminobenzidine
DAPC	Dystrophin-Associated Protein Complex
Dapi	Diamidino-2-phenylindole
DHPR	Dihydropyridine Receptor
DMD	Duchenne Muscular Dystrophy
EBD	Evans Blue Dye
EDL	Extensor Digitorum Longus
ERK	Extracellular-Regulated-Signal Kinases
f-actin	Filamentous actin
FKBP	FK506 Binding Protein
GABP	GA-Binding Protein
GAPDH	Glyceraldehyde-3-phosphate dehydrogenase
GSK3-β	Glycogen-Synthase kinase3-β
H&E	Hematoxylin and Eosin
HA	Haemaglutinin
HDAC	Histone Deacetylase

HPRT	Hypoxanthine-guanine Phospho Ribosyl Transferase
HRP	Horse Radish Peroxidase
HSP	Heat Shock Protein
HW/BW	Heart Weight-to-Body Weight
IF	Immunofluorescence
IGF-1	Insulin Growth Factor-I
IGF-R	Insulin Growth Factor-I Receptor
IRS	Insulin Receptor Substrate
JNK	Janus-N-Terminal Kinase
LG	Lateral Gas
MAFbx	Muscle Atrophy F-box
MAPK	Mitogen Activated Protein Kinase
MCIP	Modulatory Calcineurin-Interacting Protein
MLP	Muscle LIM Protein
MRF	Muscle Regulatory Factor
mTOR	mammalian Target Of Rapamycin
Myf	Myogenic factor
MyHC	Myosin Heavy Chain
MyoD	Myogenic Determination factor
NES	Nuclear Export Signal
NFAT	Nuclear Factor of Activated T cells
NF-$_\kappa$B	Nuclear Factor-$_\kappa$B
NHR	N-Homology Region
NLS	Nuclear Localization Signal
NMJ	Neuromuscular Junction
Pax	Paired box
PDK	Phospho-Inositide-Dependent Kinase
PFA	Paraformaldehyde
PI	Phosphatidyl-Inositol
PKB	Protein Kinase B
PKC	Protein Kinase C
PMSF	Phenylmethanesulfonyl Fluoride
PPN	Peripheral Purkinje Network
PV	Parvalbumin
PVDF	Polyvinyl difluoride
RCAN	Regulator of Calcineurin
RHR	Rel-Homology Region
RPL13	60S Ribosomal Protein L13
RyR	Ryanodine Receptor
S6K	S6 kinase
SAN	Sinoatrial Node
SDS	Sodium Dodecyl Sulfate
SDS	Succinate Dehydrogenase
SERCA	Sarcoplasmic Reticulum-Ca^{2+}-ATPases
SGK	Serum and Glucocorticoid-regulated Kinase
Six	Sine oculis-related homeobox

SP	Serine-Proline
SR	Sarcoplasmic Reticulum
SRR	Serine-Rich Regions
T/TBS	Tween/Tris Buffered Saline
TA	Tibialis Anterior
TAD	Transactivation Domain
TBP	TATA-Binding Protein
TEMED	Tetramethylethylenediamine
TGF	Transforming Growth Factor
TnIs	Troponin I slow promoter
TonEBP	Tonicity-response Enhancer-Binding Protein
T-tubules	Transverse tubules
WT	Wild-Type
α-SMA	Alpha Smooth Muscle Actin

Chapter 1 : General Introduction

1.1 Muscle structure, contraction and development

1.1.1 Muscle structure and contraction

Muscle tissue is a highly vascularized organ used for contraction. All muscles show biochemical specialization which allows them to produce body movement [1]. There are three basic types of muscle tissue: skeletal, cardiac and smooth (Figure 1.1). Skeletal muscle cells are long, cylindrical, voluntary-controlled, multi-nucleated and striated cells formed by fusing hundreds of myoblasts end-to-end. Skeletal muscles stabilize the position of the skeleton, generate heat and protect internal organs. Cardiac muscle cells (cardiomyocytes) are long, branched involuntary-controlled cells that are mono-nucleated but still show a striated pattern. Intercalated discs connect these cells whose main functions are to circulate blood and maintain blood pressure. Smooth muscle cells are mono-nucleated, involuntary-controlled cells with no striations. They are found in the walls of hollow internal structures such as blood vessels, urinary bladder, respiratory, digestive and reproductive tracts. Smooth muscles function to move foods, urine and reproductive tract secretions, regulate the diameter of blood vessels and control the width of respiratory passage ways [1].
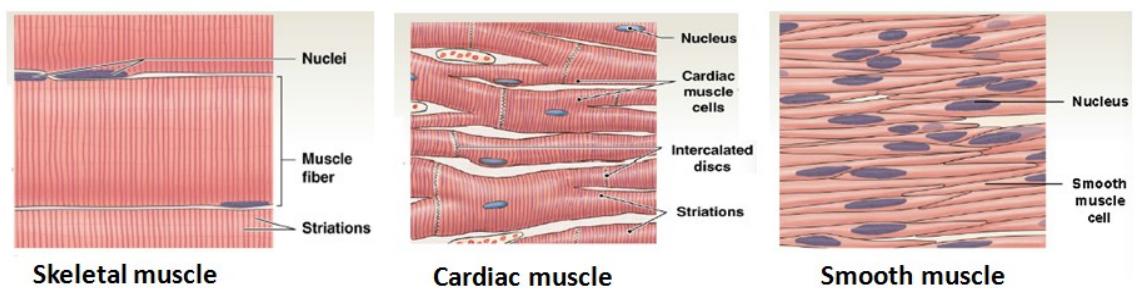
Figure 1.1: The general structures of skeletal, cardiac and smooth muscles [1]

Each skeletal muscle fiber is enveloped by a plasma membrane called the sarcolemma, which surrounds a cytoplasm (called sarcoplasm) and contains a Sarcoplasmic Reticulum (SR). Most of the cytoplasm is occupied by cylindrical bundles of contractile proteins called myofibrils, each of which measures approximately 1-2 μm in diameter. The sarcomere is the repeating subunit of myofibrils and the functional unit of muscle contraction [2]. Filamentous actin (f-actin), titin and nebulin are the three filament systems of the sarcomere that interact with the Z-disc (also known as the Z-band or Z-line), which forms the borders of the sarcomere (Figure 1.2), whereas myosin-based thick filaments do not directly interact with the Z-disc [3]. Those thick filaments are located in the central portion of the sarcomere, while the thin filaments that are composed of actin, are situated at the extremities of the functional unit and bind myosin to perform the muscle contraction process.

During contraction, myosin heads bind to actin. This interaction is regulated by two proteins, tropomyosin and troponin, which are bound to the thin filaments and are capable of covering the binding sites for myosin. At this stage, myosin cannot bind to actin and thus, muscle contraction is inhibited [2]. In a process known as excitation-contraction coupling, a nerve impulse triggers the release of the neurotransmitter Acetylcholine (Ach) from the presynaptic terminus into the synaptic cleft. The released Ach binds to its receptor (AchR) on the postsynaptic muscle surface, and induces a conformational change causing this channel to open for ion flux. For instance, Na^+ influx leads to membrane depolarization and propagation of an action potential. This action potential is transmitted into the Transverse tubules (T-tubules; special extensions of the sarcolemma) where it opens the SR Ca^{2+} channel. Upon the increase of sarcoplasmic Ca^{2+}

3

concentration, troponin binds Ca^{2+}, causing a conformational change, which pulls tropomyosin away from its blocking position. Consequently, as the actin binding sites become uncovered for myosin to bind, the contraction process begins [2].
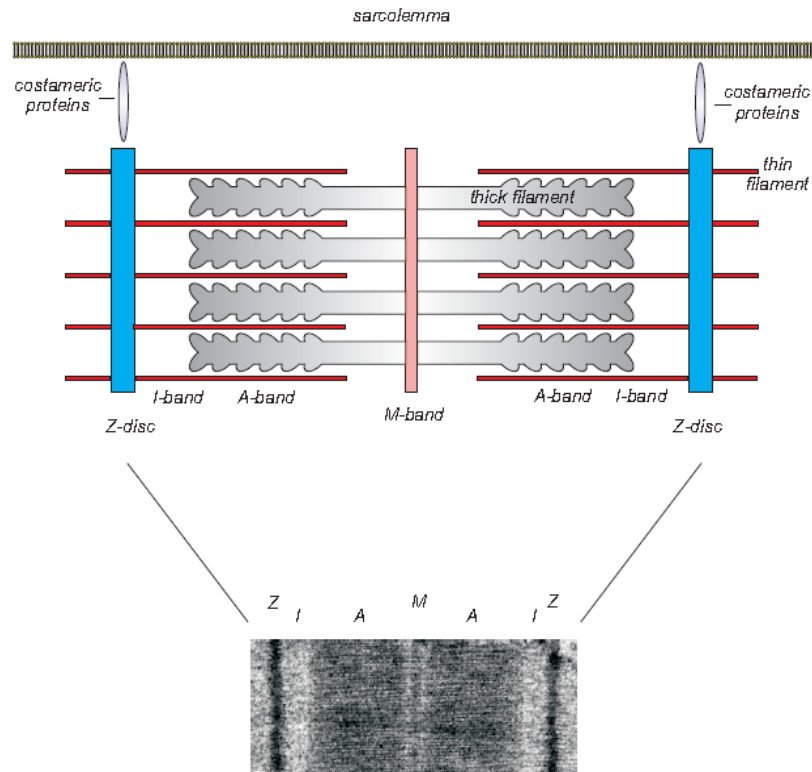
Figure 1.2: A schematic drawing of the sarcomere [4]

The f-actin-containing thin filaments anchor at the Z-disc and interdigitate with the myosin-containing thick filaments at the level of the A-band. Costameric proteins ensure lateral force transduction and linkage to the sarcolemma and its associated protein complexes.

1.1.2 Skeletal muscle development

The process of generating muscle (myogenesis) is divided into several stages [5]. The initial muscle fibers of the body are created by mesoderm, which is a derived structure that develops during embryonic development. Subsequently, additional fibers are formed from the template fibers [5, 6]. In the course of maintaining homeostasis,

adult skeletal muscle relies on a compensatory mechanism for the turnover of terminally differentiated cells. This compensatory mechanism involves activation of satellite cells that are capable of differentiation into new fibers [7, 8]. Satellite cells can be activated after damage caused by mechanical stress or chemical injection [9, 10]. In both embryonic myogenesis and regeneration of skeletal muscle processes, there are common transcription factors and signaling molecules that are utilized (Figure 1.3) [5].
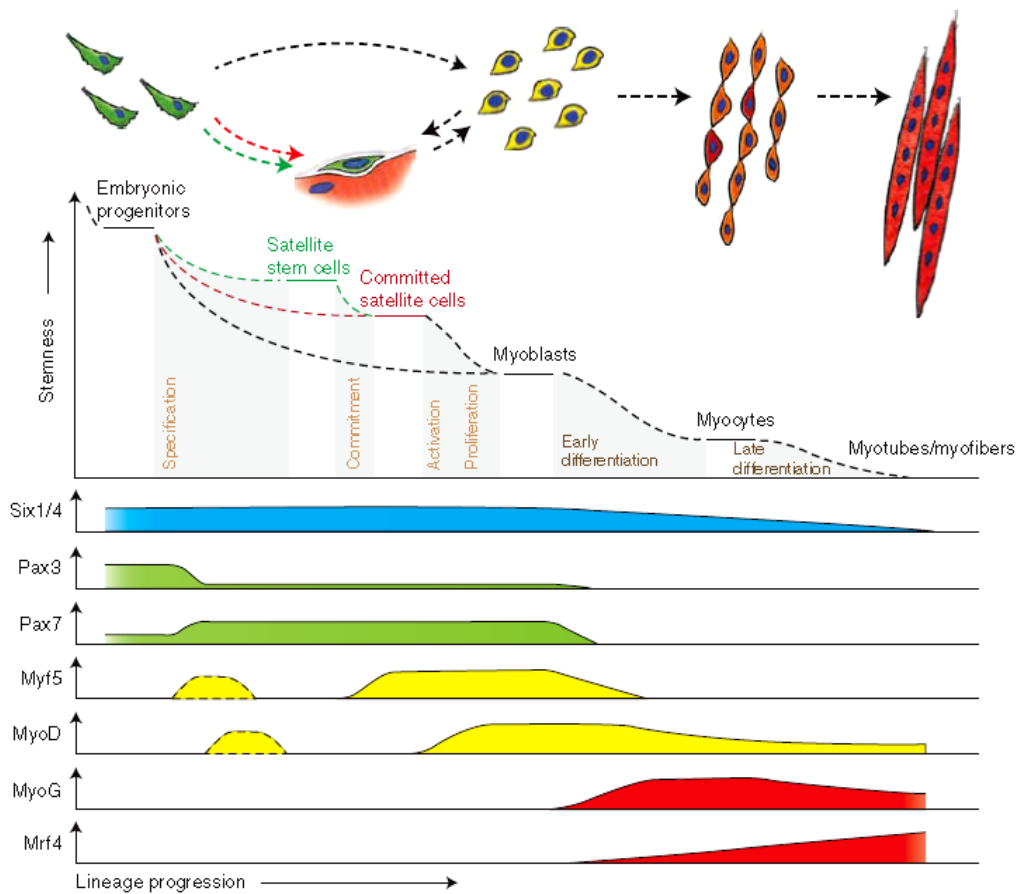
Figure 1.3: Transcription factors regulating myogenesis [11]

Muscle progenitors that are involved in embryonic muscle differentiation skip the quiescent satellite cell stage and directly become myoblasts. Some progenitors remain as satellite cells in postnatal muscle and form stem and committed cells. Six1/4 and Pax3/7 are master regulators of early lineage specification, whereas Myf5 and MyoD commit cells to the myogenic program. Expression of the terminal differentiation genes required for the fusion of myocytes and the formation of myotubes, are performed by both myogenin (MyoG) and MRF4.

Myogenesis is a well-controlled process that is separated into two steps: 1) proliferation of cells and 2) differentiation and maturation of proliferated cells. The basic helix-loop-helix Myogenic Determination factor (MyoD) is capable of transforming a group of cell types such as fibroblasts into cells that fuse into myotubes [12]. Myogenic factor 5 (Myf5), myogenin and Muscle Regulatory Factor 4 (MRF4, also known as Myf6) are three other myogenic basic helix-loop-helix factors which induce myoblast traits in non-muscle cell lines [13, 14]. Collectively, these four transcription factors are referred to as Myogenic Regulatory Factors (MRFs) [15]. Each of these factors has a critical function in myogenesis. While Myf5 has a role in myoblast proliferation, MyoD and myogenin promote myoblast differentiation [16-18], and MRF4 is essential for myoblast maturation [19, 20]. The Paired box (Pax) 3 and 7 are additional factors involved in satellite cell differentiation and proliferation, as well as in the myogenesis process [21, 22]. Additionally, myostatin, an important negative regulator of muscle mass, is present in satellite cells and myoblasts [23]. Interestingly, myostatin overexpression downregulates Pax7 expression while myostatin inhibition upregulates Pax7 expression [24]. Moreover, the Sine oculis-related homeobox transcription factors (Six) 1 and 4 are also master regulators of early lineage specification. Thus, Six1 and 4 proteins act as cofactors to activate Six target genes such as Pax3 and MRFs [25].

1.1.3 Cardiac muscle development

Cardiac muscle development (cardiogenesis) is an additive process in which additional layers of complexity are added throughout the evolution of a simple structure (linear heart tube) [26]. The earliest stages of heart development are nearly identical

among all vertebrates unlike the subsequent septation of the chambers and the outflow tract, which vary between species depending on utilization of the lungs [26]. The heart field is the region of the embryonic mesoderm that contains the cardiac progenitor cells. The mesodermal cells are committed to the heart by the early gastrulation stage. These pre-heart cells migrate toward the anterior embryonic pole to condense in bilateral areas of the splanchnic mesoderm. Soon after formation, the precardiac areas migrate to the embryonic midline, fuse under the endodermal foregut and form the primitive tubular heart. The precardiac mesoderm contains both endocardial and myocardial precursors [27]. In vivo, precardiac mesodermal cells express transcription factors including Transforming Growth Factors as TGFβ1, TGFβ2 and activin A, which regulate the expression of α-Myosin Heavy Chain (α-MyHC), an initial marker of cardiac differentiation [27, 28]. Furthermore, cell-cell interactions within the precardiac mesoderm also may have a significant influence on cardiac differentiation. At the organ level, the adequate integration of the different heart components ultimately results in the development of heart shape and function [28].

Cardiac looping arises from the coordinated integration of the different components of the heart tube [27]. The mechanisms involved in looping are still under discussion. After the initial fusion of the paired primordial cells, a single heart tube is formed in the embryonic midline. This primitive heart represents the future trabeculated part of the right ventricle. Continued fusion of the paired primordium brings about the merging of the trabeculated part of the left ventricle, the atrium and the sinus venosus, which are progressively incorporated into the developing heart [29]. The myocardium is formed throughout looping of a single population of developing myocytes. Molecular

7

modifications in cellular proliferation, transformation, migration and death are thought to be involved in the process of looping, but the relative contributions of these cellular mechanisms are still unknown [29]. When looping is complete, the heart progressively acquires an adult configuration. Internally, independent septa develop in the atrial and ventricular chambers, the bulbus cordis, and the atrioventricular canal. These septa reunite in the center of the heart to transform the cardiac tube into a four chambered organ (two atria and two ventricles; left and right) (Figure 1.4). This system is connected to the blood entry system by the inferior and the superior vena cavae from one side and by the pulmonary veins from the other side [30].
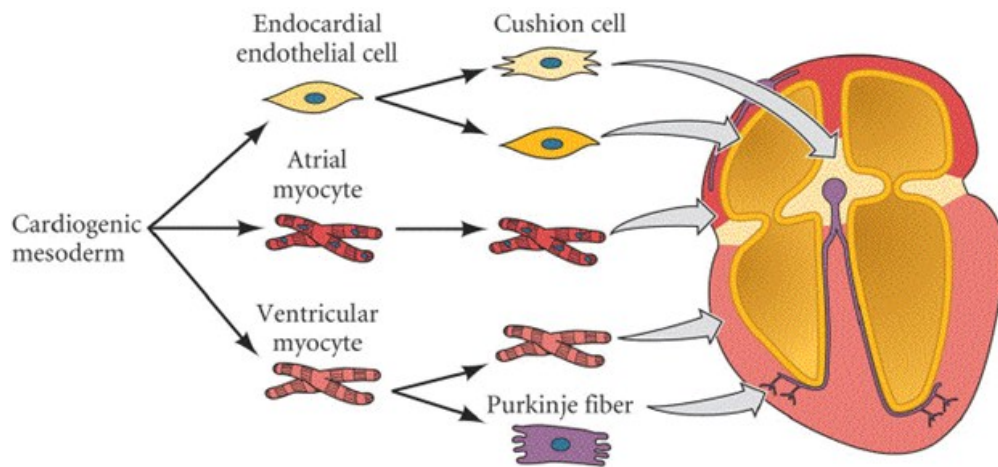
Figure 1.4: A schematic drawing of cardiac mesoderm differentiation [31]

In the formed heart, it is critical to distinguish between the working myocardium (whose main function is contraction) and the conduction system (which is responsible for generation and conduction of the electrical impulse from the sinusal node formed at the atrial junction) [32]. The conduction system comprises separate components with distinct functions. The Sino-Atrial Node (SAN), which contains the leading pacemaker, generates

8

the impulse that is subsequently conducted, via the atrial myocardium toward the Atrio-Ventricular Node (AVN), with a delay. The impulse is then rapidly transmitted from the AVN via the bundle branches and the Peripheral Purkinje Network (PPN) to ensure a coordinated activation of the ventricular myocardium from apex to base. Hence, the development of the conduction system does not require the invention of new building blocks, but a remodeling of existing components [32].

1.1.4 Muscle fiber types

Skeletal muscles comprise fiber types with distinctive contractile and metabolic properties. Scientists used to distinguish skeletal muscles based on their colors as red or white and on their contractile properties as fast and slow. However, during the last 40 years, the classification of muscle fiber types changed such that now four major fiber types are recognized in adult mammalian skeletal muscles [33]. Since 1968-1970, fast-white muscles have been identified as those specialized for phasic activity, whereas slow-red muscles are those dedicated for more continuous activity [34]. Using histochemical-physiological studies, fast-twitch fibers have been shown to display large variations in levels of Succinate Dehydrogenase (SDH) as an indication of variable resistance to fatigue [35]. Simultaneously, two fast fiber populations (named type IIa and IIb), which are distinct from the slow type I fibers have been identified [36, 37]. Additionally, skeletal muscle fibers can be classified into slow oxidative, fast-twitch oxidative glycolytic and fast-twitch glycolytic muscle fibers based on the levels of glycolytic and oxidative enzymes they possess [38]. Biochemical analysis also identified a third fast fiber type called type IIx or IId which has a strong SDH staining [39, 40] with an

intermediate maximal velocity of shortening between that of IIa and IIb fibers [41, 42]. The properties of the major skeletal muscle fiber types are demonstrated in Figure 1.5.

Fiber type switching is possibly induced by electric stimulation that causes changes in nerve activity [43]. For instance, phasic high-frequency electrical stimulation leads to a slow-to-fast fiber switch in the direction I→ IIa→ IIx→ IIb, whereas tonic-low frequency electrical stimulation causes a fast-to-slow switch in the direction IIb→ IIx → IIa →I [43]. Moreover, fast muscles have the capacity to adapt in the range IIb↔ IIx↔ IIa, while slow muscles adapt in the range I↔ IIa↔ IIx [44].

MyHC type	Twitch duration	Shortening velocity	Cross-sectional area	Metabolism	Endurance	Energy efficiency
I	Slow	Slow	Small	Oxidative	High	High
IIa						
IIx						
IIb	Fast	Fast	Large	Glycolytic	Low	Low

Figure 1.5: MyHC isoforms in skeletal muscle and their properties [45]

The classification of muscle fibers in cardiomyocytes is different from that of skeletal muscles. Thus, in cardiac cells, there are two types of MyHC protein; α and β. The expression of these two isoforms is correlated to the contractile velocity of cardiac muscles [46]. However, the skeletal slow MyHC and the cardiac β-MyHC are the same isoform [47]. Cardiomyocytes expressing α-MyHC are found in adult hearts, have a more contractile velocity and are quicker to fatigue than β-MyHC. In contrast, cardiomyocytes expressing more β-MyHC are present in fetal and developing hearts, have a great capability of force generation and are more resistant to fatigue (Figure 1.6) [46, 48].

MyHC type	Location	ATP source	ATPase activity	Contraction velocity	Fatigue rate
α-MyHC	Adult hearts	Glycolysis	Fast	Fast	Fast
β-MyHC	Fetal hearts	Oxidative phosphorylation	Slow	Slow	Slow

Figure 1.6: Cardiac MyHC isoforms and their properties (information taken from [47])

Like in skeletal muscles, several pathological stimuli cause a shift in the MyHC composition from α to β [46]. β-MyHC is re-activated in cardiovascular diseases that usually cause pathophysiological cardiac growth and hypertrophy, leading to heart failure and death [49].

1.2 Muscle function and signal transduction

1.2.1 Calcium and calmodulin

Skeletal muscle plasticity is the ability of muscles to adapt to variations in activity and work [50]. This process is linked to the Ca^{2+} handling system, which displays Ca^{2+} influx into the cells via depolarization and Ca^{2+} release to the SR [51]. The Ca^{2+} handling system controls all functions of muscle including contraction and relaxation. The major mechanism involved in the latter process is the troponin-tropomyosin system, which is restricted to skeletal and cardiac muscles and has been previously described in depth [51].

A variety of Ca^{2+} binding proteins such as Calmodulin (CaM), calpains, Calcineurin (Cn), sorcin and annexins might be important for muscle performance and plasticity,

although they are not directly involved in the process of muscle contraction and relaxation. The Ryanodine Receptor (RyR) causes release of Ca^{2+} from the SR (Figure 1.7). Additionally, the high-affinity Ca^{2+}-binding protein Parvalbumin (PV) facilitates Ca^{2+} translocation from the myofibril to the SR in fast muscle fibers [51]. The SR-ATPase, in turn regulates Ca^{2+} uptake into the SR. Inside the SR, Ca^{2+} binds to the high-capacity and low affinity Ca^{2+}-binding protein calsequestrin. Elevated cytoplasmic Ca^{2+} may cause a variety of muscle diseases, leading to changes in muscle fiber transcription and transformation, necrosis and apoptosis [51]. The Ca^{2+} handling process and the effects of elevated cytoplasmic Ca^{2+} levels are explained in Chapter 2 of this thesis.
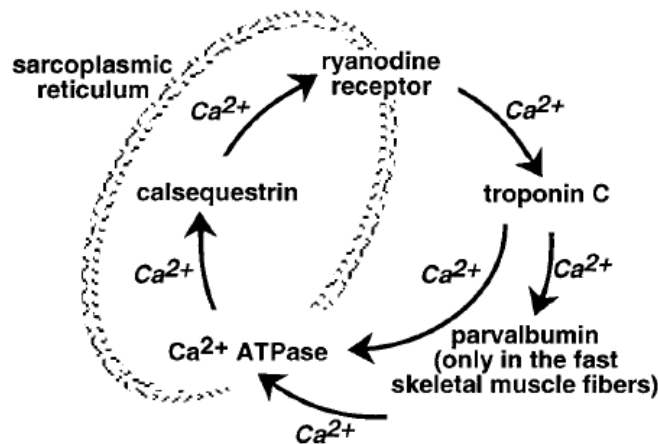
Figure 1.7: A schematic presentation for the Ca^{2+} binding proteins involved in the Ca^{2+} cycle[51]

CaM is one of the major Ca^{2+} binding proteins that is involved in many signaling pathways. It is a small protein of 148 residues (17 kDa), containing four EF-hand motifs that bind Ca^{2+} [52]. The term EF-hand refers to the two COOH-terminal α-helical sequence stretches, which are oriented in a perpendicular position and present in a large number of Ca^{2+} binding proteins. Each motif binds one Ca^{2+} ion in the central loop region

[53-55]. In the absence of Ca^{2+}, CaM appears in a closed or semi-open conformation [52]. When the intracellular Ca^{2+} $[Ca^{2+}]_i$ levels increase, Ca^{2+} binds to the Ca^{2+} binding loops, causing conformational changes in the EF-hand motifs from the semi-open to the more 'open' shape (Figure 1.8), promoting the binding of other target proteins including kinases and phosphatases [51]. Furthermore, CaM might have a regulatory role in other muscle activities such as metabolism and activation of CaM-dependent Protein Kinases (CaMK) including glycogen synthase kinase and CaMK II, and phosphatases including Cn [56-58].
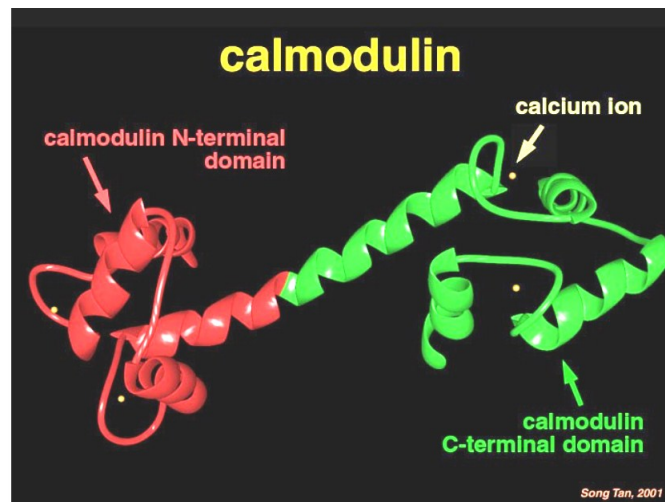
Figure 1.8: The crystal structure of calmodulin (Song Tan, University Park, PA 2001)

1.2.2 Calcineurin (Cn)

Cn is a Calcium/Calmodulin (Ca^{2+}/CaM) dependent serine-threonine phosphatase that plays an important role in cell signaling and the immune system. The administration of immunosuppressive drugs such as Cyclosporine A (CsA) and FK506, decreases Cn activity [59, 60]. Cn exists as a heterodimer comprising the Calcineurin A (CnA) subunit with catalytic activity and the Calcineurin B (CnB), which is a calcium binding subunit

that helps regulate Cn activity (Figure 1.9A). CnA is made up of two domains; the catalytic domain, which is located at the N-terminal region and the regulatory domain, which is located at the C-terminal region. The regulatory domain has three binding sites; CnB, CaM and autoinhibitory binding domains [61]. At rest, the $[Ca^{2+}]_i$ levels are low and thus the autoinhibitory domain covers the catalytic domain of CnA and renders Cn in an inactive conformation (Figure 1.9B). The opposite takes place during physical activity, where the $[Ca^{2+}]_i$ levels increase and Ca^{2+} binds to the CnB subunit, causing a conformational change that releases the inhibition caused by the autoinhibitory domain (Figure 1.9C). This in turn exposes the CaM binding domain where activated CaM binds to activate Cn phosphatase activity [62, 63].

CnAα, CnAβ and *CnAγ* are three genes that encode for CnA. The first two are ubiquitously expressed, whereas *CnAγ* is expressed only in brain and testis [61, 64]. *CnAβ* exists in two splice variants, *CnAβ1* and *CnAβ2*, whose proteins differ in their C-terminal domains [61]. CnAβ1 lacks the typical autoinhibitory domain present in CnAβ2, which is replaced by an alternative C-terminal domain, generated by the translation of intronic sequences [64]. It is noteworthy that CnAβ1 displays a cardio-protective function via activation of the Akt (a protein kinase) and Serum and Glucocorticoid-regulated Kinase (SGK) pathways, thus decreasing inflammation [65].
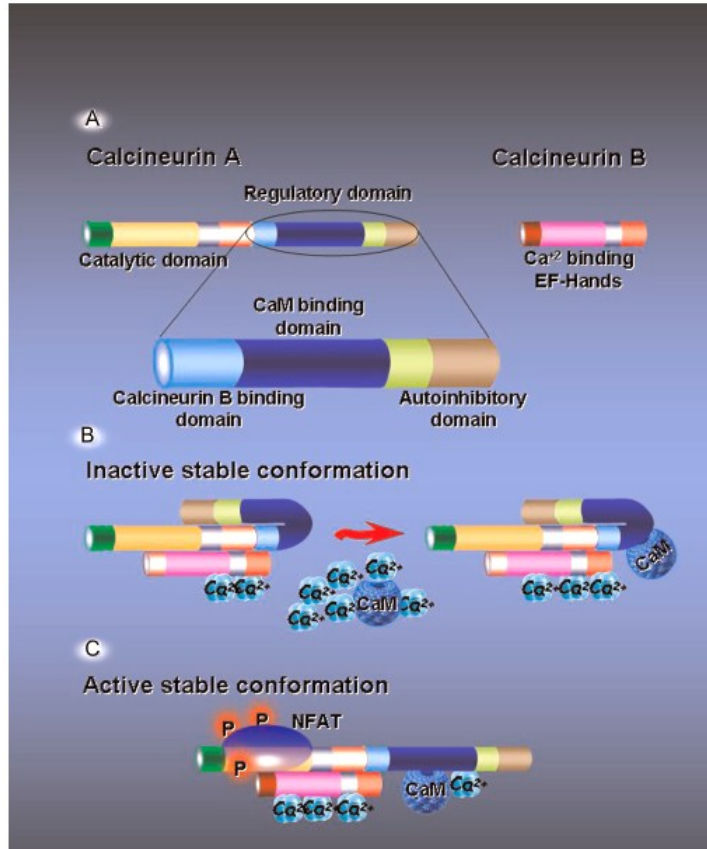
Figure 1.9: Calcineurin structure and its active and inactive conformations[52]

(**A**) The heterodimeric structure of calcineurin consists of two subunits catalytic-regulatory (calcineurin A) and a Ca^{2+}-binding (calcineurin B). Calcineurin A contains two domains, the N-terminal catalytic and C-terminal regulatory, which consists of three domains: the calcineurin binding site, calmodulin binding site and an auotoinhibitory site. (**B**) In resting skeletal muscle cells where the intracellular Ca^{2+} level is low, calcineurin is in the inactive conformational state. Increased intracellular Ca^{2+} levels activate calmodulin which, in turn, binds to the heterodimer calcineurin, inducing its active conformational changes. (**C**) In its active stable conformational state, the auotoinhibitory domain has been displaced from the catalytic domain where the nuclear factor of activated T-cell (NFAT) protein binds.

Cn interacts with numerous transcription factors, scaffolding and cytoskeleton proteins. Thus, Cn regulates various functions in muscle, which potentially affect both skeletal and cardiac muscles [66]. For instance, the hypertrophy of skeletal muscle cells in culture is induced by activating Cn, while inhibition of Cn blocks the hypertrophy induced by Insulin Growth Factor-I (IGF-I) [67, 68], suggesting that Cn has a prominent

role in skeletal muscle hypertrophy either alone or with other signals that might be important for activation of Cn-dependent genes [69, 70]. Additionally, when CsA is administered to heat-stressed Wistar rats exercised at 41°C for 60 minutes, a smaller hypertrophic response is induced in their soleus muscles [71].

1.2.3 NFAT proteins; structure and regulation

Cn regulates several signaling pathways through dephosphorylation of a majority of proteins such as the Nuclear Factor of Activated T cells (NFAT) [72]. NFAT proteins belong to the Rel-family of transcription factors and have a molecular weight that varies between 70 to 200 kDa, due to the presence of different splicing of genes (Figure 1.10) [72].
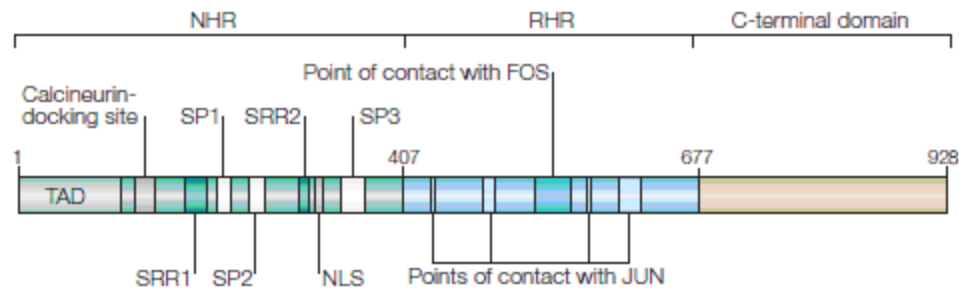
Figure 1.10: The primary structure of NFAT proteins [73]

The NHR includes the calcineurin-docking site, the nuclear localization signal (NLS), the serine-rich regions (SRRs) and the SPXX-repeat motifs (SPs). An inducible phosphorylation site has also been described in the N-terminal transactivation domain (TAD) of NFAT. The RHR contains the DNA-binding domain, points of contact with FOS and JUN, which allows the formation of the synergistic NFAT–FOS–JUN–DNA quaternary complex. The phosphoserines that are targeted by calcineurin dephosphorylation are located in the SP2, SP3 and SRR1 motifs.

NFAT transcription factors consist of five isoforms; The first four including NFATc1 (also called NFAT2, or NFATc), NFATc2 (also called NFAT1, or NFATp),

NFATc3 (also called NFAT4, or NFATx) and NFATc4 (also called NFAT3) reside in the cytoplasm in unstimulated cells but rapidly move to the nucleus in response to stimulation triggered by Ca^{2+} mobilization [74]. Therefore, these isoforms have well-known roles in both skeletal and cardiac muscles [72, 75]. The fifth one is called NFAT5 or Tonicity-response Enhancer-Binding Protein (TonEBP) and is insensitive to Cn signaling due to the absence of SPRIEIT sequence. The latter sequence allows Cn to bind to NFAT and dephosphorylate thirteen serine residues of the NFAT protein [76].

Structurally, NFAT consists of three domains: a conserved N-Homology Region (NHR), a conserved Rel-Homology Region (RHR) and a non-conserved C-Terminal Domain (CTD). The first 407 amino acid residues form the N-homology region, which contains a Transactivation Domain (TAD) required for NFAT binding to the promoter region of genes and transcriptional initiation, a Cn docking domain that contains the SPRIEIT sequence, a Nuclear Localization Signal (NLS), Serine-Rich Regions (SRR) and repeating Ser-Pro-X-X motifs (SP) (X refers to any amino acid). Additionally, there is a Nuclear Export Signal (NES) but its exact location in the NFAT primary structure is still unknown [77, 78]. Residues 408 to 677 constitute the RHR domain, which is conserved among all Rel proteins [79]. Finally, residues from 678 to 928 form the CTD whose role is still unclear due to the discrepancy in the length of this domain among NFAT isoforms. Yet, many scientists suggest that it may be responsible for NFAT transcriptional activity [75, 80]. Having this critical structure, an important question could be raised, how does NFAT shuttle between the nucleus and the cytoplasm?

In resting cells, NFAT proteins are located in the cytoplasm. Upon activation, they become dephosphorylated by Cn and then transported to the nucleus [74, 81]. To

examine how phosphorylation controls localization and function of NFAT, the Okamura group in 2000 used a combination of mass spectrometry and systematic mutational analysis. They showed that thirteen out of fourteen conserved phosphoserine residues of NFAT are dephosphorylated by Cn, in an event that contributes to NFAT transcriptional activity [82]. Upon dephosphorylation, the NES sequence of NFAT is hidden, whereas the NLS sequence becomes unmasked allowing NFAT to enter the nucleus. Inside the nucleus, a number of kinases phosphorylate the same serine residues of NFAT that are targeted by Cn, and thus regulate NFAT transcriptional activity. Those kinases include the Mitogen Activated Protein Kinase (MAPK) family that consists of p38, Janus-N-Terminal Kinase (JNK) and Extracellular-Regulated Signal Kinases (ERK). Other kinases include Casein Kinase (CK) and Glycogen-Synthase Kinase3-β (GSK3-β) [83-86]. Upon rephosphorylation, the NES sequence becomes re-exposed whereas the NLS sequence becomes masked, leading to the nuclear export of NFAT back to the cytoplasm [82]. Those regulatory kinases are classified into maintenance kinases that phosphorylate NFAT in the cytoplasm preventing its nuclear import, and export kinases that phosphorylate NFAT in the nucleus promoting its nuclear export. GSK3-β acts as an export kinase on the SPXX repeat motifs; SP2 and SP3 of NFATc1 and on SP2 of NFATc2 [73, 87], whereas CK functions as both a maintenance and an export kinase on SRR1 of NFATc2 [88]. Furthermore, JNK phosphorylates NFATc1, while p38 phosphorylates NFATc2 [84, 86].

18

1.2.4 Cn/NFAT signaling and Duchenne muscular dystrophy

Activation of Cn signaling is initiated in response to increased levels of $[Ca^{2+}]_i$, which binds to Cn and activates its phosphatase activity. It has been shown that Cn signaling can distinguish between different patterns in the amplitude of changes in $[Ca^{2+}]_i$ [89, 90]. Cn signaling activity responds to sustained, low-amplitude release of $[Ca^{2+}]_i$, which is characteristic of nerves innervating slow muscles [89]. However, phasic nerve activity, which is characteristic of nerves innervating fast fibers leads to high-amplitude of $[Ca^{2+}]_i$ that is insufficient to activate the Cn pathway [89].

Activation of Cn leads to dephosphorylation and nuclear localization of dephosphorylated NFAT, which in turn binds to the promoter regions of many genes and potentiates their expressions [91-93]. Some of these genes, such as *utrophin*, are implicated in skeletal muscle diseases, whereas others are linked to cardiac hypertrophy. The autosomal gene *utrophin* is one of the most critical downstream targets of NFAT. The therapeutic value of this gene arises from the high degree of sequence identity that it shares with the *dystrophin* gene [94].

The *dystrophin* gene encodes for the muscle sarcolemmal protein dystrophin, which is 427 kDa and an integral part of the <u>D</u>ystrophin-<u>A</u>ssociated <u>P</u>rotein <u>C</u>omplex (DAPC) family [95]. Three tissue-specific promoters of dystrophin include brain (B), muscle (M), and purkinje (P) [96]. The M promoter drives high levels of dystrophin expression in skeletal muscles and cardiomyocytes [96, 97]. Dystrophin is linked to the sarcolemma of normal muscle by DAPC, which is composed of at least 10 different proteins (Figure 1.11). Together with other members of DAPC, dystrophin links the

extracellular matrix with the actin network [98]. Structurally, dystrophin contains four separate regions (Figure 1.12); an actin binding domain at the NH_2 terminus, a central rod domain composed of 24 repeating units giving the molecule a flexible rod-like structure, a WW domain that mediates the interaction between β-dystroglycan (a member of DAPC) and dystrophin, a cysteine-rich domain and a COOH-terminal domain [94].
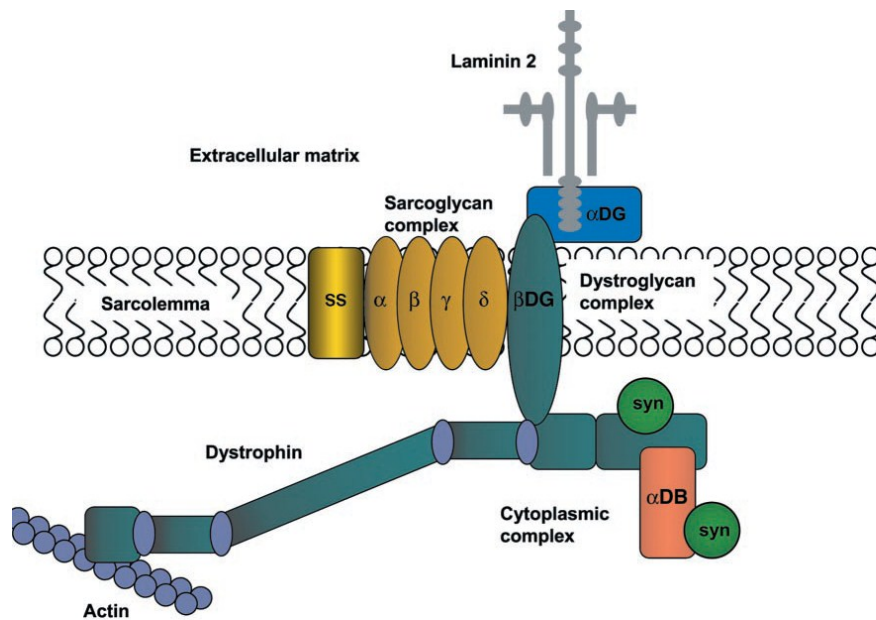
Figure 1.11: Dystrophin associated protein complex. Modified from [94]

Dystrophin binds to cytoskeletal actin at its NH2 terminus. At its COOH terminus, dystrophin is associated with a number of integral and peripheral membrane proteins. β-dystroglycan binds to dystrophin and completes the link between the actin-based cytoskeleton and the extracellular matrix.

Duchenne Muscular Dystrophy (DMD) is a neuromuscular disease caused by loss of dystrophin [95]. Becker Muscular Dystrophy (BMD) is a much milder form of the disease, where patients have much longer survival than DMD [94]. Both disorders are characterized by muscle wasting and early death, and caused by mutations in the gene encoding dystrophin leading to truncated, non-functional protein [94]. Many mutations

have been identified in DMD and BMD affecting almost all domains of dystrophin [94]. DMD mutations lead to the absence or much reduced levels of dystrophin protein, due to premature termination of translation associated with protein instability. BMD mutations lead to some partially functional but smaller dystrophin protein, due to the expression of truncated transcripts without affecting the reading frame [94]. Early results show that the cysteine-rich domain is not deleted in BMD, and mutations in this domain and the COOH-terminal domain cause severe clinical phenotypes, suggesting that these domains are critical for dystrophin function [94].

Studies have shown that the regulation of $[Ca^{2+}]_i$ is disrupted in dystrophic muscle fibers due to abnormal fluxes of Ca^{2+} from the SR [94, 99], leading to extensive cycles of degeneration and regeneration accompanied by invasion of free radicals and related oxidative stress [99, 100]. The loss of functional dystrophin, mechanical disruption of the sarcolemma and activation of the Ca^{2+}-dependent protein calpain lead to Ca^{2+} leakage and the triggering of a pathophysiological Ca^{2+} concentration in the cytosol [101, 102].

Currently, there is a limited efficacy for the pharmacological interventions to treat patients with DMD [94]. Glucocorticoids have been used to minimize the inflammatory responses, as well as to enhance the respiratory function of patients [103]. Yet, the side effects of steroids might negatively affect the progression of the disease. Furthermore, non-steroidal anti-inflammatory drugs have been shown recently to ameliorate muscle morphology and reduce macrophage infiltration, without affecting the levels of the dystrophin-homologue protein utrophin [104]. Several studies have shown that upregulating utrophin protein levels at the muscle sarcolemma can compensate for the loss of dystrophin in dystrophin-deficient animal models [105, 106]. In addition, exon

skipping in combination with other measures very often has been considered for correcting the gene defect in DMD and expressing the missing dystrophin protein [107-109]. Additionally, Deflazacort has been considered the "gold standard" drug therapy in DMD [110, 111], as it reduces muscle fiber necrosis caused by membrane damage [112, 113]. In addition to its anti-inflammatory effect, Deflazacort upregulates Cn/NFAT pathway activity, which increases utrophin expression [114, 115]. Therefore, utrophin has been considered a strong candidate among therapeutic strategies for treating DMD [105].

The *utrophin* gene is located on chromosome 6 in humans and on chromosome 10 in mice, and encodes a protein with a predicted molecular mass of 395 kDa [116, 117]. The predicted structure of utrophin shares similarity with dystrophin, and both proteins have conserved binding domains (Figure 1.12). Utrophin is highly expressed in most organs including smooth, skeletal and cardiac muscles in addition to vascular endothelia and platelets [118-120]. In healthy adult muscle fibers, utrophin is confined to the Neuromuscular Junctions (NMJ) [119], but in developing muscle, it is located at the sarcolemma [121, 122]. Unlike utrophin, dystrophin accumulates in the cytoplasm (Figure 1.13) [123, 124]. Acetylcholine receptors (AchR) clusters colocalize with utrophin at the NMJ in developing muscle and in cultured muscle cells [125-127]. In myasthenia gravis, an autoimmune neuromuscular disorder caused by circulating antibodies that block AchRs at the NMJ, utrophin is also lost from the NMJ [128, 129]. In DMD, utrophin can relocalize to the sarcolemma and compensate for the lack of dystrophin due to its ability to bind to other components of DAPC [130].
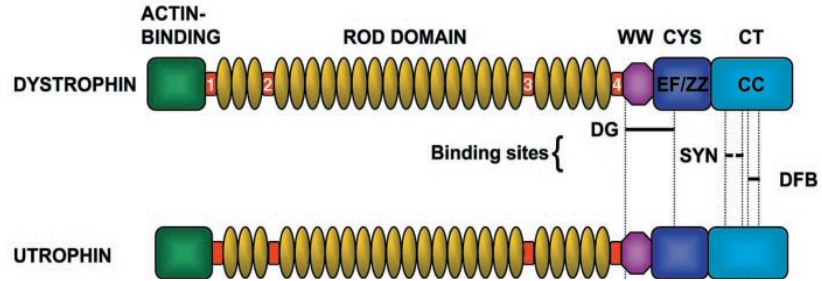
Figure 1.12: Dystrophin and utrophin protein structures. Modified from [94]

An 800 bp fragment of the utrophin promoter is essential for its expression in muscle. The promoter contains: 1) an E-box motif, which is a characteristic motif for muscle specific proteins and binds myogenic transcription factors [131, 132] and 2) an N-box motif essential for directing synapse-specific gene expression [133]. There are two different isoforms of utrophin; utrophin-A and utrophin-B. Utrophin-A is expressed in mature skeletal muscle fibers and utrophin-B is expressed in the endothelial cells [105, 134]. Both isoforms contain different 5' exons and are transcribed from different promoters. In skeletal muscles, the A and B transcripts are relatively equal [134]. Since utrophin-B promoter does not contain an N-box motif, it might not induce the synapse-specific expression of utrophin-B transcripts and this explains the presence of utrophin transcripts in extrasynaptic regions of muscle fibers [134, 135].
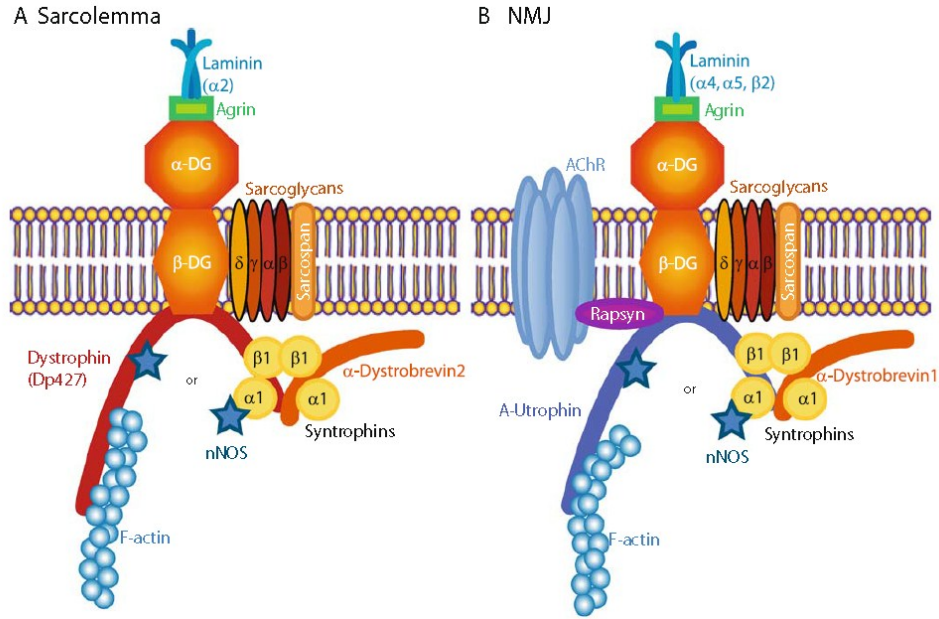
Figure 1.13: Schematic diagram showing dystrophin in the cytoplasm and utrophin at the NMJ [136]

The *mdx* mouse model has been developed to study and represent DMD, as it lacks the full-length dystrophin protein due to a point mutation in exon 23 of the *dystrophin* gene, leading to a premature stop codon [99]. The lack of functional dystrophin protein in *mdx* mice leads to reduced stability of the sarcolemma and necrosis of muscle fibers during a crisis period at 3-4 weeks of age [137, 138]. After this period, extensive degeneration and regeneration of muscle fiber continues, leading to increased proportions of myofibers with centrally located nuclei (a marker for muscle necrosis and regeneration), large variations in myofiber size, elevated levels of muscle enzymes and defective regulation of energy metabolism [137, 139, 140], until mice eventually die due to muscle wasting and respiratory failure [141]. It is clear that DMD and *mdx* mice share common features of the disease including the onset, progression, complexity and severity [94]. Therefore, the *mdx* mouse has been considered a key resource in the identification

of dystrophic pathophysiology and potential therapies [94]. However, Cn serum levels are shown to be lower in DMD patients than *mdx* mice [142] possibly due to insufficient utrophin and impairment of muscle regeneration. To study the importance of utrophin, other knockout (-/-) mice have been generated. *Utrophin*-/- mice do not show any obvious functional abnormalities, but do exhibit reduced numbers of AchRs [143]. Mice deficient for both dystrophin and utrophin show more severe progressive muscular dystrophy than *mdx* mice, resulting in premature death [144, 145]. Thus, the double mutant mouse may provide a useful model for studying human DMD disease and potential therapies using utrophin [146, 147].

Targeting Cn/NFAT signaling is essential to prevent the progression of DMD, knowing that transgenic mice overexpressing Cn (CnA*), where the C-terminal autoinhibitory domain is cleaved, display shifting towards slower MyHC fiber-type, upregulation of utrophin around the sarcolemma and improvement of sarcolemmal integrity [105, 106]. Inhibition of the latter pathway using CsA, leads to skeletal muscle degeneration and impairment of the muscle regeneration process [148]. Interestingly, this mechanism is supported by the finding that Deflazacort attenuates the progression of DMD via activating Cn/NFAT signaling, which mediates gene expression [115]. However, caution should be taken as the increase in Cn levels also might cause severe side effects such as cardiac hypertrophy [149]. Accordingly, DMD patients are susceptible to heart failure when activated Cn is used to alleviate the dystrophic symptoms. The process of upregulating utrophin at the muscle sarcolemma of slow muscle fibers in *mdx* mice via the Cn/NFAT pathway is thoroughly explained in Chapter 2 of this thesis.

In addition to utrophin, overexpressing the Heat Shock Protein 70 (HSP70) in *mdx* and *mdx/utrophin-/-* mouse models has been shown to play a role in the rescue of the dystrophic phenotype [150]. The mechanism by which HSP70 improves the dystrophic symptoms is still unclear. However, HSP70 binds to and enhances the function of the Sarcoplasmic Reticulum-Ca^{2+}-ATPases (SERCA) in the removal of $[Ca^{2+}]_i$ from the cytoplasm by an unknown mechanism [151]. Further, overexpression of HSP70 in rat soleus muscles protect skeletal muscle from atrophy [152]. These effects might explain the importance of targeting HSP70 for the treatment of muscle dystrophy.

1.2.5 Cn/NFAT signaling and cardiac hypertrophy

The role of Cn signaling in cardiac hypertrophy has been under debate for many years. Several studies have shed light on the ability of Cn to trigger reprogramming of gene expression and hypertrophic growth in the heart upon release of $[Ca^{2+}]_i$ [81, 149]. The immunosuppressant drugs CsA and FK506 are highly specific inhibitors of Cn and therefore, can block hypertrophic responses in neonatal cardiomyocytes which have been exposed to hypertrophic agonists. Thus, such drugs can be used in treatment of cardiac hypertrophy associated with heart diseases [153]. Moreover, the direct Cn modulators such as Modulatory Calcineurin-Interacting Protein (MCIP) (recently known as RCAN), also can block the hypertrophic response in cultured cardiomyocytes [154].

The Cn/NFAT pathway is initiated upon $[Ca^{2+}]_i$ release and activation of Cn. Subsequently, Cn dephosphorylates members of the NFAT family, specifically NFATc4, which translocates to the nucleus and binds to the promoter of the cardiac-restricted Zinc finger transcription factor GATA4 (Figure 1.14) [155]. The two conserved Zinc fingers

of GATA4, are required for binding to the consensus DNA sequences 5'-(A/T)GATA(A/G)-3' [156-158]. GATA4 has been shown to regulate the expression of cardiac structural genes during development [159-161]. Many cardiac fetal genes are activated during physiological and/or pathological heart growth [156]. However, the major ones highlighted in Chapter 4 of this thesis are *β-MyHC*, Atrial Natriuretic Peptide (*ANP*) and Brain Natriuretic Peptide (*BNP*). Thus, binding of NFATc4 to GATA4 leads to the activation of those fetal cardiac genes, which are responsible for physiological cardiac growth during heart development. However, in adult hearts, the activation of these genes would be responsible for pathological cardiac growth [155]. It is noteworthy that in CnA* mice, other Cn-dependent signaling events are augmented. For instance, specific c-Jun N-terminal kinases are activated [162, 163]. Additionally, Calmodulin-dependent protein Kinase (CaMK), a potent inducer of cardiac hypertrophy, is also activated where it targets the Histone Deacetylase (HDAC) protein complexes, leaving HDAC free (Figure 1.14) [164-166].

Furthermore, the relative Heart Weight to Body Weight (HW/BW) ratio of CnA* transgenic mice is three-fold higher than that of Wild-Type (WT) counterparts. These mice also display a two-fold increase in Cross Sectional Area (CSA) of cardiomyocytes and are more susceptible to death than WT mice. Such effects are blocked by treating CnA* mice with CsA [149]. GATA4 also is phosphorylated by GSK3-β, a negative regulator of cardiac hypertrophy. This phosphorylation leads to the export of GATA4 from the nucleus and thus minimizes the consequences of cardiac hypertrophy [167, 168]. Other kinases that target GATA4 include ERK1/2 and P38 MAPK that phosphorylate

27

GATA4 at serine 105, leading to increased DNA binding affinity during heart failure [169, 170].
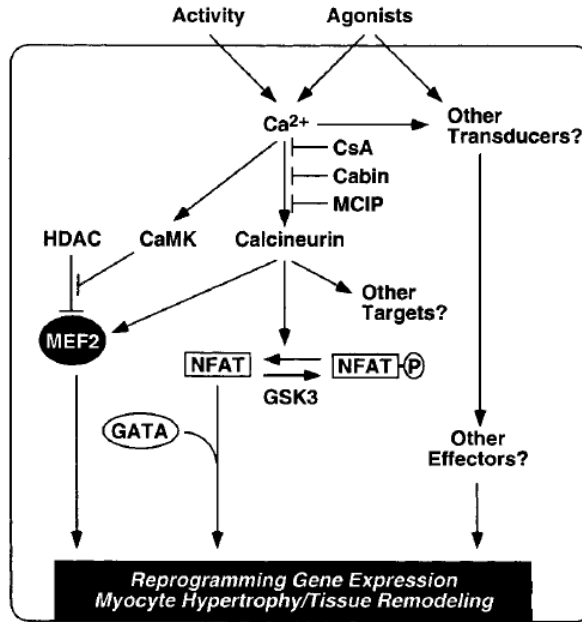
Figure 1.14: Ca^{2+} signaling pathways implicated in cardiac hypertrophy [153]

1.2.6 IGF-1-Akt signaling and cardiac hypertrophy

Stimulation of cardiac hypertrophy is not restricted to Cn. Other signaling pathways have been shown to play a critical role in this process [171]. One major pathway is the IGF-1-Akt/PKB pathway. The importance of Akt, a <u>P</u>rotein <u>K</u>inase <u>B</u>, (PKB) in heart diseases is based on previous data showing that short-term activation of the IGF-1-Akt/PKB pathway induces compensatory cardiac hypertrophy. Moreover, *Akt-/-* mice are not subject to physiological cardiac hypertrophy as are WT mice. On the contrary, mice overexpressing Akt demonstrate severe heart failure, suggesting an important role for Akt in cardiac hypertrophy [172, 173].

At the inner surface of the plasma membrane, IGF-1 binds to the receptor tyrosine kinase IGF-1 Receptor (IGF-R). This binding leads to the phosphorylation of Insulin Receptor Substrate (IRS) by the IGF-R. In turn, phosphorylated IRS activates Phosphatidyl-Inositol-3-Kinase (PI3K) to phosphorylate membrane phospholipids, giving rise to Phospho-Inositide-3,4,5-tri-Phoshate (PIP3) from Phospho-Inositide 4,5-bi-Phosphate (PIP2). At this stage, the inactive Akt translocates from the cytoplasm to the inner surface of the plasma membrane. This leads to a conformational change of Akt followed by its phosphorylation by Phospho-Inositide-Dependent Kinase 1 (PDK1) at Threonine 308, which causes its activation. Akt in turn, represses the transcription factors of the Foxo family, and inhibits protein degradation and activation of the mammalian Target Of Rapamycin (mTOR) and GSK3-β proteins that stimulate protein synthesis (Figure 1.15) [174].
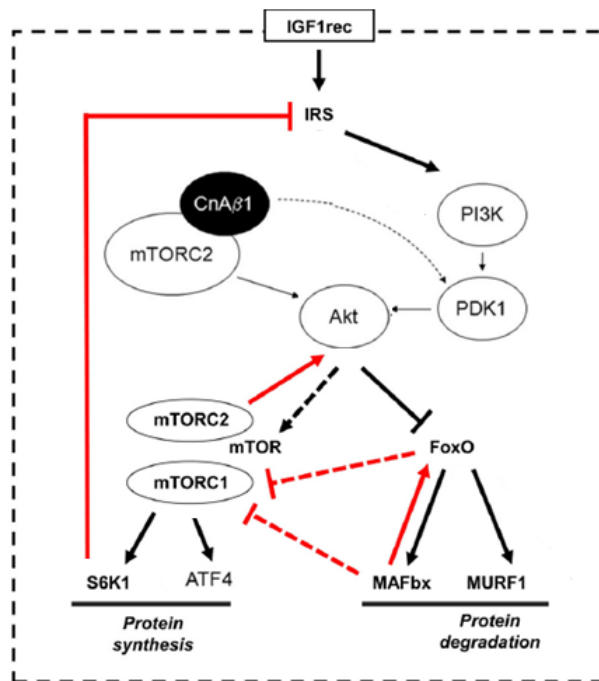
Figure 1.15: The involvement of the IGF-1-Akt pathway in protein synthesis and degradation; (Modified from [65] and [175])

29

The insulin-like growth factor 1 (IGF1)-Akt pathway controls muscle growth via mammalian target of rapamycin (mTOR) and Foxo. The internal feedback loops that control the IGF1-Akt pathway are indicated in red. The dotted line indicates that the effect of Akt on mTOR is indirect and mediated by other proteins. Protein synthesis is mediated by the activation of cardio-protective signaling via CnAβ1 and ATF4 in the heart.

Foxo factors regulate the transcriptional regulation of a ubiquitin ligase called Muscle Atrophy F-box (MAFbx) (also called atrogin-1) and Murf-1, leading to protein degradation via the proteosome [175]. There are two isoforms of mTOR; mTORC1 and mTORC2 [176]. While mTORC2 is required for Akt phosphorylation and activation, mTORC1 phosphorylates S6 Kinase (S6K), which phosphorylates S6 and thus stimulates protein synthesis [177].

To control the IGF-Akt pathway, two feedback loops exist; a negative one which inhibits IRS phosphorylation by S6K leading to degradation and altered localization, and a positive one where mTORC2 phosphorylates Akt at Serine 473 and Threonine 308, by which Akt is activated and protein synthesis is stimulated [178, 179]. Other factors involved in the Akt pathway include the β_1 isoform of the CnA subunit (CnAβ$_1$), which has an essential role in the activation of Akt and thus, is sufficient to produce a protective mechanism [64, 65]. It is possible that CnAβ$_1$ enters the Akt pathway below PI3K (Figure 1.15) and then interacts with mTORC2 through its C-terminal domain, which is critical for the activation of Akt [65]. Further, the Activating Transcription Factor 4 (ATF4) is considered a potential mediator of the cardio-protective effect produced by CnAβ$_1$. ATF4 is also a downstream target of mTORC1, and has been shown to activate the amino acid biosynthesis program and induce the expression of a protective growth factor [65, 180, 181]. The role of both the Cn/NFAT and Akt pathways in cardiac hypertrophy are explained in Chapter 4 of this thesis.

1.3 Direct calcineurin modulators

It has been postulated that the direct Cn modulators are part of a feedback inhibition mechanism to control the regulation of the Cn/NFAT pathway and expression of myofiber genes [182, 183]. The importance of the Cn modulators originated from studying different kinds of cardiac myopathy and heart hypertrophy, where the majority of these proteins exhibit a cardio-protective effect [4, 184, 185]. Since utrophin expression in skeletal muscles is regulated by Cn [105], studying the direct regulators of Cn might be essential when seeking pharmacological interventions for DMD. Therefore, we are interested in studying these modulators in skeletal muscles to see if they have a protective role in certain diseases such as muscle dystrophy, especially when various manipulations in the Cn/NFAT pathway are conducted. Some of these modulators are Z-line proteins, such as the Calcineurin-Interacting proteins (Calsarcins) and Muscle LIM Protein (MLP), while others have direct interactions with Cn and/or NFAT, such as Regulator of Calcineurin 1 (RCAN 1) and Calcineurin Inhibitor (CAIN). In both cases, these modulators are major regulators for Cn activity (Figure 1.16).

1.3.1 Z-line proteins

The Z-lines are defined as the lateral boundaries of the basal contractile unit of the myocyte (Figure 1.2) [3]. The Z-disc consists of parallel layers of α-actinin, which is a 97 kDa actin-binding cytoskeletal protein and a member of the dystrophin family, in which the central rod domain is used for interaction with actin and titin filaments from neighboring sarcomeres [186]. It has been shown that α-actinin is essential for stabilizing the muscle sarcolemma at the beginning of the contraction process [187]. Yet, other

proteins can partially substitute for the loss of α-actinin function during myofibrillogenesis (the assembly of myofibrils in skeletal muscles) [188]. Z-disc-associated proteins play a major role in mechanotransduction, a process by which biomechanical stress is sensed by cardiac myocytes and translated to cardiac hypertrophy [189-191].
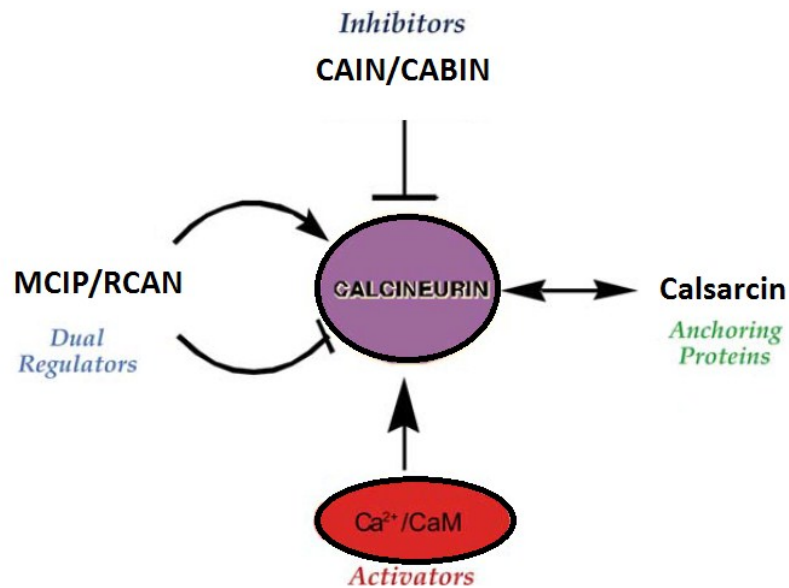
Figure 1.16: Classes of calcineurin binding and regulatory proteins (modified from [192])

Calsarcins, a family of Cn-interacting proteins, tether Cn to α-actinin at the Z- line of cardiac and skeletal muscle cells and inhibit Cn activity, which in turn affects utrophin regulation [184, 193]. Members of this family include calsarcin-1 and calsarcin-2, which are expressed in developing cardiac and skeletal muscles during embryogenesis. In addition, calsarcin-1 is expressed specifically in adult cardiac and slow twitch skeletal muscles, whereas calsarcin-2 is restricted to fast-twitch skeletal muscles [194]. Calsarcin-3 is expressed specifically in skeletal muscle and is enriched in fast-twitch muscles [195].

All members of this family bind to α-actinin, colocalize with Cn and interact with the following Z-line proteins: telethonin, γ filamin, ZASP/oracle and myotilin (reviewed in [190]). It has been reported that mice overexpressing calsarcin-1 are protected against Angiotensin II (Ang II)-induced cardiac hypertrophy, whereas *calsarcin-1-/-* mice suffer from sensitization to pathological stimuli through pressure overload, excessive Cn activity and exacerbated hypertrophy (reviewed in [4]).

MLP, also known as Cysteine Rich Protein3 (CSRP3), contains two LIM domains (tandem zinc fingers consisting of a cysteine-rich consensus) each followed by a glycine rich domain [196]. MLP is tethered to calsarcin-1 and colocalizes with Cn at the sarcomeric Z-disc, thereby affecting Cn activity [197]. It has been revealed that MLP is found in the sarcomeric Z-discs of different species [197-199], in the cytoplasm where it binds with titin [200] and in the nucleus [199]. MLP also binds to the following Z-line proteins: α-actinin, telethonin, Zyxin, N-Rap and β-spectrin [4]. Hypertrophy and dilated cardiac myopathy are reported in MLP-deficient animals, suggesting MLP negatively regulates skeletal and cardiac myofibers [196], whereas overexpression of MLP in differentiating myoblasts, promotes myogenic differentiation [200].

1.3.2 RCAN

RCAN belongs to a family of endogenous Cn regulators that are conserved from yeast to humans. This Cn regulator functions in a negative feedback loop to inhibit Cn activity via its N-terminus [201, 202]. Two different isoforms are identified; RCAN1.1 and RCAN1.4 [203]. Both bind near or at the catalytic domain of CnA and inhibit its activity [204-206].Yet, the expression of the RCAN1.4 isoform is under the control of Cn

through the NFAT binding sites located in exon 4 of the *RCAN* gene [207]. GSK3 phosphorylates the RCAN1 isoform, allowing it to bind and inhibit Cn activity [201]. MAPK can also phosphorylate RCAN1 at five sites giving rise to the phospho-RCAN, which is a good candidate for Cn. Nevertheless, this phosphorylation decreases RCAN affinity to Cn suggesting that the phosphorylated form reduces the inhibitory effect on Cn by RCAN [202]. Binding of RCAN to Cn specifically affects its phosphatase activity, but does not interfere with binding of either Ca^{2+}/CaM complex or the regulatory subunit (B) to the catalytic subunit (A) of Cn [208]. It has been shown that overexpression of RCAN1 in mice causes sustained cardiac function after myocardial infarction [185]. Additionally, those mice show *in vitro* and *in vivo* inhibition of Cn activity through direct association with the catalytic subunit [185]. On the contrary, *RCAN1-/-* mice show reduction in cardiac activity, impaired NFAT activation and diminished hypertrophic response to pressure overload similar to mice lacking $CnA\beta_1$ [185, 209].

1.3.3 CAIN

CAIN, also known as Cabin1, is a soluble cytosolic novel Cn-binding 240 kDa protein with no significant similarity to any known protein [182]. CAIN is widely expressed in various tissues as well as in the brain in a similar manner to Cn, suggesting a physiological relationship between the two proteins [182]. Despite its high molecular weight, CAIN contains a putative Cn-binding domain through a very small portion of its COOH terminus, where binding to Cn leads to inhibition of its catalytic activity [182, 210]. Moreover, CAIN functions as a scaffolding protein that is linked to other proteins like kinases and phosphatases in addition to Cn. Yet, it is not clear so far, whether

phosphorylation affects its activity or not [182]. It has been shown that mice overexpressing CAIN have repressed NFAT dephosphorylation [211], whereas *cain-/-* mice show no gross defects in Cn activity *in vitro* compared to their WT counterparts [212]. However, the cellular Cn activity of these knockout mice was not measured *in vivo* [213]. The roles of RCAN1, calsarcins and MLP in DMD disease are thoroughly discussed in Chapter 3 of this thesis.

1.4 Thesis organization and hypotheses

Cn/NFAT is one of the most critical Ca^{2+} signaling pathways involved in muscle adaptation and disease. Further, other pathways might interfere with the regulation of this pathway. Thus, it is worth exploring the roles of these molecules, which will provide a better understanding of the regulation of Cn and its modulators in both skeletal muscle and heart diseases. In this manuscript-based thesis, we used transgenic and knockout models in addition to animal breeding to study the role of Ca^{2+} and Cn in DMD and cardiac hypertrophy. For each chapter, I have included background that should be read before the manuscript to help understand the basics of the content. Here is a summary for the chapters:

Chapter 2: The role of the Cn/NFAT pathway and the expression of the Heat Shock Protein 70 (HSP70) are discussed in transgenic mice overexpressing the Ca^{2+} buffering protein PV in an *mdx* background. Due to the impairment of Ca^{2+} signaling and the subsequent downregulation of Cn activity, we hypothesize a dramatic exacerbation in the pathology of slow muscle fibers of *mdx*/PV with no changes in HSP70 expression. In this chapter, the role of HSP70 is further studied in *mdx* mice crossed with transgenic mice overexpressing either Cn (which upregulates utrophin expression) or Calmodulin-Binding

Protein (CaMBP), (which attenuates Cn activity and reduces utrophin expression). Herein, we hypothesize a constant HSP70 level with such changes in utrophin expression.

Chapter 3: The roles of direct Cn modulators are investigated in different transgenic models in an *mdx* background. These regulators have a major feedback mechanism, which is essential for regulating Cn activity. Therefore, they may be of great importance in the treatment of DMD. In this context, we hypothesize that the expression of these proteins would be regulated with changes in Cn activity. Thus, the final objective would be to inhibit these inhibitors, for the sake of rendering Cn active through a reasonable mechanism that does not cause severe side effects such as cardiac hypertrophy.

Chapter 4: The role of the NFATc2 transcription factor is studied in the hearts of adult *NFATc2*-/- mice, where we hypothesize that NFATc2 would be more essential in later stages of normotensive adult hearts than in young mice. Additionally, the importance of this transcription factor is thoroughly revealed in the hearts of *NFATc2*+/+ and *NFATc2*-/- mice stimulated by AngII administration for 14 and 28 days. The objective behind this stress, is to inspect the role of NFATc2 and changes in different signaling molecules when adult hearts are exposed to an additional workload via Ang II implantation.

Chapter 2 : **Distinct calcineurin-related transgenic approaches rescue or exacerbate the dystrophic phenotype in fibers from crossbred *mdx* mice despite constant HSP70 expression**

Manal Al Zein[1], Bernard J. Jasmin[2] and Robin N. Michel[1]

[1]*Department of Exercise Science, Concordia University, Montreal, QC, Canada,* [2]*University of Ottawa, Ottawa, ON, Canada*

2.1 Background

In Chapter 2, we are interested in looking at the Calcineurin/Nuclear Factor of Activated T cells (Cn/NFAT) signaling in *mdx* mice, an animal model for Duchenne Muscular Dystrophy (DMD), particularly in the context of overexpression of the transgene Parvalbumin (PV) that attenuates Cn activity [214]. Herein, we shed light on the effect of this transgene on the downstream targets of Cn including NFAT and utrophin. Unlike previous animal models, the transgene in this study targets $[Ca^{2+}]_i$ kinetics and causes a shift in Ca^{2+} oscillations from low to high amplitude spikes, a characteristic of fast fibers. These high amplitude spikes are insufficient to activate the Cn/NFAT pathway and thus affect utrophin expression and the progression of the disease [89, 214]. Additionally, we seek to investigate the role of the Heat Shock Protein 70 (HSP70) that is linked to the Ryanodine Receptor (RyR) and Sarcoplasmic Reticulum-Ca^{2+}-ATPases (SERCA), which are considered critical parts of the Ca^{2+} cycle and play a major role in maintaining Ca^{2+} homeostasis [51].

The results of this chapter are to be submitted for publication to *The FASEB Journal,* which is a premier journal for biomedical and cell biology research. Our work emphasizes the effectiveness of the strategies promoting the slower high oxidative myofiber program via Ca^{2+}/Cn signaling in the treatment of muscle dystrophy. Additionally, they give new insights into the role of HSP70 in rescuing DMD.

Note: Special thanks to Daniel Spensieri who helped in cutting tissues for HSP70 staining.

2.2 Abstract

We have shown the dystrophic phenotype to be rescued by driving the slower oxidative myogenic program via Calcineurin/Nuclear Factor of Activated T cells (Cn/NFAT) signaling together with an increase in utrophin-A expression (Chakkalakal *et al.,* 2004). In this study, we set out to determine the impact of interfering with Ca^{2+}/Cn-based signaling in targeted dystrophin-deficient myofibers. We thus crossbred *mdx* mice with transgenic mice expressing the Ca^{2+}-buffering protein Parvalbumin (PV), driven by the fiber-specific Troponin I slow promoter (TnIs). This approach forced expression of this non-native fast Ca^{2+}-regulatory protein in slow fibers, thus lowering their Cn activity. Consistent with impairments in Cn, we observed significant reduction in utrophin-A expression together with a clear exacerbation of the dystrophic phenotype in *mdx*/PV slow fibers exemplified by several pathological indices. However, a recent study suggests an alternate strategy in the rescue of the dystrophic phenotype by overexpressing the Heat Shock Protein 70 (HSP70), without necessary changes in utrophin-A expression (Gehrig *et al.,* 2012). Therefore, we examined HSP70 expression in *mdx* mice crossbred with mice expressing transgenes either stimulating or attenuating Cn activity. Immunoblotting results showed changes in utrophin-A despite constant levels of HSP70, indicating that the regulation of these two proteins is not correlated. Further, immunofluorescence showed colocalization of HSP70 with MyHC I in transgenic-modified *mdx* slow fibers displaying impaired Cn signaling with exacerbation of the dystrophic phenotype. These results not only underscore the therapeutic potential of targeting Ca^{2+}/Cn-based signaling intermediates as effective countermeasures for muscle dystrophy, but also raise questions about the role of HSP70 in rescuing the dystrophic pathology.

2.3 Introduction

"<u>D</u>uchenne <u>M</u>uscular <u>D</u>ystrophy" (DMD), the most prevalent inherited neuromuscular disorder, is caused by the loss of the muscle sarcolemmal protein dystrophin [95]. Dystrophin is an integral part of the <u>D</u>ystrophin-<u>A</u>ssociated <u>P</u>rotein <u>C</u>omplex (DAPC) family, which is composed of at least 10 different proteins [94]. Together with other members of DAPC, dystrophin links the extracellular matrix with the actin network [98]. Many mutations have been identified in the *dystrophin* gene preventing the synthesis of the full length protein in DMD patients [94]. These mutations lead to instability of the sarcolemma due to the loss of the linkage provided by dystrophin [215, 216]. Currently, pharmacological interventions show limited efficacy in treating patients with DMD [193].

It has been shown that the regulation of intracellular calcium concentration $[Ca^{2+}]_i$ is disrupted in dystrophic muscle fibers [99]. In healthy muscles, excitation of muscle fiber via a motor nerve generates an action potential that spreads along the sarcolemma and the <u>T</u>ransverse tubular system (T-tubules). Accordingly, the <u>D</u>ihydropyridine <u>R</u>eceptor (DHPR), senses the membrane depolarization, causes conformational changes and activates the <u>R</u>yanodine <u>R</u>eceptor (RyR) leading to the release of Ca^{2+} from the <u>S</u>arcoplasmic <u>R</u>eticulum (SR) [217]. In addition, the rapid re-uptake of Ca^{2+} ions is facilitated by the <u>S</u>arcoplasmic <u>R</u>eticulum-<u>C</u>a^{2+}-<u>A</u>TPase (SERCA) enzymes and the Ca^{2+} binding protein calsequestrin [101]. The disruption in $[Ca^{2+}]_i$ kinetics in DMD is caused by abnormal fluxes of Ca^{2+} from the SR (reviewed in [94]), leading to chronic inflammation and extensive cycles of degeneration and regeneration accompanied by invasion of free radicals and related oxidative stress [99, 100]. Such impairment of Ca^{2+}

handling in DMD occurs due to loss of functional dystrophin, mechanical disruption of the sarcolemma and activation of the Ca^{2+}-dependent protein calpain, leading to Ca^{2+} leakage and the triggering of a pathophysiological Ca^{2+} concentration in the cytosol [101, 102].

Utrophin, a neuromuscular junctional protein that shares a high degree of sequence identity with dystrophin, has been considered a strong candidate among therapeutic strategies for treating DMD [105]. Several studies have shown that upregulating utrophin at the muscle sarcolemma, compensates for the loss of dystrophin in DMD and dystrophin-deficient animal models [218, 219]. Along with these findings, studies on the *mdx* mouse, an animal model of DMD, have shown that overexpression of utrophin in skeletal muscles results in improvement of the pathological symptoms of the disease [220-222]. The relevance of utrophin as a therapeutic target for DMD has been correlated to its location. Thus, utrophin normally accumulates at the neuromuscular junction sites of slow and fast muscle fibers but extrajunctionally along the sarcolemma in slow fibers [98]. In the *mdx* mouse, utrophin expression is upregulated within extrajunctional regions of slow but not fast fibers via stimulation of the Calcineurin/Nuclear Factor of Activated T cells (Cn/NFAT) pathway. This event explains utrophin compensation for the loss of dystrophin and the rescuing of the slow fibers but not their fast counterparts, leading to degeneration and eventual death [98].

Of the two isoforms of utrophin, only utrophin-A is expressed in mature skeletal muscle fibers and is under the regulation of the Cn/NFAT pathway, whereas utrophin-B is expressed in endothelial cells [105, 133, 134]. To this end, we have previously shown that utrophin-A expression in slow muscle fibers is regulated by the Cn/NFAT signaling

pathway which promotes the slower, high oxidative myofiber gene program [105]. Ca^{2+} and Calmodulin (CaM), a calcium binding protein, are regulators for Cn and CaM Kinase (CaMK) activities [216]. These enzymes modulate the activity of various transcriptional regulators[89]. Once activated, the phosphatase activity of Cn leads to dephosphorylation of NFAT, followed by nuclear translocation and binding to target promoters to stimulate the expression of the slower myofiber genes including *utrophin* [66, 89]. Utrophin-A expression also is influenced by nerve-derived factors including agrin and heregulin, which promote a series of transcriptional reactions that stimulate the activity of the GA-Binding Protein (GABP) α and β [223]. When activated, GABP binds to the N-box motif of the utrophin-A promoter and stimulates utrophin-A expression [223].

To further establish the role of the Cn/NFAT pathway in regulating utrophin-A expression, we and others illustrated the concept that strategies aimed at promoting the slower high oxidative myofiber program in muscle play a role in the treatment of DMD [98, 224, 225]. In our laboratory, the latter strategy was established by crossbreeding *mdx* mice with transgenic mice expressing an activated form of Cn (CnA*), leading to an increase in utrophin-A expression [106]. Moreover, the transgene expression of a small peptide inhibitor called Calmodulin-Binding Protein (CaMBP) driven by the fiber-specific Troponin-slow I promoter (TnIs) in *mdx* mice, leads to a reduction in the levels of utrophin-A and the transcript of slow Myosin Heavy Chain I (MyHC I), thus exacerbating the dystrophic phenotype [98]. This strategy establishes the impact of interfering with Ca^{2+}/CaM-based signaling in dystrophin-deficient slow myofibers.

Another strategy in the rescue of the dystrophic phenotype involves overexpressing the Heat Shock Protein 70 (HSP70) in *mdx* and *mdx/utrophin-/-* mouse

models [150]. Early studies on human DMD tissues have shown elevated levels of HSP70 suggesting an autoprotective role for this protein [226]. Further, overexpression of HSP70 in rat soleus muscles inhibits skeletal muscle atrophy and therefore is cytoprotective [152]. From this perspective, we have shown earlier that constitutive expression of HSP70 is restricted to the slower, high oxidative fibers (MyHC I and IIa) in rat plantaris [227]. In addition, this heat shock protein binds to and protects the function of the SERCA enzymes [151]. The reason for this protection is not very well understood. However, it might be due to the ability of HSP70 to prevent protein aggregation [228]. Taken together, these findings might explain the potential role of HSP70 in the treatment of muscle dystrophy.

In this study, we introduce a new approach for targeting the Cn/NFAT pathway by forced transgenic expression of the Ca^{2+} buffering protein Parvalbumin (PV) in slow fibers of crossbred *mdx* mice. PV is an EF-hand protein normally expressed only in fast fibers [229], but the transgene is driven by the TnIs, linked to the Haemaglutinin (HA) epitope and forced expressed in slow fibers leading to a decrease in Cn activity and a turning off of the Cn/NFAT pathway [214]. Our strategy is based on different types of nerve activities controlling fast and slow gene expression programs [89]. Tonic motor nerve activity, which is characteristic of nerves innervating slow muscles leads to low-amplitude sustained $[Ca^{2+}]_i$ that activates the Cn/NFAT pathway [89]. However, phasic nerve activity, which is characteristic of nerves innervating fast fibers leads to high-amplitude of $[Ca^{2+}]_i$ that is insufficient to activate the Cn/NFAT pathway [89]. In agreement, PV overexpression in slow fibers, leads to expression of a fast fiber gene and

metabolic profile via shifting Ca^{2+} oscillations from low to high amplitude spikes and subsequent attenuation of Cn signaling [214].

The objective of this study is first to investigate if PV overexpression in *mdx* slow muscle fibers would interfere with Cn/NFAT signaling via utrophin and exacerbate the dystrophic phenotype. Second, we sought to determine if attenuation of the latter pathway and the change in Ca^{2+} dynamics have influenced HSP70, RyR and SERCA isoform expressions. Indeed, PV overexpression led to a prominent exacerbation of the dystrophic phenotype in soleus muscles as exemplified by reduction in utrophin-A expression and higher hallmarks of *mdx* cellular damage. However, reduction of utrophin expression was not accompanied by differences in HSP70 protein levels between *mdx* and *mdx* crossed with PV (*mdx*/PV) mice. In addition, RyR1 (an isoform that is expressed mainly in skeletal muscles) was considerably increased in mice expressing the PV transgene, whereas SERCA 1 and 2 protein levels did not change between *mdx* and *mdx*/PV soleus muscles. Additionally, the role of HSP70 was examined in *mdx* mice crossed with transgenes expressing either CnA* (*mdx*/CnA*) that rescues the dystrophic phenotype, by upregulation of utrophin-A [106] or CaMBP (*mdx*/CaMBP) that exacerbates muscular dystrophy, by downregulation of utrophin-A [98]. Our results showed constant HSP70 levels with either an increase in utrophin-A levels in T̲ibialis A̲nterior (TA) muscles of *mdx*/CnA* or a decrease in utrophin-A expression in soleus muscles of *mdx*/CaMBP mice. Finally, immunofluorescence experiments (IFs) showed colocalization of HSP70 with MyHC I fibers in *mdx* and *mdx*/PV mice and with both MyHC I and IIa in *mdx*/CnA* mice but not with utrophin positive fibers.

These results collectively emphasize that strategies promoting the slower high oxidative myofiber gene program via Ca^{2+}/Cn signaling are considered effective countermeasures in the treatment of DMD, but independent of HSP70. Additionally, they raise questions about the potential role of HSP70 in rescuing the dystrophic pathology.

2.4 Methods

2.4.1 Animals

Animal care and experimental procedures were performed in accordance to the guidelines of the Canadian Council of Animal Care. Transgenic mice expressing either CnA*, CaMBP or PV proteins were generated as described previously [163, 214, 230]. Female *mdx* mice were crossed with CnA*, CaMBP or PV tagged with HA (PV-HA) transgenic mice resulting in pups having the dystrophic pathology. Male pups were selected for the experiments and the presence of the transgene in PV and *mdx*/PV mice was identified by PCR screening of genomic DNA extracted from tails using primers recognizing PV-TnIs (Sigma Genosys). Immunoblotting of soleus proteins using anti-PV antibody (Swant) was also performed to detect PV whereas, Extensor Digitorum Longus (EDL) tissues were used as a negative control. Wild-Type (WT), PV, CnA*, CaMBP, *mdx*, *mdx*/PV, *mdx*/CnA* and *mdx*/CaMBP of 10-12 week old male mice were utilized for all subsequent analyses.

2.4.2 Mice genotyping

Mdx genotyping was performed by amplifying DNA from mouse tails as described earlier [231]. Briefly, 5 µl of DNA was added to 4 µl Taq buffer with KCl

(Fermentas), 2 mM MgCl$_2$ (Fermentas), 0.2 mM dNTP (Invitrogen), 0.66 µM primers (Sigma Aldrich) and 1µl Taq DNA polymerase (Fermentas) yielding a final volume of 20 µl. The following primers were used; a common forward primer: 5'-GCGCGAAACTCATCAAATATGCGTGTTAGTGT-3', a mutant reverse primer: 5'-CGGCCTGTCACTCAGATAGTTGAAGCCATTTTA-3 and a WT reverse primer: 5'-GATACGCTGCTTTAATGCCTTTAGTCACTCAGATAGTTGAAGCCATTTTG-3'. Cycling conditions were as follows: 1) initial denaturation at 95ºC for two minutes, 2) five cycles of first-stage amplification including: denaturation at 95ºC for 20 seconds, primer annealing at 60ºC for 20 seconds and extension at 72ºC for 20 seconds, 3) 23 cycles of the second-stage amplification including: denaturation at 95ºC for 20 seconds, primer annealing at 64ºC for 20 seconds and extension at 72ºC for 20 seconds, 4) final extension at 72ºC for one minute. PCR products were loaded on a 3% agarose gel stained with ethidium bromide and resolved, after electrophoresis, under UV irradiation using the Alpha Innotec FluorChem system (Cell Biosciences).

Detection of CnA* and CaMBP transgenes was thoroughly described in earlier studies [98, 106]. Similarly, PV-HA in PV transgenic mice was identified by extracting DNA from mouse tails followed by the addition of 2 µl DNA to 1X Taq buffer with KCl (Fermentas), 2 mM MgCl$_2$ (Fermentas), 0.2 mM dNTP (Invitrogen), 0.5 mM primers (Sigma Aldrich) and 0.5 µl Taq DNA polymerase (Fermentas) yielding a final volume of 25 µl. The following forward and reverse primers were used: 5'-CCCACCAGCCC AGCTTTTCTA-3'and 5'-TTAGGCGTAGTCGGGCACGTCATATGGGTAGCTTT GG CCAC-3' respectively. Cycling conditions were as follows: 1) initial denaturation at 95ºC for five minutes, 2) denaturation at 94ºC for 30 seconds, 3) primer annealing at 65 ºC for

one minute and extension at 72ºC for one minute, 4) repeat steps 2 and 3 for 24 cycles, 5) final extension at 72ºC for ten minutes. PCR products were loaded on 1.5% agarose gel stained with ethidium bromide and visualized as described above.

2.4.3 Muscle extraction and preservation

Mice were anesthetized by a mixture of 100 mg/ml ketamine hydrochloride (Bimeda-MTC Animal Health Inc.) and 20 mg/ml xylazine (Bayer HealthCare) in a volume ratio of 1.6:1. A dosage of 0.04 ml/30 g of body weight was administered intramuscularly to each mouse. Muscles were extracted and frozen directly in liquid nitrogen for biochemical use or embedded with Tissue-Tek Optimum Cutting Temperature compound (Fisher Scientific) and frozen in a pool of melting isopentane cooled in liquid nitrogen for histology. Samples were then stored at -86ºC until used. Animals were euthanized after extraction using CO_2 gas.

2.4.4 Immunofluorescence

Assessment of NFATc1 nuclear localization was done as described earlier [106]. In summary, soleus muscle cross sections (10 μm thick) were fixed with 4% Paraformaldehyde (PFA), blocked and permeabilized with 2% goat serum and 0.2% Triton X-100, then washed with 1X phosphate buffer saline (PBS) and incubated at 4ºC overnight with primary antibodies recognizing NFATc1. This was followed by incubation with secondary antibodies coupled with fluorescent molecules for one hour, with subsequent washing and mounting with Vectashield containing 4',6-diamidino-2-phenylindole (Dapi) (Vector laboratories). Quantification of NFATc1 nuclear localization

was performed by counting the number of myonuclei positively stained for NFATc1 in cross sectional views of myofibers and calculating the percentage of nuclear NFATc1.

Colocalization of utrophin with MyHC I and IIa was performed as described previously [193]. Co-staining was achieved by applying anti-utrophin antibody together with either anti-MyHC I or IIa antibodies at 4°C overnight. On the following day, secondary antibodies for utrophin detection with secondary antibodies for either MyHC I or IIa were applied for one hour. This was followed by washing, mounting with Vectashield with Dapi and detection using fluorescent microscopy. Additionally, the percentage of fibers with central nucleation in positively stained MyHC I fibers was calculated and compared in *mdx* and *mdx*/PV mice. Further, the colocalization of HSP70 with MyHC I, MyHC IIa, MyHC IIb and utrophin was done as previously discussed [193]. Serial sections (10 μm thick) were fixed, blocked and incubated with primary and secondary antibodies as described above. The same areas were captured at 40X magnification to detect the presence or absence of co-staining using a Zeiss Axioplan fluorescence microscope mounted with a Lumenera Infinity 3-1C1.4 camera (Ottawa, ON, Canada). Negative control slides without primary antibodies revealed the absence of background staining at the acquisition time used. Colocalization analysis was performed using ImagePro Plus version 6.2 software (Olympus, Markham, ON, Canada). All primary and secondary antibodies and their proper conditions are listed in Table 2.1.

Table 2.1: Antibodies and conditions for immunofluorescence

PROTEIN	SUPPLIER	1°ANTIBODY (overnight)	2°ANTIBODY (1 hour)
NFATc1	Santa Cruz# sc-13033	1:50	1:100 Alexa Fluor® 488 Goat anti-rabbit IgG (Invitrogen# A-11008)

Utrophin	Santa Cruz# sc-15377	1:40	1:100 Alexa Fluor® 546 Goat anti-rabbit IgG (Invitrogen# A-11010)
MyHC I	DSHB# A4.840	1:100	1:200 anti-mouse IgM FITC conjugate (Sigma Aldrich# F9259)
MyHC IIa	DSHB# SC-71	1:10	1:100 Alexa Fluor® 488 Goat anti-mouse IgG (Invitrogen# A-11001)
MyHC IIb	DSHB# BF-F3	1:25	1:100 anti-mouse IgM FITC conjugate (Sigma Aldrich# F9259)
HSP70	Enzo Life Sciences# ADI-SPA-812)	1:10	1:100 Alexa Fluor® 546 Goat anti-rabbit IgG (Invitrogen# A-11010)

2.4.5 Fiber typing

Immunohistochemistry of MyHC I and IIa in slow muscle fibers from *mdx* and *mdx*/PV mice was conducted using specific antibodies. Briefly, soleus cross sections were blocked for one hour, incubated with anti-MyHC I or IIa overnight at 4°C, washed and further incubated for two hours with secondary anti-mouse IgM (A8786, Sigma Aldrich) and anti-mouse IgG (A8924, Sigma Aldrich) to detect MyHC I and IIa, respectively. Slides then were washed for several times, incubated with 3,3'-diaminobenzidine (DAB) (Thermoscientific) for five minutes and finally dried, mounted and visualized. The percentage of fibers stained for each of MyHC I and IIa was calculated in three 20X cross sectional views of myofibers from the mid-belly regions of soleus muscles, from four animals per group. Cross sectional areas also were measured and analyzed in the corresponding tissues.

2.4.6 RNA extraction and quantitative real time PCR (qPCR)

Skeletal muscles were homogenized in a solution of guanidinium thiocyanate (Sigma Aldrich), sodium citrate, N-laurylsarcosine (Sigma Aldrich) and 2-mercaptoethanol (Bioshop), followed by addition of sodium acetate (pH 4.0) with vortexing, phenol (Sigma Aldrich) and chloroform:isoamyl alcohol until a white emulsion appeared. Samples were cooled on ice for fifteen minutes, and then centrifuged at 10,000 x g for ten minutes at 4ºC. Afterwards, two volumes of 99% ethanol were added to the aqueous layer with vortexing and centrifugation again at 10,000 x g for ten minutes at 4ºC. The ethanol was decanted and the RNA was suspended in 200 μl of 70% ethanol and centrifuged at 10,000 x g for ten minutes at 4ºC. The ethanol again was decanted and the RNA pellet was dried and suspended in 15 μl of RNAse free H_2O (Bioshop) per 10 mg of tissue with subsequent vortexing and heating at 70ºC for 3 minutes. The RNA concentration was measured and its integrity was validated using an Eppendorf Biophotometer (Eppendorf) at 260nm. About 2 μg of RNA was mixed with a 2:1 formamide:ethidium bromide, formaldehyde (Sigma Aldrich), 10X MOPS (pH 7.0) and bromophenol blue, heated at 65ºC for ten minutes and loaded on a 1.5% agarose gel containing 1X MOPS and formaldehyde. All rRNA bands; 5S, 18S and 28S were visualized indicating RNA integrity. The changes in the abundance of *utrophin*, *utrophin-A*, *MyHC I* and *MyHC IIa* were assessed using real time PCR. Briefly, 2 μg of freshly extracted RNA was reverse transcribed to cDNA using iScript reverse transcription supermix (Bio-Rad) and qPCR was performed using gene specific primers together with proper reference genes for quantification (CFX96 Real-Time System, Bio-Rad). Relative quantities then were normalized by the Real-time System software to the average relative

quantities of the *36B4*, *beta actin* and *gamma actin* housekeeping genes. All primer
sequences used for qPCR in this study are listed in Table 2.2.

Table 2.2: Primers for quantitative real-time PCR

Gene	Forward Primer	Reverse Primer	Product Size(bp)
Utrophin	5'- gtttgaggtgcttcctcagc -3'	5'- gcgctatctggtagctgtcc -3'	203
Utrophin-A	5'- tggaccatttttcagattta -3'	5'- atcgagcgtttatccatttg -3'	207
MyHC I	5'- ctcccaaggagagacgactg-3'	5'-ttaagcaggtcggctgagtt-3'	252
MyHC IIa	5'- gaaccctcccaagtacgaca-3'	5'- taagggttgacggtgacaca -3'	147
36B4	5'- gctccaagcagatgcagca -3'	5'- ccggatgtgaggcagcag -3'	143
β- actin	5'- ccagccatgtacgtagccatccag -3'	5'- cacgcacgatttccctctcagctgt -3'	244
γ- actin	5'- acccaggcattgctgacaggatgc-3'	5'-ccatctagaagcatttgcggtggacg-3'	216

2.4.7 Protein extraction and Immunoblotting

Protein levels of PV, utrophin, HSP70, RyR1, SERCA1 and SERCA2 were
measured by immunoblotting using extracts from soleus tissues of WT, PV, *mdx* or
mdx/PV mice. Similarly, utrophin and HSP70 protein levels were detected in TA muscles
of *mdx* and *mdx*/CnA* mice and in soleus muscles of *mdx* or *mdx*/CaMBP mice using
commercially available primary and secondary antibodies coupled to horse radish
peroxidase (HRP). Briefly, tissues were homogenized in 1X RIPA buffer solution (6
μl/mg tissue) consisting of 1X PBS, 1% Igepal, 0.5% Sodium Deoxycholate, 0.1%
Sodium Dodecyl Sulfate (SDS), 0.001 M Sodium Orthovanadate, 0.01 M Sodium
Fluoride, 0.01 mg/ml Aprotinin, 0.01 mg/ml Leupeptin and 1 mM
Phenylmethanesulfonyl fluoride (PMSF). Homogenates were centrifuged at 15,000 x g
for twenty minutes and the supernatant layers were collected and re-centrifuged.

Protein concentrations were measured using Quick Start Bradford dye reagent (Bio-Rad), followed by loading 40 µg of soleus or TA and 5 µg of EDL proteins, with electrophoresis using SDS-PAGE (5% gel for utrophin and RyR1 and 12% for PV, HSP70, SERCA1 and SERCA2) at 120V and transfer at 30V for 90 minutes, using Borax (Bioshop), to a Polyvinyl difluoride (PVDF) membrane (Millipore). This was followed by blocking for one hour using either 5% non-fat milk in Tween/Tris Buffered Saline (T/TBS) or 1% Bovine Serum Albumin (BSA) in 0.1% T/TBS. Primary antibodies were incubated on a shaker at a moderate speed and at 4ºC overnight. Membranes then were washed and incubated with secondary antibodies (Sigma Aldrich and Cell Signaling) coupled to HRP on a shaker at room temperature and moderate speed for one hour, followed by washing and developing with enhanced chemi-luminescence reagents (Millipore) using the Alpha Innotec FluorChem system (Cell Biosciences). Bands were then quantified and their intensities were measured using the Alpha Innotec FluorChem software. Alpha tubulin was used as a loading control and groups were normalized to WT. All information about antibodies, suppliers and conditions are listed in Table 2.3.

Table 2.3: Antibodies and their conditions for immunoblotting

PROTEIN	SUPPLIER	PRODUCT SIZE (kDa)	1°ANTIBODY (overnight)	2°ANTIBODY (1 hour)
Utrophin	Novacastra #NCL-DRP2	395	1:500 in T/TBS	1:500 in T/TBS (anti-mouse)
PV-HA	Swant	Endogenous=12 Transgene=14	1:2000 for soleus and 1:10000 for EDL in 5%milk	1:2000 for soleus and 1:10000 for EDL in 5% milk (anti-rabbit)
HSP70	Enzo Life Sciences #ADI-SPA-810	70	1:2000 in 5%milk	1:2000 in 5%milk (anti-mouse)

RyR1	Abcam #ab2868	565	1:500 in 5%milk	1:5000 in 5%milk (anti-mouse)
SERCA1	Pierce # MA3-912	110	1:1000 in 5%milk	1:5000 in 5%milk (anti-rabbit)
SERCA2	Pierce #MA3-919	110	1:500 in 5%milk	1:5000 in 5%milk (anti-rabbit)
α-tubulin	Cell Signaling #2125	52	1:2000 in 5%milk	1:2000 in 5%milk (anti-rabbit)

2.4.8 Assessment of central nucleation and muscle fiber size

Necrosis and regeneration of soleus muscles was assessed using Hematoxylin and Eosin (H&E) to examine the percentage of fibers with centrally located nuclei. Hematoxylin stains the nucleus purple, whereas eosin stains the cytoplasm pink. Simply, cross sections (10 µm thick) from soleus muscles were stained with H&E, dehydrated through a series of alcohol solutions, cleared with xylene and mounted using permount (Fisher Scientific). The sections were visualized using a standard light microscope, and images were captured and used to count the number of fibers with centrally located nuclei. The extent of regeneration occurring in soleus muscles was determined by counting the number of fibers having central nucleation relative to the total number of fibers and then comparing the average percentage of fibers with central nuclei between samples [106]. To assess size variability of fibers within dystrophic mice, a pathological feature of *mdx* mice [232], cross sectional area for each individual fiber was measured using ImagePro Plus Software. The average standard deviation from three 20X cross sectional views of myofibers from the mid-belly of muscles from four animals per group was calculated and the values were compared between *mdx* and *mdx*/PV mice.

2.4.9 Evans Blue uptake and staining

Evans Blue dye (EBD) injections were carried out as described elsewhere [233]. Briefly, 50 µl/10 g of body weight of EBD (Fisher Scientific) was injected intraperitoneally. Muscles were isolated 12 to 16 hours later, frozen in isopentane, then in liquid nitrogen and finally removed and stored at -86ºC. Prior to visualizing the tissues under the microscope, 10 µm sections were collected, fixed in 4% PFA for 20 minutes, washed five times for five minutes with PBS and mounted with Vectashield mounting medium. The intensity level of Evans blue dye was determined using ImagePro Plus Software by converting images to 8-bit gray scale and determining the total and average gray intensity in cytosolic regions of myofibers as a measure of Evans blue dye fluorescence. The average gray intensity was then compared between groups with three animals per group. Three 10X cross sectional views from soleus mid-belly regions were used to obtain average intensities.

2.4.10 Statistical analyses

Statistical analyses were performed using the SPSS software program version 17.0. (IBM SPSS, Chicago, IL, USA). Results were expressed as means ± SEM. Statistical differences between individual groups (P<0.05) were analyzed using One Way Analysis of Variance (Anova) to test for differences among four groups of different phenotypes. Student's *t*-test was applied when comparing only two groups with one variable. Analyses for Chapter 2 are fully explained in Appendix I.

2.5 Results

2.5.1 Generation and identification of *mdx*/PV mice

To assess the role of $[Ca^{2+}]_i$ kinetics in a dystrophin-deficient background, we generated *mdx* mice expressing the PV transgene specifically in slow muscle fibers. Our previous findings determined that PV-TnIs mice are healthy and capable of breeding [214]. PCR-based screening was used to identify animals expressing the PV transgene in addition to a spontaneous nonsense mutation in exon 23 of the *dystrophin* gene in *mdx* mice [234, 235] (Figure 2.1a). Immunoblotting analyses of soleus and EDL muscles from WT, PV, *mdx* and *mdx*/PV mice demonstrated the presence of endogenous PV in both soleus (Figure 2.1b) and EDL (Figure 2.1c) muscles of all mice and the expression of the PV-HA transgene solely in soleus muscles of PV and *mdx*/PV mice with no detectable levels in EDL muscles.

2.5.2 Forced expression of PV transgene leads to impairment of downstream Ca²⁺/CaM-based signaling

To assess the consequences of impaired CaM signaling in slow muscle fibers from *mdx*/PV mice, we sought to determine the nuclear localization of NFATc1, which has been shown to be regulated by the Cn pathway [66, 236, 237]. IFs of soleus muscles demonstrated changes in NFATc1 nuclear localization (Figure 2.1d). Quantitative assessment revealed a significant decrease in the nuclear localization of NFATc1 in PV, *mdx* and *mdx*/PV compared to WT and in *mdx*/PV compared to *mdx* soleus muscles (Figure 2.1e).
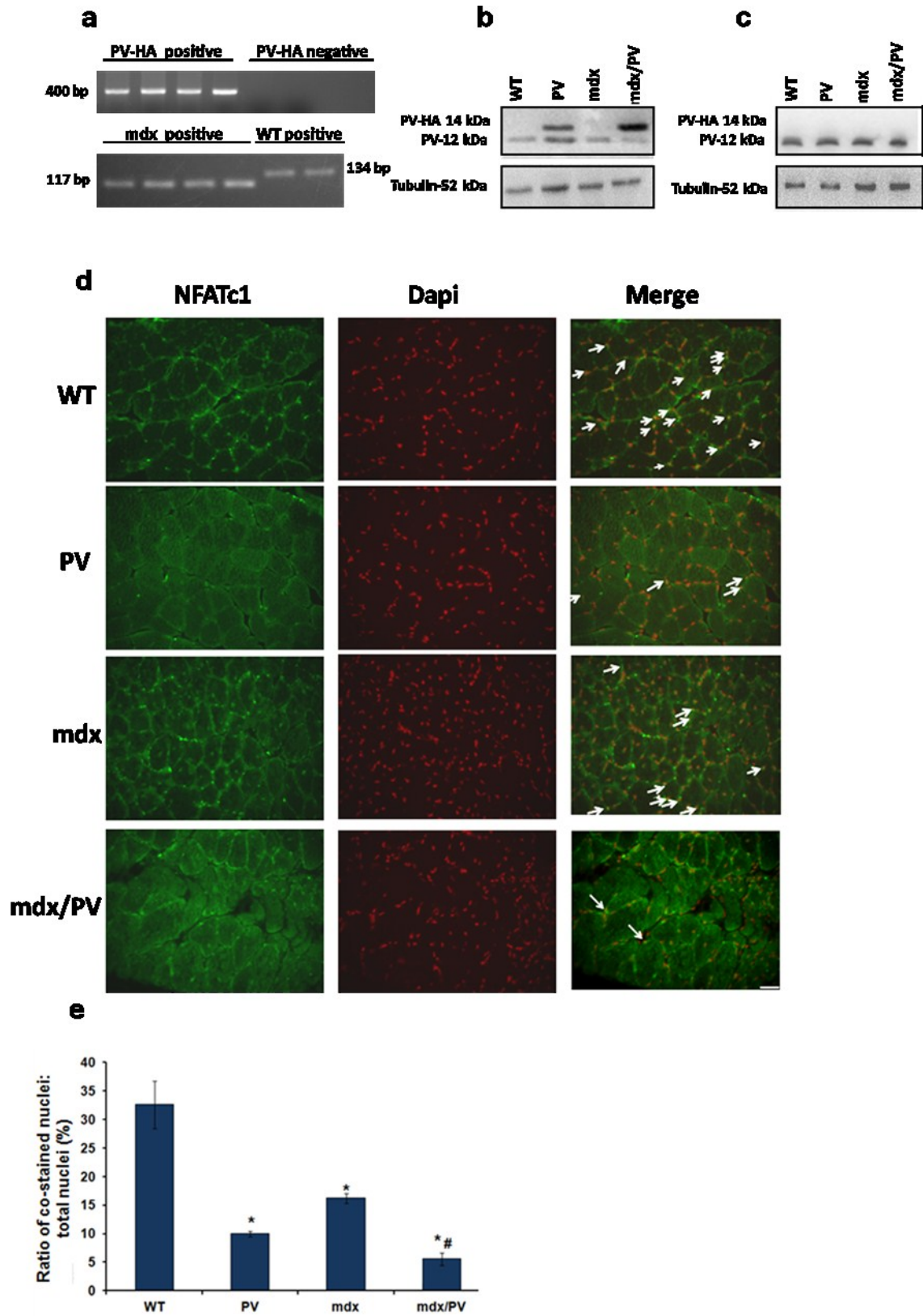
Figure 2.1: Forced expression of PV in *mdx* slow fibers decreases Cn signaling via NFATc1 nuclear localization

(**a**) Representative photomicrographs depicting DNA products of PV-HA and *mdx* genotyping, using a forward primer from the PV-cDNA and a reverse primer from the HA epitope tag, which was inserted at the 3' end of the cDNA to generate a 400 bp product representing the PV-HA cDNA. For *mdx*, the first five nucleotides of the common forward and the mutant reverse primers are not present in the *dystrophin* gene, whereas the first 23 nucleotides of the WT mutant primer were chosen arbitrarily to give a larger product (134 bp in WT *vs* 117 bp in *mdx*). (**b-c**) Representative immunoblots for PV-HA in soleus (**b**) and EDL (negative control) (**c**) muscles giving products of 12 kDa for the endogenous PV and 14 kDa for the PV-HA transgene. The 2 kDa difference is due to the HA epitope tag. (**d**) Representative photomicrographs for NFATc1 nuclear localization by IF. Arrows indicate nuclei positively stained for NFATc1. (**e**) Quantification reveals signficant reduction in PV, *mdx* and *mdx*/PV compared to WT (*) and in *mdx*/PV compared to *mdx* (#) (n=3; P<0.05). Scale bars, 20µm. Means ± SEM are shown.

We previously have assessed alterations in gene expression of fiber type-specific genes that may be downstream of a Ca^{2+}-regulated transcriptional pathway. These changes are accompanied by the overexpression of PV [214]. We also have shown that changes in mRNA levels for these proteins are related to alterations in Cn activity [214]. Furthermore, Cn signaling has been shown to be involved in controlling the slow oxidative myofiber program, as well as the transcriptional activity of slower isoforms of MyHC genes [89, 91, 238-241]. Therefore, we tested the mRNA levels of both *MyHC I* and *MyHC IIa*. Accordingly, *mdx* and *mdx*/PV soleus muscles did not show significant differences in the transcript levels of both isoforms (Figures 2.2a and 2.2b).

Further, immunohistochemical analyses showed no fiber-type switching between MyHC I and MyHC IIa in soleus muscles of *mdx*/PV compared to *mdx* mice (Figures 2.2c and 2.2d), suggesting that the changes in Cn downstream signaling accompanied by the expression of the PV transgene are not due to fiber type switching.
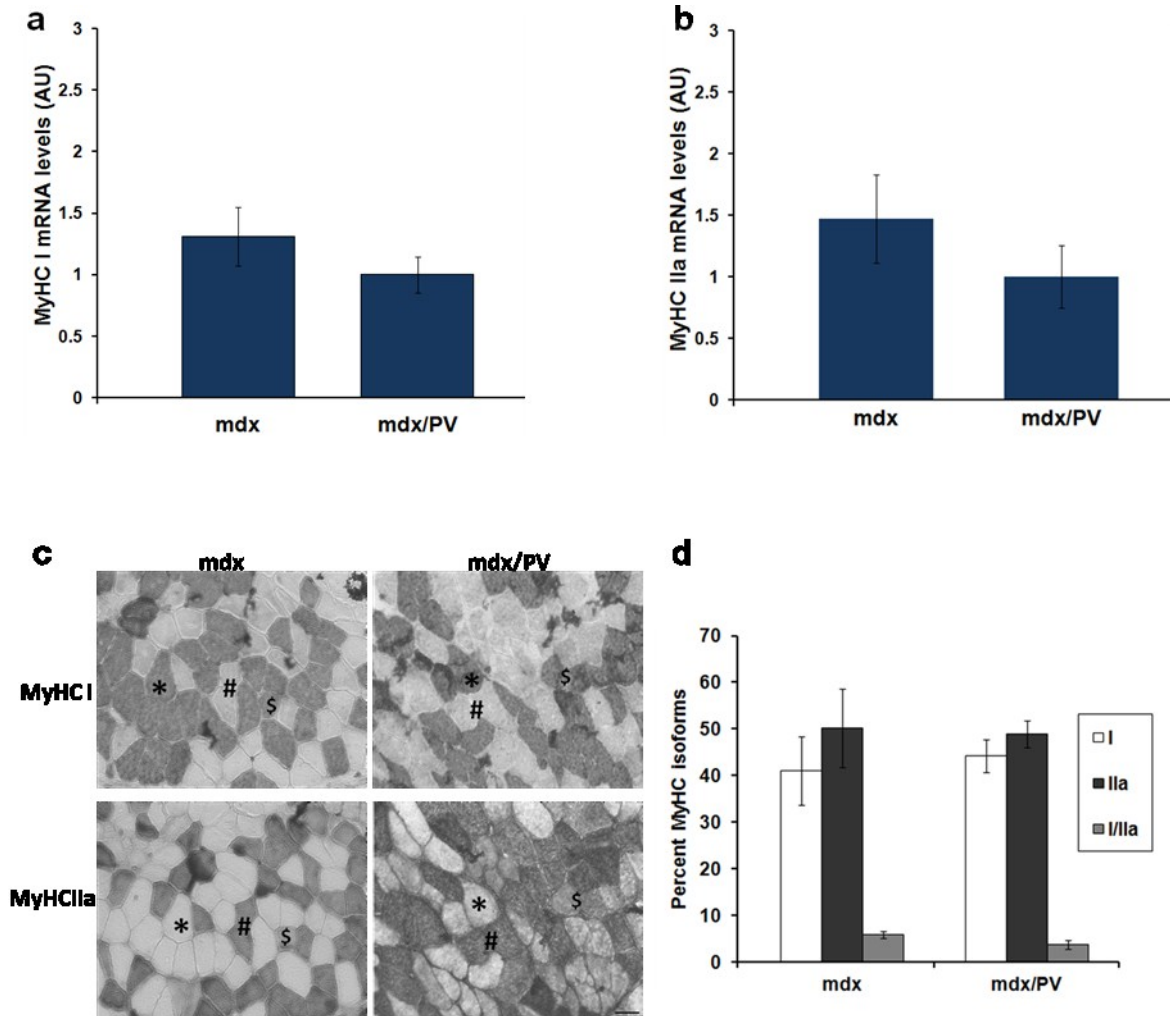
Figure 2.2: PV expression does not cause fiber type conversions in *mdx* soleus muscles

QPCR histograms of mRNA levels of *MyHC I* (**a**) and *MyHC IIa* (**b**) in soleus muscles of *mdx* and *mdx*/PV mice. Relative quantities are normalized to *36B4*, *beta* and *gamma actin* (n=4). AU represents Arbitrary Units. (**c**) Representative photomicrographs of cross sections from *mdx*, and *mdx*/PV soleus muscles processed to detect MyHC I and MyHC IIa. Fibers labeled with (*) and (#) express MyHC I and MyHC IIa respectively and the ones labeled ($) co-express both MyHC I and IIa in the different cross sections. Scale bars, 40μm (**d**) MyHC fiber type proportions in *mdx* soleus are not changed by the PV transgene (n=4). Means ± SEM are shown.

2.5.3 Utrophin and utrophin-A expressions are reduced in *mdx*/PV soleus muscles

Repeatedly, we have correlated changes in utrophin expression with changes in Cn activity [98, 106]. In the present study, we hypothesized that the impairment of Cn activity driven by PV overexpression would have affected utrophin and utrophin-A expression in slow muscle fibers. Indeed, qPCR analyses showed reduction in the mRNA levels of both *utrophin* and *utrophin-A* in PV compared to WT soleus muscles and in *mdx*/PV compared to *mdx* soleus muscles (Figures 2.3a and 2.3b). In these experiments, EDL was used as a negative control to show first, that expression of the transgene did not affect *utrophin* and *utrophin-A* expression in EDL *mdx*/PV muscle fibers and secondly, to show the significant differences in the expression of the latter genes between soleus and EDL muscle fibers from WT mice, confirming previous semi- quantitative RT-PCR data [242].

In agreement with the qPCR results, immunoblotting experiments showed a significant reduction of total utrophin protein levels in *mdx*/PV compared to *mdx* soleus muscles, while *mdx* muscles showed a significant increase compared to WT and PV soleus muscles (Figures 2.3c and 2.3d).

Utrophin expression in *mdx* mice is upregulated within extrajunctional regions of slow but not fast fibers, which plays a critical role in compensation for the loss of dystrophin. This compensation rescues slow but not fast fibers, which will eventually die [98]. Therefore, we next examined whether Cn pathway impairment compromised slow fibers due to reduced utrophin expression. IFs revealed reduced utrophin staining in both

MyHC I and IIa fibers of *mdx*/PV soleus muscles, suggesting that these fibers were not rescued from damage. However, there was positive utrophin staining in MyHC I fibers of *mdx* soleus muscles indicating that these fibers were rescued by utrophin and protected from damage (Figures 2.3e and 2.3f).

Thus, expression of the PV transgene in slow dystrophin-deficient muscle fibers resulted in impaired activity of downstream targets for CaM-based signaling, including NFATc1 as well as utrophin expression in slow myofibers.

e

	Utrophin	MyHC I	Merge
mdx			
mdx/PV			

f

	Utrophin	MyHC IIa	Merge
mdx			
mdx/PV			
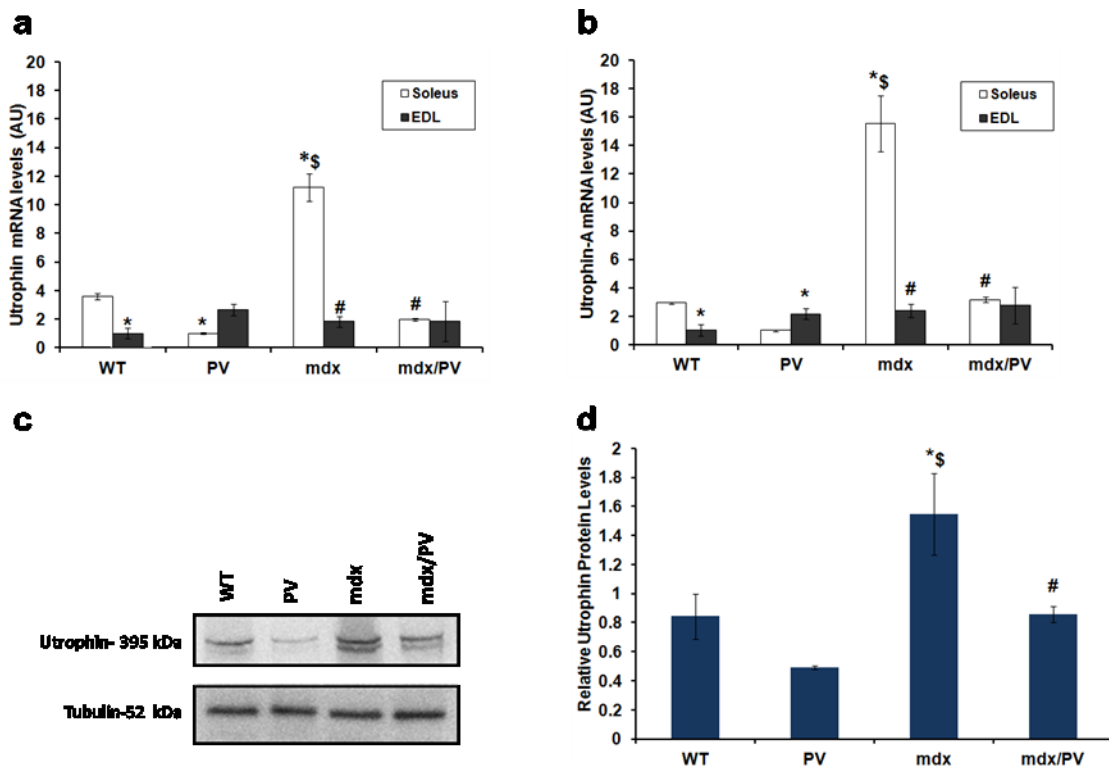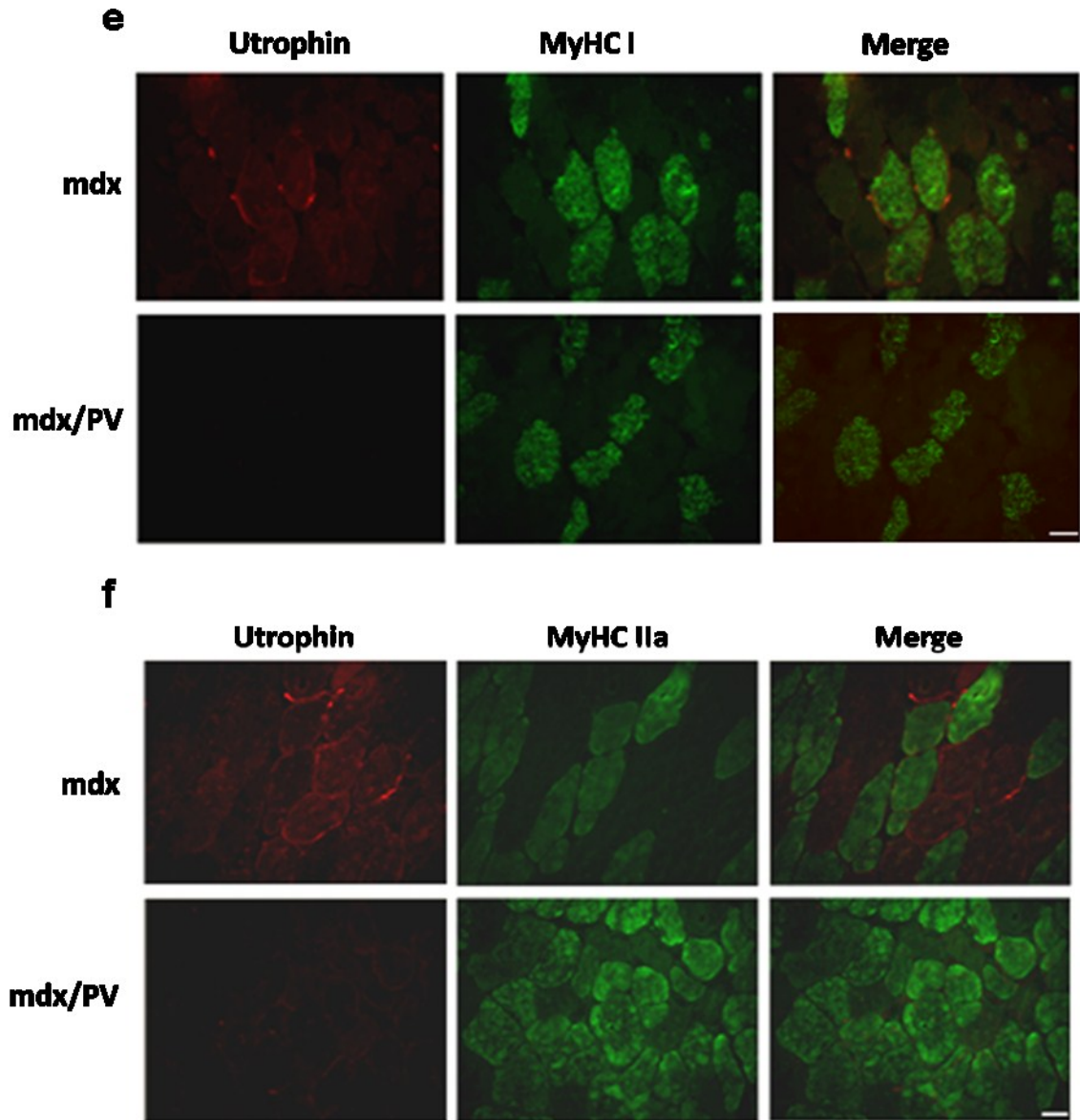
Figure 2.3: PV expression in WT and *mdx* soleus muscles leads to decreased utrophin expression

QPCR of mRNA levels of *utrophin* (**a**) and *utrophin-A* (**b**) in soleus and EDL tissues of WT, PV, *mdx* and *mdx*/PV mice. Relative quantities are normalized to *36B4, beta* and *gamma actin* (n=4 for soleus and n=3 for EDL). AU represents Arbitrary Units. (**c-d**) Representative immunoblot and quantification for total utrophin protein levels in the soleus muscle of WT, PV, *mdx* and *mdx*/PV mice. Relative quantities are normalized to α-tubulin (n=3; P<0.05). *compared to WT soleus; $compared to PV soleus, #compared to *mdx* soleus. Means ± SEM are shown. (**e-f**) IFs for utrophin co-staining with MyHC I (**e**) and MyHC IIa (**f**) in *mdx* and *mdx*/PV soleus muscles (n=3). Scale bars, 20μm.

2.5.4 Dystrophic slow fibers expressing PV exhibit more hallmarks of *mdx* cellular damage

Reduced utrophin expression in *mdx* mice has been correlated with augmented severity in dystrophic pathology [144, 146]. To determine whether impairment of Cn signaling and reduced utrophin expression have affected the pathological features in slow fibers of *mdx*/PV mice, we assessed several morphological indices in soleus muscles from *mdx*/PV mice.

H&E staining of muscle sections revealed an exacerbated appearance and extended infiltration in *mdx*/PV muscle fibers compared to *mdx* counterparts. The left column shows more central nucleation, whereas the right column shows more fibrosis and infiltrate in *mdx*/PV compared to *mdx* (Figure 2.4a). Quantification and measurement showed a ~ 20% increase in the percentage of fibers with central nucleation in *mdx*/PV compared to *mdx* soleus muscles (Figure 2.4b), indicating extensive cycles of regeneration and degeneration in those fibers. The latter suggests, once again, the role of the Cn pathway in the improvement and/or exacerbation of the dystrophic phenotype [98, 106]. Additionally, healthy skeletal muscle exhibits relatively uniform size in individual muscle fibers [234]. Among the several pathological parameters, dystrophic muscle fibers display more variations in fiber size than normal muscles [234]. Quantitative evaluation of fiber size variability determined by the averaged standard deviation of the cross sectional areas of soleus muscles, revealed higher variability in *mdx*/PV compared to *mdx* (Figure 2.4b). This exacerbation is in agreement with our previous findings that impairment of the Cn pathway has a critical role in the pathological features of *mdx* muscle fibers [98, 106].

To test for membrane integrity that might have been affected by reduced utrophin expression, we injected *mdx* and *mdx*/PV mice with the small dye Evans Blue (EB) and monitored, using fluorescence microscopy, the uptake of the dye in myofibers (Figure 2.4c). This dye is normally excluded from cytosolic regions of normal muscle fibers except if lesions take place in the sarcolemma [233]. Quantitative assessment of the average intensity of EB staining showed a significant increase in soleus muscles from *mdx*/PV compared to *mdx* mice (Figure 2.4d). These results add to the pathological features of *mdx*/PV soleus muscle fibers and suggest a correlation with reduced utrophin expression.

Fast fibers are more susceptible than their slower counterparts to damage stimulated by forced lengthening contractions [243, 244], whereas slow muscle fibers in *mdx* mice are rescued by upregulation of utrophin [220]. Therefore, we hypothesized that slow muscle fibers of *mdx*/PV would be more sensitive than *mdx* slow muscle fibers. This was tested by measuring the percentage of slow fibers with central nucleation in soleus tissues stained with MyHC I in both *mdx* and *mdx*/PV mice (Figure 2.4e). Quantification revealed more central nucleation in MyHC I positive fibers of *mdx*/PV compared to *mdx* MyHC I positive fibers (Figure 2.4f).
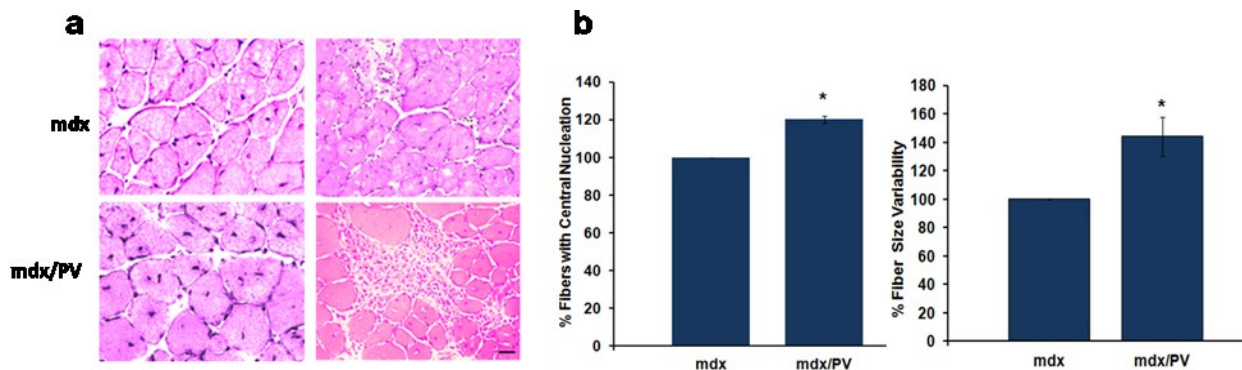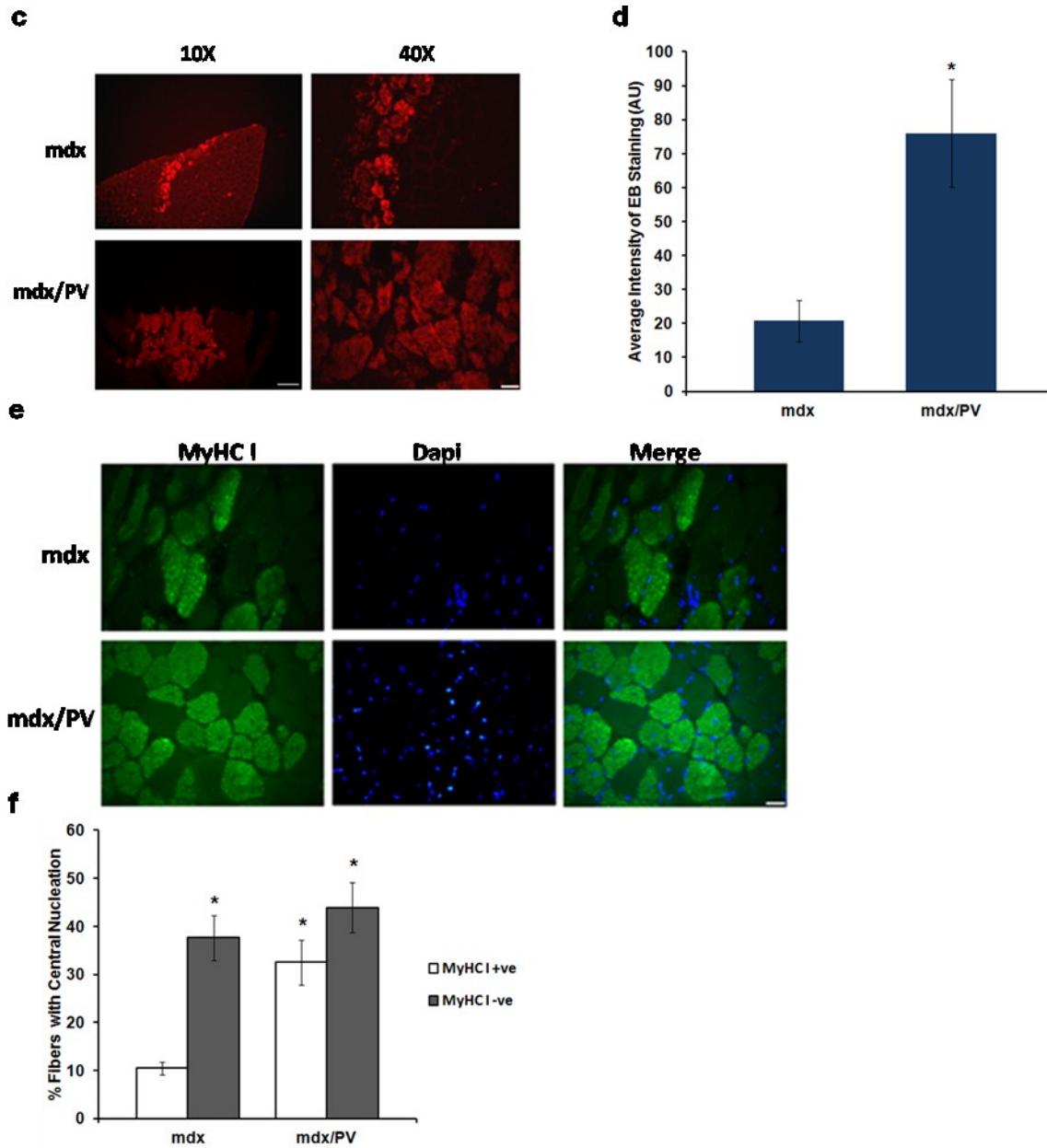
Figure 2.4: Dystrophic slow fibers expressing PV exhibit more hallmarks of *mdx* cellular damage

(**a**) Representative photomicrographs of cross sections from *mdx* and *mdx*/PV muscles processed for hematoxylin and eosin staining. Scale bars, 50μm. (**b**) Quantitative evaluation of central nucleation and size variability. Values are normalized to mdx and then multiplied by 100 (n=4; *p<0.05). (**c**) Cross sectional views of Evans blue dye-positive regions of soleus muscles from *mdx* and *mdx*/PV mice intraperitoneally injected (images taken at 10X; scale bars, 100μm and 40X; scale bars, 20μm). (**d**) Assesment of Evans blue dye staining in damaged regions of *mdx* and *mdx*/PV mice (n=3; *p<0.05). AU represents Arbitrary Units. (**e-f**) IFs for MyHC I showing

central nucleation in MyHC I +ve fibers of *mdx* and *mdx*/PV mice. Scale bars, 20μm. (n=4 for *mdx* and n=3 for *mdx*/PV; *P<0.05). Means ± SEM are shown.

2.5.5 HSP70 expression does not change in soleus msucle of *mdx*/PV with reduction in utrophin level

Early studies done on human DMD tissues have shown elevated levels of HSP70, suggesting an autoprotective role for this protein [226]. Moreover, it has been recently demonstrated that pharmacological induction of HSP70 preserves muscle strength and contractile function in *mdx* mice. Yet, this amelioration is not accompanied by a significant increase in utrophin transcript levels in both diaphragm and TA muscles [150]. Therefore, we sought to investigate if HSP70 expression was changed in *mdx*/PV soleus muscles with reduced utrophin levels. Using immunoblotting analysis, HSP70 protein levels did not change in soleus muscles between *mdx* and *mdx*/PV mice, suggesting that the expression of HSP70 and utrophin is not co-regulated (Figures 2.5a and 2.5b). In agreement, IFs on soleus muscles showed colocalization of HSP70 with MyHC I and utrophin positive fibers in *mdx* mice. HSP70 also was colocalized with MyHC I-positive fibers in *mdx*/PV soleus tissues. Nevertheless, both HSP70 and MyHC I positive fibers were not stained for utrophin. On the contrary, they showed more central nucleation when stained with Dapi (Figure 2.5c).

2.5.6 RyR1 is significantly increased, while SERCA1 & 2 protein levels are not changed by PV expression in *mdx* soleus muscles

RyR is an intracellular Ca^{2+} release channel located at the SR membrane [245]. This receptor is activated when muscle fibers are excited via motor nerves that generate

an action potential, thus leading to the release of Ca^{2+} from the SR [217]. In addition, PV facilitates Ca^{2+} translocation from the myofibril to the SR in fast muscle fibers, whereas SR-Ca^{2+}-ATPases (SERCA) enzymes regulate Ca^{2+} uptake into the SR [51]. Furthermore, the maximal activity of SERCA enzymes decreases with alterations in Ca^{2+} binding and ATP binding domains [151]. In addition, HSP70 binds SERCA and enhances its activity in cases of cellular stresses [151]. Thus, we next examined whether the expression of PV has affected RyR1 or SERCA1 or 2 expressions in *mdx* soleus muscles.

Being expressed predominantly in fast skeletal muscles, RyR1 transcript was significantly increased in PV soleus muscles compared to WT counterparts, suggesting a possible regulation of this protein with alterations in Ca^{2+} handling [214]. Our current findings, showed an increase in RyR1 protein level in PV compared to WT and in *mdx*/PV compared to *mdx* soleus muscles. However, SERCA1 (mostly expressed in fast fibers) and SERCA2 (mostly expressed in slow fibers) did not change between the corresponding groups (Figures 2.5d and 2.5e). Thus, higher levels of RyR1, without changes in SERCA isoforms suggest that the additional chelation of $[Ca^{2+}]_i$ by PV led to a faster profile and produced a reciprocal effect to Cn in slow *mdx* fibers.
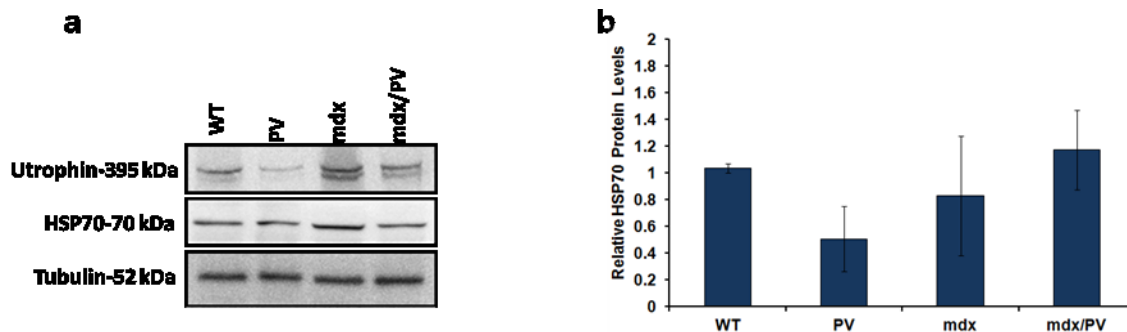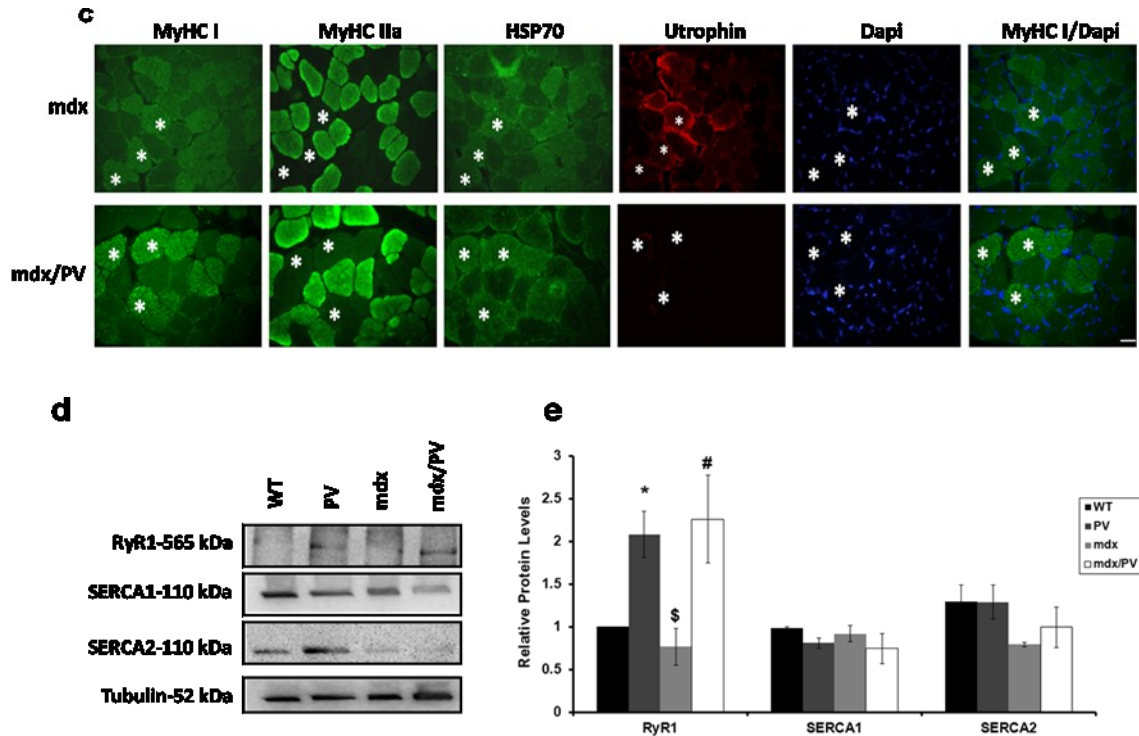
Figure 2.5: Decreased utrophin expression in *mdx*/PV slow fibers appears independent of HSP70 and SERCA1 and 2 expressions but associated with higher fast RyR1 protein levels

(a-b) Representative immunoblots and quantification of HSP70 protein levels in *mdx* and *mdx*/PV soleus muscles (n=3). (c) IFs showing HSP70, MyHC I, MyHC IIa and utrophin expression in *mdx* and *mdx*/PV soleus muscles. Asterisks indicate fibers stained for both MyHC I and HSP70 (n=3). Scale bars, 20μm. (d-e) Representative immunoblots and quantification of RyR1, SERCA1 and SERCA2 protein levels in *mdx* and *mdx*/PV soleus muscles. Relative quantities are normalized to α-tubulin (n=4; P<0.05). *compared to WT; $compared to PV, #compared to *mdx*. Means ± SEM are shown.

2.5.7 Transgenic models known to rescue [106, 193] or exacerbate [98] the dystrophic phenotype in *mdx* mice via utrophin regulation, display constant muscle HSP70 levels

We then wanted to investigate if HSP70 and utrophin proteins are regulated differently in other transgenic models. Thus, we studied HSP70 expression in *mdx* mice crossed with mice expressing an activated form of Cn (*mdx*/CnA*) where utrophin

expression is upregulated [106] and in *mdx* mice crossed with transgenic mice expressing

CaMBP (*mdx*/CaMBP) where utrophin expression is downregulated [98].
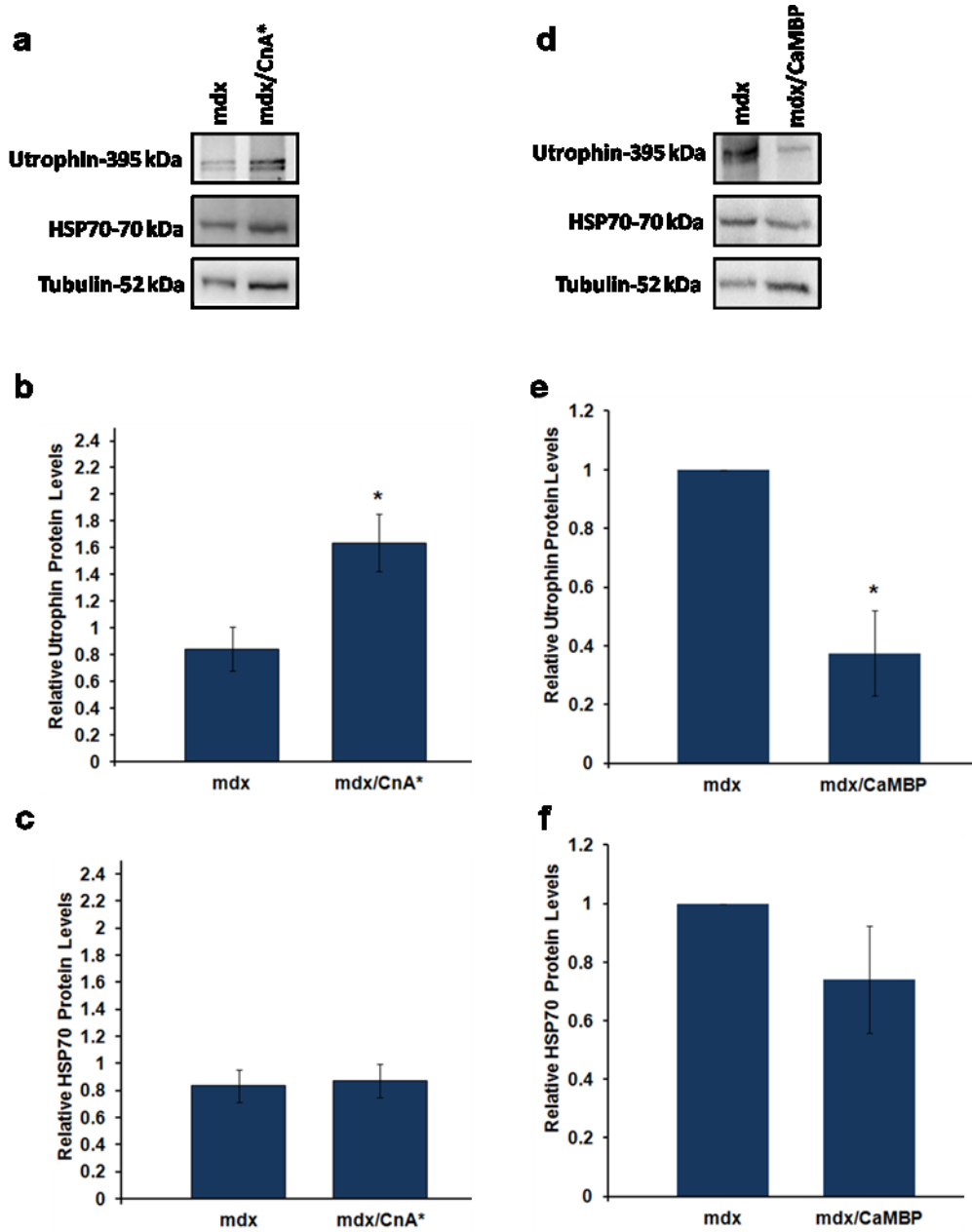
Figure 2.6: Transgenic models known to rescue [106, 193] or exacerbate[98] the dystrophic phenotype in muscles of *mdx* mice via utrophin regulation [93], display constant muscle HSP70 levels

(**a,d**) Representative immunoblots for utrophin and HSP70 proteins in the TA muscles of *mdx* and *mdx*/CnA* mice and in the soleus muscles of *mdx* and *mdx*/CaMBP mice. (**b,e**) Quantifications of utrophin protein levels. (**c,f**) Quantifications of HSP70 protein levels. Relative quantities are normalized to α-tubulin (n=3; $P<0.05$). *compared to *mdx*. Means ± SEM are shown.

Immunoblotting analysis suggests that activation of Cn signaling in TA muscles of *mdx*/CnA* leads to increased utrophin but not HSP70 expressions supporting our previous results [98] (Figures 2.6a, 2.6b and 2.6c). Similarly, attenuation of Cn signaling in soleus muscles of *mdx*/CaMBP leads to reduced utrophin but not HSP70 expression [98] (Figures 2.6d, 2.6e and 2.6f). These results suggest, once again, that HSP70 is not regulated with changes in Cn signaling.

To further support this observation, data from IFs in Lateral Gas (LG) tissues of both *mdx* and *mdx*/CnA* mice showed colocalization of HSP70 with MyHC I and MyHC IIa but not with MyHC IIb muscles confirming our previous data [227]. Those MyHC IIb fibers were shown to be rescued by increased utrophin expression and reduced central nucleation accompanied by the expression of the CnA* transgene. Additionally, utrophin positive fibers were not necessarily stained for HSP70 in *mdx*/CnA*, suggesting that HSP70 is not affected with the regulation of the slow myofiber gene program accompanied by manipulations in Cn activity (Figures 2.7a and 2.7b).
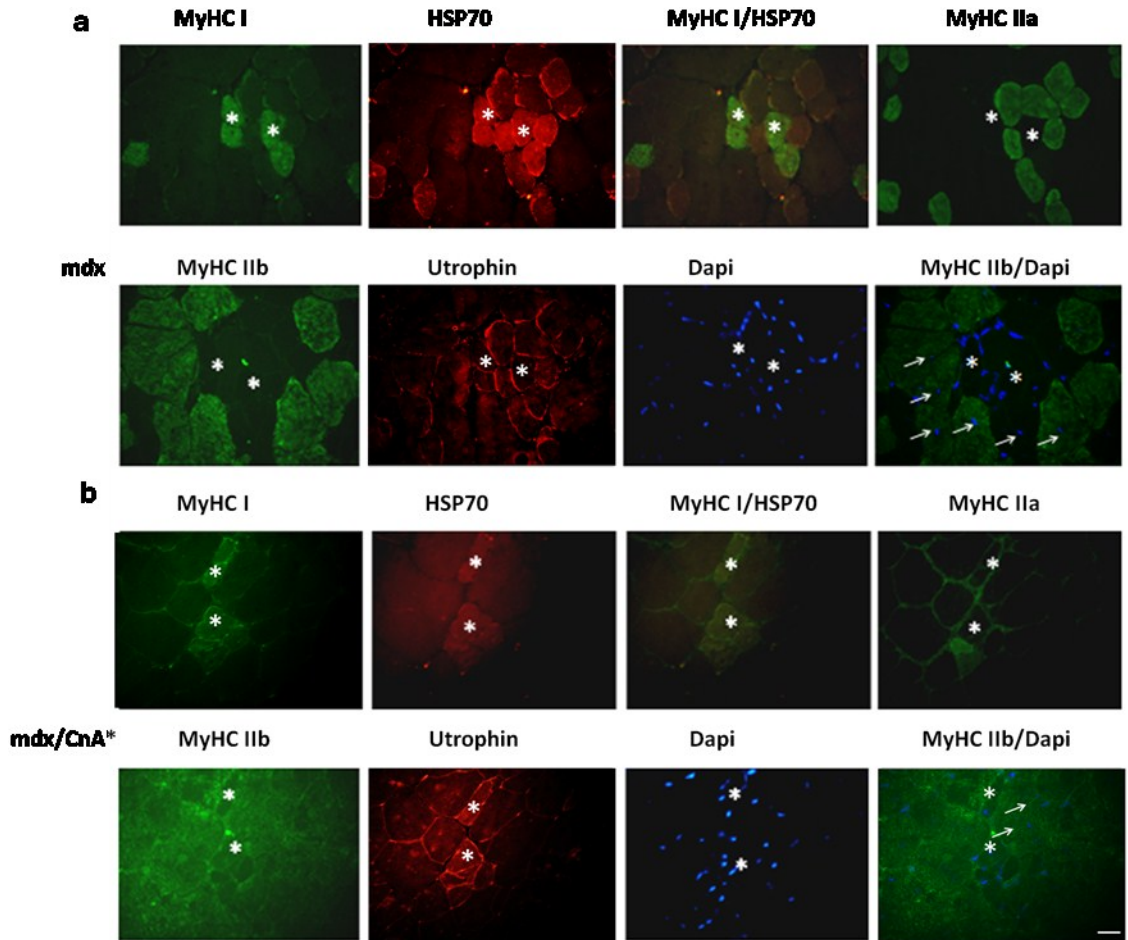
Figure 2.7: HSP70 expression does not change in Lateral Gas muscles between *mdx* and *mdx*/CnA* mice

IFs demonstrate colocalization of HSP70 with MyHC I and MyHC IIa but not MyHC IIb fibers in *mdx* (**a**) and *mdx*/CnA* (**b**) Lateral Gas muscles. Asterisks indicate fibers positively stained for MyHC I and HSP70. Arrows indicate central nucleation in MyHC IIb positive fibers (n=3). Scale bars, 20μm.

2.6 Discussion

Our lab previously has demonstrated the involvement of the Cn/NFAT signaling pathway in the regulation of utrophin-A expression in slow muscle fibers [98, 106]. Therefore, we and others illustrated the concept that strategies aimed at regulating the slower, high oxidative myofiber program in muscle could play a role in the treatment or exacerbation of DMD [98, 106, 224, 225]. In the current study, we attenuated Ca^{2+}/CaM-based signaling in dystrophin-deficient slow muscle fibers by crossbreeding *mdx* mice with transgenic mice expressing PV, which is normally expressed only in fast fibers [229]. This transgene is driven by the TnIs promoter and forced expressed in slow fibers, leading to attenuation of Cn activity [214]. Having done that, slow *mdx* fibers became more stressed and subject to deterioration. Unlike our previous approaches, the transgene in the present study causes alterations in $[Ca^{2+}]_i$ kinetics in slow fibers which would interfere with Cn/NFAT signaling [214]. Indeed, expression of PV in *mdx* slow muscle fibers inhibited the latter pathway via reducing utrophin expression, decreased NFATc1 nuclear localization and drastic increase in the hallmarks of *mdx* cellular damage.

Attenuation of the Cn/NFAT pathway has a well-known effect on the downstream targets of Cn [98]. Herein, we observed reduced percentage of nuclear NFATc1 in PV compared to its WT soleus muscles and in *mdx*/PV compared to *mdx* soleus muscles possibly due to reduced Cn activity (Figure 2.1). Surprisingly, *mdx* soleus muscle showed also reduced NFATc1 nuclear localization compared to WT counterparts despite the increase in the $[Ca^{2+}]_i$ levels in *mdx* mice. This increased $[Ca^{2+}]_i$ levels is due to that the total Ca^{2+} content in muscle biopsies from *mdx* mice is double that in muscle biopsies from WT mice, in addition to the increased $[Ca^{2+}]_i$ influx through the cellular membrane

[246, 247]. Such an increase in $[Ca^{2+}]_i$ should theoretically stimulate the Cn pathway and NFATc1 nuclear localization. However, altered $[Ca^{2+}]_i$ levels also can affect other transcriptional factors such as the Mitogen Activated Protein Kinase (MAPK) family that consists of Janus-N-Terminal Kinase (JNK), leading to their activation [248]. The increased JNK activity observed in dystrophic muscles might result in increased interactions with NFATc1, causing its transport out of the nucleus [106, 114]. Furthermore, the reduced NFATc1 nuclear localization in *mdx*/PV soleus muscles could be explained in part via activation of the MAPK-JNK pathway and also via Ca^{2+} buffering caused by expression of the PV transgene.

Our previous findings did not show changes in fiber type conversion due to overexpression of PV [214]. Neither did our current study comparing *mdx*/PV to *mdx* mice. In 2003, it was suggested that PV would buffer additional Ca^{2+} in non-stressed fibers. It is also possible that the amplitude and duration of the Ca^{2+} transients are altered by PV through an unknown mechanism. Yet, there might be an alteration in contractile and biochemical characteristics in soleus muscles without any fiber type conversion [214]. We did not observe changes in *MyHC I* or *IIa* transcripts in *mdx*/PV compared to *mdx* soleus muscles (Figure 2.2). These results together with our previous ones, suggest a selective role for Ca^{2+}-dependent transcriptional pathways in regulating muscle energetics but not all fiber type-related muscle characteristics [214]. It is also possible that complete transformation from slow to fast muscles, might require additional regulation of Ca^{2+} and perhaps other signaling pathways.

The involvement of Cn/NFAT signaling in regulating utrophin-A expression has previously been discussed [105, 249]. In addition to reduced NFATc1 nuclear

localization, the expression of PV in *mdx* slow muscles has caused reduction in utrophin and utrophin-A expression (Figure 2.3). The absence of a difference in utrophin expression between *mdx* and *mdx*/PV EDL muscle fibers, supports the fact that the transgene is solely expressed in slow muscle fibers. With respect to these findings, it is critical to mention that adult *mdx* fast muscles are more susceptible to the damage caused by forced lengthening contractions than are slow muscles [243]. Since this damage is rescued by upregulation of utrophin and due to that slow fibers are capable of expressing more utrophin, the latter fibers can overcome the pathological progression of the disease [105, 220, 242]. In the current study, IF co-staining of utrophin and MyHC I revealed positive utrophin staining in MyHC I fibers of *mdx* soleus muscle confirming the rescue provided by utrophin. However, and due to reduced utrophin staining in both MyHC I and IIa fibers of *mdx*/PV soleus muscles, this rescue was abolished in both slow and fast muscle fibers of dystrophic mice expressing the PV transgene (Figures 2.3e and 2.3f). Moreover, the increase in central nucleation and invasion of EBD staining in *mdx*/PV slow fibers compared to the rescued *mdx* counterparts support the fact that only fast fibers are sensitive to death in *mdx* mice and that the most exacerbated fibers were indeed those where the PV transgene was being expressed (Figure 2.4). Taken together, these results clearly show the detrimental effects of attenuating Cn activity in muscular dystrophy.

The pharmacological induction of HSP70, as well as its overexpression in *mdx*/*utrophin*-/- mice, have been shown recently to rescue the dystrophic phenotype [150]. Further, HSP70 can improve the function of SERCA enzymes in the removal of excess Ca^{2+} from the cytosol [150]. Nevertheless, our current results did not show significant changes in HSP70 and SERCA1 and 2 expressions between *mdx* and *mdx*/PV

slow fibers (Figure 2.5). In agreement, Gehrig *et al.,* [150] also showed no differences in SERCA1 and 2 protein levels between 10 week old WT and *mdx* mice. In the same context, Chin *et al.,* [214] showed no differences in the transcript level of SERCA2 between WT and PV soleus muscles. Moreover, our IFs showed colocalization of HSP70 with MyHC I positive fibers in both *mdx* and *mdx*/PV. Interestingly, utrophin negative fibers that were stained positive for HSP70 in *mdx*/PV soleus muscles, showed more central nucleation than utrophin and HSP70 positive fibers in *mdx* mice. These data indicate that utrophin but not HSP70 might have rescued those fibers. They further suggest that both HSP70 and SERCA proteins are not regulated via the Cn/NFAT pathway.

In addition to the PV model, other transgenic approaches in our study that manipulate the Cn/NFAT pathway showed that HSP70 expression was constant despite increased utrophin expression in *mdx*/CnA* mice and decreased utrophin levels in *mdx*/CaMBP mice (Figure 2.6). Accordingly, IFs revealed colocalization of HSP70 in MyHC I and IIa fibers and in utrophin positive fibers as well, but not in MyHC IIb fibers in *mdx* LG muscles. In *mdx*/CnA* mice, MyHC IIb fibers were rescued by increased expression of utrophin and decreased central nucleation compared to *mdx*. However, those rescued fibers were not positive for HSP70, suggesting once again, that HSP70 is not regulated via the Cn/NFAT pathway (Figure 2.7). In this context, HSP70 has been shown to prevent disuse muscle fiber atrophy via inhibition of Foxo3a, which in turn prevents the increase of atrogin-1 and Murf1 promoter activities [152]. In this case, rescuing muscular dystrophy by HSP70 might be correlated to the prevention of muscle atrophy via the Akt-growth pathway. HSP70 also inhibits Nuclear Factor-$_K$B (NF-$_K$B)

activity during muscle disuse but without affecting atrogin-1 and Murf1 promoter activities [152]. It also has been shown that the pharmacological blockade or genetic manipulations of the NF-$_K$B pathway reduces inflammation and ameliorates muscular dystrophy [250, 251]. Therefore, another possibility for the regulation of HSP70 might be via the NF-$_K$B pathway, which needs further investigation.

Simultaneously, RyR1, a marker of increased SR [Ca^{2+}]$_i$ release, was significantly increased in PV compared to WT and in *mdx*/PV compared to *mdx* mice (Figure 2.5). Interestingly, Chin *et al.,* [214] showed a significant increase in *RyR1* transcript level in PV compared to WT soleus muscle. In our study, RyR1 expression did not change between WT and *mdx* soleus muscles. In agreement, no difference in RyR1 expression was shown between WT and *mdx* mice [252], suggesting that changes in Ca^{2+} homeostasis in *mdx* mice might not be due to changes in RyR1 expression but to other signaling molecules. In addition, the changes in RyR1, but not SERCA isoforms, suggest that the additional chelation of [Ca^{2+}]$_i$ by PV led to a faster profile and produced a reciprocal effect to Cn in *mdx* slow fibers. The increase in RyR1 expression in PV and *mdx*/PV mice also suggests an activation of the Ca^{2+}-sensitive RyR to uptake more Ca^{2+} from the SR to the cytoplasm.

Collectively, our data from the current study would be of great influence in studying the regulation of the Cn/NFAT pathway, promoting the slower, more oxidative myofiber gene program and eventually in the treatment of DMD. Further, this study increases the chances of understanding the physiological and pathological features of the disease. It also raises the possibility that HSP70 acts upon different mechanisms in the rescue of muscular dystrophy.

Chapter 3 : **Direct calcineurin modulators regulate Calcineurin/NFAT signaling in *mdx* crossbreeds**

Manal Al Zein and Robin N. Michel

Department of Exercise Science, Concordia University, Montreal, QC, Canada

3.1 Background

In Chapter 3, we seek to understand the regulation of direct Calcineurin (Cn) modulators in different transgenic models in an *mdx* background. The transgenic models either stimulate or inhibit Cn activity and utrophin expression. The Cn modulators have a major feedback mechanism, which is essential for regulating Cn activity. Therefore, they may be of great value in the treatment of Duchenne Muscular Dystrophy (DMD) disease. Our preliminary results illustrate changes in the expression of these proteins suggesting a critical role in *mdx* mice, which will need further investigation.

The results of this chapter, once completed, could be submitted for publication to a scientific journal that publishes topics in chemistry, biology and/or genetics. Our work provides new insights into the regulation of Cn in *mdx* mice and unveils some facts about Cn modulators, which could be essential for future research. All these collectively, increase the chances for finding good therapeutic targets for muscle dystrophy.

3.2 Abstract

We have previously shown that dystrophic symptoms are ameliorated by stimulation of the Calcineurin/Nuclear Factor of Activated T cells (Cn/NFAT) pathway and an increase in utrophin-A expression. Further, we have shown exacerbation of the dystrophic phenotype upon impairment of Cn signaling and reduction in utrophin-A levels (Chakkalakal *et al.,* 2004, 2006). Additionally, alterations in $[Ca^{2+}]_i$ kinetics by forced expression of the fast protein Parvalbumin (PV) in slow fibers of crossbred *mdx* mice also exacerbates the dystrophic phenotype (Chapter 2). The direct Cn modulators were first identified in various types of cardiac diseases, where the majority provide cardio-protective effect. However, little is known about the role of these molecules in Duchenne Muscular Dystrophy (DMD). Therefore, we set out to determine the role of various Cn modulators in *mdx* mice, an animal model of DMD, particularly with respect to changes in the Cn/NFAT signaling pathway. Herein, we hypothesize that the expression of the Cn modulators is modified upon changing Cn activity and that the inhibition of these inhibitors, may be of therapeutic value since inhibiting the inhibitors will maintain effective Cn levels. Using qPCR and immunoblotting analyses, our results showed an upregulation in the mRNA level of *RCAN1.4*, whereas RCAN1, calsarcin-1 and MLP protein levels did not change between *mdx* and *mdx* crossed with PV (*mdx*/PV) soleus muscles. On the contrary, the expression levels of RCAN1 did not change in *mdx* crossed with mice over expressing CnA (*mdx*/CnA*). However, calsarcin-2 protein level was significantly lower in *mdx*/CnA* compared to CnA* mice. These preliminary results confirm the dual regulation of RCAN and open discussions on the regulation and the roles of these proteins in muscle dystrophy.

3.3 Introduction

Duchenne Muscular Dystrophy (DMD) is a disease characterized by muscle wasting and early death and caused by the loss of the cytoskeletal protein dystrophin [94, 95]. Although there has been limited success in the use of pharmacological drugs to treat DMD patients [193], stimulating the Cn pathway has shown positive effects in increasing the expression of the dystrophin-homologue protein utrophin-A [106, 224]. Utrophin-A relocalizes at the muscle sarcolemma in slow but not fast *mdx* muscle fibers, to compensate for the loss of dystrophin [98]. Such compensation rescues slow fibers, but leads to eventual death of their fast counterparts [98]. Therefore, targeting Calcineurin/Nuclear Factor of Activated T cells (Cn/NFAT) signaling may be a useful approach when considering an effective treatment for DMD [98, 106]. One of the possible concepts in targeting the Cn pathway involves regulation of a group of modulators, which directly regulate Cn activity. Being linked to cardiac hypertrophy, the direct Cn modulators have initially been identified to regulate diseases linked to Cn [4, 184, 185]. They are well-characterized in heart diseases such as cardiac myopathy and heart hypertrophy [4, 184, 185]. In this context, overexpression of most of these regulators has been shown to provide cardio-protective effects [4, 185]. However, little is known about the role of these Cn regulators in the progression of neuromuscular diseases such as DMD. Such information may be useful in planning strategies for ameliorating the effects of the disease.

The Cn modulators are introduced as a replacement for the non specific pharmacological drugs that inhibit Cn but cause severe side effects [213]. Drugs such as Cyclosporin A (CsA) and FK506 inhibit the phosphatase activity of Cn in a unique

manner [253]. Cn dephosphorylates NFAT at its N-terminal regulatory domain [82]. There are multiple domains in NFAT, called "anchors", which are used for interaction with different sites on the phosphatase Cn. One important anchoring sequence lying in the N-terminal region of NFAT contains the consensus site "PXIXIT", in which X represents any amino acid. This sequence is sufficient for Cn-substrate docking [254]. While CsA binds to the cytosolic receptor protein cyclophilin, FK506 binds to FK506-Binding Protein (FKBP) [255, 256]. Thus, the immunophilins cyclophilin and FKBP might either have a direct interaction with Cn or just serve in an allosteric manner to fix the drugs in a certain conformation that interact with Cn. Therefore, both drugs and immunophilins are necessary for significant inhibition of Cn [213]. However, these drugs are not specific for the immune system since they cause neurotoxicity and nephrotoxicity side effects [257]. Hence, the PXIXIT sequence required for any substrate to interact with Cn, has been utilized in the development of NFAT-specific inhibitors of Cn, which are direct Cn modulators or inhibitors. These modulators affect NFAT dephosphorylation solely without causing any side effects such as neurotoxicity or nephrotoxicity, as these novel inhibitors do not affect dephosphorylation of other substrates [213].

The direct Cn inhibitors are classified into three major groups based on the way they affect Cn: inhibitors of Cn, dual regulators and Anchoring proteins. Inhibitors of Cn bind to and inhibit Cn activity, such as Calcineurin Inhibitor (CAIN/Cabin1). Dual regulators have both inhibitory and stimulatory effects, driven by a feedback mechanism such as Regulator of Calcineurin (RCAN) or called Modulatory Calcineurin-Interacting Protein (MCIP). Anchoring proteins tether Cn to other signaling proteins such as the Z-line family of proteins "Calsarcins" (reviewed in [192]).

CAIN/Cabin1 is a phospho-protein, discovered in a mouse T-cell cDNA library. It is highly expressed in the brain, and accumulates in the cytoplasm and the nucleus [182]. CAIN may serve in a negative regulatory loop. Thus, upon activation of Protein Kinase C (PKC), CAIN becomes hyperphosphorylated, which increases its affinity to Cn (reviewed in [192]).

The RCAN family is the only known family of Cn inhibitors that is conserved from yeast to humans. RCAN is known by its dual regulation of Cn, acting as an activator at low concentration and an inhibitor at high concentration [204, 258, 259]. Two splice variants of RCAN are identified: RCAN1.1 and RCAN1.4 [207]. Like CAIN, RCAN also serves as a feedback inhibitor of Cn. Upon activation of Cn signaling, the dephosphorylated NFAT binds to the putative NFAT binding site in RCAN1.4 promoter region and stimulates its expression. RCAN1.4 protein then binds and inactivates Cn [207, 258].

Anchoring proteins include Muscle LIM Protein (MLP), calsarcin-1, which is expressed specifically in adult cardiac and slow-twitch skeletal muscles and calsarcin-2, which is expressed in fast-twitch skeletal muscles. These proteins also function as Cn modulators [194]. Calsarcins link Cn to α-actinin at the Z-line of cardiac and skeletal muscle, whereas MLP is tethered to calsarcin-1 and colocalizes with Cn at the Z-disc. Accordingly, both calsarcins and MLP inhibit Cn activity [184, 197].

We set out to learn more about the Cn pathway by monitoring changes in the expression of Cn modulators in various mutant conditions. Thus, we decided to examine the expression of RCAN, calsarcins and MLP in different transgenic models in an *mdx* background. In a previous study, we showed that crossbreeding *mdx* mice with transgenic

mice expressing an activated form of Cn (CnA*) upregulates utrophin-A and improved the pathological symptoms of DMD [106]. In addition, crossbreeding *mdx* mice with transgenic mice expressing a small peptide inhibitor called Calmodulin-Binding Protein (CaMBP) leads to a reduction in the levels of utrophin-A and the transcript of slow myosin heavy chain I (MyHC I) [98]. Recently, we showed that alterations in $[Ca^{2+}]_i$ kinetics by forced expression of the fast protein Parvalbumin (PV) in slow fibers of crossbred *mdx* mice, interfered with Cn/NFAT signaling via reduction in utrophin expression and exacerbation of the dystrophic phenotype (Chapter 2). Herein, we hypothesize that the expression of the Cn modulators would be modified in *mdx* mice expressing either the CnA* transgene (which stimulates Cn activity) or the PV transgene (which attenuates Cn activity). Understanding how these proteins are regulated may eventually help in maintaining Cn in an activated state.

Using quantitative real time PCR (qPCR) and immunoblotting analyses, our results showed an upregulation in the mRNA levels but no change in protein levels of RCAN1 in the soleus muscles of *mdx*/PV compared to *mdx* mice. Further, we showed *calsarcin-1* mRNA levels to be increased in *mdx*/PV compared to Wild-Type (WT) mice, with no difference between *mdx* and *mdx*/PV mice at the transcript or protein level. In contrast, we saw no changes in the expression levels of RCAN1 in the Extensor Digitorum Longus (EDL) muscles of *mdx*/CnA* mice compared to *mdx* mice but a downregulation of *calsarcin-2* mRNA level in EDL tissue of *mdx*/CnA* mice compared to those of CnA* mice. MLP protein level also showed a significant decrease in *mdx*/CnA* mice compared to WT mice.

These preliminary results confirm the dual regulation of RCAN and raise questions about the role of these proteins in DMD. Further, understanding the different effectors that control various Cn regulators will possibly assist in controlling those inhibitors, to maintain Cn activity and high levels of utrophin-A in *mdx* mice.

3.4 Methods

3.4.1 Animals

Animal care and experimental procedures were performed in accordance to the guidelines of the Canadian Council of Animal Care. Transgenic mice expressing either PV or CnA* proteins were generated [163, 214]. Female *mdx* mice were crossed with male PV or CnA* transgenic mice, resulting in pups having the dystrophic pathology. Male pups were selected for the experiments and the presence of the transgene in PV and *mdx*/PV mice was identified by PCR screening of genomic DNA extracted from tails using primers encoding PV-TnIs (Sigma Genosys). WT, PV, CnA*, *mdx*, *mdx*/PV and *mdx*/CnA* of 10-12 week old were utilized for all subsequent analyses. Details about mice genotyping techniques and the primers used are explained in Chapter 2 of this thesis.

3.4.2 Muscle extraction and preservation

Mice were anesthetized by a mixture of 100 mg/ml ketamine hydrochloride (Bimeda-MTC Animal Health Inc.) and 20 mg/ml xylazine (Bayer HealthCare) in a volume ratio of 1.6:1. A dosage of 0.04 ml/30 g of body weight was administered intramuscularly to each mouse. Muscles were extracted and frozen directly in liquid

nitrogen for biochemical use. Samples were stored at -86ºC until used. Animals were euthanized after extraction using CO_2 gas.

3.4.3 RNA extraction and quantitative real time PCR (qPCR)

Soleus and EDL skeletal muscles were homogenized in a solution made up of 4 M guanidinium thiocyanate (Sigma Aldrich), 25 mM sodium citrate, 0.5% (v/v) N-laurylsarcosine (Sigma Aldrich) and 0.1 M 2-mercaptoethanol (Bioshop), followed by addition of 0.2 M sodium acetate (pH 4.0) with vortexing, phenol (Sigma Aldrich) and chloroform:isoamyl alcohol with vortexing until the appearance of a white emulsion. Samples were cooled on ice for fifteen minutes, and then centrifuged at 10,000 x g for ten minutes at 4ºC. Afterwards, two volumes of 99% ethanol were added to the aqueous layer with vortexing and centrifugation again at 10,000 x g for ten minutes at 4ºC. The ethanol was decanted and the RNA was suspended in 200 μl of 70% ethanol and centrifuged at 10,000 x g for ten minutes at 4ºC. The ethanol again was decanted and the RNA pellet was left to dry and re-suspended in 15 μl of RNAse free H_2O (Bioshop) per 10 mg of tissue with subsequent vortexing and heating at 70ºC for 3 minutes. To test RNA integrity, the RNA concentration was determined using an Eppendorf Biophotometer (Eppendorf) at 260nm. Subsequently, 2 μg of RNA was mixed with a 2:1 formamide:ethidium bromide, formaldehyde (Sigma Aldrich), 10X MOPS (pH 7.0) and bromophenol blue, heated at 65ºC for ten minutes and loaded on a 1.5% agarose gel containing 1X MOPS and formaldehyde. The three rRNA bands: 5S, 18S and 28S were visualized to indicate RNA integrity.

The changes in abundance of *RCAN1.4*, *calsarcin-1*, *calsarcin-2* and *MLP* were assessed using real time PCR. Briefly, 2 µg of freshly extracted RNA was reverse transcribed to cDNA using iScript reverse transcription supermix (Bio-Rad) and qPCR was performed, using gene specific primers together with appropriate reference genes for quantification (CFX96 Real-Time System, Bio-Rad). Relative quantities were then normalized by the Real-time System software to the average relative quantities of *36B4*, *beta actin*, *gamma actin* and/or *28S* rRNA housekeeping genes. All primer sequences are listed in Table 3.1.

Table 3.1: Primers for quantitative real-time PCR

Gene	Forward Primer	Reverse Primer	Product Size(bp)
RCAN1.4	5'-aaggaacctccagcttgggct-3'	5'-ccctggtctcactttcgctg-3'	160
Calsarcin-1	5'-gccaaaggggtgggtatct-3'	5'-tgccctaagcagaccaacag-3'	156
Calsarcin-2	5'-accgaggctccaagatgttc-3'	5'-cagagccctgctgatgacg -3'	243
MLP	5 '-gtcttcaccatgccaaac-3'	5'-agctttcctgcaggccatgc-3'	138
28S	5'-ttgttgccatggtaatcctgctcagta-3'	5'-tctgacttagaggcgttcagtcataatc-3'	132
36B4	5'-gctccaagcagatgcagca-3'	5'-ccggatgtgaggcagcag-3'	143
β- actin	5'-ccagccatgtacgtagccatccag -3'	5'-cacgcacgatttccctctcagctgt-3'	244
γ- actin	5'-acccaggcattgctgacaggatgc-3'	5'-ccatctagaagcatttgcggtggacg-3'	216

3.4.4 Protein extraction and Immunoblotting

The expression levels of RCAN1, calsarcin-1, calsarcin-2 and MLP were measured by immunoblotting using extracts from soleus tissues of WT, PV, *mdx* and *mdx*/PV mice and EDL or Tibialis Anterior (TA) tissues of WT, CnA*, *mdx* and

mdx/CnA* mice. Relative protein levels were measured using commercially available primary antibodies and secondary antibodies coupled to horse radish peroxidase (HRP). Briefly, whole tissues were homogenized in 1X RIPA buffer solution (6 µl/mg tissue) consisting of 1X PBS, 1% Igepal, 0.5% Sodium Deoxycholate, 0.1% Sodium Dodecyl Sulfate (SDS), 0.001 M Sodium Orthovanadate, 0.01 M Sodium Fluoride, 0.01 mg/ml Aprotinin, 0.01 mg/ml Leupeptin and 1 mM Phenylmethanesulfonyl fluoride (PMSF). Homogenates were centrifuged at 15,000 x g for twenty minutes and the supernatant layers were collected and re-centrifuged.

Protein concentrations were measured using Quick Start Bradford dye reagent (Bio-Rad), followed by loading 40 µg of proteins with electrophoresis on 10% SDS-PAGE at 120V and transfer at 30V for 90 minutes, using Borax (Bioshop), to a Polyvinyl difluoride (PVDF) membrane (Millipore) followed by blocking in 5% non-fat milk in 0.1% Tween/Tris Buffered Saline (T/TBS) for one hour. Primary antibodies were incubated with the blot on a shaker at 4ºC overnight. The following primary antibodies and concentrations were used; RCAN1 (NBP1-46853, Novus Biologicals; 1:500), calsarcin-1 (rabbit polyclonal antibody; a gift from Drs. Norbert Frey and Derk Frank; 1:2000), calsarcin-2 (13160-1-AP, Cedarlane; 1:1000) and MLP (10721-1-AP, Cedarlane; 1:1000). Membranes were washed with 0.1% T/TBS and incubated with secondary antibodies (Sigma Aldrich and Cell Signaling; 1:2000), coupled to HRP on a shaker at room temperature for one hour, followed by washing and developing with enhanced chemi-luminescence reagents (Millipore), using the Alpha Innotec FluorChem system (Cell Biosciences). Bands were then quantified and their intensities were

measured using the Alpha Innotec FluorChem software. Alpha tubulin (2125, Cell Signaling) was used as a loading control and groups were normalized to WT.

3.4.5 Statistical analyses

Statistical analyses were performed using the SPSS software program version 17.0. (IBM SPSS, Chicago, IL, USA). Results were expressed as means ± SEM. Statistical differences between individual groups (P<0.05) were analyzed using One Way Analysis of Variance (Anova) to test for differences among four groups of different phenotypes. Kruskal Wallis non-parametric test was used for the statistical analysis of the mRNA levels of RCAN in EDL samples of the PV models. Analyses for Chapter 3 are fully explained in Appendix II.

3.5 Results

3.5.1 RCAN1.4 and calsarcin-1 transcript levels are increased while MLP does not change in soleus muscle of *mdx*/PV

The expression of the direct Cn modulators including RCAN1, calsarcins and MLP was assessed by generating *mdx* mice expressing a PV or an activated form of Cn (CnA*) transgene. PV is normally expressed only in fast fibers [229], but was driven by the fiber-specific TnIs promoter to express the transgene in slow fibers [214]. CnA* is a transgene driven by the fast muscle creatine kinase promoter [260].

Concurrent with the reduction in Cn activity and accompanied by the expression of PV [214], we showed previously a reduction in the expression of the NFAT down stream target, utrophin (Chapter 2). Being another NFAT target [207], RCAN was

hypothesized to be reduced with a reduction in Cn activity, but since RCAN1 also functions in a negative feedback loop to inhibit Cn activity [201, 202], we expected to see different results in its expression. Additionally, calsarcin-1 tethers Cn to α-actinin at the Z- line of cardiac and skeletal muscle cells, and inhibits Cn activity [184]. MLP as well, colocalizes with Cn at the sarcomeric Z-disc and probably affects Cn activity [197]. Besides Z-disc, MLP also is found in the cytoplasm and the nucleus [199, 200]. Moreover, multiple proteins might interact with MLP and influence its expression. Yet, it is still unclear if calsarcin and MLP work through a negative feedback loop as RCAN does.

To assess whether downregulation of the Cn signaling pathway, caused by overexpression of PV, affected Cn modulators expression, we sought to determine the transcript levels of *RCAN1.4*, *calsarcin-1* and *MLP* in soleus muscles. Our qPCR results showed constant *RCAN1.4* mRNA levels among WT, PV and *mdx* mice, but a significant increase in *mdx*/PV mice compared to the other three groups (Figure 3.1a), suggesting a possible feed back regulation of RCAN or interference with other transcription factors. Similarly, *calsarcin-1* mRNA levels did not change within the soleus muscles of WT, PV and *mdx* mice but instead there was a significant increase in the *mdx*/PV mice compared to WT mice. A slight but insignificant increase in *calsarcin-1* mRNA levels in the *mdx*/PV mice compared to the *mdx* mice also was seen (Figure 3.1b). In addition, *MLP* expression was constant in the groups tested (Figure 3.1c). In these experiments, the fast muscle, EDL, was used as a negative control since the PV transgene is solely expressed in slow muscle fibers [214], and thus should not affect the expression of the Cn modulators in EDL muscles.
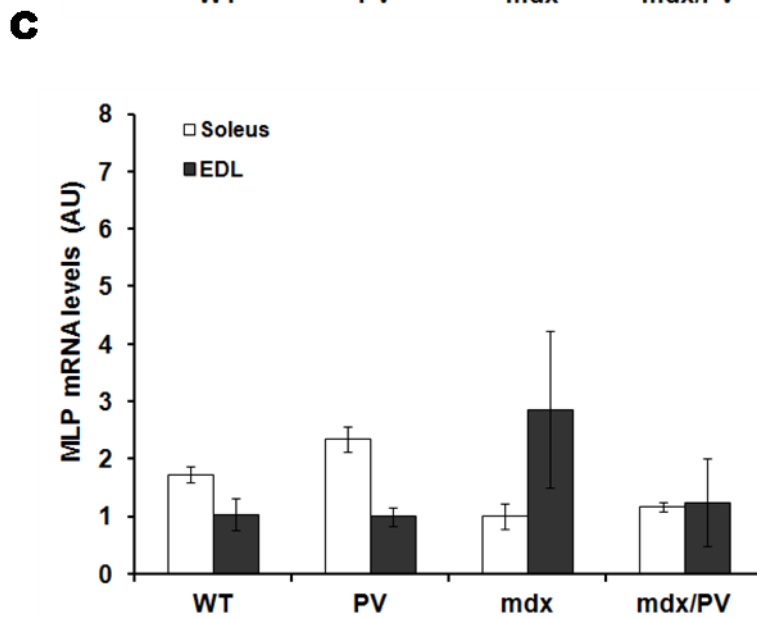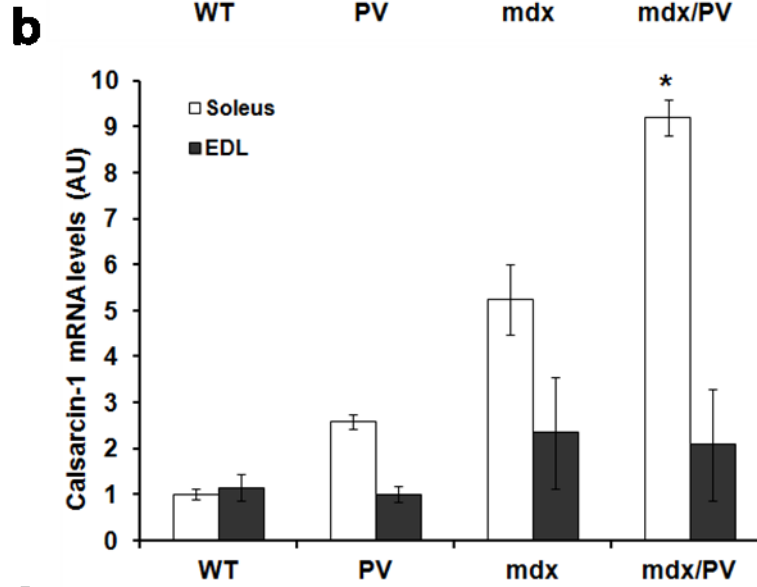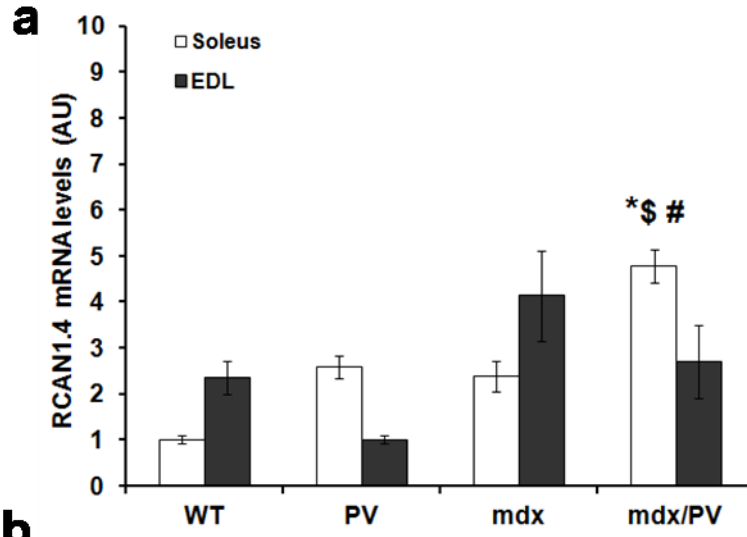
Figure 3.1: *RCAN1.4* **and** *calsarcin-1* **mRNA levels are increased in** *mdx***/PV while MLP level does not change in soleus slow muscles**

(**a**) QPCR histograms showing mRNA levels of *RCAN1.4* in soleus muscles of WT, PV, *mdx* and *mdx*/PV mice. (**b**) QPCR histograms showing mRNA levels of *calsarcin-1* in soleus muscles of WT, PV, *mdx* and *mdx*/PV mice. (**c**) QPCR histograms showing mRNA levels of *MLP* in soleus muscles of WT, PV, *mdx* and *mdx*/PV mice. Note that EDL is used as a negative control in these experiments. Relative quantities are normalized to *36B4*, *beta* and *gamma actin* (n=4 for soleus and n=3 for EDL; P<0.05). AU represents Arbitrary Units. *compared to soleus WT, $compared to soleus PV, #compared to soleus *mdx*. Means ± SEM are shown.

3.5.2 RCAN1, calsarcin-1 and MLP protein levels are not changed in the soleus muscle of *mdx*/PV

To examine the effect of the PV transgene on protein levels, we next asessed the levels of RCAN1, calsarcin-1 and MLP in soleus tissues of WT PV, *mdx* and *mdx*/PV mice. Unexpectedly, our immunoblotting experiments showed downregulation in RCAN1 protein levels in the soleus muscle of *mdx*/PV compared to *mdx*, with no changes in other phenotypes (Figures 3.2a and 3.2b). Although the latter effect is insignificant (P=0.15), it suggests that the mRNA and protein levels of RCAN1 are regulated independently.

Although there was a significant increase in calsarcin-1 mRNA levels in *mdx*/PV compared to WT, there was no change in calsarcin-1 protein levels among WT, PV, *mdx* and *mdx*/PV mice (Figures 3.2c and 3.2d), suggesting a possible post transcriptional modification of calsarcin-1.

In agreement with the calsarcin-1 expression results, MLP protein levels did not change among WT, PV, *mdx* and *mdx*/PV mice (Figures 3.2e and 3.2f). This might be due to potential interactions with other Z-line proteins.
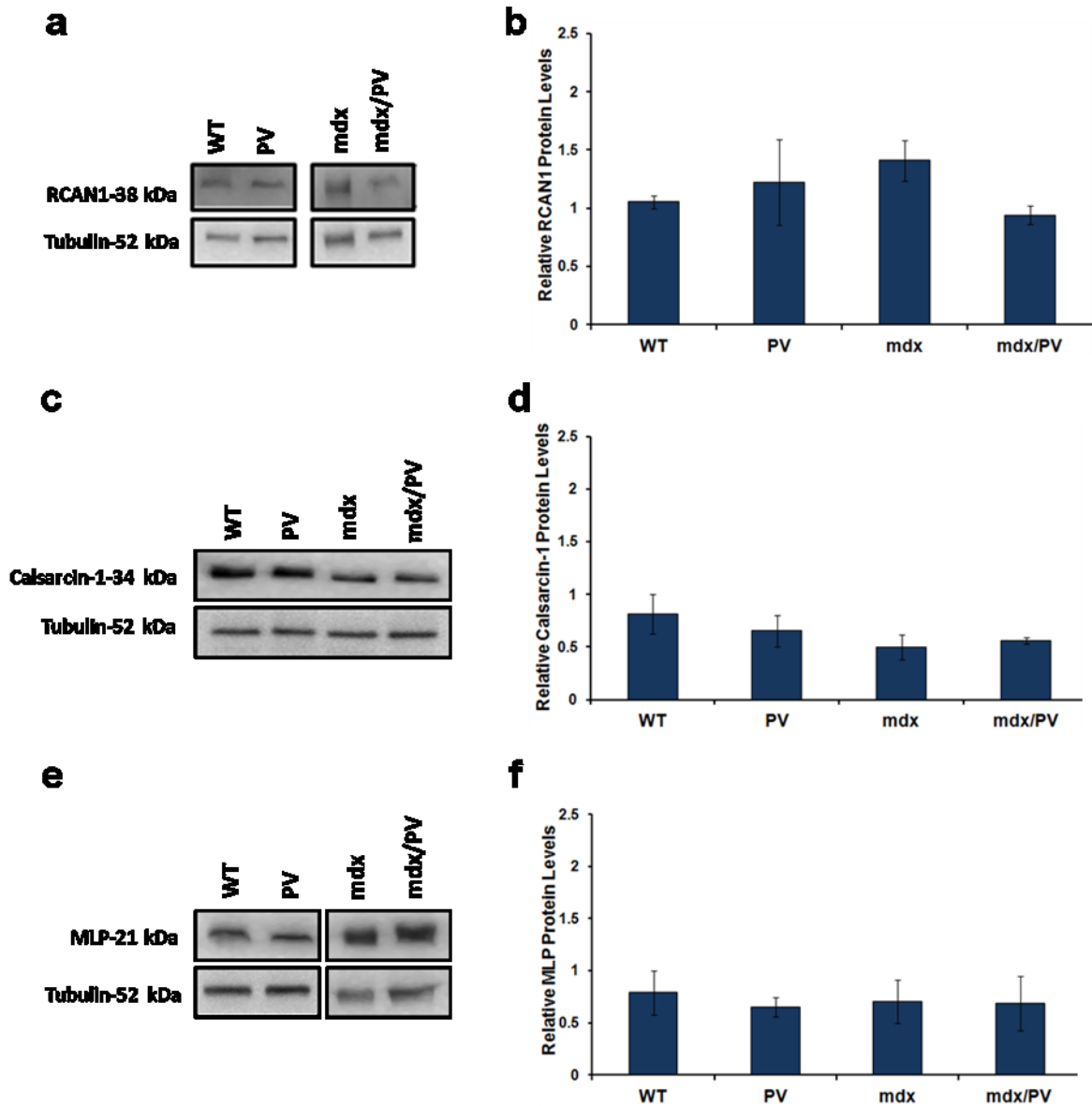
Figure 3.2: RCAN1, calsarcin-1 and MLP protein levels are not changed in the soleus muscle of *mdx*/PV

(**a,c,e**) Representative immunoblots for RCAN1, calsarcin-1 and MLP proteins in the soleus muscles of WT, PV, *mdx* and *mdx*/PV mice. (**b,d,f**) Quantifications of the immunoblots showing RCAN1, calsarcin-1 and MLP expression. Relative quantities are normalized to α-tubulin (n=3). Means ± SEM are shown.

3.5.3 *RCAN1.4, calsarcin-2* and *MLP* transcript levels do not change in *mdx* and *mdx*/CnA* EDL fast muscles

Being linked to the fast muscle creatine kinase promoter, the transgene that overexpresses Cn is expressed in fast fibers causing stimulation of the slow myofiber gene program [260]. Accordingly, EDL fast muscle was used to test the trasncript levels of *RCAN1.4*, *calsarcin-2* and *MLP*. Since Cn activity is stimulated with overexpression of CnA, we hypothesized an increase in *RCAN1.4*, *calsarcin-2* and/or *MLP* mRNA levels in EDL tissues of CnA and *mdx*/CnA mice.

Our qPCR results showed constant *RCAN1.4* and *MLP* mRNA levels between WT and CnA* EDL tissues. They both showed a tendency for a decrease in *mdx* and *mdx*/CnA* where Cn activity is high, but with no difference between *mdx* and *mdx*/CnA* mice (Figure 3.3a and Figure 3.3c).

In additon, *calsarcin-2*, which is expressed in fast-twitch skeletal muscles, showed no difference in transcript levels between *mdx* and *mdx*/CnA* EDL muscles (Figure 3.3b).
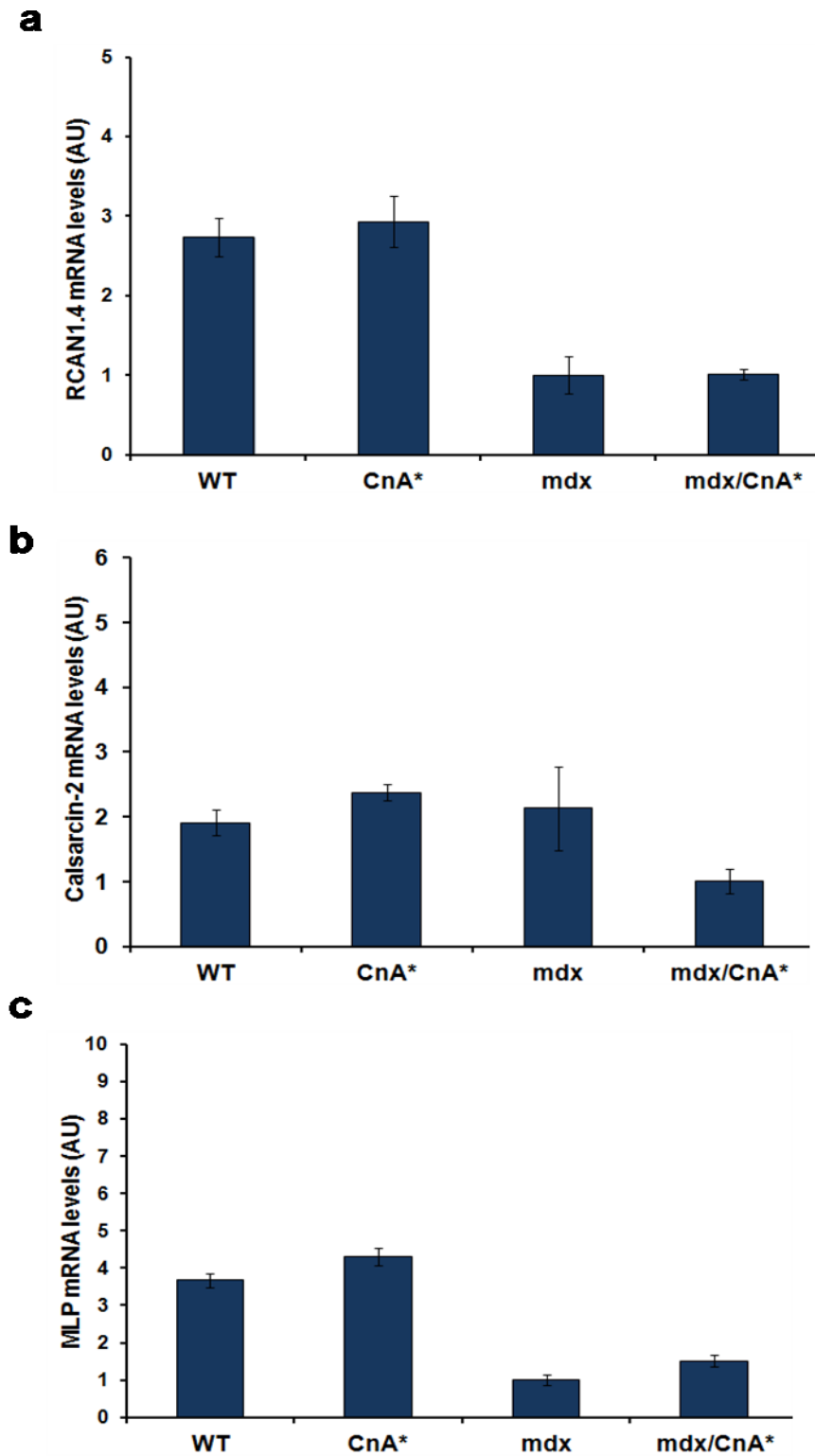
Figure 3.3: *RCAN1.4*, *calsarcin-2* and *MLP* mRNA levels do not show significant changes between *mdx* and *mdx*/CnA* mice

(**a**) QPCR histograms showing mRNA levels of *RCAN1.4* in EDL muscles of WT, CnA*, *mdx* and *mdx*/CnA* mice. (**b**) QPCR histograms showing mRNA levels of *calsarcin-2* in EDL muscles of WT, CnA*, *mdx* and *mdx*/CnA* mice. (**c**) QPCR histograms showing mRNA levels of *MLP* in EDL muscles of WT, CnA*, *mdx* and *mdx*/CnA* mice. AU represents Arbitrary Units. Relative quantities are normalized to *36B4* and *28S* (n=3). Means ± SEM are shown.

3.5.4 Calsarcin-2 and MLP protein levels are reduced while RCAN1 does not change in *mdx*/CnA* mice

To see the effect of the transgene on the translational level of the Cn modulators, we then examined the protein levels of RCAN1, calsarcin-2 and MLP in fast muscles of WT, CnA*, *mdx* and *mdx*/CnA* mice (EDL muscle was used for RCAN1 and calsarcin-2 and TA muscle was used for MLP).

Our imunblotting results for RCAN1 expression showed similar levels in WT, CnA*, *mdx* and *mdx*/CnA* in agreement with the qPCR results (Figures 3.4a and 3.4b). In addition, the calsarcin-2 protein level was significantly reduced in *mdx*/CnA* mice compared to CnA* mice with a tendency for downregulation compared to *mdx* mice (P=0.1) (Figures 3.4c and 3.4d). Finally, MLP protein level was not changed between WT and CnA, or between *mdx* and *mdx*/CnA* muscle fibers. Yet, there was a significant decrease in MLP protein level in *mdx*/CnA* mice compared to WT and a tendency for downregulation in MLP protein level in *mdx*/CnA* mice compared to CnA* mice (P=0.06) (Figures 3.4e and 3.4f). These results were also unexpected, as we hypothesized an increase in MLP expression to inhibit any additional Cn.
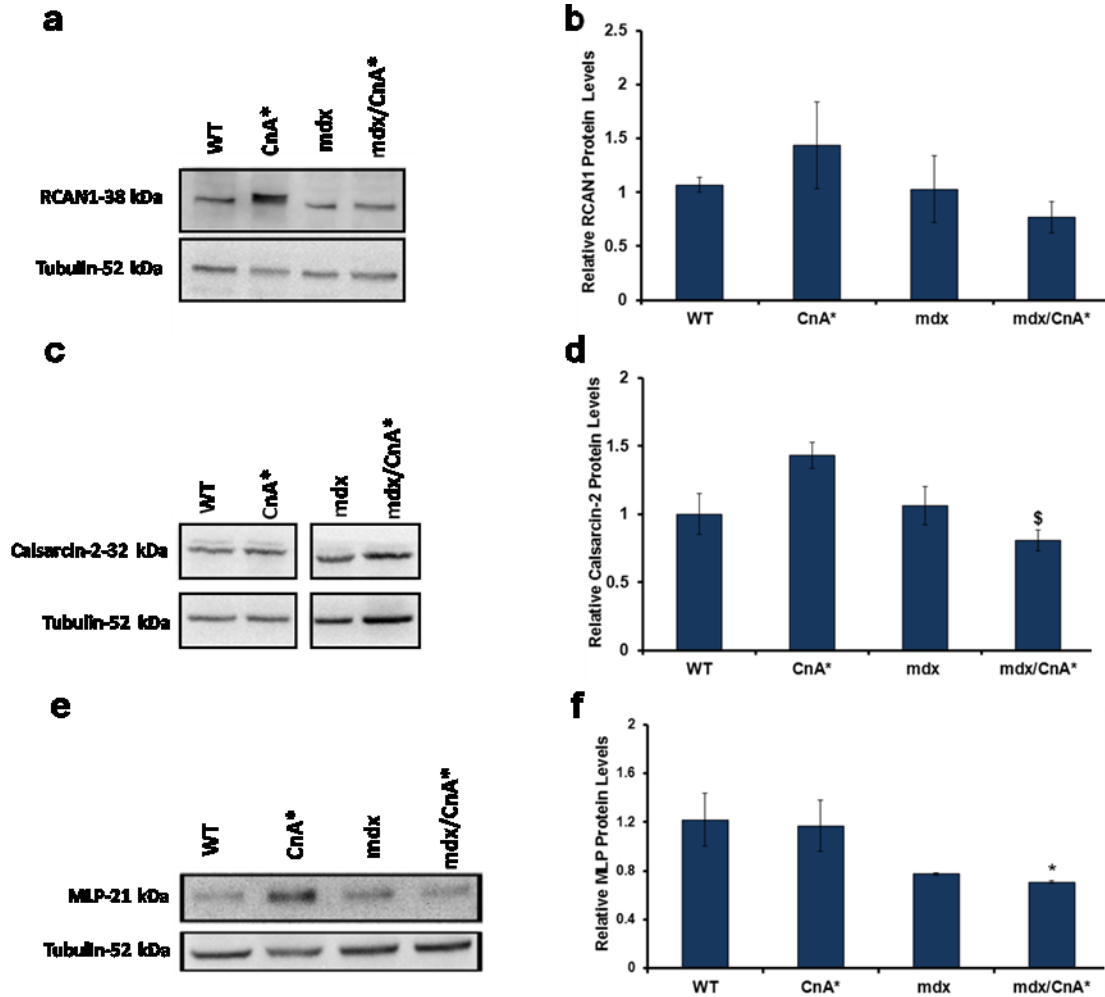
Figure 3.4: RCAN1, calsarcin-2 and MLP protein levels in WT, CnA*, *mdx* and *mdx*/CnA* mice

(**a,c,e**) Representative immunoblots for RCAN1, calsarcin-2 and MLP proteins in WT, CnA*, *mdx* and *mdx*/CnA* mice. (**b,d,f**) Quantification of the immunoblots showing RCAN1, calsarcin-2 and MLP expression. Relative quantities are normalized to α-tubulin (n=3; P<0.05). *compared to WT, \$compared to CnA*. Means ± SEM are shown.

3.6 Discussion

DMD, the most prevalent inherited neuromuscular disorder, is caused by the loss of the muscle sarcolemmal protein dystrophin, which is a 427 kDa cytoskeletal protein [95]. Utrophin, a neuromuscular junctional protein that shares a high degree of sequence identity with dystrophin, has been considered a strong candidate among therapeutic strategies for treating DMD [105]. Several studies have shown that upregulating utrophin-A at the muscle sarcolemma by stimulating the Cn/NFAT pathway, can compensate for the loss of dystrophin [105, 106]. Our lab previously has demonstrated the involvement of the Cn/NFAT signaling pathway in the regulation of utrophin-A expression in slow muscle fibers, and thus in the treatment of DMD [98, 106]. In 2003, our lab defined a new approach to knock down Ca^{2+}/CaM-based signaling in slow muscle fibers by overexpressing the transgene PV [214].

Recently, we crossbred *mdx* mice with transgenic mice expressing PV, which is normally expressed only in fast fibers [229]. This transgene is driven by the TnIs promoter, which leads to the force expression of PV in slow fibers leading to alterations in $[Ca^{2+}]_i$ kinetics and attenuation of Cn activity [214]. Thus, we showed that overexpression of PV in *mdx* slow muscle fibers reduces utrophin expression and increases the hallmarks of *mdx* cellular damage accompanied with an increase in the severity of the dystrophic pathology (Chapter 2). To better understand utrophin regulation, we started looking at proteins, which might have a role in regulating Cn activity and thus utrophin expression. The direct Cn modulators have been identified in Cn related-diseases such as cardiac hypertrophy [4, 184, 185]. However, their role in

skeletal muscle diseases is still not clear. Consequently, we set out to determine the expression levels of the direct Cn modulators in DMD disease using different transgenic models crossed with *mdx* mice.

Our preliminary results showed a mixture of expected and unexpected findings, which might be correlated to different types of regulation of these proteins. These differences might be driven by changes in the Cn/NFAT pathway and the various phosphatases and kinases affecting it. For instance, *RCAN1.4* mRNA levels were increased in the soleus muscle of *mdx*/PV mice compared to those of WT, PV and *mdx* mice (Figure 3.1). There was a tendency for downregulation in the RCAN1 protein level in *mdx*/PV mice compared to *mdx* mice (P=0.15) (Figure 3.2). In the fast EDL tissue, we did not find significant changes in RCAN1.4 mRNA and protein levels between *mdx* and *mdx*/CnA* mice (Figures 3.3 and 3.4). Therefore, there seems to be different regulation of RCAN1 expression upon changes in Cn activity driven by different transgenes.

RCAN is known to have a dual regulatory effect on Cn, thus acting as both an activator at low concentrations and an inhibitor at high concentrations [204, 258, 259]. The dual regulation of RCAN for Cn has been observed earlier by the Olson group while investigating the role of RCAN1 in cardiac hypertrophy. They have shown that deletion of the *RCAN* gene leads to a significant reduction in Cn activity, with similar levels of Cn expression in *RCAN* knockout (*RCAN*-/-) and WT mice [261]. Moreover, under conditions of high Cn activity, RCAN1 suppresses Cn signaling and exacerbates cardiac hypertrophy but not to the same extent as other transgenic models do [149, 261]. Not only in mice but also in other organisms such as yeast, the dual regulation exists, supporting our finding [258]. Furthermore, upon activation of Cn signaling, RCAN1.4 is

induced and then binds and inactivates Cn in a part of a feedback inhibition mechanism [207, 258]. This suggests that our results might be correlated to the time the expression of RCAN was measured. Thus measurement of RCAN could have been performed either during its induction or after being induced to go back and further inhibit Cn, as well as the expression of the downstream targets of NFAT including RCAN. In the future, it might be worth measuring RCAN expression in different time points; during development, in young and in adult mice. Additionally, the Olson group has shown no changes in Cn protein level in *RCAN1*-/- mice, but an increase in RCAN1 protein stability in the presence of Cn [261]. In our transgenic models in an *mdx* background, it would be interesting to look at RCAN1 protein stability bearing in mind the different kinases that might phosphorylate RCAN and affect its stability. One more thing that would be useful is to knockout the *RCAN* gene in *mdx* mice, with either impaired Cn activity such as *mdx*/PV or stimulated Cn activity such as *mdx*/CnA*. This will better underscore the role of RCAN in the Cn/NFAT pathway.

In this study, we observed an unexpected increase in *calsarcin-1* mRNA levels with impairment of Cn activity in the soleus muscle of *mdx*/PV mice compared to WT but not to *mdx* mice (Figure 3.1). However, protein levels did not change in the same transgenic models (Figure 3.2). Moreover, the mRNA levels of *calsarcin-2*, the isoform that is expressed in fast-twitch muscles, was also unchanged between *mdx* and *mdx*/CnA* (Figure 3.3), whereas the protein level showed a significant reduction in *mdx*/CnA* compared to CnA* EDL tissues (Figure 3.4). So, what is controlling the expression of calsarcins and how do they exert their function on Cn?

It has been shown that mice lacking the *calsarcin-1* gene have normal hearts but increased NFAT activity [262]. Like the RCAN studies, mice lacking *calsarcin-1* crossed with CnA* mice show an enhanced hypertrophic response [262]. Moreover, *calsarcin-1* is a known cardio-protective gene whose overexpression prevents Angiotensin II and Endothelin-1-induced hypertrophy in the heart [263]. However, does the same protection effect exist in skeletal muscles? If so, then the increase in *calsarcin-1* transcript level that we saw in *mdx*/PV mice might be related to protection provided by *calsarcin-1* in a failed attempt to rescue the dystrophic phenotype, as we did not see the same increase at the translational level. Additionally, calsarcin-1 is not restricted to the Z-disc, it also can shuttle to the nucleus [194]. Whether it interacts with NFAT in the nucleus is not yet established. Like RCAN1, calsarcin-1 could be phosphorylated, but the kinases responsible for this phosphorylation are still to be determined [264]. Further, Vondrisk's group has documented phosphorylation and post-translational processing of calsarcin-1 in the heart in a trial to establish growth-signaling mechanisms during heart diseases [265]. This regulation of calsarcin-1 is worth looking into in the future work. In regard to calsarcin-2, it has been shown, again by the Olson group, that *calsarcin-2-/-* mice exhibit improved running distances in exercise studies via the regulation of the Cn/NFAT pathway [184]. It is possible that calsarcin-2 was downregulated in our *mdx*/CnA* mice as a result of the improved performance carried out by stimulating the Cn/NFAT pathway. Yet, the latter needs further study. Thus, research on the role of calsarcins in the sarcomere function and their medical value particularly in DMD remains to be explored.

Finally yet importantly, we showed that there was no change in MLP expression in the soleus tissues of *mdx*/PV mice compared to *mdx* mice (Figures 3.1 and 3.2).

Nevertheless, we saw a down regulation in MLP protein levels in the TA tissues of *mdx*/CnA* compared to WT mice (Figure 3.4). As in RCAN1 and calsarcin-1, mice lacking *MLP* display hypertrophy and dilated cardiac myopathy, suggesting MLP negatively regulates skeletal and cardiac myofibers [196]. It was also shown that *MLP-/-* cardiomyocytes are not able to induce the Brain Natriuretic Peptide (BNP) when exposed to mechanical stimulation, where BNP together with the Atrial Natriuretic Peptide (ANP) decrease blood volume and thus lower systemic blood pressure [266]. These data suggest that MLP has a cardio-protective role. However, it is essential to figure out whether the decrease in the protein level that we detected in *mdx*/CnA* is related to Cn inhibition or considered as a negative reaction toward the protection provided by stimulating Cn in those mice.

One important Cn modulator whose role should not be ruled out is CAIN. The latter protein works in a negative regulatory loop. Thus, it becomes hyperphosphorylated upon activation of Protein Kinase C (PKC), which in turn affects Cn activity (reviewed in [192]). The importance of CAIN, has been well discussed in T-lymphocytes where CAIN could shuttle between the nucleus and the cytoplasm just like calsarcin-1 (Fan Pan and J.O.L, unpublished data). Further, CAIN contains a putative Cn-binding and Myocyte Enhancer Factor 2 (MEF2)-binding domain at its COOH terminus [182, 210, 212]. Knocking down these two binding domains in the C-terminus of CAIN, leads to upregulation of cytokines including interleukin-2 (IL-2) in response to stimulation by T-cell receptor agonists, yet with no changes in Cn activity. This might be explained in part by the low sensitivity of the NFAT dephosphorylation assay, in which low differences are undetectable. It can also be explained by the nature of T-lymphocytes, where CAIN may

have other functions rather than Cn inhibition [192]. Additionally, there might be competition between CAIN and NFAT or other substrates of Cn [192]. Therefore, it is worth exploring the expression and binding of CAIN with other transcription factors like MEF2. This might help understanding how this protein works to inhibit and regulate Cn.

Together, RCAN1, calsarcins, MLP and CAIN are four examples of Cn-interacting proteins which are quite important in regulating Cn and muscle diseases. Nevertheless, they require further studies on their regulation. It might be worthwhile to overexpress and/or knockdown the genes encoding these proteins in order to understand the importance of their roles in skeletal muscles particularly in certain types of muscle diseases such as muscle dystrophy. In case these proteins have only inhibitory effects on Cn, it would be interesting in the future to inhibit those inhibitors in order to maintain high but effective levels of Cn, which could stimulate utrophin expression in *mdx* mice and DMD patients.

Chapter 4 : **The role of the NFATc2 transcription factor in Calcineurin-dependent cardiac hypertrophy in adult mice**

Manal Al Zein, Patrick Sin-Chan, Mathieu St-Louis and Robin N. Michel

Department of Exercise Science, Concordia University, Montreal, QC, Canada

4.1 Background

In Chapter 4, we are interested in investigating the role of the NFATc2 transcription factor in the hearts of adult mice. A new manipulation in the Calcineurin/Nuclear Factor of Activated T cells (Cn/NFAT) pathway includes the knockout of the functional NFATc2 isoform in the heart. It has been demonstrated that young (1-2 month old) *NFATc2-/-* mice display a complete inhibition of forced hypertrophy and reduced fibrosis, suggesting a clear protection against pathological cardiac remodeling in the absence of NFATc2 [267]. However, we observed that adult (6-9 month old) *NFATc2-/-* mice were more susceptible to sudden death and had enlarged hearts when autopsied. Hence, we wanted to shed light on the role of the NFATc2 transcription factor in Cn-mediated cardiac hypertrophy, in normotensive and Angiotensin II (Ang II)-stressed hearts.

The results of this chapter are to be submitted for publication to the *Journal of Molecular and Cellular Cardiology.* This journal publishes work advancing knowledge of the mechanisms responsible for both normal and diseased cardiovascular function. Our work emphasizes a hidden role of the NFATc2 transcription factor in the adult heart and the regulation of some genes that might have an essential role in cardiac hypertrophy.

Patrick Sin-Chan has generated Figures 1-4 (Appendix IV). I added data to Figure 4a and performed the calculations and analyses for Figures 4d-4f. Patrick has also interpreted the results of the mentioned Figures, which are part of his MSc thesis. Dr. Mathieu St-Louis carried out NFATc1 immunofluorescence in the 14 day Ang II stimulated animals. I performed the calculations and generated the corresponding graphs.

4.2 Abstract

Cardiac hypertrophy is an overall increase in heart mass without improved contractile function. In this abnormality, the heart can no longer supply adequate amounts of blood to meet the body's hemodynamic demands, resulting in cardiac dilatation, decrease in contractile effectiveness, organ failure and death. The Ca^{2+}-dependent phosphatase, Calcineurin (Cn) and its downstream target, the Nuclear Factor of Activated T cells (NFAT), are major intracellular modulators of cardiac hypertrophy. In young mice, the NFATc2 transcription factor has been identified as the major NFAT isoform responsible for Cn-mediated cardiac hypertrophy. Surprisingly, we observed that adult *NFATc2* null (*NFATc2*-/-) mice were more prone to sudden death, suggesting that NFATc2 might be essential at later rather than earlier stages of life. Hence, we raised a question as to the role of NFATc2 in the hearts of adult mice. Our histological analysis showed that *NFATc2*-/- mice displayed left ventricular inner chamber dilatation, which might cause death to those mice. Nevertheless, Angiotensin II (Ang II)-stimulated cardiac growth for 14 days displayed alterations of transcriptional mechanisms in *NFATc2*-/- mice but no changes in the damage hallmarks compared to their Wild-Type (*NFATc2*+/+) counterparts. Additionally, Ang II stimulation for 28 days showed more damage in the stressed hearts compared to normotensive ones, with no detectable changes between *NFATc2*+/+ and *NFATc2*-/- mice. Our data collectively suggest a cardio-protective role for *NFATc2* in normotensive adult mice to maintain normal heart function and signaling. This protection is compromised when stressing the hearts for 14 and 28 days of Ang II stimulation. This study moves the discussion toward a better understanding of the role of NFATc2 in Cn-mediated cardiac hypertrophy in adult mice.

4.3 Introduction

Cardiovascular disease represents one of the leading causes of death in the modern world. An abnormality associated with the majority of cardiovascular diseases is pathological cardiac hypertrophy in which hearts are subjected to increased workload and decreased contractile efficiency [268]. Individuals living with this disease have a greater susceptibility to cardiac arrhythmias, organ failure and sudden death [268]. Further, prolonged cardiac hypertrophy leads to heart failure in which the heart cannot supply the body with enough blood and can no longer sustain the increased workload required to meet the body's hemodynamic demands as a healthy heart can, causing left ventricular dilatation. This enlargement of the left ventricle causes irregular heartbeats (arrhythmia), thinning of the myocardial walls and an overall decrease in heart contraction and function resulting in sudden death [269, 270]. The Ca^{2+}/Calmodulin (CaM)-dependent phosphatase, Calcineurin (Cn) and its downstream transcriptional target, the Nuclear Factor of Activated T cells (NFAT), are major intracellular modulators of pathological cardiac hypertrophy [155, 271-273]. Of the five known NFAT isoforms, four (NFATc1, NFATc2, NFATc3, NFATc4) are regulated by Cn signaling and their presence has been detected in the heart [72, 274]. Cn dephosphorylates NFAT triggering its nuclear transit, where it interacts with other cardiac factors to activate the transcription of cardiac fetal genes including β-Myosin Heavy Chain (*β-MyHC*), Atrial Natriuretic Peptide (*ANP*) and Brain Natriuretic Peptide (*BNP*), thereby initiating the hypertrophic gene program [156]. *In vivo* and *in vitro* studies previously have demonstrated the effectiveness of Cn/NFAT signaling in the mediation of cardiac hypertrophy and heart failure [72, 149, 155, 275-282]. Another well-characterized inducer of cardiac hypertrophy is the GATA4

transcription factor. Transgenic mice overexpressing *GATA4* display increased heart sizes, cardiomyopathy and reactivation of the cardiac fetal genes [283]. In addition, GATA4 has been shown to cooperate with NFATc4 to synergistically activate the BNP promoter to induce cardiac hypertrophy [149].

Genetic loss-of-function studies have identified that NFATc2 is the major NFAT isoform responsible for Cn-induced pathological cardiac hypertrophy. Thus, 1-2 month old *NFATc2*-/- mice display a complete inhibition of forced hypertrophy, decreased cardiac fetal gene expression, reduced fibrosis and restored contractile functions suggesting a clear protection against pathological cardiac remodeling [267]. However, we observed that 6-9 month *NFATc2*-/- mice are physically frailer in appearance, more susceptible to sudden death and have larger hearts upon autopsy. These observations suggest that in younger *NFATc2*-/- mice, other transcription factors may be compensating for the absence of functional NFATc2. Over time, these compensatory transcription factors might not be able to completely restore normal cardiomyocyte growth and function, predisposing these mice to heart failure. Having this difference between early findings on young mice and our observations on adult mice, we decided to examine the role of NFATc2 transcription factor in the hearts of adult mice in normotensive and Angiotensin II (Ang II)-stimulated hearts for 14 and 28 days. Ang II performs a physiologic stimulus, which promotes myocyte growth and cardiac hypertrophy [267].

Our results on normotensive adult *NFATc2*-/- mice showed a similar Heart Weight-to-Body Weight (HW/BW) ratio as *NFATc2*+/+ mice. However, *NFATc2*-/- mice displayed left ventricular inner chamber dilatation and thinning of the right ventricular wall, which might be correlated with heart failure. We also demonstrated that *NFATc2*-/-

mice have increased GATA4 expression and both NFATc1 and GATA4 nuclear translocation, suggesting a compensatory mechanism induced by these factors for the loss of NFATc2 in an attempt to rescue cardiomyocyte growth. Moreover, when inducing cardiac hypertrophy using Ang II implantation for 14 days, we observed that the overall heart morphology of Ang II-stimulated *NFATc2-/-* mice was similar to those of *NFATc2+/+* mice. We also showed that the expression of cardiac fetal genes may be regulated by separate mechanisms, since the change in their expression did not show the same pattern. However, the mRNA levels of the cardio-protective genes *calsarcin-1*, the beta 1 isoform of Calcineurin A (*CnAβ1*) and the Activating Transcription Factor 4 (*ATF4*), were either reduced or unchanged in the stimulated *NFATc2-/-* hearts compared to their *NFATc2+/+* counterparts. The protein levels of phospho-Akt (pAkt) (Ser473), phospho-Foxo3a (pFoxo3a) (Ser253) and CnAβ were unchanged in the 14 day Ang II-stimulated *NFATc2-/-* mice compared to their *NFATc2+/+* counterparts. Additionally, Haematoxylin and Eosin (H&E), picrosirius red, CD45 and the fibroblast markers Alpha Smooth Muscle Actin (α-SMA) and Vimentin did not show any differences between the 14 day stimulated *NFATc2-/-* mice and their *NFATc2+/+* counterparts. Comparable to the 14 day stimulation, the 28 day Ang II-stimulated *NFATc2+/+* and *NFATc2-/-* hearts were both overstressed showing the same degree of damage, collagen infiltrate and fibrosis.

Our results collectively, suggest that the NFATc2 transcription factor does not cause pathological cardiac hypertrophy in normotensive hearts. On the contrary, it might have a protective role in maintaining normal heart function and regulating growth-mediated biochemical signaling. In addition, upon stressing the hearts with Ang II, the loss of NFATc2 does not confer any protection against damage and failure since both

stimulated *NFATc2-/-* and *NFATc2+/+* hearts show similar degree of inflammation and fibrosis. In all cases, we propose that normal Cn/NFAT signaling is required for proper heart function. Simultaneously, abnormalities driven by Ang II are able to induce changes in this signaling pathway, thereby produce an exacerbated pathological situation.

4.4 Methods

4.4.1 Mouse model, breeding and maintenance

Transgenic *NFATc2* null (*NFATc2-/-*) mice were generously provided by Drs. Grace Pavlath (Emory University) and Laurie Glimcher (Harvard University). As a result of NFATc2 gene disruption, a loss of function mutation is produced as previously described [284]. Breeding of heterozygous (*NFATc2+/-*) or homozygous (*NFATc2-/-*) mice yielded a second generation *NFATc2-/-* mice. For the experimental design, *NFATc2-/-* mice were age and sex-matched with Wild-Type (*NFATc2+/+*) counterparts, which were purchased from (Charles River Laboratories) or generated from breeding. All mice were housed under standard environmental conditions (20-22ºC) and provided with standard rodent food and tap water. Mice between 6 and 9 months of age were used for all subsequent analyses. Animal care and experimental procedures were performed in accordance to the guidelines of the Canadian Council of Animal Care.

4.4.2 Mice genotyping

DNA from mouse tails was amplified by adding 2 μl of DNA to 1X Taq buffer with KCl (Fermentas), 2 mM $MgCl_2$ (Fermentas), 0.2 mM dNTP (Invitrogen), 0.5 mM primers (Sigma Aldrich) and 20 U Taq DNA polymerase (Fermentas), yielding a final

volume of 20 μl. The following primers were used 5' -gcaagcctcagtgacaaagtatccacttca-3', 5'-ccacgagctgcccatggtggagagacaaga-3' and 5'-agcgttggctacccgtgatattgctgaaga-3'. Cycling conditions were as follows: 1) initial denaturation at 95ºC for five minute, 2) denaturation at 94ºC for one minute, 3) primer annealing at 60 ºC for one minute, extension at 72ºC for one minute, 4) repeat steps 2 and 3 for 36 cycles, 5) final extension at 72ºC for ten minutes. PCR products were loaded on a 1.5% agarose gel stained with ethidium bromide and resolved, after electrophoresis, under UV irradiation using the Alpha Innotec FluorChem system (Cell Biosciences).

4.4.3 Muscle extraction and preservation

Prior to muscle extraction, mice were anesthetized by an intramuscular injection of a 1.6:1 volume ratio mixture of 100 mg/ml ketamine hydrochloride (Bimeda-MTC Animal Health Inc.) and 20 mg/ml xylazine (Bayer Health Care). A dosage of 0.04 ml/30 g of body weight was administered to each mouse. Animals were euthanized after extraction using CO_2 gas. Hearts for biochemical use were extracted and frozen directly in liquid nitrogen. For histology, the hearts were stimulated with an equal volume of 5% gelatin (Sigma Aldrich) in each ventricle, embedded with Tissue-Tek *Optimum Cutting Temperature* compound (Fisher Scientific) and frozen in a pool of melting isopentene cooled in liquid nitrogen. All samples were stored at -86ºC until used.

4.4.4 RNA extraction and semi-quantitative RT-PCR

Mouse hearts were homogenized in a solution made up of guanidinium thiocyanate (Sigma Aldrich), 25 mM sodium citrate, 0.5% (v/v) N-laurylsarcosine

(Sigma Aldrich) and 0.1 M 2-mercaptoethanol (Bioshop), followed by addition of 0.2 M sodium acetate (pH 4.0) with vortexing, phenol (Sigma Aldrich) and chloroform:isoamyl alcohol with vortexing until the appearance of a white emulsion. Samples were cooled on ice for fifteen minutes, and then centrifuged at 10,000 x g for ten minutes at 4ºC. Afterwards, two volumes of 99% ethanol were added to the aqueous layer with vortexing and centrifugation again at 10,000 x g for ten minutes at 4ºC. The ethanol was decanted and the RNA was suspended in 200 μl of 70% ethanol and centrifuged at 10,000 x g for ten minutes at 4ºC. The ethanol again was decanted and the RNA pellet was left to dry and re-suspended in 15 μl of RNAse free H_2O (Bioshop) per 10 mg of tissue with subsequent vortexing and heating at 70ºC for 3 minutes. To test RNA integrity, the RNA concentration was determined using an Eppendorf Biophotometer (Eppendorf) at 260nm. Subsequently, 2 μg of RNA was mixed with a 2:1 formamide:ethidium bromide, formaldehyde (Sigma Aldrich), 10X MOPS (pH 7.0) and bromophenol blue, heated at 65ºC for ten minutes and loaded on a 1.5% agarose gel containing 1X MOPS and formaldehyde. The three rRNA bands: 5S, 18S and 28S were visualized to verify RNA integrity.

RT-PCR was performed by combining 2 μg of RNA and ultrapure water, to a final volume of 10 μl. The final volume of the RT mixture was 40 μl, and consisted of 0.625 μM random primer hexamers (Invitrogen), 1X RT-buffer (Ambion), 0.5 μM dNTP (Invitrogen), 40 U of RNase Inhibitor (Ambion) and 100 U of MMLV-RT (Ambion). The RT-PCR program (fifteen minutes at 20ºC, one hour at 37ºC, and ten minutes at 65 º C) was performed using an MJ Research PTC-100 thermalcycler. As a negative control, RT

samples were duplicated in the absence of MMLV-RT. The cDNA was stored at -20ºC until used.

The cDNA was amplified by adding 2.5 μl of cDNA to 1X Taq buffer with KCl (Fermentas), 1.5 mM MgCl$_2$ (Fermentas), 0.1 mM dNTP (Invitrogen), 0.2 mM primers (Sigma Aldrich) and 0.5 μl Taq DNA polymerase (Fermentas), yielding a final volume of 50 μl. Cycling conditions were as follows: 1) initial denaturation at 94ºC for one minute, 2) denaturation at 94ºC for one minute, 3) primer annealing at 55 ºC for one minute and extension at 72ºC for one minute, 4) repeat steps 2 and 3 for X number of cycles, 6) final extension at 72ºC for ten minutes, using an MJ Research PTC-100 thermalcycler. PCR products were loaded on a 1.5% agarose gel stained with ethidium bromide and resolved under UV irradiation using the Alpha Innotec FluorChem system (Cell Biosciences) after electrophoresis. The primer sequences used for semi-quantitative RT-PCR are listed in Table 4.1.

Table 4.1: Primers for semi-quantitative PCR

Gene	Forward Primer	Reverse Primer	Product Size (bp)
NFATc1	5'-ttccagcaccttcggaagggtgc-3'	5'-agtgagccctgtggtgagac -3'	205
NFATc2	5'-tctgctgttctcatggatgccc-3'	5'-ggatgcagtcacagggatgct-3'	282
NFATc3	5'-cgatctgctcaagaactccc-3'	5'-ggcagatgtaactgctgggt-3'	246
NFATc4	5'-ctgaggatcgaggtacagcc-3'	5'-ttgttctctgggagcaaggt -3'	293
28S	5'-ttgttgccatggtaatcctgctcagta-3'	5'-tctgacttagaggcgttcagtcataatc-3'	132
β-MHC	5'-gccaacaccaacctgtccaagttc-3'	5'-tgcaaaggctccaggtctgagggc-3'	205
ANP	5'-ttggcttccaggccataattg-3'	5'-aagagggcagatctatcgga-3'	282
BNP	5'-atggatctcctgaaggtgct-3'	5'-tcttgtgcccaaagcagctt-3'	505

4.4.5 Real time quantitative-PCR (qPCR)

Changes in gene expression for *calsarcin-1*, *CnAβ1*, *ATF4*, *Foxo3a* and *myostatin* were assessed by qPCR. Briefly, 2 μg of freshly extracted heart RNA was reverse transcribed to cDNA using iScript reverse transcription supermix (Bio-Rad) and qPCR was performed using gene-specific primers together with appropriate reference genes for quantification (CFX96 Real-Time System, Bio-Rad). Relative quantities then were normalized by the Real-time System software to the relative quantities of Hypoxanthine-guanine Phospho-Ribosyl Transferase (*HPRT*), 60S Ribosomal Protein L13 (*RPL13*) and/or TATA-Binding Protein (*TBP*) housekeeping genes. The primer sequences used for qPCR are listed in Table 4.2.

Table 4.2: Primers for quantitative real-time PCR

Gene	Forward Primer	Reverse Primer	Product Size(bp)
Calsarcin-1	5'-gccaaagggggtgggtatct-3'	5'-tgccctaagcagaccaacag-3'	156
CnAβ1	5'-agaaggtgaagaccagt-3'	5'-agcaagttgcataacatcatt-3'	144
ATF4	5'-atgctctgtttcgaatgga-3'	5'-gtctgaggggggctccttatt-3'	121
Foxo3a	5'-caaagcagaccctcaaactga-3'	5'-caaaggtgtcaagctgtaaacgg-3'	102
MSTN	5'-taaccttcccaggaccagga-3'	5'-cactctccagagcagtaatt-3'	223
RPL13	5'-aaggtggtggtcgtacgctgtg-3'	5'-gcgccagaaaatgcggctgg-3'	153
HPRT	5'-ccagcgtcgtgattagcgatgatg-3'	5'-gagcaagtctttcagtcctgtcc-3'	135
TBP	5'-caccaatgactcctatgacc-3'	5'-gtttacagccaagattcacg-3'	111

4.4.6 Protein extraction and Immunoblotting

Briefly, whole hearts were homogenized in 1X RIPA buffer solution (6 µl/mg tissue) consisting of 1X PBS, 1% Igepal, 0.5% Sodium Deoxycholate, 0.1% Sodium Dodecyl Sulfate (SDS), 0.001 M Sodium Orthovanadate, 0.01 M Sodium Fluoride, 0.01 mg/ml Aprotinin, 0.01 mg/ml Leupeptin and 1 mM Phenylmethanesulfonyl fluoride (PMSF). Homogenates were centrifuged at 15,000 x g for twenty minutes and the supernatant layers were collected and re-centrifuged. Protein concentrations were measured using Quick Start Bradford dye reagent (Bio-Rad) and extracts were stored at -86ºC until used. For nuclear-cytosolic protein extraction, fractionation into cytoplasmic and nuclear proteins was performed using the NE-PER® Nuclear and Cytoplasmic Extraction Kit (Pierce Biotechnology) according to the manufacturer's protocol.

Between 50-100 µg of protein were loaded on an SDS polyacrylamide gel consisting of a 5% w/v stacking gel composed of 3.9% acrylamide (Sigma Aldrich), 0.125 M Tris (pH 6.8), 0.1% SDS, 0.06% ammonium persulfate and 0.14% Tetramethylethylenediamine (TEMED) (Bioshop), and a 10% w/v separating gel composed of 9.9% acrylamide, 0.375 M Tris (pH 8.8), 0.1% SDS, 0.06% ammonium persulfate and 0.25% TEMED. Samples were electrophoresed at 120V until the protein sizes of interest were visibly separated using the Amersham Full-Range Rainbow Molecular Weight Markers (GE Healthcare Bio-Sciences Corp). Proteins were transferred to a PVDF membrane (Millipore) at 30V for 90 minutes using Borax (Bioshop), followed by blocking in 5% non-fat milk or bovine serum albumin in 0.1% Tween/Tris Buffered Saline (T/TBS) for one hour. Primary antibodies to GATA4

(1:1000; sc-25310, Santa Cruz), α-tubulin (1:2000; 2125, Cell Signaling), Histone H3 (1:1000; 9715, Cell Signaling), GAPDH (1:2000; ab9484, Abcam), pAkt (Ser473) (1:1000; 9271, Cell Signaling), total Akt (1:1000; 610861, BD Biosciences), Alpha smooth muscle actin (1:1000; ab5694, Abcam), pFoxo3a (Ser 253) (1:500; sc-101683, Santa Cruz), total Foxo3a (1:500; sc-11351, Santa Cruz), CnAβ (1:1000; ADI-SPA-610, Enzo Life Sciences), Vimentin (1:500; C0390, Assay BioTech) and calsarcin-1 (1:2000; rabbit polyclonal antibody; a gift from Drs. Norbert Frey and Derk Frank) were added to membranes based on the manufacturer's recommendation and incubated on a shaker at 4ºC overnight. The following day, membranes were washed three times with 0.1% T/TBS and incubated with secondary antibodies (1:2000, Sigma Aldrich and Cell Signaling) coupled to horse radish peroxidase (HRP) for one hour. Membranes were washed three times with 0.1% T/TBS and developed with enhanced chemi-luminescence reagents (Millipore) using the Alpha Innotec FluorChem system.

4.4.7 Angiotensin II infusion

Alzet 2002 micro-osmotic pumps (Alzet) were placed through a small dorsal incision in the skin between the scapulae in 6-9 month old female mice anesthetized as described above. Pumps were filled with Ang II (Sigma Aldrich), administered in a dosage of 432 μg·kg^{-1}·day^{-1} in 150 mM NaCl-0.01N acetic acid. Ang II was continuously stimulated into mice for a period of 14 days. The hearts were then extracted as described earlier. For the 28 day stimulated hearts, the incision was opened and the pump was replaced by another one to give an additional dose for 14 more days before the hearts were extracted.

4.4.8 Histology, Staining and Microscopy

Hearts embedded in *Optimum Cutting Temperature* were transversally sectioned in 10 μm cuts, using a Leica CM3060S cryostat (Leica Microsystems Inc.) and collected on Superfrost Plus microslides (VWR).

For H&E, samples were incubated in 0.5% Harris haematoxylin (Sigma Aldrich) for five minutes, rinsed with water, quickly immersed in 1% HCl/70% ethanol solution, rinsed with water, incubated in 1% eosin (Fisher Scientific) for three minutes and rinsed with water. Slides were subsequently incubated in 70%, 80% and 90% ethanol solution for two minutes each and immersed in xylene (Fisher Scientific) for thirty seconds. Slides were air dried and mounted in Permount (Fisher Scientific). Images were captured on a Nikon SMZ1500 stereomicroscope or Zeiss microscope.

Picrosirius red staining for collagen infiltrate was performed using the picrosirius red kit (Polysciences, Inc.) as follows: hearts from the normotensive and Ang II stimulated mice were transversally sectioned in 10 μm cuts. Slides were fixed in 4% paraformaldehyde (PFA) for 30 minutes, followed by washing with distilled water and incubation in 20% of the stock solution A (Phosphomolybdic acid hydrate) for 5 minutes. Slides then were rinsed in distilled water and further incubated in 20% of the stock solution B (Trinitrophenol) for 30 minutes. This was followed by rinsing with distilled water and incubation in 20% of the stock solution C (Hydrogen chloride) for 2 minutes. Slides were finally dehydrated in 70% ethanol for 30 seconds, cleared with xylene for fifteen seconds, air dried and mounted in Permount. Images were visualized and captured using a microdissection microscope (Applied Biosystems).

For immunofluorescence (IF), samples were fixed in 2% PFA and washed with 1X PBS three times for five minutes. Tissues were blocked and permeabilized with 2% goat serum (Sigma Aldrich) and 0.2% Triton X-100 (Sigma Aldrich) for one hour. Samples were incubated overnight at 4ºC with primary antibodies; 1:50 NFATc1 (sc-13033), 1:25 NFATc2 (sc-13034), 1:25 NFATc3(sc-8321), 1:50 NFATc4 (sc-13036) (Santa Cruz), 1:50 CD45 (05-1413, Millipore), 1:50 α-SMA (ab5694, Abcam) or 1:50 Vimentin (C0390, Assay BioTech) in 1X PBS containing 1% goat serum and 0.05% Triton X-100. The following day, samples were washed three times with 1X PBS and incubated with 1:100 Alexa Fluor® 488 Goat Anti-mouse IgG (A-11001) (Invitrogen) for mouse primary antibodies or 1:100 Alexa Fluor® 546 Goat Anti-rabbit IgG (A-11010) (Invitrogen) for rabbit primary antibodies in 1X PBS, containing 1% goat serum and 0.05% Triton X-100 for one hour at room temperature. Slides were washed five times with 1X PBS, dried and mounted with Vectashield with 4',6-diamidino-2-phenylindole (Dapi) (Vector Laboratories Inc.). Images were captured at 40X magnification using a Zeiss Axioplan fluorescence microscope mounted with a Lumenera Infinity 3-1C1.4 camera (Ottawa, ON, Canada). Negative control slides without primary antibodies revealed the absence of background staining at the acquisition time used. Colocalization analysis was performed using ImagePro Plus version 6.2 software (Olympus, Markham, ON, Canada).

4.4.9 Statistical analyses

The levels of cDNA and protein expression were quantified by measuring the density of the band of interest with respect to a control using the Alpha Innotec

FluorChem system. Differences between experimental groups were evaluated for statistical significance using One Way Analysis of Variance (ANOVA) with necessary Post-Hoc tests. Student's *t* test was used for comparing two groups with one variable. Values were considered to be statistically significant if P<0.05. Analyses for Chapter 4 are fully explained in Appendix III.

4.5 Results

4.5.1 Characterization of heart phenotype in *NFATc2-/-* mice

NFATc2-/- mice were generated by substituting the NFATc2 N-terminal DNA binding domain of the NFAT <u>R</u>el <u>H</u>omology <u>D</u>omain (RHD) with a neomycin cassette, using homologous recombination [284]. The genotypes of experimental mice were validated by amplifying DNA isolated from tails by PCR (Appendix IV; Figure 1a). Normotensive hearts of *NFATc2*-/- mice displayed a comparable overall gross morphology (Appendix IV; Figure 1b) and a similar relative HW/BW ratio compared to *NFATc2*+/+ mice (Appendix IV; Figure 1c).

We monitored changes in the sizes of heart ventricles and myocardial wall thickness, well-characterized markers of heart disease and failure (Appendix IV; Figure 1d). The ratio of the left ventricular chamber inner diameter to total heart diameter showed that the left ventricular chamber of *NFATc2*-/- mice was approximately 28% more dilated than *NFATc2*+/+ hearts (Appendix IV; Figure 1e). Additionally, the right ventricular wall was approximately 25% thinner than in *NFATc2*+/+ hearts. However, the latter effect was not significant (Appendix IV; Figure 1f). The changes in both ventricular

dilatation and thickness of the myocardial wall suggest that adult *NFATc2*-/- mice might be more susceptible to heart failure and sudden death.

4.5.2 NFATc1 has increased nuclear localization in the hearts of *NFATc2-/-* mice

To monitor the ability of NFATc1, NFATc3 and NFATc4 to compensate for the absence of functional NFATc2 at the mRNA level, semi-quantitative RT-PCR was conducted on RNA isolated from experimental hearts. Although mRNA transcript levels showed no differences between *NFATc2*+/+ and *NFATc2*-/- hearts (Appendix IV; Figure 2a), IFs showed that NFATc1 had a significantly higher nuclear presence, whereas NFATc3 and NFATc4 were unchanged in the hearts of *NFATc2*-/- compared to *NFATc2*+/+ mice (Appendix IV; Figures 2b and 2c). This suggests that NFATc1 may have increased nuclear translocation in order to potentially compensate for the absence of the non-functional NFATc2 in the adult hearts.

4.5.3 The GATA4 transcription factor has a higher protein expression and nuclear transit in the *NFATc2-/-* compared to *NFATc2+/+* hearts

GATA4 transcription factor is one of the most well-characterized proteins required for cardiac morphogenesis and a marker of adult cardiac failure [285]. It has been demonstrated that GATA4 can interact with NFATc4 to synergistically activate the transcription of genes leading to cardiac growth and eventually heart failure [149]. Although GATA4 was not altered in the hearts of adult *NFATc2*-/- mice at the transcript level (data not shown), it was significantly upregulated at the protein level (Appendix IV; Figures 3a and 3b), suggesting that the synthesis of GATA4 protein was increased maybe

to compensate for the loss of a functional DNA binding domain in the NFATc2 protein. To determine whether there also was increased nuclear transit of GATA4 in the hearts of adult *NFATc2-/-* mice, we fractionated the hearts into cytoplasmic and nuclear protein extracts and used Glyceraldehyde-3-Phosphate Dehydrogenase (GAPDH) as a cytosolic loading control and Histone H3 as a nuclear loading control (Appendix IV; Figure 3c). Results showed that GATA4 expression was comparable in the cytoplasmic fraction of *NFATc2+/+* and *NFATc2-/-* hearts, whereas GATA4 was significantly upregulated in the nuclear fraction of *NFATc2-/-* hearts, compared to the *NFATc2+/+* counterparts (Appendix IV; Figures 3d and 3e). Thus, as a molecular partner of NFATc2, GATA4 had an increased expression as well as increased nuclear transit in the absence of functional NFATc2.

4.5.4 The 14 day Ang II-stimulated *NFATc2-/-* mice have morphological and anatomical markers of heart failure comparable to *NFATc2+/+* counterparts

Because normotensive adult *NFATc2-/-* mice displayed both physiological and biochemical alterations indicative of heart failure, we induced acute cardiac hypertrophy in those mice using Ang II administration for 14 days. We hypothesized that imposing further strain on *NFATc2-/-* mice by using a functional overload, the hearts of these mice would display a more severe pathological state. Ang II-mediated cardiac hypertrophy was validated by a 20% increased HW/BW ratio in both stimulated *NFATc2+/+* and *NFATc2-/-* hearts compared to their normotensive counterparts (Appendix IV; Figure 4a). When comparing the left ventricular inner chamber diameter and thickness of the right ventricular wall in Ang II-stimulated *NFATc2+/+* and *NFATc2-/-* mice, we visually

observed some differences (Appendix IV; Figure 4b). Yet, there was no significant change in the left ventricular chamber inner wall diameter or the right ventricular wall diameter between stimulated *NFATc2+/+* and *NFATc2-/-* hearts (data not shown), implying that imposed acute pharmacological stress on these mice might have caused some but not major changes.

In addition, we saw alterations in the expression of the cardiac fetal genes, *β-MyHC*, *ANP* and *BNP* (Appendix IV; Figure 4c). The reactivation of the cardiac fetal genes is another hallmark feature of hearts undergoing pathophysiological hypertrophy and damage [156]. We showed that of all fetal genes tested, only the *β-MyHC* gene was increased in expression, whereas *ANP* and *BNP* did not change between Ang II-induced *NFATc2-/-* and their *NFATc2+/+* counterparts (Appendix IV; Figures 4d, 4e and 4f).

4.5.5 The 14 day Ang II-stimulated *NFATc2-/-* mice display altered cardio-protective gene expressions

In addition to cardiac fetal genes, we monitored gene expression of regulators of cardiac growth following 14 days of Ang II-induced hypertrophy in *NFATc2-/-* mice. Based on our previous findings on normotensive *NFATc2-/-* mice that had altered cardiac fetal gene expression, we predicted that genes with a cardio-protective function would be downregulated, whereas genes involved in heart failure and damage would be increased in expression. Interestingly, we observed that genes with cardio-protective roles; *calsarcin-1* and *CnAβ1*, were significantly increased in Ang II-stimulated *NFATc2+/+* mice compared to *NFATc2+/+* counterparts. However, *calsarcin-1* was unchanged and *CnAβ1* was reduced in Ang II-stimulated *NFATc2-/-* mice compared to their *NFATc2+/+*

counterparts (Figures 4.1a and 4.1b). In agreement with this observation, *ATF4*, a downstream target of the <u>m</u>ammalian <u>T</u>arget <u>Of</u> <u>R</u>apamycin (mTORC1) and a potential mediator of the cardio-protective effect produced by *CnAβ₁* [64, 175, 180, 181], had a tendency for an increase (P=0.09) in stimulated *NFATc2+/+* compared to normotensive *NFATc2+/+* mice. However, this increase was lost in stimulated *NFATc2-/-* hearts (Figure 4.1c).

Additionally, the expression levels of genes with known roles in cardiac damage and atrophy were measured [174, 286-289]. *Foxo3a* was upregulated in stimulated *NFATc2-/-* mice compared to normotensive *NFATc2-/-* mice, whereas *myostatin* was increased in stimulated *NFATc2-/-* mice compared to all other groups (Figures 4.1d and 4.1e).
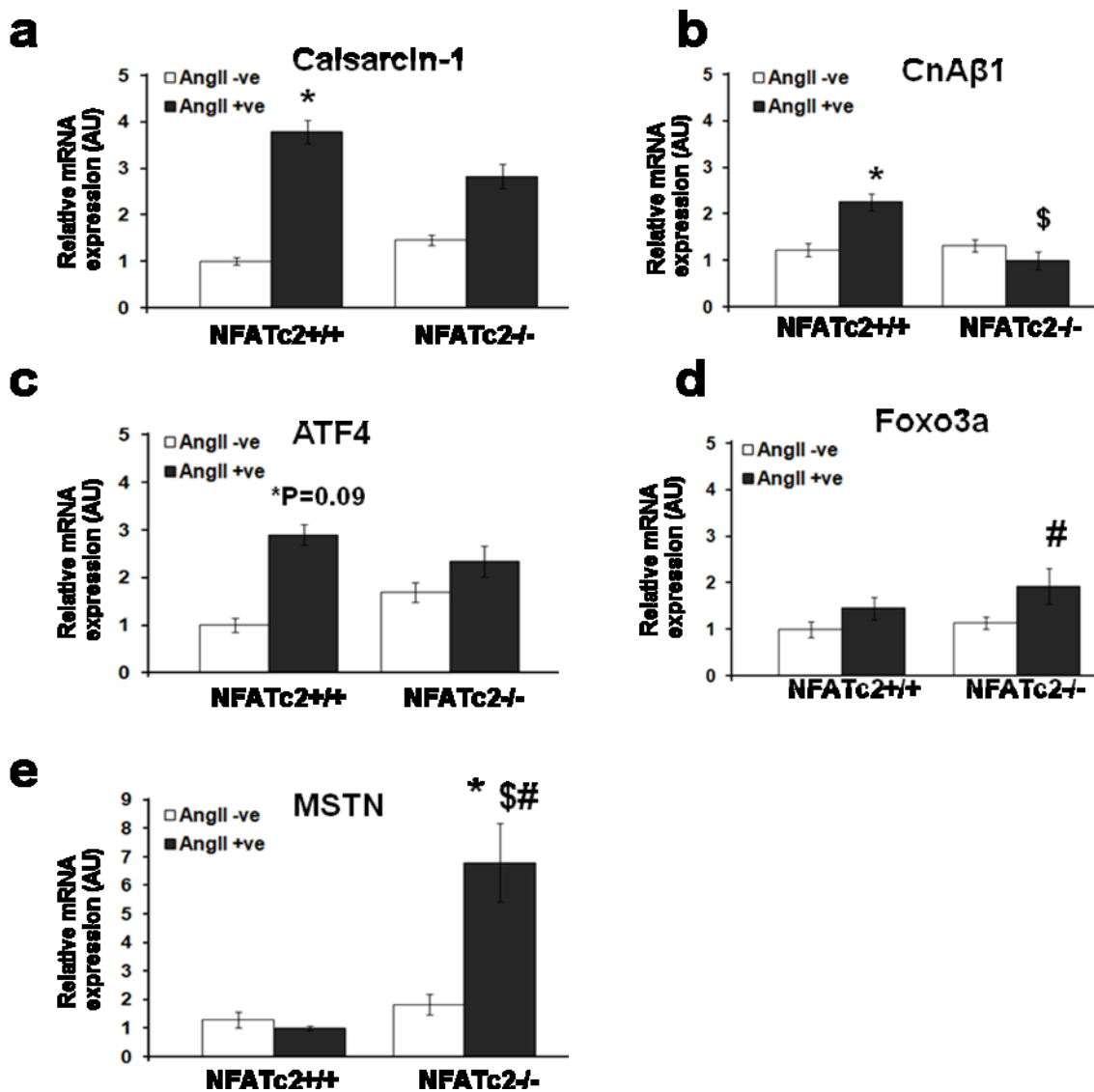
Figure 4.1: The 14 day Ang II-stimulated *NFATc2*-/- mice display less protective properties

QPCR showing changes in relative mRNA expression levels of *calsarcin-1* (**a**), *CnAβ1* (**b**), *ATF4* (**c**), *Foxo3a* (**d**) and *myostatin* (MSTN) (**e**) in normotensive as well as in the hearts of Ang II-stimulated *NFATc2*+/+ and *NFATc2*-/- mice. Relative quantities are normalized to *HPRT*, *TBP* and/or *RPL13* (n=3 for calsarcin-1, CnAβ1 and Foxo3a and n=4 for ATF4 and MSTN; P<0.05). AU represents Arbitrary Units. *compared to normotensive *NFATc2*+/+, $compared to stimulated *NFATc2*+/+, #compared to normotensive *NFATc2*-/-. Means ± SEM are shown.

4.5.6 The 14 day Ang II-stimulated hearts show similar signs of damage as normotensive hearts

In order to determine if changes in the expression of cardiac fetal genes driven by Ang II stimulation had generated any damage hallmarks in the hearts of *NFATc2-/-* mice, we next assessed various pathological indices. Picrosirius red, a strong anionic dye, was introduced to substitute for Acid Fuchsin in Van Gieson's trichrome method. This dye specifically stains collagen by direct interaction between the basic groups in collagen and sulphonic acid groups of sirius red [290]. Accordingly, H&E and picrosirius red staining did not show differences in visual morphological abnormalities between stimulated and normotensive *NFATc2-/-* hearts (Figure 4.2a).

CD45, also called Leukocyte common antigen, is a high molecular weight transmembrane glycoprotein, which is expressed in nucleated hematopoietic cells [291, 292]. CD45 is a member of the protein tyrosine phosphatase family, which is an essential regulator of T- and B-cell antigen receptor signaling and functions by activating various kinases required for antigen receptor signaling [292]. This protein is considered a valuable marker to identify cells of leukocyte origin as well as to distinguish naive from memory T-cells that are induced during inflammatory responses [293, 294]. Thus to investigate the presence of inflammation due to 14 day Ang II stimulation, we stained for CD45. Both stimulated *NFATc2+/+* and *NFATc2-/-* showed a similar staining for this marker (Figure 4.2a).

To detect and examine the presence of fibrosis in *NFATc2-/-* mice, we used two markers: α-SMA, a marker of fibrosis and smooth muscle differentiation, is a protein

synthesized from the myofibroblasts at the site of injury during wound healing [295]. Vimentin is the most frequent occurring intermediate filament in fibroblasts and thus a reliable fibroblast marker [296]. Both α-SMA and Vimentin showed similar staining in normotensive *NFATc2-/-*, stimulated *NFATc2+/+* and stimulated *NFATc2-/-* hearts (Figure 4.2a).

We previously saw an increased NFATc1 nuclear localization in the hearts of normotensive *NFATc2-/-* mice, which might be correlated to the ability of NFATc1 to compensate for the absence of *NFATc2* (Appendix IV; Figure 2c). In agreement with this, IFs showed that NFATc1 had a tendency for a higher nuclear presence in the hearts of the 14 day stimulated *NFATc2-/-* mice compared to the 14 day stimulated *NFATc2+/+* mice (P=0.05) (Figures 4.2b and 4.2c).
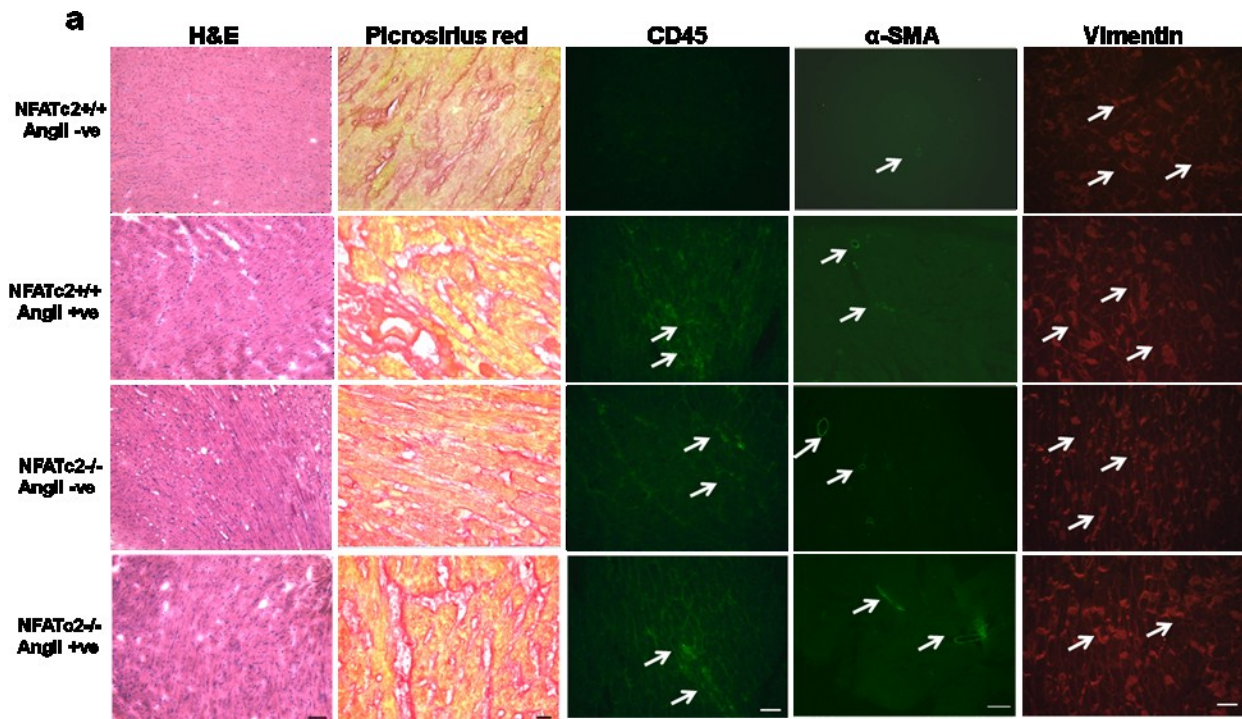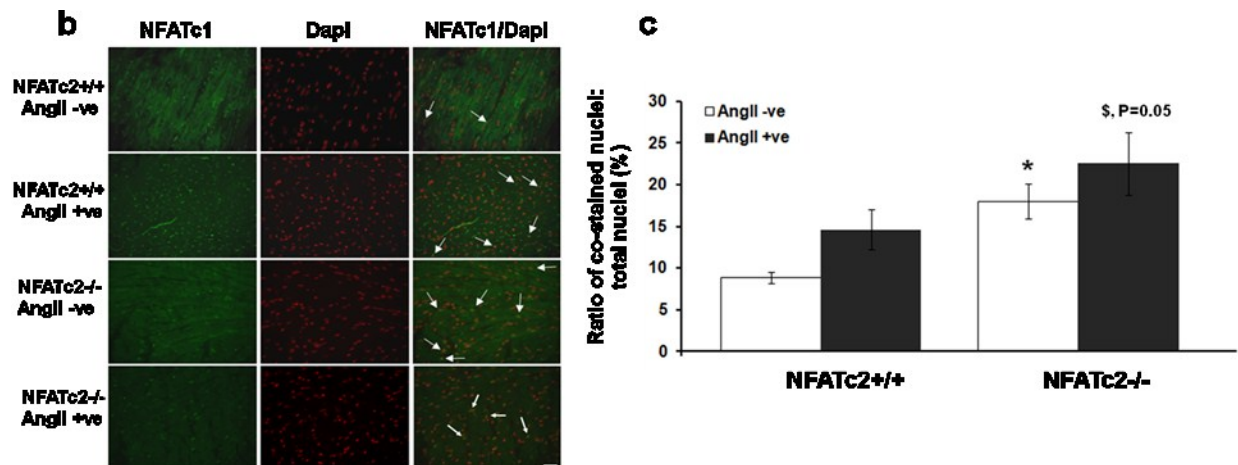
Figure 4.2: The 14 day Ang II-stimulated hearts do not show differential signs of damage from normotensive hearts

(**a**) H&E, picrosirius red staining and IFs for CD45, α-SMA and Vimentin in the hearts of normotensive and stimulated *NFATc2+/+* and *NFATc2-/-* mice (n=3). Arrows indicate positive staining. Scale bars; 50μm for (H&E), 10μm for (Picrosirius red), 20μm for (CD45 and Vimentin) and 100μm for (α-SMA). (**b**) Representative photomicrographs depicting nuclear localization of NFATc1 isoform in the heart. Arrows indicate nuclei positively stained for NFATc1. Scale bars, 20μm. (**c**) Quantification of the percentage of myonuclei stained for NFATc1 in normotensive *NFATc2-/-* compared to normotensive *NFATc2+/+* hearts (n=3; $P<0.05$). *compared to normotensive *NFATc2+/+*, $compared to stimulated *NFATc2+/+*. Means ± SEM are shown.

4.5.7 Phospho-Akt, α-SMA, phospho-Foxo3a and Vimentin protein levels do not change in the 14 day Ang II-stimulated *NFATc2-/-* mice

We next investigated whether pathways regulating protein translation were affected in Ang II-stimulated *NFATc2-/-* mice. The Insulin Growth Factor-I/Akt (IGF-1/Akt) signaling pathway is one of the most studied growth pathways involved in promoting both gene transcription and protein translation, as well as in inhibiting the activation of pathways resulting in protein degradation [178, 179]. We thus speculated that the expression of activated Akt would also be downregulated in Ang II-stimulated *NFATc2-/-* mice. Our results showed an upregulation of pAkt (Ser473) in the stimulated

125

NFATc2+/+ hearts compared to normotensive *NFATc2*+/+ hearts, but no change in the stimulated *NFATc2*-/- hearts compared to their *NFATc2*+/+ counterparts (Figures 4.3a and 4.3c). Although two bands were visible when probing for total Akt, the lower band was deemed unspecific in mice using alkaline phosphatase treatment and Western blots on rat muscles (data not shown). In addition, pFoxo (Ser253), which is inhibited by the active form of Akt [174], was also unchanged with Ang II stimulation in both phenotypes (Figures 4.3b and 4.3e)

We also examined the protein levels of α-SMA, Vimentin and CnAβ (Figure 4.3). Here, we showed a slight but not significant increase in the expression of α-SMA in both stimulated *NFATc2*+/+ and *NFATc2*-/- hearts compared to normotensive ones. Nevertheless, there was no difference between *NFATc2*+/+ and *NFATc2*-/- mice (Figures 4.3a and 4.3d). Likewise, there was no difference in the expression of Vimentin (Figures 4.3b and 4.3f). Unlike qPCR results, our immunoblotting did not show a difference in CnAβ expression between stimulated *NFATc2*-/- and *NFATc2*+/+ hearts but a significant decrease in stimulated *NFATc2*-/- hearts compared to their normotensive *NFATc2*-/- counterparts (Figures 4.3b and 4.3g).

Since the changes in signaling observed in normotensive *NFATc2*-/- mice were compromised after 14 days Ang II stimulation, we decided to carry out 28 days Ang II implantation to further stress the hearts and examine the role of NFATc2 under very high stressing conditions.
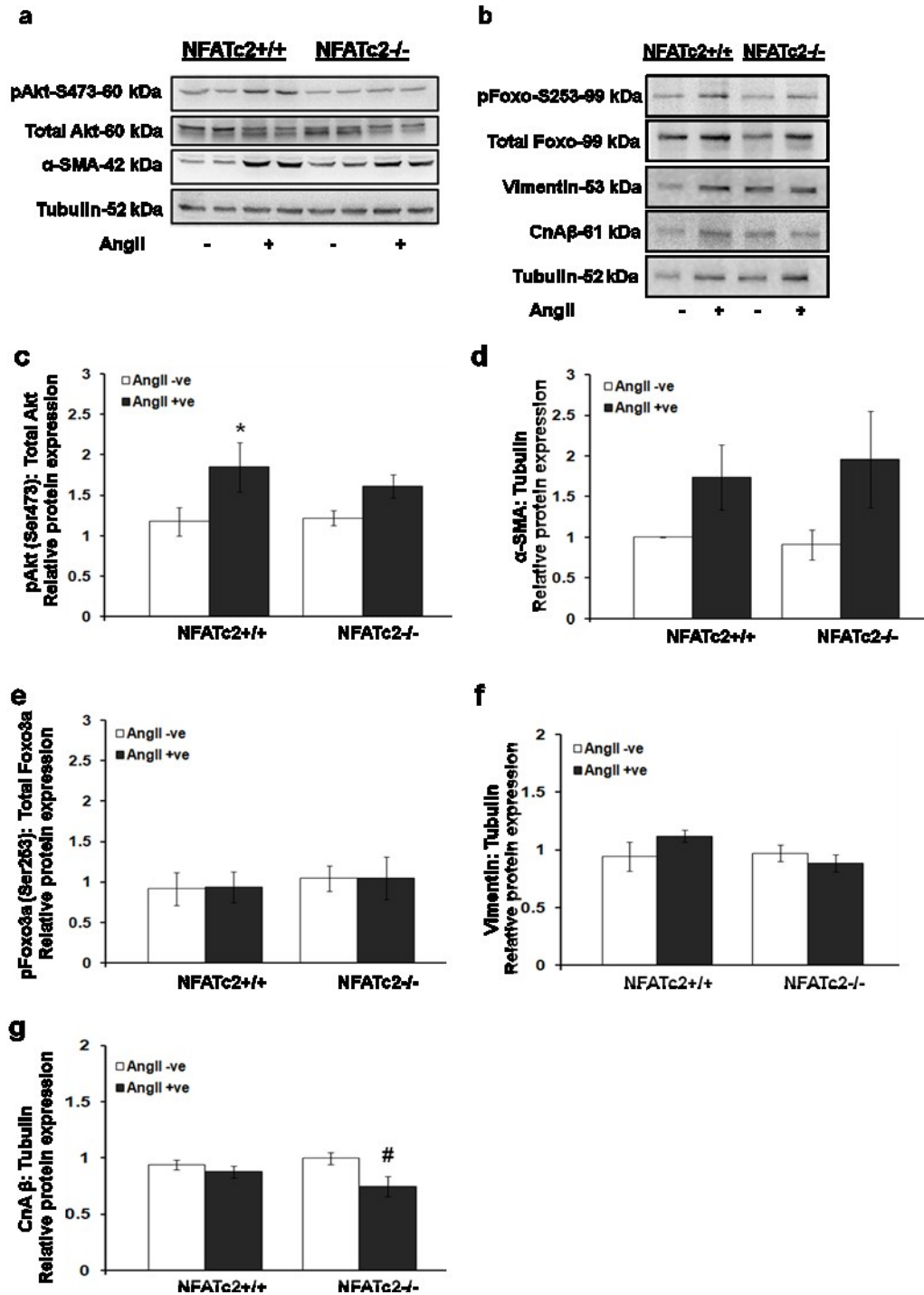
Figure 4.3: PAkt (Ser473), α-SMA, pFoxo3a (Ser253), Vimentin and CnAβ expression levels in the 14 day Ang II-stimulated mice

(**a**) Representative immunoblots for pAkt (Ser473), total Akt and α-SMA. (**b**) Representative immunoblots for pFoxo3a (Ser253), total Foxo3a, Vimentin and CnAβ. (**c-g**) Quantifications of the immunoblots normalized to α-tubulin expression (n=4; P<0.05). *compared to normotensive *NFATc2+/+*, $compared to stimulated *NFATc2+/+*, #compared to normotensive *NFATc2-/-*. Means ± SEM are shown.

4.5.8 The 28 day Ang II-stimulated *NFATc2-/-* hearts have similar features as their *NFATc2+/+* counterparts

The same collagen infiltrate, inflammatory and fibroblast markers used for the 14 day Ang II-stimulated hearts were used for the 28 day stimulated hearts. Thus, heart cross sections were stained for H&E, picrosirius red, CD45 and α-SMA (Figure 4.4a). Similar to the 14 day stimulation, we did not observe differences in those markers among the tested groups. However, picrosirius red in the stimulated hearts showed increased collagen infiltrate.

Additionally, we wanted to see if the prolonged Ang II stimulation has affected the Akt pathway. Immunoblotting for pAkt (Ser473) showed no changes in expression despite a slight increase in both stimulated *NFATc2+/+* and *NFATc2-/-* hearts (Figures 4.4b and 4.4d). In agreement with this finding, pFoxo3a (Ser253), was also unchanged with Ang II stimulation for 28 days in both phenotypes (Figures 4.4b and 4.4e).

We next set out to monitor the expression of the fibroblast markers Vimentin and α-SMA (Figures 4.4b and 4.4c). Both targets did not show any differences in expression between stimulated *NFATc2-/-* and stimulated *NFATc2+/+* hearts (Figures 4.4f and 4.4g). Interestingly, α-SMA was significantly higher in stimulated *NFATc2+/+* and *NFATc2-/-* compared to normotensive ones (Figure 4.4g).

In addition, we tested the expression of the cardio-protective genes *calsarcin-1* and *CnAβ* (Figure 4.4c). Interestingly calsarcin-1 was lower, whereas CnAβ was not changed in the stimulated hearts (Figures 4.4h and 4.4i).
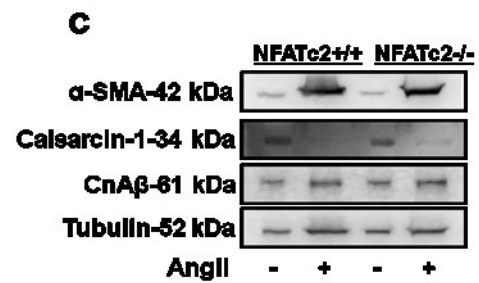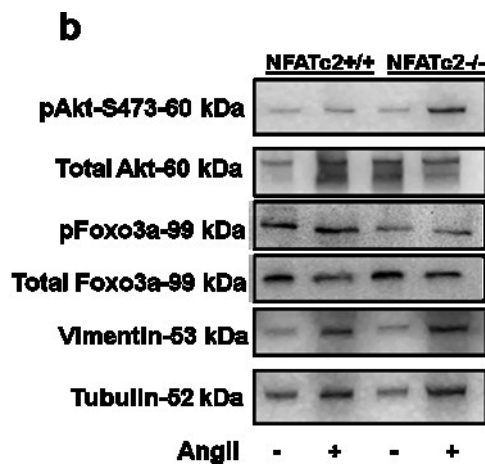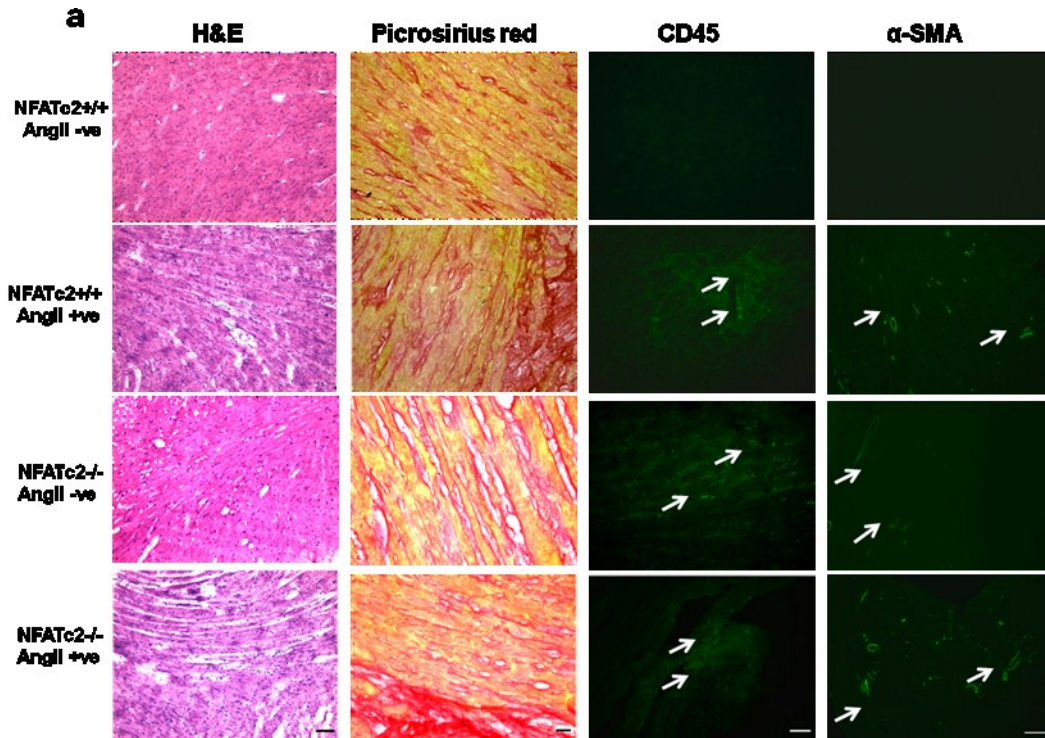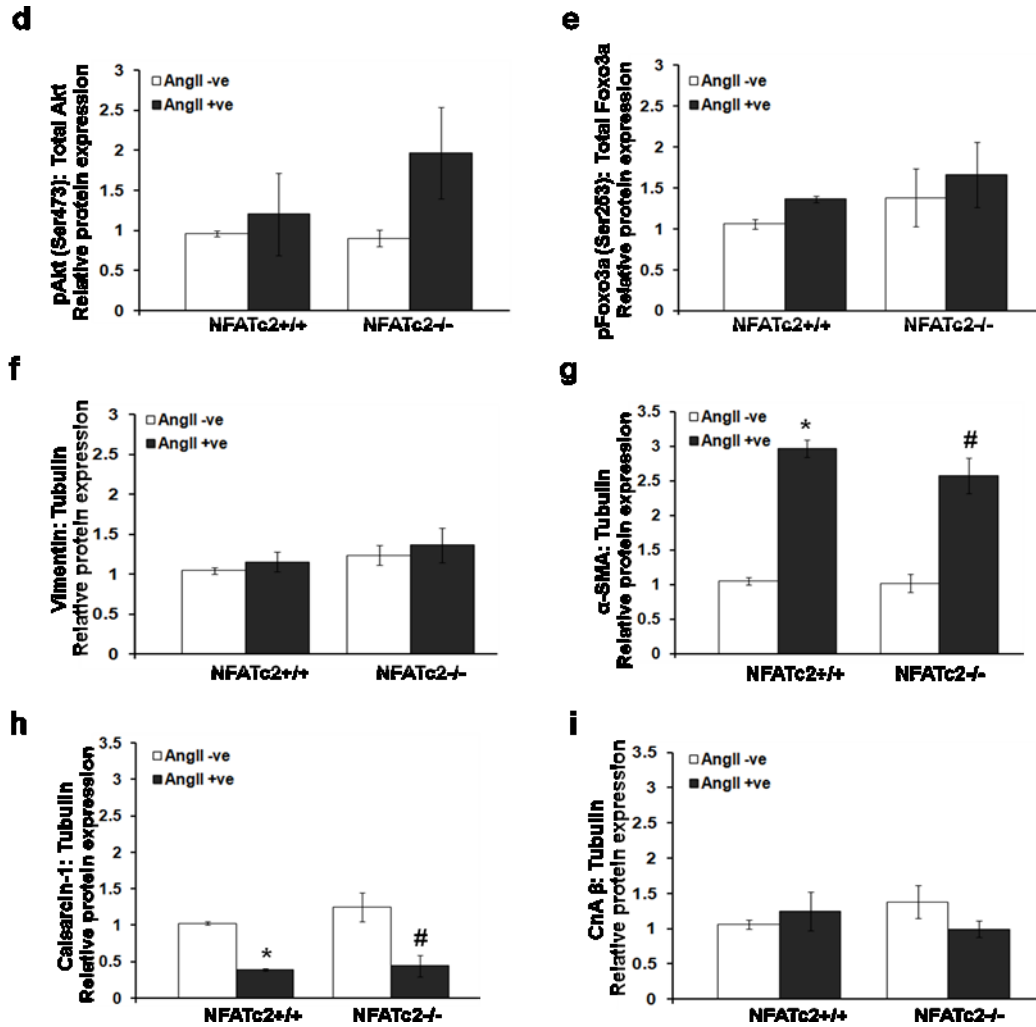
Figure 4.4: Absence of signaling changes between the hearts of the 28 day Ang II-stimulated *NFATc2*-/- mice and their *NFATc2*+/+ counterparts

(**a**) H&E, picrosirius red staining and IFs for CD45 and α-SMA demonstrate similar staining in the hearts of stimulated *NFATc2*-/- mice compared to *NFATc2*+/+ mice (n=3). Arrows indicate positive staining. Scale bars; 50µm for (H&E), 10µm for (Picrosirius red), 20µm for (CD45) and 100µm for (α-SMA). (**b-c**) Representative immunoblots for pAkt (Ser473), total Akt, pFoxo3a (Ser253), total Foxo3a, Vimentin, α-SMA, Calsarcin-1 and CnAβ expressions. (**d-i**) Quantifications of the immunoblots normalized to α-tubulin expression (n=3; P<0.05). *compared to normotensive *NFATc2*+/+, #compared to normotensive *NFATc2*-/-. Means ± SEM are shown.

4.6 Discussion

During the initial phase of our study, we observed that adult 6-9 month old *NFATc2*-/- mice were susceptible to sudden death and had enlarged hearts when autopsied. However, it has been demonstrated that 1-2 month old *NFATc2*-/- mice display a complete inhibition of forced hypertrophy, decreased cardiac fetal gene expression and reduced fibrosis, suggesting a clear protection against pathological cardiac remodeling in the absence of the NFATc2 [267]. Hence, we wanted to shed light on the role of NFATc2 transcription factor in Cn-mediated cardiac hypertrophy taking into consideration the age differences between our mice and the mice in the earlier study.

Although the hearts of 6-9 month old *NFATc2*-/- mice shared an overall similar gross morphology and HW/BW ratio as age and sex-matched *NFATc2*+/+ mice, only normotensive *NFATc2*-/- mice displayed a more dilated left ventricular chamber inner diameter and a thinner right ventricle wall, which are characteristics of compromised cardiac contractility and eventual heart failure (Appendix IV; Figure 1). In this case, the heart cannot supply the body with enough blood causing left ventricular enlargement and sudden death. Previous work has demonstrated that hearts of 1-2 month old *NFATc2*-/- mice display no significant change in left ventricular internal diameter and contractility of the left ventricle compared to *NFATc2*+/+ mice [267], which correlates with our findings in adult stimulated mice.

NFATc2 has been shown to be the major isoform responsible for cardiac hypertrophy [267], but other transcription factors are possibly compensating for its loss, raising questions about the cardio-protective role of NFATc2 at later stages of life.

Because no compensation by NFATc1, NFATc3 and NFATc4 was detected at the transcript level for the absence of functional NFATc2, we decided to monitor NFAT cellular localization. As transcription factors, NFAT proteins become active after being dephosphorylated by Cn, which enables nuclear translocation leading to increased expression of the cardiac fetal genes. Our IFs indicate that the nuclear translocation of NFATc1 was significantly higher in the normotensive hearts of *NFATc2-/-* mice, whereas nuclear NFATc3 and NFATc4 levels were unchanged (Appendix IV; Figure 2). Thus, NFATc1 may be compensating for NFATc2 in an attempt to increase growth-mediated transcription.

Dunn *et al.,* [297] have shown that Cn-mediated dephosphorylation of NFATc1 is correlated with increased muscle usage. They showed that normal weight-bearing soleus and functional overload-induced plantaris muscles express more dephosphorylated NFATc1. In addition, Shen *et al.,* [298] have demonstrated that NFATc1 has a higher cytoplasmic to nuclear shuttling rate in resting skeletal muscle cells compared to other NFAT proteins, which suggests that Cn/NFAT has a higher basal activity than other NFAT isoforms. In addition, the role of the NFATc1 transcription factor in heart function remains poorly understood since *NFATc1-/-* mice are embryonic lethal, whereas other *NFAT* knockout mice remain viable [299]. This suggests that NFATc1 is likely an important factor for physiological heart growth, which may explain why NFATc1 is the only isoform that compensates for the genetic loss of NFATc2 function in the heart. Nevertheless, NFATc1 might not be able to fully restore proper cardiomyocyte growth, function and size because *NFATc2-/-* mice display changes in the ventricles, which are characteristic of heart failure.

NFAT transcription factors can interact with molecular partners in the nucleus to re-activate cardiac fetal genes in response to hypertrophic stimuli leading to heart failure [79, 92, 149, 300]. Our results showed that nuclear protein expression of GATA4 is significantly elevated in both whole homogenate and fractionated hearts of *NFATc2-/-* mice (Appendix IV; Figure 3). As a well-characterized marker of cardiac hypertrophy, such an increased level of GATA4 protein might be a strong indicator of a diseased, overly stressed and most likely failed heart. Both *in vitro* and *in vivo* overexpression of GATA4 is necessary and sufficient to induce morphological, functional, molecular and structural changes resulting in cardiomyocyte remodeling and failure [283, 301, 302]. The significant increase in GATA4 protein expression and nuclear import in *NFATc2-/-* mice suggests that GATA4 is compensating for the absence of functional NFATc2. Similar to NFATc1, GATA4 may be attempting to promote transcriptional growth in the hearts of *NFATc2-/-* mice, but cannot completely compensate for the lack of NFATc2, causing these hearts to fail in adulthood.

Because some changes in signaling were minimal or absent in normotensive hearts, we stimulated cardiac hypertrophy in mice using Ang II for 14 and 28 days. As observed in normotensive hearts, the HW/BW ratio of 6 month old 14 day Ang II-stimulated *NFATc2-/-* mice was similar to that of Ang II-stimulated *NFATc2+/+* mice, but it was higher in stimulated hearts compared to normotensive ones, suggesting a preserved ability of these hearts to develop hypertrophy due to induced stress (Appendix IV; Figure 4a). These results differ from previous work showing that 1-2 month old Ang II-stimulated *NFATc2-/-* mice display a HW/BW ratio that is significantly lower than *NFATc2+/+* counterparts [267]. The latter suggests that there could be a difference

between young and adult mice in the role of NFATc2 in the heart, and this interesting possibility should be confirmed by future studies with direct side-by-side comparison of the two age groups.

We initially expected that the transcript expression of *β-MyHC*, *ANP* and *BNP* would be increased in Ang II-stimulated adult *NFATc2-/-* mice, which would suggest that these mice are more vulnerable to cardiac disease. Although we observed increased *β-MyHC* expression, *ANP* and *BNP* expression did not change in Ang II-stimulated *NFATc2-/-* mice compared to their *NFATc2+/+* counterparts (Appendix IV; Figures 4c-4f). As a major structural protein in the myocardial sarcomeric contractile unit, β-MyHC is thought to be a more representative indirect marker of pathological cardiac hypertrophy and failure [303]. Abraham *et al.,* [303] found that *β-MyHC* transcript expression incrementally declines when patients having idiopathic dilated cardiomyopathy are treated with β-blockers, whereas ANP expression decreases in both placebo and β-blocker treated groups. This indicates that ANP responds non-specifically to the method of treatment and that the regulation of other cardiac fetal genes might be controlled by a separate mechanism from that of the cardiac MyHC isoforms. In addition, it seems that once hearts are hypertrophied with Ang II, changes in contractile protein expression take place causing these hearts to fail.

As a known negative regulator of Cn signaling in the heart, *in vitro* and *in vivo* work has shown that overexpression of *calsarcin-1* attenuates Ang II-mediated cardiac hypertrophy [263]. In *NFATc2+/+* mice, *calsarcin-1* was increased in expression following stimulation as an initial cellular reaction to increased load and as a rescue response. However, it was not changed in Ang II-stimulated *NFATc2-/-* mice compared

to stimulated *NFATc2+/+* mice, indicating decreased protective properties in NFATc2-deficient hearts (Figure 4.1a). Moreover, calsarcin-1 protein level was downregulated in the 28 day Ang II-stimulated mice compared to normotensive hearts, suggesting the absence of cardio-protection (Figure 4.4h). Whether NFATc2 has a role in regulating *calsarcin-1* gene expression as a manner for preventing heart failure remains unclear.

Recent studies have demonstrated that mice overexpressing cardiac *CnAβ1* are not subject to hypertrophy, but rather display a cardio-protective function through activation of the Akt and S̲erum and G̲lucocorticoid-regulated K̲inase (SGK) pathway [65]. In our study, *CnAβ1* expression was increased following 14 day Ang II treatment in *NFATc2+/+* mice, suggesting that its expression is activated as a protective measure in response to induced stress. In contrast, *CnAβ1* expression was decreased in stimulated *NFATc2-/-* mice, which indicates that additional exerted stress by Ang II treatment may have caused those hearts to pass a critical stage for recovery and to lose the cardio-protective functions of CnAβ1 (Figure 4.1b). It is noteworthy that the change in CnAβ expression between stimulated *NFATc2-/-* and *NFATc2+/+* mice was restricted to the transcript, but not protein level suggesting a possible post-transcriptional modification of CnAβ in the hearts of *NFATc2-/-* mice (Figures 4.3g and 4.4i).

Further, ATF4 activates an amino acid biosynthesis program and mediates the cardio-protective effect produced by CnAβ$_1$ [65, 180, 181]. Here, ATF4 worked in concert with CnAβ1, and showed a tendency for upregulation in the stimulated *NFATc2+/+* mice perhaps to produce a protective effect. However, it was unchanged in the stimulated *NFATc2-/-* compared to normotensive ones, suggesting once more the loss of protection after Ang II stimulation (Figure 4.1c).

Foxo factors are the downstream targets of pAkt which represses Foxo transcription and thus inhibits protein degradation [174]. All members of the Foxo family except Foxo6 are essential for cardiac function [304]. Akt phosphorylates Foxo3a at Ser253, which masks its nuclear localization sequence, leading to its export from the nucleus to the cytoplasm [305, 306]. Thus, Akt signaling is a major regulator of Foxo activity. In this context, we showed an upregulation of Foxo3a only at the transcript level in the stimulated *NFATc2-/-* mice compared to normotensive *NFATc2-/-* mice but with no significant difference compared to stimulated *NFATc2+/+* mice, suggesting a possible shift toward protein degradation in the knockout stressed hearts (Figure 4.1d).

The exact role of myostatin in the heart is still being established and several studies have reported an elevated myostatin expression in mammalian models of heart failure [286-289]. Heineke *et al.,* [307] showed that the heart can actively secrete myostatin to skeletal muscles to induce cachexia in an endocrine manner and that the genetic deletion of myostatin in the heart inhibits skeletal muscle wasting. Another report has shown that myostatin inhibition could contribute to repairing damaged cardiac muscle fibers by increasing contractility and Ca^{2+} influx into cardiomyocytes, both of which are features of physiological cardiac hypertrophy [308]. Furthermore, myostatin plasma levels correlate with biomarkers of heart failure severity [288]. In agreement with Foxo3a expression levels, we showed that *myostatin* is significantly upregulated in the hearts of stimulated *NFATc2-/-* mice, which signifies that these mice have a greater susceptibility to heart failure (Figure 4.1e). The collective findings that *CnAβ1* is lowered, and that *myostatin* and *Foxo3a* are elevated in the hearts of Ang II-treated *NFATc2-/-* mice, suggest that these hearts may have passed a critical stage of heart failure

severity in which rescue is not feasible. These results also suggest that induced cardiac hypertrophy causes a shift in gene expression profiles toward a more damaged status.

Additionally, both the 14 and 28 day stimulated hearts from *NFATc2+/+* and *NFATc2-/-* mice did not show variations in any of the damage markers used in this study, suggesting that NFATc2 is neither protecting nor exacerbating the hearts of adult mice exposed to pathological stress (Figures 4.2a and 4.4a).

Upon imitating cardiac workload by Ang II stimulation, we observed that activated pAkt (Ser473) was higher in the hearts of the 14 day Ang II-stimulated *NFATc2+/+* mice than in normotensive mice supporting previous findings [309]. This observation suggests that the upregulation of pAkt expression in the stimulated *NFATc2+/+* was an attempt to overcome the stress produced by Ang II. However, this attempt did not work with the stimulated *NFATc2-/-* hearts since the expression of pAkt was unchanged in the hearts of the 14 day Ang II-stimulated *NFATc2-/-* mice, which suggests an inactivation of translational-mediated cardiac growth in *NFATc2-/-* mice (Figure 4.3c). After 28 days of Ang II stimulation no change was observed, suggesting an inactivation of the Akt growth pathway due to Ang II stimulation as opposed to the loss of NFATc2 (Figure 4.4d).

The knockdown of α-SMA in embryonic stem cells using RNA interference has been shown to affect cardiac differentiation [310]. In addition, it has been shown that α-SMA is expressed during pressure-overload hypertrophy [311]. Another study has found an absence of α-SMA in cardiomyocytes during various pathological situations [312]. We showed a non-significant increase in the expression of α-SMA in the 14 day stimulated *NFATc2+/+* and *NFATc2-/-* hearts compared to their normotensive controls, without any

difference between the stimulated hearts (Figure 4.3d). In the 28 day Ang II-stimulated hearts, there was a significant increase in α-SMA in the stimulated hearts compared to the normotensive ones, which is most likely due to prolonged Ang II stimulation (Figure 4.4g).

Vimentin also has been used as a reliable fibroblast marker in many recent studies to identify cardiac myofibroblasts [313, 314]. Vimentin expression was unchanged among the tested groups in both the 14 and 28 day Ang II-stimulated hearts (Figures 4.3f and 4.4f). This indicates that prolonged Ang II stimulation does not affect the expression of Vimentin, which was not the case for α-SMA expression in the 28 day Ang II-stimulated hearts.

Our work provides evidence that Cn/NFAT signaling has a crucial role in the normal function of the adult heart, contrary to the general theory which postulates that Cn signaling is responsible for cardiac disorders, heart failure and sudden death. Physiological and biochemical signaling alterations in the hearts of *NFATc2-/-* mice indicate that these mice are susceptible to disease, which provides further insights toward understanding the importance of the Cn/NFATc2 pathway in the adult heart. Bourajjaj *et al.,* [267] provided additional evidence that the absence of NFATc2 produces clear protection against cardiac hypertrophy in young mice. Our study showed that NFATc2 might produce cardio-protection in adult non-stressed hearts. However, this protection was minimized after stressing the hearts for 14 days and completely lost after 28 days of Ang II-stimulation. Nevertheless, the loss of NFATc2 isoform neither exacerbated the response of the hearts of adult mice nor prevented hypertrophy.

Moreover, NFATc1 nuclear localization was significantly higher in normotensive *NFATc2-/-* mice compared to normotensive *NFATc2+/+* mice (Appendix IV; Figure 2c), and nuclear localization had a tendency to increase (P=0.05) in the hearts of 14 day stimulated *NFATc2-/-* mice compared to their *NFATc2+/+* counterparts (Figure 4.6c). Thus, our results from this study implicate a compensation for loss of NFATc2 by the NFATc1 isoform. Another explanation might be related to the fact that stressing the hearts for 14 or even 28 days with a potent drug like Ang II, might have caused a level of damage which masked any difference between *NFATc2-/-* and *NFATc2+/+* mice, as those hearts have reached a damaged point which could not be exceeded. Over time, changes in growth-mediated signaling may predispose these mice to eventual heart deterioration and overt heart failure due to Ang II-mediated stress rather than through loss of the NFATc2 isoform. Therefore, there is still much to be explored about this branch of Cn-mediated cardiac hypertrophy.

Bourajjaj *et al.,* [267] proposed that because the hearts of young 1-2 month old *NFATc2-/-* or *NFATc3-/-* mice are either totally or partially impaired in their ability to grow in response to Cn-mediated hypertrophy, a combined *NFATc2c3-/-* mouse would display more complete inhibition to hypertrophy. Whether similar effects would be seen in adult *NFATc3-/-*, remains to be elucidated. Additionally, there are many signaling effectors that can regulate both physiological and pathophysiological cardiac growth and it is difficult to identify which other pathways could be activated or inactivated in the *NFATc2-/-* mouse model. An interesting pathway to investigate in *NFATc2-/-* mice would be that involving the Ca^{2+}/CaM dependent Kinases (CaMK). It is likely that a disruption of Cn/NFATc2 signaling may be compensated by a parallel branch of the Ca^{2+}/CaM

pathway. Transgenic mice overexpressing CaMK II in the heart are subject to cardiac hypertrophy, which is likely caused by increased nuclear export and dissociation of class II Histone Deacetylases (HDAC) from the DNA, allowing the Myocyte Enhancer Factor 2 (MEF2) and other transcription factors to bind DNA more readily to compensate for the absence of NFATc2 [171, 285, 315, 316].

All these data collectively will help explain the role of NFATc2 in Cn-mediated cardiac hypertrophy in normal hearts and following biochemical stress, which leads to deterioration, further damage and eventual death.

Chapter 5 : **General conclusions**

The Ca^{2+}/calmodulin-dependent phosphatase, Calcineurin (Cn) and its downstream transcriptional target, the Nuclear Factor of Activated T cells (NFAT) play a major role in controlling a variety of muscle diseases. Strategies that aim to control the amount of Cn may be of great value in identifying novel pharmacological targets for the treatment of muscle disorders. This research provides new insights into understanding different mechanisms by which Cn regulates and affects muscle diseases. The involvement of the Cn/NFAT pathway in Duchenne Muscular Dystrophy (DMD) has been thoroughly discussed in previous studies. These studies manipulated the activity of Cn, using several transgenic models that target either Cn or calmodulin [98, 106]. However, the study presented here is the first that shows manipulation of Ca^{2+} kinetics and the effect of such manipulation on Cn activity as well as on the expression of important genes such as *utrophin*. We provide information about the expression of other proteins including the Heat Shock Protein 70 (HSP70) in *mdx* and *mdx* crossbreeds. This protein recently has been shown to be involved in ameliorating the symptoms of DMD in the absence of utrophin [150]. Our results show no correlation between utrophin and HSP70 suggesting that the two proteins are regulated by different mechanisms. This looks exciting, as it shows the possibility that other pathways are involved in the regulation of DMD. Thus, targeting more than one pathway might be a more effective countermeasure for treating muscle dystrophy. Additionally, understanding the roles of various Cn modulators will help to clarify what is still unknown about this disease. Figure 5.1 illustrates the three transgenes used in this thesis and shows the effect of the PV transgene on the Cn/NFAT pathway. It also shows that HSP70 does not work through the same pathway suggesting alternative explanations.
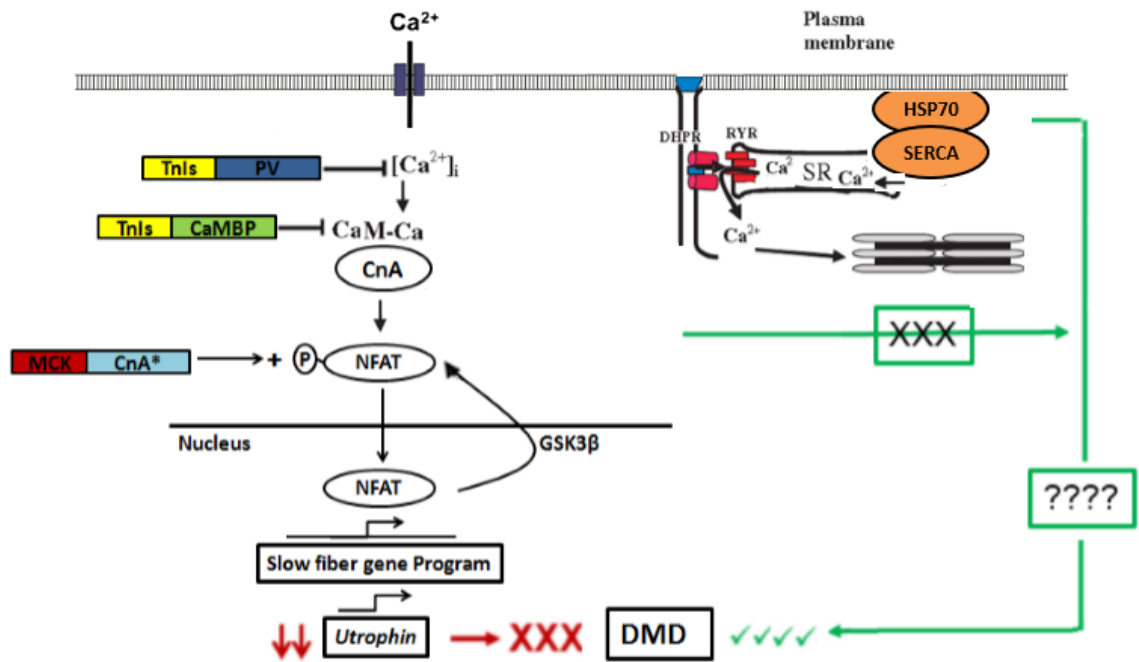
Figure 5.1: Schematic diagram showing the three transgenes used to manipulate the Cn/NFAT pathway and showing the effect of HSP70 on DMD

In addition, our research provides evidence that normal Cn/NFAT signaling has a crucial role in the function of the adult heart. Thus, it is not the high Cn activity that causes deterioration in cardiac hypertrophy, but the inability to adapt to and utilize high Cn levels. In accordance, we provide new insights toward understanding the importance of the Cn/NFAT pathway in the adult heart. Interestingly, our study might help in investigating pharmacological interventions to treat cardiac disorders.

Chapter 6 : **Future Directions**

As it is one of the crucial Ca^{2+} signaling pathways involved in muscle diseases, it is important to continue research involving the Cn/NFAT pathway. This will lead to a better understanding of the regulation of Cn and its modulators in muscle disorders. In this manuscript-based thesis, we dealt with two important muscle diseases: Duchenne muscular dystrophy and cardiac hypertrophy, in which Cn and its effectors play a major role in their progression. The results of the second chapter (First manuscript): "Distinct calcineurin-related transgenic approaches rescue or exacerbate the dystrophic phenotype in fibers from crossbred *mdx* mice despite constant HSP70 expression" are completed and ready for submission to one of the most effective journals in the field such as *The FASEB Journal,* which has many contributions to health. As our results showed that utrophin-A and HSP70 are regulated by different mechanisms, I believe the next manuscript should involve research on the pathways that might be regulating HSP70 as well as other HSP isoforms, which also might have roles in muscle dystrophy. Suggestions for such pathways are included in the discussion of Chapter 2 in this thesis.

Similarly, the results of the fourth chapter (Third manuscript): "The role of NFATc2 transcription factor in Calcineurin-dependent cardiac hypertrophy in adult mice" are completed and ready for submission to one of the important cardiology journals such as the *Journal of Molecular and Cellular Cardiology.* Since our work investigates the role of the NFATc2 transcription factor and since little is known about the role of NFATc3 in the heart, it would be interesting for the next manuscript to involve research on the role of the double knockout model *NFATc2c3-/-* in the hearts of adult mice. In our laboratory, we already have this model and mice are being bred continuously.

The third chapter of this thesis (Second manuscript): "Direct calcineurin modulators regulate calcineurin/NFAT signaling in *mdx* crossbreeds" is a manuscript in preparation, which needs a lot of work to be finalized for publication. Our preliminary results confirm the dual regulation of RCAN for Cn, which was observed earlier by the Olson group while they investigated the role of RCAN1 in cardiac hypertrophy [261]. However, RCAN could be phosphorylated by different kinases, which might affect its stability. Therefore, it would be interesting to explore those kinases and study how phosphorylation affects both the expression and stability of RCAN. Since our results might be correlated to the time the expression of RCAN was measured, as mentioned in the discussion of Chapter 3, it might be worth measuring RCAN expression in different time points; during development, in young and in adult mice. Additionally, the knockout of the *RCAN* gene in *mdx* mice, with either impaired Cn activity such as *mdx*/PV or stimulated Cn activity such as *mdx*/CnA*, might better reveal the role of RCAN in the Cn/NFAT pathway.

Similar to RCAN, mice lacking *calsarcin-1* crossed with CnA* mice show an enhanced hypertrophic response [262], suggesting a cardio-protective role for calsarcin-1. Since calsarcins can shuttle to the nucleus [194], investigating whether they interact with NFAT in the nucleus might explain the current results. Moreover, Vondrisk's group has documented phosphorylation and post-translational processing of calsarcin-1 during heart diseases [265], which is worth looking into in the future.

Since MLP is suggested to negatively regulate skeletal and cardiac myofiber responses [196], it is thus essential to study the proteins that possibly interact and affect MLP. In this context, it is noteworthy that the fast muscle EDL was used in the qPCR

reactions of MLP in WT, CnA*, *mdx* and *mdx*/CnA* mice, whereas the fast muscle TA was used for the immunoblotting reactions in the same mice. Therefore, it would be important to replicate those experiments using the same type of muscle, in case there is any discrepancy between EDL and TA tissues.

Finally, it has been shown that CAIN works in a negative regulatory loop and becomes hyperphosphorylated upon activation of PKC, which in turn affects Cn activity (reviewed in [192]). Further, it was suggested that CAIN competes with NFAT or other substrates of Cn [192]. Therefore, it is worth studying the expression and binding of CAIN with other transcription factors. This might help in understanding how this protein works to inhibit and regulate Cn.

As discussed earlier in Chapter 3, research is continuing to overexpress and/or knockdown the genes encoding Cn modulators in order to understand their roles in muscle diseases particularly in muscle dystrophy. The objective of this research would be of great value to show the importance of inhibiting Cn modulators that inhibit Cn activity. Consequently, inhibiting the inhibitors will maintain effective Cn levels, which stimulate the Cn/NFAT pathway without side effects.

References

1. Martini, F. and J. Nath, *The Tissue Level Of Organization.* Fundamentals of Anatomy & Physiology, 8th Ed., Pearson Education, Inc, 2009: p. 326-328.
2. Jenkins, G.W., C.P. Kemnitz and G.J. Tortora, *Anatomy and Physiology: from science to life.* John Wiley & Sons Inc, 2010.
3. Clark, K.A., A.S. McElhinny, M.C. Beckerle and C.C. Gregorio, *Striated muscle cytoarchitecture: an intricate web of form and function.* Annu Rev Cell Dev Biol, 2002. **18**: p. 637-706.
4. Frank, D. and N. Frey, *Cardiac Z-disc signaling network.* J Biol Chem, 2011. **286**(12): p. 9897-904.
5. Tajbakhsh, S., *Skeletal muscle stem cells in developmental versus regenerative myogenesis.* J Intern Med, 2009. **266**(4): p. 372-89.
6. Parker, M.H., P. Seale and M.A. Rudnicki, *Looking back to the embryo: defining transcriptional networks in adult myogenesis.* Nat Rev Genet, 2003. **4**(7): p. 497-507.
7. Schmalbruch, H. and D.M. Lewis, *Dynamics of nuclei of muscle fibers and connective tissue cells in normal and denervated rat muscles.* Muscle Nerve, 2000. **23**(4): p. 617-26.
8. Charge, S.B. and M.A. Rudnicki, *Cellular and molecular regulation of muscle regeneration.* Physiol Rev, 2004. **84**(1): p. 209-38.
9. Tidball, J.G. and M. Wehling-Henricks, *Macrophages promote muscle membrane repair and muscle fibre growth and regeneration during modified muscle loading in mice in vivo.* J Physiol, 2007. **578**(Pt 1): p. 327-36.
10. Hill, M., A. Wernig and G. Goldspink, *Muscle satellite (stem) cell activation during local tissue injury and repair.* J Anat, 2003. **203**(1): p. 89-99.
11. Bentzinger, C.F., Y.X. Wang and M.A. Rudnicki, *Building muscle: molecular regulation of myogenesis.* Cold Spring Harb Perspect Biol, 2012. **4**(2).
12. Davis, R.L., H. Weintraub and A.B. Lassar, *Expression of a single transfected cDNA converts fibroblasts to myoblasts.* Cell, 1987. **51**(6): p. 987-1000.
13. Braun, T., G. Buschhausen-Denker, E. Bober, E. Tannich and H.H. Arnold, *A novel human muscle factor related to but distinct from MyoD1 induces myogenic conversion in 10T1/2 fibroblasts.* EMBO J, 1989. **8**(3): p. 701-9.
14. Braun, T., E. Bober, B. Winter, N. Rosenthal and H.H. Arnold, *Myf-6, a new member of the human gene family of myogenic determination factors: evidence for a gene cluster on chromosome 12.* EMBO J, 1990. **9**(3): p. 821-31.
15. Weintraub, H., R. Davis, S. Tapscott, M. Thayer, M. Krause, R. Benezra, T.K. Blackwell, D. Turner, R. Rupp, S. Hollenberg and et al., *The myoD gene family: nodal point during specification of the muscle cell lineage.* Science, 1991. **251**(4995): p. 761-6.
16. Sabourin, L.A., A. Girgis-Gabardo, P. Seale, A. Asakura and M.A. Rudnicki, *Reduced differentiation potential of primary MyoD-/- myogenic cells derived from adult skeletal muscle.* J Cell Biol, 1999. **144**(4): p. 631-43.
17. Seale, P., A. Asakura and M.A. Rudnicki, *The potential of muscle stem cells.* Dev Cell, 2001. **1**(3): p. 333-42.
18. Cao, Y., R.M. Kumar, B.H. Penn, C.A. Berkes, C. Kooperberg, L.A. Boyer, R.A. Young and S.J. Tapscott, *Global and gene-specific analyses show distinct roles for Myod and Myog at a common set of promoters.* EMBO J, 2006. **25**(3): p. 502-11.

19.   Zhang, W., R.R. Behringer and E.N. Olson, *Inactivation of the myogenic bHLH gene MRF4 results in up-regulation of myogenin and rib anomalies.* Genes Dev, 1995. **9**(11): p. 1388-99.

20.   Ferri, P., E. Barbieri, S. Burattini, M. Guescini, A. D'Emilio, L. Biagiotti, P. Del Grande, A. De Luca, V. Stocchi and E. Falcieri, *Expression and subcellular localization of myogenic regulatory factors during the differentiation of skeletal muscle C2C12 myoblasts.* J Cell Biochem, 2009. **108**(6): p. 1302-17.

21.   Buckingham, M. and F. Relaix, *The role of Pax genes in the development of tissues and organs: Pax3 and Pax7 regulate muscle progenitor cell functions.* Annu Rev Cell Dev Biol, 2007. **23**: p. 645-73.

22.   Lagha, M., T. Sato, L. Bajard, P. Daubas, M. Esner, D. Montarras, F. Relaix and M. Buckingham, *Regulation of skeletal muscle stem cell behavior by Pax3 and Pax7.* Cold Spring Harb Symp Quant Biol, 2008. **73**: p. 307-15.

23.   McCroskery, S., M. Thomas, L. Maxwell, M. Sharma and R. Kambadur, *Myostatin negatively regulates satellite cell activation and self-renewal.* J Cell Biol, 2003. **162**(6): p. 1135-47.

24.   McFarlane, C., A. Hennebry, M. Thomas, E. Plummer, N. Ling, M. Sharma and R. Kambadur, *Myostatin signals through Pax7 to regulate satellite cell self-renewal.* Exp Cell Res, 2008. **314**(2): p. 317-29.

25.   Grifone, R., J. Demignon, C. Houbron, E. Souil, C. Niro, M.J. Seller, G. Hamard and P. Maire, *Six1 and Six4 homeoproteins are required for Pax3 and Mrf expression during myogenesis in the mouse embryo.* Development, 2005. **132**(9): p. 2235-49.

26.   Fishman, M.C. and K.R. Chien, *Fashioning the vertebrate heart: earliest embryonic decisions.* Development, 1997. **124**(11): p. 2099-117.

27.   Icardo, J.M., *Developmental biology of the vertebrate heart.* J Exp Zool, 1996. **275**(2-3): p. 144-61.

28.   Cantor, A.B. and S.H. Orkin, *Transcriptional regulation of erythropoiesis: an affair involving multiple partners.* Oncogene, 2002. **21**(21): p. 3368-76.

29.   Kathiriya, I.S. and D. Srivastava, *Left-right asymmetry and cardiac looping: implications for cardiac development and congenital heart disease.* Am J Med Genet, 2000. **97**(4): p. 271-9.

30.   Eisenberg, L.M. and R.R. Markwald, *Molecular regulation of atrioventricular valvuloseptal morphogenesis.* Circ Res, 1995. **77**(1): p. 1-6.

31.   Yihan, S., L. Guozhen and C. Tingfen, *Paraxial and intermediate mesoderm*. Online lectures on cardiac development.

32.   Moorman, A.F., F. de Jong, M.M. Denyn and W.H. Lamers, *Development of the cardiac conduction system.* Circ Res, 1998. **82**(6): p. 629-44.

33.   Schiaffino, S. and C. Reggiani, *Fiber types in mammalian skeletal muscles.* Physiol Rev, 2011. **91**(4): p. 1447-531.

34.   Schiaffino, S., M. Sandri and M. Murgia, *Activity-dependent signaling pathways controlling muscle diversity and plasticity.* Physiology (Bethesda), 2007. **22**: p. 269-78.

35.   Edstrom, L. and E. Kugelberg, *Histochemical composition, distribution of fibres and fatiguability of single motor units. Anterior tibial muscle of the rat.* J Neurol Neurosurg Psychiatry, 1968. **31**(5): p. 424-33.

36.   Brooke, M.H. and K.K. Kaiser, *Muscle fiber types: how many and what kind?* Arch Neurol, 1970. **23**: p. 369–379.

37.   Guth, L. and F.J. Samaha, *Qualitative differences between actomyosin ATPase of slow and fast mammalian muscle.* Exp Neurol, 1969. **25**: p. 138-152.

38.   Peter, J.B., R.J. Barnard, V.R. Edgerton, C.A. Gillespie and K.E. Stempel, *Metabolic profiles of three fiber types of skeletal muscle in guinea pigs and rabbits.* Biochemistry, 1972. **11**(14): p. 2627-33.

39.   Bar, A. and D. Pette, *Three fast myosin heavy chains in adult rat skeletal muscle.* FEBS Lett, 1988. **235**(1-2): p. 153-5.

40.   Schiaffino, S., L. Gorza, S. Sartore, L. Saggin, S. Ausoni, M. Vianello, K. Gundersen and T. Lomo, *Three myosin heavy chain isoforms in type 2 skeletal muscle fibres.* J Muscle Res Cell Motil, 1989. **10**(3): p. 197-205.

41.   Bottinelli, R., R. Betto, S. Schiaffino and C. Reggiani, *Unloaded shortening velocity and myosin heavy chain and alkali light chain isoform composition in rat skeletal muscle fibres.* J Physiol, 1994. **478 (Pt 2)**: p. 341-9.

42.   Bottinelli, R., S. Schiaffino and C. Reggiani, *Force-velocity relations and myosin heavy chain isoform compositions of skinned fibres from rat skeletal muscle.* J Physiol, 1991. **437**: p. 655-72.

43.   Pette, D. and G. Vrbova, *What does chronic electrical stimulation teach us about muscle plasticity?* Muscle Nerve, 1999. **22**(666-677).

44.   Ausoni, S., L. Gorza, S. Schiaffino, K. Gundersen and T. Lomo, *Expression of myosin heavy chain isoforms in stimulated fast and slow rat muscles.* J Neurosci, 1990. **10**(1): p. 153-60.

45.   Gundersen, K., *Excitation-transcription coupling in skeletal muscle: the molecular pathways of exercise.* Biol Rev Camb Philos Soc, 2011. **86**(3): p. 564-600.

46.   Nakao, K., W. Minobe, R. Roden, M.R. Bristow and L.A. Leinwand, *Myosin heavy chain gene expression in human heart failure.* J Clin Invest, 1997. **100**(9): p. 2362-70.

47.   Sieck, G.C. and M. Regnier, *Invited Review: plasticity and energetic demands of contraction in skeletal and cardiac muscle.* J Appl Physiol, 2001. **90**(3): p. 1158-64.

48.   Holubarsch, C., R.P. Goulette, R.Z. Litten, B.J. Martin, L.A. Mulieri and N.R. Alpert, *The economy of isometric force development, myosin isoenzyme pattern and myofibrillar ATPase activity in normal and hypothyroid rat myocardium.* Circ Res, 1985. **56**(1): p. 78-86.

49.   Izumo, S., A.M. Lompre, R. Matsuoka, G. Koren, K. Schwartz, B. Nadal-Ginard and V. Mahdavi, *Myosin heavy chain messenger RNA and protein isoform transitions during cardiac hypertrophy. Interaction between hemodynamic and thyroid hormone-induced signals.* J Clin Invest, 1987. **79**(3): p. 970-7.

50.   Bottinelli, R. and C. Reggiani, *Skeletal Muscle Plasticity in Health and Disease From Genes to Whole Muscle.* Springer, 2006.

51.   Berchtold, M.W., H. Brinkmeier and M. Muntener, *Calcium ion in skeletal muscle: its crucial role for muscle function, plasticity, and disease.* Physiol Rev, 2000. **80**(3): p. 1215-65.

52.   Al-Shanti, N. and C.E. Stewart, *Ca2+/calmodulin-dependent transcriptional pathways: potential mediators of skeletal muscle growth and development.* Biol Rev Camb Philos Soc, 2009. **84**(4): p. 637-52.

53.   Braunewell, K.H. and E.D. Gundelfinger, *Intracellular neuronal calcium sensor proteins: a family of EF-hand calcium-binding proteins in search of a function.* Cell Tissue Res, 1999. **295**(1): p. 1-12.

54.   Ikura, M., *Calcium binding and conformational response in EF-hand proteins.* Trends Biochem Sci, 1996. **21**(1): p. 14-7.

55.   Kretsinger, R.H., *Calcium coordination and the calmodulin fold: divergent versus convergent evolution.* Cold Spring Harb Symp Quant Biol, 1987. **52**: p. 499-510.

56.   Woodgett, J., *GSK3 Glycogen synthase kinase-3. In: The Protein Kinase Facts Book, edited by G. Hardie and S. Hanks. .* New York:Academic, 1995: p. 231-233.

57.   Kennedy, M.B., *CaMKII CaM-dependent PK II. In: The Protein Kinase Facts Book, edited by G. Hardie and S. Hanks.* New York: Academic, 1995: p. 131-134.

58.   Guerini, D., *Calcineurin. In: Guidebook to the Calcium-Binding Proteins, edited by M. R. Celio.* Oxford, UK: Oxford Univ. Press, 1996: p. 30-32.

59.   Aramburu, J., A. Rao and C.B. Klee, *Calcineurin: from structure to function.* Current topics in cellular regulation, 2000. **36**: p. 237-95.

60.   Rusnak, F. and P. Mertz, *Calcineurin: form and function.* Physiological reviews, 2000. **80**(4): p. 1483-521.

61.   Klee, C.B., H. Ren and X. Wang, *Regulation of the calmodulin-stimulated protein phosphatase, calcineurin.* J Biol Chem, 1998. **273**(22): p. 13367-70.

62.   Shibasaki, F., U. Hallin and H. Uchino, *Calcineurin as a multifunctional regulator.* J Biochem, 2002. **131**(1): p. 1-15.

63.   Yang, S.A. and C.B. Klee, *Low affinity Ca2+-binding sites of calcineurin B mediate conformational changes in calcineurin A.* Biochemistry, 2000. **39**(51): p. 16147-54.

64.   Lara-Pezzi, E., N. Winn, A. Paul, K. McCullagh, E. Slominsky, M.P. Santini, F. Mourkioti, P. Sarathchandra, S. Fukushima, K. Suzuki and N. Rosenthal, *A naturally occurring calcineurin variant inhibits FoxO activity and enhances skeletal muscle regeneration.* J Cell Biol, 2007. **179**(6): p. 1205-18.

65.   Felkin, L.E., T. Narita, R. Germack, Y. Shintani, K. Takahashi, P. Sarathchandra, M.M. Lopez-Olaneta, J.M. Gomez-Salinero, K. Suzuki, P.J. Barton, N. Rosenthal and E. Lara-Pezzi, *Calcineurin splicing variant calcineurin Abeta1 improves cardiac function after myocardial infarction without inducing hypertrophy.* Circulation, 2011. **123**(24): p. 2838-47.

66.   Liu, Y., Z. Cseresnyes, W.R. Randall and M.F. Schneider, *Activity-dependent nuclear translocation and intranuclear distribution of NFATc in adult skeletal muscle fibers.* J Cell Biol, 2001. **155**(1): p. 27-39.

67.   Semsarian, C., M.J. Wu, Y.K. Ju, T. Marciniec, T. Yeoh, D.G. Allen, R.P. Harvey and R.M. Graham, *Skeletal muscle hypertrophy is mediated by a Ca2+-dependent calcineurin signalling pathway.* Nature, 1999. **400**(6744): p. 576-81.

68.   Musaro, A., K.J. McCullagh, F.J. Naya, E.N. Olson and N. Rosenthal, *IGF-1 induces skeletal myocyte hypertrophy through calcineurin in association with GATA-2 and NF-ATc1.* Nature, 1999. **400**(6744): p. 581-5.

69.   Naya, F.J. and E. Olson, *MEF2: a transcriptional target for signaling pathways controlling skeletal muscle growth and differentiation.* Curr Opin Cell Biol, 1999. **11**(6): p. 683-8.

70.   Wu, H., B. Rothermel, S. Kanatous, P. Rosenberg, F.J. Naya, J.M. Shelton, K.A. Hutcheson, J.M. DiMaio, E.N. Olson, R. Bassel-Duby and R.S. Williams, *Activation of MEF2 by muscle activity is mediated through a calcineurin-dependent pathway.* EMBO J, 2001. **20**(22): p. 6414-23.

71.   Kobayashi, T., K. Goto, A. Kojima, T. Akema, K. Uehara, H. Aoki, T. Sugiura, Y. Ohira and T. Yoshioka, *Possible role of calcineurin in heating-related increase of rat muscle mass.* Biochem Biophys Res Commun, 2005. **331**(4): p. 1301-9.

72.   Van Rooij, E., P.A. Doevendans, C.C. de Theije, F.A. Babiker, J.D. Molkentin and L.J. de Windt, *Requirement of nuclear factor of activated T-cells in calcineurin-mediated cardiomyocyte hypertrophy.* J Biol Chem, 2002. **277**(50): p. 48617-26.

73.   Macian, F., *NFAT proteins: key regulators of T-cell development and function.* Nat Rev Immunol, 2005. **5**(6): p. 472-84.

74. Rao, A., C. Luo and P.G. Hogan, *Transcription factors of the NFAT family: regulation and function.* Annu Rev Immunol, 1997. **15**: p. 707-47.

75. Calabria, E., S. Ciciliot, I. Moretti, M. Garcia, A. Picard, K.A. Dyar, G. Pallafacchina, J. Tothova, S. Schiaffino and M. Murgia, *NFAT isoforms control activity-dependent muscle fiber type specification.* Proc Natl Acad Sci U S A, 2009. **106**(32): p. 13335-40.

76. Lopez-Rodriguez, C., J. Aramburu, A.S. Rakeman and A. Rao, *NFAT5, a constitutively nuclear NFAT protein that does not cooperate with Fos and Jun.* Proc Natl Acad Sci U S A, 1999. **96**(13): p. 7214-9.

77. Klemm, J.D., C.R. Beals and G.R. Crabtree, *Rapid targeting of nuclear proteins to the cytoplasm.* Curr Biol, 1997. **7**(9): p. 638-44.

78. Macian, F., C. Lopez-Rodriguez and A. Rao, *Partners in transcription: NFAT and AP-1.* Oncogene, 2001. **20**(19): p. 2476-89.

79. Chen, L., J.N. Glover, P.G. Hogan, A. Rao and S.C. Harrison, *Structure of the DNA-binding domains from NFAT, Fos and Jun bound specifically to DNA.* Nature, 1998. **392**(6671): p. 42-8.

80. Rinne, A., N. Kapur, J.D. Molkentin, S.M. Pogwizd, D.M. Bers, K. Banach and L.A. Blatter, *Isoform- and tissue-specific regulation of the Ca(2+)-sensitive transcription factor NFAT in cardiac myocytes and heart failure.* Am J Physiol Heart Circ Physiol, 2010. **298**(6): p. H2001-9.

81. Crabtree, G.R., *Generic signals and specific outcomes: signaling through Ca2+, calcineurin, and NF-AT.* Cell, 1999. **96**(5): p. 611-4.

82. Okamura, H., J. Aramburu, C. Garcia-Rodriguez, J.P. Viola, A. Raghavan, M. Tahiliani, X. Zhang, J. Qin, P.G. Hogan and A. Rao, *Concerted dephosphorylation of the transcription factor NFAT1 induces a conformational switch that regulates transcriptional activity.* Mol Cell, 2000. **6**(3): p. 539-50.

83. Zhu, J., F. Shibasaki, R. Price, J.C. Guillemot, T. Yano, V. Dotsch, G. Wagner, P. Ferrara and F. McKeon, *Intramolecular masking of nuclear import signal on NF-AT4 by casein kinase I and MEKK1.* Cell, 1998. **93**(5): p. 851-61.

84. Gomez del Arco, P., S. Martinez-Martinez, J.L. Maldonado, I. Ortega-Perez and J.M. Redondo, *A role for the p38 MAP kinase pathway in the nuclear shuttling of NFATp.* J Biol Chem, 2000. **275**(18): p. 13872-8.

85. Beals, C.R., C.M. Sheridan, C.W. Turck, P. Gardner and G.R. Crabtree, *Nuclear export of NF-ATc enhanced by glycogen synthase kinase-3.* Science, 1997. **275**(5308): p. 1930-4.

86. Chow, C.W., M. Rincon, J. Cavanagh, M. Dickens and R.J. Davis, *Nuclear accumulation of NFAT4 opposed by the JNK signal transduction pathway.* Science, 1997. **278**(5343): p. 1638-41.

87. Beals, C.R., N.A. Clipstone, S.N. Ho and G.R. Crabtree, *Nuclear localization of NF-ATc by a calcineurin-dependent, cyclosporin-sensitive intramolecular interaction.* Genes Dev, 1997. **11**(7): p. 824-34.

88. Okamura, H., C. Garcia-Rodriguez, H. Martinson, J. Qin, D.M. Virshup and A. Rao, *A conserved docking motif for CK1 binding controls the nuclear localization of NFAT1.* Mol Cell Biol, 2004. **24**(10): p. 4184-95.

89. Chin, E.R., E.N. Olson, J.A. Richardson, Q. Yang, C. Humphries, J.M. Shelton, H. Wu, W. Zhu, R. Bassel-Duby and R.S. Williams, *A calcineurin-dependent transcriptional pathway controls skeletal muscle fiber type.* Genes Dev, 1998. **12**(16): p. 2499-509.

90. Dolmetsch, R.E., R.S. Lewis, C.C. Goodnow and J.I. Healy, *Differential activation of transcription factors induced by Ca2+ response amplitude and duration.* Nature, 1997. **386**(6627): p. 855-8.

91. Dunn, S.E., J.L. Burns and R.N. Michel, *Calcineurin is required for skeletal muscle hypertrophy.* J Biol Chem, 1999. **274**(31): p. 21908-12.

92. Hogan, P.G., L. Chen, J. Nardone and A. Rao, *Transcriptional regulation by calcium, calcineurin, and NFAT.* Genes Dev, 2003. **17**(18): p. 2205-32.

93. Michel, R.N., E.R. Chin, J.V. Chakkalakal, J.K. Eibl and B.J. Jasmin, *Ca2+/calmodulin-based signalling in the regulation of the muscle fibre phenotype and its therapeutic potential via modulation of utrophin A and myostatin expression.* Appl Physiol Nutr Metab, 2007. **32**(5): p. 921-9.

94. Blake, D.J., A. Weir, S.E. Newey and K.E. Davies, *Function and genetics of dystrophin and dystrophin-related proteins in muscle.* Physiol Rev, 2002. **82**(2): p. 291-329.

95. Emery, A.E., *Population frequencies of inherited neuromuscular diseases--a world survey.* Neuromuscul Disord, 1991. **1**(1): p. 19-29.

96. Boyce, F.M., A.H. Beggs, C. Feener and L.M. Kunkel, *Dystrophin is transcribed in brain from a distant upstream promoter.* Proceedings of the National Academy of Sciences of the United States of America, 1991. **88**(4): p. 1276-80.

97. Chelly, J., G. Hamard, A. Koulakoff, J.C. Kaplan, A. Kahn and Y. Berwald-Netter, *Dystrophin gene transcribed from different promoters in neuronal and glial cells.* Nature, 1990. **344**(6261): p. 64-5.

98. Chakkalakal, J.V., S.A. Michel, E.R. Chin, R.N. Michel and B.J. Jasmin, *Targeted inhibition of Ca2+ /calmodulin signaling exacerbates the dystrophic phenotype in mdx mouse muscle.* Hum Mol Genet, 2006. **15**(9): p. 1423-35.

99. Hoffman, E.P., R.H. Brown, Jr. and L.M. Kunkel, *Dystrophin: the protein product of the Duchenne muscular dystrophy locus.* Cell, 1987. **51**(6): p. 919-28.

100. Austin, L., M. de Niese, A. McGregor, H. Arthur, A. Gurusinghe and M.K. Gould, *Potential oxyradical damage and energy status in individual muscle fibres from degenerating muscle diseases.* Neuromuscul Disord, 1992. **2**(1): p. 27-33.

101. Culligan, K.G. and K. Ohlendieck, *Abnormal Calcium Handling in Muscular Dystrophy.* Basic Appl Myol, 2002. **12**(4): p. 147-157.

102. Petrof, B.J., *Molecular pathophysiology of myofiber injury in deficiencies of the dystrophin-glycoprotein complex.* Am J Phys Med Rehabil, 2002. **81**(11 Suppl): p. S162-74.

103. Buyse, G.M., N. Goemans, M. van den Hauwe and T. Meier, *Effects of glucocorticoids and idebenone on respiratory function in patients with duchenne muscular dystrophy.* Pediatr Pulmonol, 2012.

104. Serra, F., M. Quarta, M. Canato, L. Toniolo, V. De Arcangelis, A. Trotta, L. Spath, L. Monaco, C. Reggiani and F. Naro, *Inflammation in muscular dystrophy and the beneficial effects of non-steroidal anti-inflammatory drugs.* Muscle Nerve, 2012. **46**(5): p. 773-84.

105. Chakkalakal, J.V., M.A. Stocksley, M.A. Harrison, L.M. Angus, J. Deschenes-Furry, S. St-Pierre, L.A. Megeney, E.R. Chin, R.N. Michel and B.J. Jasmin, *Expression of utrophin A mRNA correlates with the oxidative capacity of skeletal muscle fiber types and is regulated by calcineurin/NFAT signaling.* Proc Natl Acad Sci U S A, 2003. **100**(13): p. 7791-6.

106. Chakkalakal, J.V., M.A. Harrison, S. Carbonetto, E. Chin, R.N. Michel and B.J. Jasmin, *Stimulation of calcineurin signaling attenuates the dystrophic pathology in mdx mice.* Hum Mol Genet, 2004. **13**(4): p. 379-88.

107. Verhaart, I.E. and A. Aartsma-Rus, *The effect of 6-thioguanine on alternative splicing and antisense-mediated exon skipping treatment for duchenne muscular dystrophy.* PLoS Curr, 2012. **4**.

108.   Malerba, A., J.K. Kang, G. McClorey, A.F. Saleh, L. Popplewell, M.J. Gait, M.J. Wood and G. Dickson, *Dual Myostatin and Dystrophin Exon Skipping by Morpholino Nucleic Acid Oligomers Conjugated to a Cell-penetrating Peptide Is a Promising Therapeutic Strategy for the Treatment of Duchenne Muscular Dystrophy.* Mol Ther Nucleic Acids, 2012. **1**: p. e62.

109.   Kendall, G.C., E.I. Mokhonova, M. Moran, N.E. Sejbuk, D.W. Wang, O. Silva, R.T. Wang, L. Martinez, Q.L. Lu, R. Damoiseaux, M.J. Spencer, S.F. Nelson and M.C. Miceli, *Dantrolene enhances antisense-mediated exon skipping in human and mouse models of duchenne muscular dystrophy.* Sci Transl Med, 2012. **4**(164): p. 164ra160.

110.   Biggar, W.D., L. Politano, V.A. Harris, L. Passamano, J. Vajsar, B. Alman, A. Palladino, L.I. Comi and G. Nigro, *Deflazacort in Duchenne muscular dystrophy: a comparison of two different protocols.* Neuromuscul Disord, 2004. **14**(8-9): p. 476-82.

111.   Biggar, W.D., M. Gingras, D.L. Fehlings, V.A. Harris and C.A. Steele, *Deflazacort treatment of Duchenne muscular dystrophy.* J Pediatr, 2001. **138**(1): p. 45-50.

112.   Cousins, J.C., K.J. Woodward, J.G. Gross, T.A. Partridge and J.E. Morgan, *Regeneration of skeletal muscle from transplanted immortalised myoblasts is oligoclonal.* J Cell Sci, 2004. **117**(Pt 15): p. 3259-69.

113.   Morrison, J., Q.L. Lu, C. Pastoret, T. Partridge and G. Bou-Gharios, *T-cell-dependent fibrosis in the mdx dystrophic mouse.* Lab Invest, 2000. **80**(6): p. 881-91.

114.   Kolodziejczyk, S.M., G.S. Walsh, K. Balazsi, P. Seale, J. Sandoz, A.M. Hierlihy, M.A. Rudnicki, J.S. Chamberlain, F.D. Miller and L.A. Megeney, *Activation of JNK1 contributes to dystrophic muscle pathogenesis.* Curr Biol, 2001. **11**(16): p. 1278-82.

115.   St-Pierre, S.J., J.V. Chakkalakal, S.M. Kolodziejczyk, J.C. Knudson, B.J. Jasmin and L.A. Megeney, *Glucocorticoid treatment alleviates dystrophic myofiber pathology by activation of the calcineurin/NF-AT pathway.* FASEB J, 2004. **18**(15): p. 1937-9.

116.   Tinsley, J.M., D.J. Blake, A. Roche, U. Fairbrother, J. Riss, B.C. Byth, A.E. Knight, J. Kendrick-Jones, G.K. Suthers, D.R. Love and et al., *Primary structure of dystrophin-related protein.* Nature, 1992. **360**(6404): p. 591-3.

117.   Love, D.R., D.F. Hill, G. Dickson, N.K. Spurr, B.C. Byth, R.F. Marsden, F.S. Walsh, Y.H. Edwards and K.E. Davies, *An autosomal transcript in skeletal muscle with homology to dystrophin.* Nature, 1989. **339**(6219): p. 55-8.

118.   Pons, F., A. Robert, E. Fabbrizio, G. Hugon, J.C. Califano, J.A. Fehrentz, J. Martinez and D. Mornet, *Utrophin localization in normal and dystrophin-deficient heart.* Circulation, 1994. **90**(1): p. 369-74.

119.   Nguyen, T.M., J.M. Ellis, D.R. Love, K.E. Davies, K.C. Gatter, G. Dickson and G.E. Morris, *Localization of the DMDL gene-encoded dystrophin-related protein using a panel of nineteen monoclonal antibodies: presence at neuromuscular junctions, in the sarcolemma of dystrophic skeletal muscle, in vascular and other smooth muscles, and in proliferating brain cell lines.* The Journal of cell biology, 1991. **115**(6): p. 1695-700.

120.   Earnest, J.P., G.F. Santos, S. Zuerbig and J.E. Fox, *Dystrophin-related protein in the platelet membrane skeleton. Integrin-induced change in detergent-insolubility and cleavage by calpain in aggregating platelets.* The Journal of biological chemistry, 1995. **270**(45): p. 27259-65.

121.   Lin, S., F. Gaschen and J.M. Burgunder, *Utrophin is a regeneration-associated protein transiently present at the sarcolemma of regenerating skeletal muscle fibers in dystrophin-deficient hypertrophic feline muscular dystrophy.* Journal of neuropathology and experimental neurology, 1998. **57**(8): p. 780-90.

122. Takemitsu, M., S. Ishiura, R. Koga, K. Kamakura, K. Arahata, I. Nonaka and H. Sugita, *Dystrophin-related protein in the fetal and denervated skeletal muscles of normal and mdx mice.* Biochemical and biophysical research communications, 1991. **180**(3): p. 1179-86.

123. Khurana, T.S., S.C. Watkins, P. Chafey, J. Chelly, F.M. Tome, M. Fardeau, J.C. Kaplan and L.M. Kunkel, *Immunolocalization and developmental expression of dystrophin related protein in skeletal muscle.* Neuromuscular disorders : NMD, 1991. **1**(3): p. 185-94.

124. Ohlendieck, K., J.M. Ervasti, K. Matsumura, S.D. Kahl, C.J. Leveille and K.P. Campbell, *Dystrophin-related protein is localized to neuromuscular junctions of adult skeletal muscle.* Neuron, 1991. **7**(3): p. 499-508.

125. Bewick, G.S., C. Young and C.R. Slater, *Spatial relationships of utrophin, dystrophin, beta-dystroglycan and beta-spectrin to acetylcholine receptor clusters during postnatal maturation of the rat neuromuscular junction.* Journal of neurocytology, 1996. **25**(7): p. 367-79.

126. Campanelli, J.T., S.L. Roberds, K.P. Campbell and R.H. Scheller, *A role for dystrophin-associated glycoproteins and utrophin in agrin-induced AChR clustering.* Cell, 1994. **77**(5): p. 663-74.

127. Phillips, W.D., P.G. Noakes, S.L. Roberds, K.P. Campbell and J.P. Merlie, *Clustering and immobilization of acetylcholine receptors by the 43-kD protein: a possible role for dystrophin-related protein.* The Journal of cell biology, 1993. **123**(3): p. 729-40.

128. Sieb, J.P., S. Kraner, M. Rauch and O.K. Steinlein, *Immature end-plates and utrophin deficiency in congenital myasthenic syndrome caused by epsilon-AChR subunit truncating mutations.* Human genetics, 2000. **107**(2): p. 160-4.

129. Slater, C.R., C. Young, S.J. Wood, G.S. Bewick, L.V. Anderson, P. Baxter, P.R. Fawcett, M. Roberts, L. Jacobson, J. Kuks, A. Vincent and J. Newsom-Davis, *Utrophin abundance is reduced at neuromuscular junctions of patients with both inherited and acquired acetylcholine receptor deficiencies.* Brain : a journal of neurology, 1997. **120 (Pt 9)**: p. 1513-31.

130. Matsumura, K., J.M. Ervasti, K. Ohlendieck, S.D. Kahl and K.P. Campbell, *Association of dystrophin-related protein with dystrophin-associated proteins in mdx mouse muscle.* Nature, 1992. **360**(6404): p. 588-91.

131. Arnold, H.H. and B. Winter, *Muscle differentiation: more complexity to the network of myogenic regulators.* Current opinion in genetics & development, 1998. **8**(5): p. 539-44.

132. Black, B.L. and E.N. Olson, *Transcriptional control of muscle development by myocyte enhancer factor-2 (MEF2) proteins.* Annual review of cell and developmental biology, 1998. **14**: p. 167-96.

133. Fromm, L. and S.J. Burden, *Synapse-specific and neuregulin-induced transcription require an ets site that binds GABPalpha/GABPbeta.* Genes Dev, 1998. **12**(19): p. 3074-83.

134. Burton, E.A., J.M. Tinsley, P.J. Holzfeind, N.R. Rodrigues and K.E. Davies, *A second promoter provides an alternative target for therapeutic up-regulation of utrophin in Duchenne muscular dystrophy.* Proc Natl Acad Sci U S A, 1999. **96**(24): p. 14025-30.

135. Gramolini, A.O., C.L. Dennis, J.M. Tinsley, G.S. Robertson, J. Cartaud, K.E. Davies and B.J. Jasmin, *Local transcriptional control of utrophin expression at the neuromuscular synapse.* J Biol Chem, 1997. **272**(13): p. 8117-20.

136. Pilgram, G.S., S. Potikanond, R.A. Baines, L.G. Fradkin and J.N. Noordermeer, *The roles of the dystrophin-associated glycoprotein complex at the synapse.* Mol Neurobiol, 2010. **41**(1): p. 1-21.

137. Hoffman, E.P., *Topics in Membranes* 1991. **38**: p. 113-154.

138. Tanabe, Y., K. Esaki and T. Nomura, *Skeletal muscle pathology in X chromosome-linked muscular dystrophy (mdx) mouse.* Acta neuropathologica, 1986. **69**(1-2): p. 91-5.

139. Coulton, G.R., N.A. Curtin, J.E. Morgan and T.A. Partridge, *The mdx mouse skeletal muscle myopathy: II. Contractile properties.* Neuropathology and applied neurobiology, 1988. **14**(4): p. 299-314.

140. Hardiman, O., *Dystrophin deficiency, altered cell signalling and fibre hypertrophy.* Neuromuscular disorders : NMD, 1994. **4**(4): p. 305-15.

141. Muntoni, F., A. Mateddu, F. Marchei, A. Clerk and G. Serra, *Muscular weakness in the mdx mouse.* Journal of the neurological sciences, 1993. **120**(1): p. 71-7.

142. Sundaram, J.S., V.M. Rao, A.K. Meena and M.P. Anandaraj, *Decreased calcineurin activity in circulation of Duchenne muscular dystrophy.* Clin Biochem, 2007. **40**(7): p. 443-6.

143. Deconinck, A.E., A.C. Potter, J.M. Tinsley, S.J. Wood, R. Vater, C. Young, L. Metzinger, A. Vincent, C.R. Slater and K.E. Davies, *Postsynaptic abnormalities at the neuromuscular junctions of utrophin-deficient mice.* The Journal of cell biology, 1997. **136**(4): p. 883-94.

144. Deconinck, A.E., J.A. Rafael, J.A. Skinner, S.C. Brown, A.C. Potter, L. Metzinger, D.J. Watt, J.G. Dickson, J.M. Tinsley and K.E. Davies, *Utrophin-dystrophin-deficient mice as a model for Duchenne muscular dystrophy.* Cell, 1997. **90**(4): p. 717-27.

145. Li, D., Y. Yue and D. Duan, *Marginal level dystrophin expression improves clinical outcome in a strain of dystrophin/utrophin double knockout mice.* PloS one, 2010. **5**(12): p. e15286.

146. Grady, R.M., H. Teng, M.C. Nichol, J.C. Cunningham, R.S. Wilkinson and J.R. Sanes, *Skeletal and cardiac myopathies in mice lacking utrophin and dystrophin: a model for Duchenne muscular dystrophy.* Cell, 1997. **90**(4): p. 729-38.

147. Chen, S., C. Zhang, X. Liu, L. Gao, W. Zhang, W. Huang, X. Lu and Z. Wang, *[Study on the gene knockout model mice of Duchenne muscular dystrophy].* Sichuan da xue xue bao. Yi xue ban = Journal of Sichuan University. Medical science edition, 2003. **34**(2): p. 210-3.

148. Stupka, N., P. Gregorevic, D.R. Plant and G.S. Lynch, *The calcineurin signal transduction pathway is essential for successful muscle regeneration in mdx dystrophic mice.* Acta Neuropathol, 2004. **107**(4): p. 299-310.

149. Molkentin, J.D., J.R. Lu, C.L. Antos, B. Markham, J. Richardson, J. Robbins, S.R. Grant and E.N. Olson, *A calcineurin-dependent transcriptional pathway for cardiac hypertrophy.* Cell, 1998. **93**(2): p. 215-28.

150. Gehrig, S.M., C. van der Poel, T.A. Sayer, J.D. Schertzer, D.C. Henstridge, J.E. Church, S. Lamon, A.P. Russell, K.E. Davies, M.A. Febbraio and G.S. Lynch, *Hsp72 preserves muscle function and slows progression of severe muscular dystrophy.* Nature, 2012. **484**(7394): p. 394-8.

151. Tupling, A.R., A.O. Gramolini, T.A. Duhamel, H. Kondo, M. Asahi, S.C. Tsuchiya, M.J. Borrelli, J.R. Lepock, K. Otsu, M. Hori, D.H. MacLennan and H.J. Green, *HSP70 binds to the fast-twitch skeletal muscle sarco(endo)plasmic reticulum Ca2+ -ATPase (SERCA1a) and prevents thermal inactivation.* J Biol Chem, 2004. **279**(50): p. 52382-9.

152. Senf, S.M., S.L. Dodd, J.M. McClung and A.R. Judge, *Hsp70 overexpression inhibits NF-kappaB and Foxo3a transcriptional activities and prevents skeletal muscle atrophy.* FASEB J, 2008. **22**(11): p. 3836-45.

153. Olson, E.N. and R.S. Williams, *Calcineurin signaling and muscle remodeling.* Cell, 2000. **101**(7): p. 689-92.

154. Taigen, T., L.J. De Windt, H.W. Lim and J.D. Molkentin, *Targeted inhibition of calcineurin prevents agonist-induced cardiomyocyte hypertrophy.* Proc Natl Acad Sci U S A, 2000. **97**(3): p. 1196-201.

155. Wilkins, B.J., Y.S. Dai, O.F. Bueno, S.A. Parsons, J. Xu, D.M. Plank, F. Jones, T.R. Kimball and J.D. Molkentin, *Calcineurin/NFAT coupling participates in pathological, but not physiological, cardiac hypertrophy.* Circ Res, 2004. **94**(1): p. 110-8.

156. Oka, T., J. Xu and J.D. Molkentin, *Re-employment of developmental transcription factors in adult heart disease.* Semin Cell Dev Biol, 2007. **18**(1): p. 117-31.

157. Merika, M. and S.H. Orkin, *DNA-binding specificity of GATA family transcription factors.* Mol Cell Biol, 1993. **13**(7): p. 3999-4010.

158. Ko, L.J. and J.D. Engel, *DNA-binding specificities of the GATA transcription factor family.* Mol Cell Biol, 1993. **13**(7): p. 4011-22.

159. Grepin, C., L. Dagnino, L. Robitaille, L. Haberstroh, T. Antakly and M. Nemer, *A hormone-encoding gene identifies a pathway for cardiac but not skeletal muscle gene transcription.* Mol Cell Biol, 1994. **14**(5): p. 3115-29.

160. Molkentin, J.D., D.V. Kalvakolanu and B.E. Markham, *Transcription factor GATA-4 regulates cardiac muscle-specific expression of the alpha-myosin heavy-chain gene.* Mol Cell Biol, 1994. **14**(7): p. 4947-57.

161. Thuerauf, D.J., D.S. Hanford and C.C. Glembotski, *Regulation of rat brain natriuretic peptide transcription. A potential role for GATA-related transcription factors in myocardial cell gene expression.* J Biol Chem, 1994. **269**(27): p. 17772-5.

162. De Windt, L.J., H.W. Lim, S. Haq, T. Force and J.D. Molkentin, *Calcineurin promotes protein kinase C and c-Jun NH2-terminal kinase activation in the heart. Cross-talk between cardiac hypertrophic signaling pathways.* J Biol Chem, 2000. **275**(18): p. 13571-9.

163. O'Keefe, S.J., J. Tamura, R.L. Kincaid, M.J. Tocci and E.A. O'Neill, *FK-506- and CsA-sensitive activation of the interleukin-2 promoter by calcineurin.* Nature, 1992. **357**(6380): p. 692-4.

164. Lu, J., T.A. McKinsey, R.L. Nicol and E.N. Olson, *Signal-dependent activation of the MEF2 transcription factor by dissociation from histone deacetylases.* Proc Natl Acad Sci U S A, 2000. **97**(8): p. 4070-5.

165. Passier, R., H. Zeng, N. Frey, F.J. Naya, R.L. Nicol, T.A. McKinsey, P. Overbeek, J.A. Richardson, S.R. Grant and E.N. Olson, *CaM kinase signaling induces cardiac hypertrophy and activates the MEF2 transcription factor in vivo.* J Clin Invest, 2000. **105**(10): p. 1395-406.

166. Wu, H., F.J. Naya, T.A. McKinsey, B. Mercer, J.M. Shelton, E.R. Chin, A.R. Simard, R.N. Michel, R. Bassel-Duby, E.N. Olson and R.S. Williams, *MEF2 responds to multiple calcium-regulated signals in the control of skeletal muscle fiber type.* EMBO J, 2000. **19**(9): p. 1963-73.

167. Haq, S., G. Choukroun, Z.B. Kang, H. Ranu, T. Matsui, A. Rosenzweig, J.D. Molkentin, A. Alessandrini, J. Woodgett, R. Hajjar, A. Michael and T. Force, *Glycogen synthase kinase-3beta is a negative regulator of cardiomyocyte hypertrophy.* J Cell Biol, 2000. **151**(1): p. 117-30.

168. Morisco, C., K. Seta, S.E. Hardt, Y. Lee, S.F. Vatner and J. Sadoshima, *Glycogen synthase kinase 3beta regulates GATA4 in cardiac myocytes.* J Biol Chem, 2001. **276**(30): p. 28586-97.

169. Charron, F., G. Tsimiklis, M. Arcand, L. Robitaille, Q. Liang, J.D. Molkentin, S. Meloche and M. Nemer, *Tissue-specific GATA factors are transcriptional effectors of the small GTPase RhoA.* Genes Dev, 2001. **15**(20): p. 2702-19.

170. Liang, Q., R.J. Wiese, O.F. Bueno, Y.S. Dai, B.E. Markham and J.D. Molkentin, *The transcription factor GATA4 is activated by extracellular signal-regulated kinase 1- and 2-mediated phosphorylation of serine 105 in cardiomyocytes.* Mol Cell Biol, 2001. **21**(21): p. 7460-9.

171. Chien, K.R., *Meeting Koch's postulates for calcium signaling in cardiac hypertrophy.* J Clin Invest, 2000. **105**(10): p. 1339-42.

172. Heineke, J. and J.D. Molkentin, *Regulation of cardiac hypertrophy by intracellular signalling pathways.* Nat Rev Mol Cell Biol, 2006. **7**(8): p. 589-600.

173. Matsui, T., L. Li, J.C. Wu, S.A. Cook, T. Nagoshi, M.H. Picard, R. Liao and A. Rosenzweig, *Phenotypic spectrum caused by transgenic overexpression of activated Akt in the heart.* J Biol Chem, 2002. **277**(25): p. 22896-901.

174. Manning, B.D. and L.C. Cantley, *AKT/PKB signaling: navigating downstream.* Cell, 2007. **129**(7): p. 1261-74.

175. Schiaffino, S. and C. Mammucari, *Regulation of skeletal muscle growth by the IGF1-Akt/PKB pathway: insights from genetic models.* Skelet Muscle, 2011. **1**(1): p. 4.

176. Zoncu, R., A. Efeyan and D.M. Sabatini, *mTOR: from growth signal integration to cancer, diabetes and ageing.* Nat Rev Mol Cell Biol, 2011. **12**(1): p. 21-35.

177. Guertin, D.A., D.M. Stevens, C.C. Thoreen, A.A. Burds, N.Y. Kalaany, J. Moffat, M. Brown, K.J. Fitzgerald and D.M. Sabatini, *Ablation in mice of the mTORC components raptor, rictor, or mLST8 reveals that mTORC2 is required for signaling to Akt-FOXO and PKCalpha, but not S6K1.* Dev Cell, 2006. **11**: p. 859-871.

178. Harrington, L.S., G.M. Findlay, A. Gray, T. Tolkacheva, S. Wigfield, H. Rebholz, J. Barnett, N.R. Leslie, S. Cheng and P.R. Shepherd, *The TSC1-2 tumor suppressor controls insulin-PI3K signaling via regulation of IRS proteins.* J Cell Biol, 2004. **166**: p. 213-223.

179. Sarbassov, D.D., D.A. Guertin, S.M. Ali and D.M. Sabatini, *Phosphorylation and regulation of Akt/PKB by the rictor-mTOR complex.* Science, 2005. **307**(5712): p. 1098-101.

180. Adams, C.M., *Role of the transcription factor ATF4 in the anabolic actions of insulin and the anti-anabolic actions of glucocorticoids.* J Biol Chem, 2007. **282**(23): p. 16744-53.

181. Cao, H., S. Yu, Z. Yao, D.L. Galson, Y. Jiang, X. Zhang, J. Fan, B. Lu, Y. Guan, M. Luo, Y. Lai, Y. Zhu, N. Kurihara, K. Patrene, G.D. Roodman and G. Xiao, *Activating transcription factor 4 regulates osteoclast differentiation in mice.* J Clin Invest, 2010. **120**(8): p. 2755-66.

182. Lai, M.M., P.E. Burnett, H. Wolosker, S. Blackshaw and S.H. Snyder, *Cain, a novel physiologic protein inhibitor of calcineurin.* J Biol Chem, 1998. **273**(29): p. 18325-31.

183. Bassel-Duby, R. and E.N. Olson, *Role of calcineurin in striated muscle: development, adaptation, and disease.* Biochem Biophys Res Commun, 2003. **311**(4): p. 1133-41.

184. Frey, N., D. Frank, S. Lippl, C. Kuhn, H. Kogler, T. Barrientos, C. Rohr, R. Will, O.J. Muller, H. Weiler, R. Bassel-Duby, H.A. Katus and E.N. Olson, *Calsarcin-2 deficiency increases exercise capacity in mice through calcineurin/NFAT activation.* J Clin Invest, 2008. **118**(11): p. 3598-608.

185. Van Rooij, E., P.A. Doevendans, H.J. Crijns, S. Heeneman, D.J. Lips, M. van Bilsen, R.S. Williams, E.N. Olson, R. Bassel-Duby, B.A. Rothermel and L.J. De Windt, *MCIP1 overexpression suppresses left ventricular remodeling and sustains cardiac function after myocardial infarction.* Circ Res, 2004. **94**(3): p. e18-26.

186. Djinovic-Carugo, K., P. Young, M. Gautel and M. Saraste, *Structure of the alpha-actinin rod: molecular basis for cross-linking of actin filaments.* Cell, 1999. **98**(4): p. 537-46.

187. Fyrberg, C., A. Ketchum, E. Ball and E. Fyrberg, *Characterization of lethal Drosophila melanogaster alpha-actinin mutants.* Biochem Genet, 1998. **36**(9-10): p. 299-310.

188. Knoll, R., M. Hoshijima and K.R. Chien, *Z-line proteins: implications for additional functions.* European Heart Journal, 2002. **4**: p. I13-I17.

189. Knoll, R., M. Hoshijima and K. Chien, *Cardiac mechanotransduction and implications for heart disease.* J Mol Med (Berl), 2003. **81**(12): p. 750-6.

190. Frank, D., C. Kuhn, H.A. Katus and N. Frey, *The sarcomeric Z-disc: a nodal point in signalling and disease.* J Mol Med (Berl), 2006. **84**(6): p. 446-68.

191. Hoshijima, M., *Mechanical stress-strain sensors embedded in cardiac cytoskeleton: Z disk, titin, and associated structures.* Am J Physiol Heart Circ Physiol, 2006. **290**(4): p. H1313-25.

192. Liu, J.O., *Endogenous protein inhibitors of calcineurin.* Biochem Biophys Res Commun, 2003. **311**(4): p. 1103-9.

193. Stupka, N., D.R. Plant, J.D. Schertzer, T.M. Emerson, R. Bassel-Duby, E.N. Olson and G.S. Lynch, *Activated calcineurin ameliorates contraction-induced injury to skeletal muscles of mdx dystrophic mice.* J Physiol, 2006. **575**(Pt 2): p. 645-56.

194. Frey, N., J.A. Richardson and E.N. Olson, *Calsarcins, a novel family of sarcomeric calcineurin-binding proteins.* Proc Natl Acad Sci U S A, 2000. **97**(26): p. 14632-7.

195. Frey, N. and E.N. Olson, *Calsarcin-3, a novel skeletal muscle-specific member of the calsarcin family, interacts with multiple Z-disc proteins.* The Journal of biological chemistry, 2002. **277**(16): p. 13998-4004.

196. Arber, S., J.J. Hunter, J. Ross, Jr., M. Hongo, G. Sansig, J. Borg, J.C. Perriard, K.R. Chien and P. Caroni, *MLP-deficient mice exhibit a disruption of cardiac cytoarchitectural organization, dilated cardiomyopathy, and heart failure.* Cell, 1997. **88**(3): p. 393-403.

197. Heineke, J., H. Ruetten, C. Willenbockel, S.C. Gross, M. Naguib, A. Schaefer, T. Kempf, D. Hilfiker-Kleiner, P. Caroni, T. Kraft, R.A. Kaiser, J.D. Molkentin, H. Drexler and K.C. Wollert, *Attenuation of cardiac remodeling after myocardial infarction by muscle LIM protein-calcineurin signaling at the sarcomeric Z-disc.* Proc Natl Acad Sci U S A, 2005. **102**(5): p. 1655-60.

198. Mery, A., O. Taghli-Lamallem, K.A. Clark, M.C. Beckerle, X. Wu, K. Ocorr and R. Bodmer, *The Drosophila muscle LIM protein, Mlp84B, is essential for cardiac function.* J Exp Biol, 2008. **211**(Pt 1): p. 15-23.

199. Boateng, S.Y., R.J. Belin, D.L. Geenen, K.B. Margulies, J.L. Martin, M. Hoshijima, P.P. de Tombe and B. Russell, *Cardiac dysfunction and heart failure are associated with abnormalities in the subcellular distribution and amounts of oligomeric muscle LIM protein.* Am J Physiol Heart Circ Physiol, 2007. **292**(1): p. H259-69.

200. Arber, S., G. Halder and P. Caroni, *Muscle LIM protein, a novel essential regulator of myogenesis, promotes myogenic differentiation.* Cell, 1994. **79**(2): p. 221-31.

201. Vega, R.B., J. Yang, B.A. Rothermel, R. Bassel-Duby and R.S. Williams, *Multiple domains of MCIP1 contribute to inhibition of calcineurin activity.* The Journal of biological chemistry, 2002. **277**(33): p. 30401-7.

202. Ma, L., H. Tang, Y. Ren, H. Deng, J. Wu and Z. Wang, *p38alpha MAP kinase phosphorylates RCAN1 and regulates its interaction with calcineurin.* Sci China Life Sci, 2012. **55**(7): p. 559-66.

203. Rothermel, B.A., R.B. Vega, R.B. Vega, R.B. Vega and R.S. Williams, *The role of modulatory calcineurin-interacting proteins in calcineurin signaling.* Trends Cardiovasc Med, 2003. **13**(1): p. 15-21.

204. Rothermel, B.A., R.B. Vega, J. Yang, H. Wu, R. Bassel-Duby and R.S. Williams, *A protein encoded within the Down syndrome critical region is enriched in striated muscles and inhibits calcineurin signaling.* J Biol Chem, 2000. **275**(12): p. 8719-25.

205. Fuentes, J.J., L. Genesca, T.J. Kingsbury, K.W. Cunningham, M. Perez-Riba, X. Estivill and S. de la Luna, *DSCR1, overexpressed in Down syndrome, is an inhibitor of calcineurin-mediated signaling pathways.* Hum Mol Genet, 2000. **9**(11): p. 1681-90.

206. Ryeom, S., R.J. Greenwald, A.H. Sharpe and F. McKeon, *The threshold pattern of calcineurin-dependent gene expression is altered by loss of the endogenous inhibitor calcipressin.* Nat Immunol, 2003. **4**(9): p. 874-81.

207. Yang, J., B. Rothermel, R.B. Vega, N. Frey, T.A. McKinsey, E.N. Olson, R. Bassel-Duby and R.S. Williams, *Independent signals control expression of the calcineurin inhibitory proteins MCIP1 and MCIP2 in striated muscles.* Circ Res, 2000. **87**(12): p. E61-8.

208. Davies, K.J., G. Ermak, B.A. Rothermel, M. Pritchard, J. Heitman, J. Ahn, F. Henrique-Silva, D. Crawford, S. Canaider, P. Strippoli, P. Carinci, K.T. Min, D.S. Fox, K.W. Cunningham, R. Bassel-Duby, E.N. Olson, Z. Zhang, R.S. Williams, H.P. Gerber, M. Perez-Riba, H. Seo, X. Cao, C.B. Klee, J.M. Redondo, L.J. Maltais, E.A. Bruford, S. Povey, J.D. Molkentin, F.D. McKeon, E.J. Duh, G.R. Crabtree, M.S. Cyert, S. de la Luna and X. Estivill, *Renaming the DSCR1/Adapt78 gene family as RCAN: regulators of calcineurin.* The FASEB journal : official publication of the Federation of American Societies for Experimental Biology, 2007. **21**(12): p. 3023-8.

209. Sanna, B., E.B. Brandt, R.A. Kaiser, P. Pfluger, S.A. Witt, T.R. Kimball, E. van Rooij, L.J. De Windt, M.E. Rothenberg, M.H. Tschop, S.C. Benoit and J.D. Molkentin, *Modulatory calcineurin-interacting proteins 1 and 2 function as calcineurin facilitators in vivo.* Proc Natl Acad Sci U S A, 2006. **103**(19): p. 7327-32.

210. Sun, L., H.D. Youn, C. Loh, M. Stolow, W. He and J.O. Liu, *Cabin 1, a negative regulator for calcineurin signaling in T lymphocytes.* Immunity, 1998. **8**(6): p. 703-11.

211. Sieber, M. and R. Baumgrass, *Novel inhibitors of the calcineurin/NFATc hub - alternatives to CsA and FK506?* Cell Commun Signal, 2009. **7**: p. 25.

212. Esau, C., M. Boes, H.D. Youn, L. Tatterson, J.O. Liu and J. Chen, *Deletion of calcineurin and myocyte enhancer factor 2 (MEF2) binding domain of Cabin1 results in enhanced cytokine gene expression in T cells.* J Exp Med, 2001. **194**(10): p. 1449-59.

213. Liu, J.O., *Calmodulin-dependent phosphatase, kinases, and transcriptional corepressors involved in T-cell activation.* Immunol Rev, 2009. **228**(1): p. 184-98.

214. Chin, E.R., R.W. Grange, F. Viau, A.R. Simard, C. Humphries, J. Shelton, R. Bassel-Duby, R.S. Williams and R.N. Michel, *Alterations in slow-twitch muscle phenotype in transgenic mice overexpressing the Ca2+ buffering protein parvalbumin.* J Physiol, 2003. **547**(Pt 2): p. 649-63.

215. Lapidos, K.A., R. Kakkar and E.M. McNally, *The dystrophin glycoprotein complex: signaling strength and integrity for the sarcolemma.* Circ Res, 2004. **94**(8): p. 1023-31.

216. Petrof, B.J., J.B. Shrager, H.H. Stedman, A.M. Kelly and H.L. Sweeney, *Dystrophin protects the sarcolemma from stresses developed during muscle contraction.* Proc Natl Acad Sci U S A, 1993. **90**(8): p. 3710-4.

217. Jurkat-Rott, K. and F. Lehmann-Horn, *Muscle channelopathies and critical points in functional and genetic studies.* J Clin Invest, 2005. **115**(8): p. 2000-9.

218. Krag, T.O., M. Gyrd-Hansen and T.S. Khurana, *Harnessing the potential of dystrophin-related proteins for ameliorating Duchenne's muscular dystrophy.* Acta Physiol Scand, 2001. **171**(3): p. 349-58.

219. Engvall, E. and U.M. Wewer, *The new frontier in muscular dystrophy research: booster genes.* FASEB J, 2003. **17**(12): p. 1579-84.

220. Tinsley, J.M., A.C. Potter, S.R. Phelps, R. Fisher, J.I. Trickett and K.E. Davies, *Amelioration of the dystrophic phenotype of mdx mice using a truncated utrophin transgene.* Nature, 1996. **384**(6607): p. 349-53.

221. Squire, S., J.M. Raymackers, C. Vandebrouck, A. Potter, J. Tinsley, R. Fisher, J.M. Gillis and K.E. Davies, *Prevention of pathology in mdx mice by expression of utrophin: analysis using an inducible transgenic expression system.* Hum Mol Genet, 2002. **11**(26): p. 3333-44.

222. Cerletti, M., T. Negri, F. Cozzi, R. Colpo, F. Andreetta, D. Croci, K.E. Davies, F. Cornelio, O. Pozza, G. Karpati, R. Gilbert and M. Mora, *Dystrophic phenotype of canine X-linked muscular dystrophy is mitigated by adenovirus-mediated utrophin gene transfer.* Gene Ther, 2003. **10**(9): p. 750-7.

223. Gramolini, A.O., L.M. Angus, L. Schaeffer, E.A. Burton, J.M. Tinsley, K.E. Davies, J.P. Changeux and B.J. Jasmin, *Induction of utrophin gene expression by heregulin in skeletal muscle cells: role of the N-box motif and GA binding protein.* Proceedings of the National Academy of Sciences of the United States of America, 1999. **96**(6): p. 3223-7.

224. Stupka, N., J.D. Schertzer, R. Bassel-Duby, E.N. Olson and G.S. Lynch, *Stimulation of calcineurin Aalpha activity attenuates muscle pathophysiology in mdx dystrophic mice.* Am J Physiol Regul Integr Comp Physiol, 2008. **294**(3): p. R983-92.

225. Selsby, J.T., K.J. Morine, K. Pendrak, E.R. Barton and H.L. Sweeney, *Rescue of dystrophic skeletal muscle by PGC-1alpha involves a fast to slow fiber type shift in the mdx mouse.* PLoS One, 2012. **7**(1): p. e30063.

226. Bornman, L., B.S. Polla, B.P. Lotz and G.S. Gericke, *Expression of heat-shock/stress proteins in Duchenne muscular dystrophy.* Muscle Nerve, 1995. **18**(1): p. 23-31.

227. O'Neill, D.E., F.K. Aubrey, D.A. Zeldin, R.N. Michel and E.G. Noble, *Slower skeletal muscle phenotypes are critical for constitutive expression of Hsp70 in overloaded rat plantaris muscle.* J Appl Physiol, 2006. **100**(3): p. 981-7.

228. Welch, W.J., *Mammalian stress response: cell physiology, structure/function of stress proteins, and implications for medicine and disease.* Physiol Rev, 1992. **72**(4): p. 1063-81.

229. Fuchtbauer, E.M., A.M. Rowlerson, K. Gotz, G. Friedrich, K. Mabuchi, J. Gergely and H. Jockusch, *Direct correlation of parvalbumin levels with myosin isoforms and succinate dehydrogenase activity on frozen sections of rodent muscle.* J Histochem Cytochem, 1991. **39**(3): p. 355-61.

230. Wang, J., B. Campos, G.A. Jamieson, Jr., M.A. Kaetzel and J.R. Dedman, *Functional elimination of calmodulin within the nucleus by targeted expression of an inhibitor peptide.* J Biol Chem, 1995. **270**(51): p. 30245-8.

231. Shin, J.H., C.H. Hakim, K. Zhang and D. Duan, *Genotyping mdx, mdx3cv, and mdx4cv mice by primer competition polymerase chain reaction.* Muscle Nerve, 2011. **43**(2): p. 283-6.

232. Wehling, M., M.J. Spencer and J.G. Tidball, *A nitric oxide synthase transgene ameliorates muscular dystrophy in mdx mice.* J Cell Biol, 2001. **155**(1): p. 123-31.

233. Straub, V., J.A. Rafael, J.S. Chamberlain and K.P. Campbell, *Animal models for muscular dystrophy show different patterns of sarcolemmal disruption.* J Cell Biol, 1997. **139**(2): p. 375-85.

234. Bulfield, G., W.G. Siller, P.A. Wight and K.J. Moore, *X chromosome-linked muscular dystrophy (mdx) in the mouse.* Proc Natl Acad Sci U S A, 1984. **81**(4): p. 1189-92.

235. Sicinski, P., Y. Geng, A.S. Ryder-Cook, E.A. Barnard, M.G. Darlison and P.J. Barnard, *The molecular basis of muscular dystrophy in the mdx mouse: a point mutation.* Science, 1989. **244**(4912): p. 1578-80.

236. Kubis, H.P., N. Hanke, R.J. Scheibe, J.D. Meissner and G. Gros, *Ca2+ transients activate calcineurin/NFATc1 and initiate fast-to-slow transformation in a primary skeletal muscle culture.* Am J Physiol Cell Physiol, 2003. **285**(1): p. C56-63.

237. McCullagh, K.J., E. Calabria, G. Pallafacchina, S. Ciciliot, A.L. Serrano, C. Argentini, J.M. Kalhovde, T. Lomo and S. Schiaffino, *NFAT is a nerve activity sensor in skeletal muscle and controls activity-dependent myosin switching.* Proc Natl Acad Sci U S A, 2004. **101**(29): p. 10590-5.

238. Allen, D.L. and L.A. Leinwand, *Intracellular calcium and myosin isoform transitions. Calcineurin and calcium-calmodulin kinase pathways regulate preferential activation of the IIa myosin heavy chain promoter.* J Biol Chem, 2002. **277**(47): p. 45323-30.

239. Allen, D.L., C.A. Sartorius, L.K. Sycuro and L.A. Leinwand, *Different pathways regulate expression of the skeletal myosin heavy chain genes.* J Biol Chem, 2001. **276**(47): p. 43524-33.

240. Olson, E.N. and R.S. Williams, *Remodeling muscles with calcineurin.* Bioessays, 2000. **22**(6): p. 510-9.

241. Schiaffino, S. and A. Serrano, *Calcineurin signaling and neural control of skeletal muscle fiber type and size.* Trends Pharmacol Sci, 2002. **23**(12): p. 569-75.

242. Gramolini, A.O., G. Belanger, J.M. Thompson, J.V. Chakkalakal and B.J. Jasmin, *Increased expression of utrophin in a slow vs. a fast muscle involves posttranscriptional events.* Am J Physiol Cell Physiol, 2001. **281**(4): p. C1300-9.

243. Moens, P., P.H. Baatsen and G. Marechal, *Increased susceptibility of EDL muscles from mdx mice to damage induced by contractions with stretch.* J Muscle Res Cell Motil, 1993. **14**(4): p. 446-51.

244. Webster, C., L. Silberstein, A.P. Hays and H.M. Blau, *Fast muscle fibers are preferentially affected in Duchenne muscular dystrophy.* Cell, 1988. **52**(4): p. 503-13.

245. Naranjo, J.R. and B. Mellstrom, *Ca2+-dependent transcriptional control of Ca2+ homeostasis.* J Biol Chem, 2012. **287**(38): p. 31674-80.

246. Bertorini, T.E., S.K. Bhattacharya, G.M. Palmieri, C.M. Chesney, D. Pifer and B. Baker, *Muscle calcium and magnesium content in Duchenne muscular dystrophy.* Neurology, 1982. **32**(10): p. 1088-92.

247. Tutdibi, O., H. Brinkmeier, R. Rudel and K.J. Fohr, *Increased calcium entry into dystrophin-deficient muscle fibres of MDX and ADR-MDX mice is reduced by ion channel blockers.* J Physiol, 1999. **515 (Pt 3)**: p. 859-68.

248. Nicol, R.L., N. Frey and E.N. Olson, *From the sarcomere to the nucleus: role of genetics and signaling in structural heart disease.* Annu Rev Genomics Hum Genet, 2000. **1**: p. 179-223.

249. Angus, L.M., J.V. Chakkalakal, A. Mejat, J.K. Eibl, G. Belanger, L.A. Megeney, E.R. Chin, L. Schaeffer, R.N. Michel and B.J. Jasmin, *Calcineurin-NFAT signaling, together with GABP and peroxisome PGC-1{alpha}, drives utrophin gene expression at the neuromuscular junction.* Am J Physiol Cell Physiol, 2005. **289**(4): p. C908-17.

250. Siegel, A.L., C. Bledsoe, J. Lavin, F. Gatti, J. Berge, G. Millman, E. Turin, W.T. Winders, J. Rutter, B. Palmeiri and C.G. Carlson, *Treatment with inhibitors of the NF-kappaB*

pathway improves whole body tension development in the mdx mouse. Neuromuscul Disord, 2009. **19**(2): p. 131-9.

251. Tang, Y., D.P. Reay, M.N. Salay, M.Y. Mi, P.R. Clemens, D.C. Guttridge, P.D. Robbins, J. Huard and B. Wang, *Inhibition of the IKK/NF-kappaB pathway by AAV gene transfer improves muscle regeneration in older mdx mice.* Gene Ther, 2010. **17**(12): p. 1476-83.

252. Morel, J.L., F. Dabertrand, N. Fritz, M. Henaff, J. Mironneau and N. Macrez, *The decrease of expression of ryanodine receptor sub-type 2 is reversed by gentamycin sulphate in vascular myocytes from mdx mice.* J Cell Mol Med, 2009. **13**(9B): p. 3122-30.

253. Liu, J., J.D. Farmer, Jr., W.S. Lane, J. Friedman, I. Weissman and S.L. Schreiber, *Calcineurin is a common target of cyclophilin-cyclosporin A and FKBP-FK506 complexes.* Cell, 1991. **66**(4): p. 807-15.

254. Li, H., L. Zhang, A. Rao, S.C. Harrison and P.G. Hogan, *Structure of calcineurin in complex with PVIVIT peptide: portrait of a low-affinity signalling interaction.* J Mol Biol, 2007. **369**(5): p. 1296-306.

255. Handschumacher, R.E., M.W. Harding, J. Rice, R.J. Drugge and D.W. Speicher, *Cyclophilin: a specific cytosolic binding protein for cyclosporin A.* Science, 1984. **226**(4674): p. 544-7.

256. Harding, M.W., A. Galat, D.E. Uehling and S.L. Schreiber, *A receptor for the immunosuppressant FK506 is a cis-trans peptidyl-prolyl isomerase.* Nature, 1989. **341**(6244): p. 758-60.

257. Sigal, N.H., F. Dumont, P. Durette, J.J. Siekierka, L. Peterson, D.H. Rich, B.E. Dunlap, M.J. Staruch, M.R. Melino, S.L. Koprak and et al., *Is cyclophilin involved in the immunosuppressive and nephrotoxic mechanism of action of cyclosporin A?* J Exp Med, 1991. **173**(3): p. 619-28.

258. Kingsbury, T.J. and K.W. Cunningham, *A conserved family of calcineurin regulators.* Genes Dev, 2000. **14**(13): p. 1595-604.

259. Gorlach, J., D.S. Fox, N.S. Cutler, G.M. Cox, J.R. Perfect and J. Heitman, *Identification and characterization of a highly conserved calcineurin binding protein, CBP1/calcipressin, in Cryptococcus neoformans.* EMBO J, 2000. **19**(14): p. 3618-29.

260. Sternberg, E.A., G. Spizz, W.M. Perry, D. Vizard, T. Weil and E.N. Olson, *Identification of upstream and intragenic regulatory elements that confer cell-type-restricted and differentiation-specific expression on the muscle creatine kinase gene.* Mol Cell Biol, 1988. **8**(7): p. 2896-909.

261. Vega, R.B., B.A. Rothermel, C.J. Weinheimer, A. Kovacs, R.H. Naseem, R. Bassel-Duby, R.S. Williams and E.N. Olson, *Dual roles of modulatory calcineurin-interacting protein 1 in cardiac hypertrophy.* Proc Natl Acad Sci U S A, 2003. **100**(2): p. 669-74.

262. Frey, N., T. Barrientos, J.M. Shelton, D. Frank, H. Rutten, D. Gehring, C. Kuhn, M. Lutz, B. Rothermel, R. Bassel-Duby, J.A. Richardson, H.A. Katus, J.A. Hill and E.N. Olson, *Mice lacking calsarcin-1 are sensitized to calcineurin signaling and show accelerated cardiomyopathy in response to pathological biomechanical stress.* Nat Med, 2004. **10**(12): p. 1336-43.

263. Frank, D., C. Kuhn, M. van Eickels, D. Gehring, C. Hanselmann, S. Lippl, R. Will, H.A. Katus and N. Frey, *Calsarcin-1 protects against angiotensin-II induced cardiac hypertrophy.* Circulation, 2007. **116**(22): p. 2587-96.

264. Leenders, J.J., Y.M. Pinto and E.E. Creemers, *Tapping the brake on cardiac growth-endogenous repressors of hypertrophic signaling.* J Mol Cell Cardiol, 2011. **51**(2): p. 156-67.

265. Paulsson, A.K., S. Franklin, S.A. Mitchell-Jordan, S. Ren, Y. Wang and T.M. Vondriska, *Post-translational regulation of calsarcin-1 during pressure overload-induced cardiac hypertrophy.* J Mol Cell Cardiol, 2010. **48**(6): p. 1206-14.

266. Knoll, R., M. Hoshijima, H.M. Hoffman, V. Person, I. Lorenzen-Schmidt, M.L. Bang, T. Hayashi, N. Shiga, H. Yasukawa, W. Schaper, W. McKenna, M. Yokoyama, N.J. Schork, J.H. Omens, A.D. McCulloch, A. Kimura, C.C. Gregorio, W. Poller, J. Schaper, H.P. Schultheiss and K.R. Chien, *The cardiac mechanical stretch sensor machinery involves a Z disc complex that is defective in a subset of human dilated cardiomyopathy.* Cell, 2002. **111**(7): p. 943-55.

267. Bourajjaj, M., A.S. Armand, P.A. da Costa Martins, B. Weijts, R. van der Nagel, S. Heeneman, X.H. Wehrens and L.J. De Windt, *NFATc2 is a necessary mediator of calcineurin-dependent cardiac hypertrophy and heart failure.* J Biol Chem, 2008. **283**(32): p. 22295-303.

268. Lorell, B.H. and B.A. Carabello, *Left ventricular hypertrophy: pathogenesis, detection, and prognosis.* Circulation, 2000. **102**(4): p. 470-9.

269. Hare, J., *The dilated, restrictive, and infiltrative cardiomyopathies. In: Bonow RO, Mann DL, Zipes DP, Libby P, eds. Braunwald's Heart Disease.* A Textbook of Cardiovascular Medicine. 9th ed. Philadelphia, Pa: Saunders Elsevier: Chapter 68., 2011.

270. Firth, B.G. and P.M. Dunnmon, *Left ventricular dilatation and failure post-myocardial infarction: pathophysiology and possible pharmacologic interventions.* Cardiovasc Drugs Ther, 1990. **4**(5): p. 1363-74.

271. Wilkins, B.J. and J.D. Molkentin, *Calcium-calcineurin signaling in the regulation of cardiac hypertrophy.* Biochem Biophys Res Commun, 2004. **322**(4): p. 1178-91.

272. Molkentin, J.D., *Calcineurin-NFAT signaling regulates the cardiac hypertrophic response in coordination with the MAPKs.* Cardiovasc Res, 2004. **63**(3): p. 467-75.

273. Bueno, O.F., E. van Rooij, J.D. Molkentin, P.A. Doevendans and L.J. De Windt, *Calcineurin and hypertrophic heart disease: novel insights and remaining questions.* Cardiovasc Res, 2002. **53**(4): p. 806-21.

274. Wilkins, B.J., L.J. De Windt, O.F. Bueno, J.C. Braz, B.J. Glascock, T.F. Kimball and J.D. Molkentin, *Targeted disruption of NFATc3, but not NFATc4, reveals an intrinsic defect in calcineurin-mediated cardiac hypertrophic growth.* Mol Cell Biol, 2002. **22**(21): p. 7603-13.

275. Zou, Y., Y. Hiroi, H. Uozumi, E. Takimoto, H. Toko, W. Zhu, S. Kudoh, M. Mizukami, M. Shimoyama, F. Shibasaki, R. Nagai, Y. Yazaki and I. Komuro, *Calcineurin plays a critical role in the development of pressure overload-induced cardiac hypertrophy.* Circulation, 2001. **104**(1): p. 97-101.

276. Sussman, M.A., H.W. Lim, N. Gude, T. Taigen, E.N. Olson, J. Robbins, M.C. Colbert, A. Gualberto, D.F. Wieczorek and J.D. Molkentin, *Prevention of cardiac hypertrophy in mice by calcineurin inhibition.* Science, 1998. **281**(5383): p. 1690-3.

277. Bueno, O.F., B.J. Wilkins, K.M. Tymitz, B.J. Glascock, T.F. Kimball, J.N. Lorenz and J.D. Molkentin, *Impaired cardiac hypertrophic response in Calcineurin Abeta -deficient mice.* Proc Natl Acad Sci U S A, 2002. **99**(7): p. 4586-91.

278. De Windt, L.J., H.W. Lim, O.F. Bueno, Q. Liang, U. Delling, J.C. Braz, B.J. Glascock, T.F. Kimball, F. del Monte, R.J. Hajjar and J.D. Molkentin, *Targeted inhibition of calcineurin attenuates cardiac hypertrophy in vivo.* Proc Natl Acad Sci U S A, 2001. **98**(6): p. 3322-7.

279. Hill, J.A., B. Rothermel, K.D. Yoo, B. Cabuay, E. Demetroulis, R.M. Weiss, W. Kutschke, R. Bassel-Duby and R.S. Williams, *Targeted inhibition of calcineurin in pressure-overload*

cardiac hypertrophy. Preservation of systolic function. J Biol Chem, 2002. **277**(12): p. 10251-5.

280. Antos, C.L., T.A. McKinsey, N. Frey, W. Kutschke, J. McAnally, J.M. Shelton, J.A. Richardson, J.A. Hill and E.N. Olson, *Activated glycogen synthase-3 beta suppresses cardiac hypertrophy in vivo.* Proc Natl Acad Sci U S A, 2002. **99**(2): p. 907-12.

281. Rothermel, B.A., T.A. McKinsey, R.B. Vega, R.L. Nicol, P. Mammen, J. Yang, C.L. Antos, J.M. Shelton, R. Bassel-Duby, E.N. Olson and R.S. Williams, *Myocyte-enriched calcineurin-interacting protein, MCIP1, inhibits cardiac hypertrophy in vivo.* Proc Natl Acad Sci U S A, 2001. **98**(6): p. 3328-33.

282. Diedrichs, H., M. Chi, B. Boelck, U. Mehlhorn and R.H. Schwinger, *Increased regulatory activity of the calcineurin/NFAT pathway in human heart failure.* Eur J Heart Fail, 2004. **6**(1): p. 3-9.

283. Liang, Q., L.J. De Windt, S.A. Witt, T.R. Kimball, B.E. Markham and J.D. Molkentin, *The transcription factors GATA4 and GATA6 regulate cardiomyocyte hypertrophy in vitro and in vivo.* J Biol Chem, 2001. **276**(32): p. 30245-53.

284. Hodge, M.R., A.M. Ranger, F. Charles de la Brousse, T. Hoey, M.J. Grusby and L.H. Glimcher, *Hyperproliferation and dysregulation of IL-4 expression in NF-ATp-deficient mice.* Immunity, 1996. **4**(4): p. 397-405.

285. Pikkarainen, S., H. Tokola, R. Kerkela and H. Ruskoaho, *GATA transcription factors in the developing and adult heart.* Cardiovasc Res, 2004. **63**(2): p. 196-207.

286. George, I., L.T. Bish, G. Kamalakkannan, C.M. Petrilli, M.C. Oz, Y. Naka, H.L. Sweeney and S. Maybaum, *Myostatin activation in patients with advanced heart failure and after mechanical unloading.* Eur J Heart Fail, 2010. **12**(5): p. 444-53.

287. Shyu, K.G., M.J. Lu, B.W. Wang, H.Y. Sun and H. Chang, *Myostatin expression in ventricular myocardium in a rat model of volume-overload heart failure.* Eur J Clin Invest, 2006. **36**(10): p. 713-9.

288. Gruson, D., S.A. Ahn, J.M. Ketelslegers and M.F. Rousseau, *Increased plasma myostatin in heart failure.* Eur J Heart Fail, 2011. **13**(7): p. 734-6.

289. Sharma, M., R. Kambadur, K.G. Matthews, W.G. Somers, G.P. Devlin, J.V. Conaglen, P.J. Fowke and J.J. Bass, *Myostatin, a transforming growth factor-beta superfamily member, is expressed in heart muscle and is upregulated in cardiomyocytes after infarct.* J Cell Physiol, 1999. **180**(1): p. 1-9.

290. Junqueira, L.C., G. Bignolas and R.R. Brentani, *Picrosirius staining plus polarization microscopy, a specific method for collagen detection in tissue sections.* Histochem J, 1979. **11**(4): p. 447-55.

291. Trowbridge, I.S., H.L. Ostergaard and P. Johnson, *CD45: a leukocyte-specific member of the protein tyrosine phosphatase family.* Biochim Biophys Acta, 1991. **1095**(1): p. 46-56.

292. Trowbridge, I.S., *CD45. A prototype for transmembrane protein tyrosine phosphatases.* J Biol Chem, 1991. **266**(35): p. 23517-20.

293. Beverley, P.C., A. Daser, C.A. Michie and D.L. Wallace, *Functional subsets of T cells defined by isoforms of CD45.* Biochem Soc Trans, 1992. **20**(1): p. 184-7.

294. Mackay, C.R., *Immunological memory.* Adv Immunol, 1993. **53**: p. 217-65.

295. Darby, I., O. Skalli and G. Gabbiani, *Alpha-smooth muscle actin is transiently expressed by myofibroblasts during experimental wound healing.* Lab Invest, 1990. **63**: p. 21-29.

296. Eriksson, J.E., T. Dechat, B. Grin, B. Helfand, M. Mendez, H.M. Pallari and R.D. Goldman, *Introducing intermediate filaments: from discovery to disease.* J Clin Invest, 2009. **119**(7): p. 1763-71.

297. Dunn, S.E., A.R. Simard, R. Bassel-Duby, R.S. Williams and R.N. Michel, *Nerve activity-dependent modulation of calcineurin signaling in adult fast and slow skeletal muscle fibers.* J Biol Chem, 2001. **276**(48): p. 45243-54.

298. Shen, T., Y. Liu, Z. Cseresnyes, A. Hawkins, W.R. Randall and M.F. Schneider, *Activity- and calcineurin-independent nuclear shuttling of NFATc1, but not NFATc3, in adult skeletal muscle fibers.* Mol Biol Cell, 2006. **17**(4): p. 1570-82.

299. de la Pompa, J.L., L.A. Timmerman, H. Takimoto, H. Yoshida, A.J. Elia, E. Samper, J. Potter, A. Wakeham, L. Marengere, B.L. Langille, G.R. Crabtree and T.W. Mak, *Role of the NF-ATc transcription factor in morphogenesis of cardiac valves and septum.* Nature, 1998. **392**(6672): p. 182-6.

300. Crabtree, G.R. and E.N. Olson, *NFAT signaling: choreographing the social lives of cells.* Cell, 2002. **109 Suppl**: p. S67-79.

301. Hasegawa, K., S.J. Lee, S.M. Jobe, B.E. Markham and R.N. Kitsis, *cis-Acting sequences that mediate induction of beta-myosin heavy chain gene expression during left ventricular hypertrophy due to aortic constriction.* Circulation, 1997. **96**(11): p. 3943-53.

302. Herzig, T.C., S.M. Jobe, H. Aoki, J.D. Molkentin, A.W. Cowley, Jr., S. Izumo and B.E. Markham, *Angiotensin II type1a receptor gene expression in the heart: AP-1 and GATA-4 participate in the response to pressure overload.* Proc Natl Acad Sci U S A, 1997. **94**(14): p. 7543-8.

303. Abraham, W.T., E.M. Gilbert, B.D. Lowes, W.A. Minobe, P. Larrabee, R.L. Roden, D. Dutcher, J. Sederberg, J.A. Lindenfeld, E.E. Wolfel, S.F. Shakar, D. Ferguson, K. Volkman, J.V. Linseman, R.A. Quaife, A.D. Robertson and M.R. Bristow, *Coordinate changes in Myosin heavy chain isoform gene expression are selectively associated with alterations in dilated cardiomyopathy phenotype.* Mol Med, 2002. **8**(11): p. 750-60.

304. Ronnebaum, S.M. and C. Patterson, *The FoxO family in cardiac function and dysfunction.* Annu Rev Physiol, 2010. **72**: p. 81-94.

305. Brownawell, A.M., G.J. Kops, I.G. Macara and B.M. Burgering, *Inhibition of nuclear import by protein kinase B (Akt) regulates the subcellular distribution and activity of the forkhead transcription factor AFX.* Mol Cell Biol, 2001. **21**(10): p. 3534-46.

306. Brunet, A., F. Kanai, J. Stehn, J. Xu, D. Sarbassova, J.V. Frangioni, S.N. Dalal, J.A. DeCaprio, M.E. Greenberg and M.B. Yaffe, *14-3-3 transits to the nucleus and participates in dynamic nucleocytoplasmic transport.* J Cell Biol, 2002. **156**(5): p. 817-28.

307. Heineke, J., M. Auger-Messier, J. Xu, M. Sargent, A. York, S. Welle and J.D. Molkentin, *Genetic deletion of myostatin from the heart prevents skeletal muscle atrophy in heart failure.* Circulation, 2010. **121**(3): p. 419-25.

308. Rodgers, B.D., J.P. Interlichia, D.K. Garikipati, R. Mamidi, M. Chandra, O.L. Nelson, C.E. Murry and L.F. Santana, *Myostatin represses physiological hypertrophy of the heart and excitation-contraction coupling.* J Physiol, 2009. **587**(Pt 20): p. 4873-86.

309. Gorin, Y., N.H. Kim, D. Feliers, B. Bhandari, G.G. Choudhury and H.E. Abboud, *Angiotensin II activates Akt/protein kinase B by an arachidonic acid/redox-dependent pathway and independent of phosphoinositide 3-kinase.* FASEB J, 2001. **15**(11): p. 1909-20.

310. Clement, S., M. Stouffs, E. Bettiol, S. Kampf, K.H. Krause, C. Chaponnier and M. Jaconi, *Expression and function of alpha-smooth muscle actin during embryonic-stem-cell-derived cardiomyocyte differentiation.* J Cell Sci, 2007. **120**(Pt 2): p. 229-38.

311. Black, F.M., S.E. Packer, T.G. Parker, L.H. Michael, R. Roberts, R.J. Schwartz and M.D. Schneider, *The vascular smooth muscle alpha-actin gene is reactivated during cardiac hypertrophy provoked by load.* J Clin Invest, 1991. **88**(5): p. 1581-8.

312. Suurmeijer, A.J., S. Clement, A. Francesconi, L. Bocchi, A. Angelini, D.J. Van Veldhuisen, L.G. Spagnoli, G. Gabbiani and A. Orlandi, *Alpha-actin isoform distribution in normal and failing human heart: a morphological, morphometric, and biochemical study.* J Pathol, 2003. **199**(3): p. 387-97.

313. Santiago, J.J., A.L. Dangerfield, S.G. Rattan, K.L. Bathe, R.H. Cunnington, J.E. Raizman, K.M. Bedosky, D.H. Freed, E. Kardami and I.M. Dixon, *Cardiac fibroblast to myofibroblast differentiation in vivo and in vitro: expression of focal adhesion components in neonatal and adult rat ventricular myofibroblasts.* Dev Dyn, 2010. **239**(6): p. 1573-84.

314. Vega-Hernandez, M., A. Kovacs, S. De Langhe and D.M. Ornitz, *FGF10/FGFR2b signaling is essential for cardiac fibroblast development and growth of the myocardium.* Development, 2011. **138**(15): p. 3331-40.

315. Frey, N., T.A. McKinsey and E.N. Olson, *Decoding calcium signals involved in cardiac growth and function.* Nat Med, 2000. **6**(11): p. 1221-7.

316. McKinsey, T.A., C.L. Zhang and E.N. Olson, *Activation of the myocyte enhancer factor-2 transcription factor by calcium/calmodulin-dependent protein kinase-stimulated binding of 14-3-3 to histone deacetylase 5.* Proc Natl Acad Sci U S A, 2000. **97**(26): p. 14400-5.

Appendix I: Chapter 2- Statistical Analyses

QPCR

1) MyHC I in PV models:

t-Test: Two-Sample Assuming Equal Variances

	Variable mdx	Variable mdx/PV
Mean	4.347084	3.560541
Variance	9.187562	11.06789
Observations	4	4
Pooled Variance	10.12773	
Hypothesized Mean Difference	0	
df	6	
t Stat	0.349528	
P(T<=t) one-tail	0.369317	
t Critical one-tail	1.94318	
P(T<=t) two-tail	0.738634	
t Critical two-tail	2.446912	

2) MyHC IIa in PV models:

t-Test: Two-Sample Assuming Equal Variances

	Variable mdx	Variable mdx/PV
Mean	2.7895737	1.7791748
Variance	2.542547	0.3444196
Observations	4	4
Pooled Variance	1.4434833	
Hypothesized Mean Difference	0	
df	6	
t Stat	1.189329	
P(T<=t) one-tail	0.1396188	
t Critical one-tail	1.9431803	
P(T<=t) two-tail	0.2792377	
t Critical two-tail	2.4469118	

3) Total utrophin levels in PV models:

Descriptives

Utrophin

	N	Mean	Std. Deviation	Std. Error	95% Confidence Interval for Mean		Minimum	Maximum
					Lower Bound	Upper Bound		
WT Sol	4	5.7668	2.08676	1.04338	2.4463	9.0873	3.48	8.10
PV Sol	4	1.5737	.44372	.22186	.8676	2.2798	1.00	2.03
mdx Sol	4	10.9832	5.36512	2.68256	2.4461	19.5202	3.68	16.03
mdx/PV Sol	4	3.5978	2.42721	1.21360	-.2644	7.4601	1.29	6.98
WT EDL	3	1.7236	.62987	.36365	.1589	3.2883	1.00	2.15
PV EDL	3	4.3659	.70876	.40920	2.6052	6.1266	3.80	5.16
mdx EDL	3	3.0469	.62411	.36033	1.4965	4.5972	2.36	3.59
mdx/PV EDL	3	3.6411	2.40612	1.38918	-2.3361	9.6182	1.24	6.05
Total	28	4.5007	3.72985	.70487	3.0544	5.9469	1.00	16.03

Test of Homogeneity of Variances

Utrophin

Levene Statistic	df1	df2	Sig.
2.807	7	20	.033

ANOVA

Utrophin

	Sum of Squares	df	Mean Square	F	Sig.
Between Groups	243.780	7	34.826	5.283	.002
Within Groups	131.838	20	6.592		
Total	375.618	27			

Multiple Comparisons

Dependent Variable: Utrophin

(I) Genotype	(J) Genotype	Mean Difference (I-J)	Std. Error	Sig.	95% Confidence Interval	
					Lower Bound	Upper Bound
WT Sol	PV Sol	4.19311*	1.81547	.032	.4061	7.9801
	mdx Sol	-5.21634*	1.81547	.009	-9.0033	-1.4293
	mdx/PV Sol	2.16898	1.81547	.246	-1.6180	5.9560
	WT EDL	4.04320	1.96094	.052	-.0472	8.1336
	PV EDL	1.40093	1.96094	.483	-2.6895	5.4914
	mdx EDL	2.71996	1.96094	.181	-1.3705	6.8104
	mdx/PV EDL	2.12574	1.96094	.291	-1.9647	6.2162
PV Sol	WT Sol	-4.19311*	1.81547	.032	-7.9801	-.4061
	mdx Sol	-9.40945*	1.81547	.000	-13.1965	-5.6224
	mdx/PV Sol	-2.02413	1.81547	.278	-5.8111	1.7629
	WT EDL	-.14992	1.96094	.940	-4.2404	3.9405
	PV EDL	-2.79219	1.96094	.170	-6.8826	1.2983
	mdx EDL	-1.47315	1.96094	.461	-5.5636	2.6173
	mdx/PV EDL	-2.06737	1.96094	.304	-6.1578	2.0231
mdx Sol	WT Sol	5.21634*	1.81547	.009	1.4293	9.0033
	PV Sol	9.40945*	1.81547	.000	5.6224	13.1965
	mdx/PV Sol	7.38532*	1.81547	.001	3.5983	11.1723
	WT EDL	9.25953*	1.96094	.000	5.1691	13.3500
	PV EDL	6.61726*	1.96094	.003	2.5268	10.7077
	mdx EDL	7.93630*	1.96094	.001	3.8459	12.0267
	mdx/PV EDL	7.34208*	1.96094	.001	3.2516	11.4325
mdx/PV Sol	WT Sol	-2.16898	1.81547	.246	-5.9560	1.6180
	PV Sol	2.02413	1.81547	.278	-1.7629	5.8111
	mdx Sol	-7.38532*	1.81547	.001	-11.1723	-3.5983
	WT EDL	1.87421	1.96094	.351	-2.2162	5.9647
	PV EDL	-.76806	1.96094	.699	-4.8585	3.3224
	mdx EDL	.55098	1.96094	.782	-3.5395	4.6414
	mdx/PV EDL	-.04324	1.96094	.983	-4.1337	4.0472
WT EDL	WT Sol	-4.04320	1.96094	.052	-8.1336	.0472
	PV Sol	.14992	1.96094	.940	-3.9405	4.2404
	mdx Sol	-9.25953*	1.96094	.000	-13.3500	-5.1691

170

	mdx/PV Sol	-1.87421	1.96094	.351	-5.9647	2.2162
	PV EDL	-2.64227	2.09633	.222	-7.0151	1.7306
	mdx EDL	-1.32323	2.09633	.535	-5.6961	3.0496
	mdx/PV EDL	-1.91745	2.09633	.371	-6.2903	2.4554
PV EDL	WT Sol	-1.40093	1.96094	.483	-5.4914	2.6895
	PV Sol	2.79219	1.96094	.170	-1.2983	6.8826
	mdx Sol	-6.61726[*]	1.96094	.003	-10.7077	-2.5268
	mdx/PV Sol	.76806	1.96094	.699	-3.3224	4.8585
	WT EDL	2.64227	2.09633	.222	-1.7306	7.0151
	mdx EDL	1.31904	2.09633	.536	-3.0538	5.6919
	mdx/PV EDL	.72482	2.09633	.733	-3.6480	5.0977
mdx EDL	WT Sol	-2.71996	1.96094	.181	-6.8104	1.3705
	PV Sol	1.47315	1.96094	.461	-2.6173	5.5636
	mdx Sol	-7.93630[*]	1.96094	.001	-12.0267	-3.8459
	mdx/PV Sol	-.55098	1.96094	.782	-4.6414	3.5395
	WT EDL	1.32323	2.09633	.535	-3.0496	5.6961
	PV EDL	-1.31904	2.09633	.536	-5.6919	3.0538
	mdx/PV EDL	-.59422	2.09633	.780	-4.9671	3.7786
mdx/PV EDL	WT Sol	-2.12574	1.96094	.291	-6.2162	1.9647
	PV Sol	2.06737	1.96094	.304	-2.0231	6.1578
	mdx Sol	-7.34208[*]	1.96094	.001	-11.4325	-3.2516
	mdx/PV Sol	.04324	1.96094	.983	-4.0472	4.1337
	WT EDL	1.91745	2.09633	.371	-2.4554	6.2903
	PV EDL	-.72482	2.09633	.733	-5.0977	3.6480
	mdx EDL	.59422	2.09633	.780	-3.7786	4.9671

*. The mean difference is significant at the 0.05 level.

Note: WT soleus and WT EDL were compared using student-t-test as done earlier [242].

t-Test: Two-Sample Assuming Equal Variances

	Variable WT Sol	Variable WT EDL
Mean	5.766813	1.72362
Variance	4.354566	0.39673
Observations	4	3

Pooled Variance	2.771431
Hypothesized Mean Difference	0
df	5
t Stat	3.179904
P(T<=t) one-tail	0.01227
t Critical one-tail	2.015048
P(T<=t) two-tail	0.024541
t Critical two-tail	2.570582

4) Utrophin-A levels in PV models:

Descriptives

Utrophin-A

	N	Mean	Std. Deviation	Std. Error	95% Confidence Interval for Mean		Minimum	Maximum
					Lower Bound	Upper Bound		
WT Sol	4	6.3575	1.17266	.58633	4.4916	8.2235	5.03	7.39
PV Sol	4	3.4053	2.77895	1.38947	-1.0166	7.8272	1.00	7.41
mdx Sol	4	65.7969	57.17105	28.58553	-25.1750	156.7688	8.80	125.92
mdx/PV Sol	4	8.9390	3.45650	1.72825	3.4389	14.4390	4.81	12.70
WT EDL	3	1.5327	.69911	.40363	-.2040	3.2694	1.00	2.32
PV EDL	3	3.1684	.67708	.39091	1.4865	4.8504	2.71	3.95
mdx EDL	3	3.5022	.76854	.44371	1.5930	5.4113	2.83	4.34
mdx/PV EDL	3	4.3730	2.17575	1.25617	-1.0318	9.7779	2.18	6.53
Total	28	13.4187	29.06918	5.49356	2.1469	24.6906	1.00	125.92

Test of Homogeneity of Variances

Utrophin-A

Levene Statistic	df1	df2	Sig.
49.915	7	20	.000

ANOVA

Utrophin-A

	Sum of Squares	df	Mean Square	F	Sig.
Between Groups	12934.202	7	1847.743	3.740	.009

Within Groups	9881.266	20	494.063			
Total	22815.468	27				

Multiple Comparisons

Dependent Variable: Utrophin-A

(I) Genotype	(J) Genotype	Mean Difference (I-J)	Std. Error	Sig.	95% Confidence Interval	
					Lower Bound	Upper Bound
WT Sol	PV Sol	2.95221	15.71724	.853	-29.8334	35.7378
	mdx Sol	-59.43936*	15.71724	.001	-92.2249	-26.6538
	mdx/PV Sol	-2.58144	15.71724	.871	-35.3670	30.2041
	WT EDL	4.82484	16.97656	.779	-30.5876	40.2373
	PV EDL	3.18910	16.97656	.853	-32.2234	38.6016
	mdx EDL	2.85537	16.97656	.868	-32.5571	38.2678
	mdx/PV EDL	1.98450	16.97656	.908	-33.4280	37.3970
PV Sol	WT Sol	-2.95221	15.71724	.853	-35.7378	29.8334
	mdx Sol	-62.39157*	15.71724	.001	-95.1772	-29.6060
	mdx/PV Sol	-5.53365	15.71724	.728	-38.3192	27.2519
	WT EDL	1.87263	16.97656	.913	-33.5399	37.2851
	PV EDL	.23689	16.97656	.989	-35.1756	35.6494
	mdx EDL	-.09684	16.97656	.996	-35.5093	35.3156
	mdx/PV EDL	-.96771	16.97656	.955	-36.3802	34.4448
mdx Sol	WT Sol	59.43936*	15.71724	.001	26.6538	92.2249
	PV Sol	62.39157*	15.71724	.001	29.6060	95.1772
	mdx/PV Sol	56.85792*	15.71724	.002	24.0723	89.6435
	WT EDL	64.26420*	16.97656	.001	28.8517	99.6767
	PV EDL	62.62846*	16.97656	.001	27.2160	98.0409
	mdx EDL	62.29472*	16.97656	.002	26.8822	97.7072
	mdx/PV EDL	61.42386*	16.97656	.002	26.0114	96.8363
mdx/PV Sol	WT Sol	2.58144	15.71724	.871	-30.2041	35.3670
	PV Sol	5.53365	15.71724	.728	-27.2519	38.3192
	mdx Sol	-56.85792*	15.71724	.002	-89.6435	-24.0723
	WT EDL	7.40628	16.97656	.667	-28.0062	42.8188
	PV EDL	5.77054	16.97656	.737	-29.6419	41.1830
	mdx EDL	5.43681	16.97656	.752	-29.9757	40.8493
	mdx/PV EDL	4.56594	16.97656	.791	-30.8465	39.9784
WT EDL	WT Sol	-4.82484	16.97656	.779	-40.2373	30.5876
	PV Sol	-1.87263	16.97656	.913	-37.2851	33.5399
	mdx Sol	-64.26420*	16.97656	.001	-99.6767	-28.8517

173

	mdx/PV Sol	-7.40628	16.97656	.667	-42.8188	28.0062
	PV EDL	-1.63574	18.14871	.929	-39.4933	36.2218
	mdx EDL	-1.96948	18.14871	.915	-39.8270	35.8881
	mdx/PV EDL	-2.84034	18.14871	.877	-40.6979	35.0172
PV EDL	WT Sol	-3.18910	16.97656	.853	-38.6016	32.2234
	PV Sol	-.23689	16.97656	.989	-35.6494	35.1756
	mdx Sol	-62.62846*	16.97656	.001	-98.0409	-27.2160
	mdx/PV Sol	-5.77054	16.97656	.737	-41.1830	29.6419
	WT EDL	1.63574	18.14871	.929	-36.2218	39.4933
	mdx EDL	-.33374	18.14871	.986	-38.1913	37.5238
	mdx/PV EDL	-1.20460	18.14871	.948	-39.0621	36.6529
mdx EDL	WT Sol	-2.85537	16.97656	.868	-38.2678	32.5571
	PV Sol	.09684	16.97656	.996	-35.3156	35.5093
	mdx Sol	-62.29472*	16.97656	.002	-97.7072	-26.8822
	mdx/PV Sol	-5.43681	16.97656	.752	-40.8493	29.9757
	WT EDL	1.96948	18.14871	.915	-35.8881	39.8270
	PV EDL	.33374	18.14871	.986	-37.5238	38.1913
	mdx/PV EDL	-.87086	18.14871	.962	-38.7284	36.9867
mdx/PV EDL	WT Sol	-1.98450	16.97656	.908	-37.3970	33.4280
	PV Sol	.96771	16.97656	.955	-34.4448	36.3802
	mdx Sol	-61.42386*	16.97656	.002	-96.8363	-26.0114
	mdx/PV Sol	-4.56594	16.97656	.791	-39.9784	30.8465
	WT EDL	2.84034	18.14871	.877	-35.0172	40.6979
	PV EDL	1.20460	18.14871	.948	-36.6529	39.0621
	mdx EDL	.87086	18.14871	.962	-36.9867	38.7284

*. The mean difference is significant at the 0.05 level.

Note: WT soleus and WT EDL were compared using student-t-test

t-Test: Two-Sample Assuming Equal Variances

	Variable WT Sol	*Variable WT EDL*
Mean	6.357532	1.53269
Variance	1.375136	0.488754
Observations	4	3
Pooled Variance	1.020583	
Hypothesized Mean Difference	0	
df	5	

t Stat	6.253174
P(T<=t) one-tail	0.000767
t Critical one-tail	2.015048
P(T<=t) two-tail	0.001533
t Critical two-tail	2.570582

Immunoblotting

1) Total utrophin levels in PV models:

Descriptives

Utrophin

	N	Mean	Std. Deviation	Std. Error	95% Confidence Interval for Mean		Minimum	Maximum
					Lower Bound	Upper Bound		
WT	3	.8433	.27140	.15669	.1691	1.5175	.53	1.00
PV	3	.4938	.02136	.01233	.4407	.5468	.48	.52
mdx	3	1.5498	.48699	.28116	.3400	2.7595	.99	1.88
mdx/PV	3	.8590	.09638	.05564	.6196	1.0984	.75	.92
Total	12	.9365	.46724	.13488	.6396	1.2333	.48	1.88

Test of Homogeneity of Variances

Utrophin

Levene Statistic	df1	df2	Sig.
7.864	3	8	.009

ANOVA

Utrophin

	Sum of Squares	df	Mean Square	F	Sig.
Between Groups	1.760	3	.587	7.322	.011
Within Groups	.641	8	.080		
Total	2.401	11			

Multiple Comparisons

Dependent Variable: Utrophin

(I) Genotype	(J) Genotype	Mean Difference (I-J)	Std. Error	Sig.	95% Confidence Interval	
					Lower Bound	Upper Bound
WT	PV	.34955	.23114	.169	-.1835	.8826
	Mdx	-.70645*	.23114	.016	-1.2395	-.1734
	mdx/PV	-.01572	.23114	.947	-.5487	.5173
PV	WT	-.34955	.23114	.169	-.8826	.1835
	Mdx	-1.05600*	.23114	.002	-1.5890	-.5230
	mdx/PV	-.36528	.23114	.153	-.8983	.1677
mdx	WT	.70645*	.23114	.016	.1734	1.2395
	PV	1.05600*	.23114	.002	.5230	1.5890
	mdx/PV	.69072*	.23114	.017	.1577	1.2237
mdx/PV	WT	.01572	.23114	.947	-.5173	.5487
	PV	.36528	.23114	.153	-.1677	.8983
	Mdx	-.69072*	.23114	.017	-1.2237	-.1577

*. The mean difference is significant at the 0.05 level.

2) HSP70 levels in PV models:

Descriptives

HSP70

	N	Mean	Std. Deviation	Std. Error	95% Confidence Interval for Mean		Minimum	Maximum
					Lower Bound	Upper Bound		
WT	3	1.0361	.06257	.03612	.8807	1.1915	1.00	1.11
PV	3	.5058	.42134	.24326	-.5409	1.5524	.26	.99
mdx	3	.8315	.77486	.44737	-1.0934	2.7564	.37	1.73
mdx/PV	3	1.1735	.51492	.29729	-.1056	2.4527	.59	1.57
Total	12	.8867	.50921	.14700	.5632	1.2103	.26	1.73

Test of Homogeneity of Variances

HSP70

Levene Statistic	df1	df2	Sig.
4.852	3	8	.033

ANOVA

HSP70

	Sum of Squares	df	Mean Square	F	Sig.
Between Groups	.758	3	.253	.966	.455
Within Groups	2.094	8	.262		
Total	2.852	11			

Multiple Comparisons

Dependent Variable: HSP70

(I) Genotype	(J) Genotype	Mean Difference (I-J)	Std. Error	Sig.	95% Confidence Interval	
					Lower Bound	Upper Bound
WT	PV	.53034	.41773	.240	-.4330	1.4936
	mdx	.20463	.41773	.637	-.7587	1.1679
	mdx/PV	-.13741	.41773	.751	-1.1007	.8259
PV	WT	-.53034	.41773	.240	-1.4936	.4330
	mdx	-.32572	.41773	.458	-1.2890	.6376
	mdx/PV	-.66775	.41773	.149	-1.6310	.2955
mdx	WT	-.20463	.41773	.637	-1.1679	.7587
	PV	.32572	.41773	.458	-.6376	1.2890
	mdx/PV	-.34204	.41773	.437	-1.3053	.6213
mdx/PV	WT	.13741	.41773	.751	-.8259	1.1007
	PV	.66775	.41773	.149	-.2955	1.6310
	mdx	.34204	.41773	.437	-.6213	1.3053

3) RyR1 levels in PV models:

Note: Multiple student t-tests were performed for RyR1, which is 565 kDa in size since PV, mdx and mdx/PV were normalized to WT in each set. Thus, the loading control tubulin (52 kDa) of the four sets was done on different gels.

t-Test: Two-Sample Assuming Equal Variances

	Variable WT	Variable PV
Mean	1	2.077784
Variance	0	0.487075
Observations	4	4
Pooled Variance	0.243537	
Hypothesized Mean Difference	0	
df	6	
t Stat	-3.08862	
P(T<=t) one-tail	0.010713	
t Critical one-tail	1.94318	
P(T<=t) two-tail	0.021426	
t Critical two-tail	2.446912	

t-Test: Two-Sample Assuming Equal Variances

	Variable PV	Variable mdx
Mean	2.077784	0.766988
Variance	0.487075	0.146738
Observations	4	4
Pooled Variance	0.316907	
Hypothesized Mean Difference	0	
df	6	
t Stat	3.292945	
P(T<=t) one-tail	0.008276	
t Critical one-tail	1.94318	
P(T<=t) two-tail	0.016553	
t Critical two-tail	2.446912	

t-Test: Two-Sample Assuming Equal Variances

	Variable mdx	Variable mdx/PV
Mean	0.766988	2.258649
Variance	0.146738	1.388342
Observations	4	4
Pooled Variance	0.76754	

Hypothesized Mean Difference	0
Df	6
t Stat	-2.40788
P(T<=t) one-tail	0.026363
t Critical one-tail	1.94318
P(T<=t) two-tail	0.052726
t Critical two-tail	2.446912

4) SERCA1 levels in PV models:

Descriptives

SERCA1

	N	Mean	Std. Deviation	Std. Error	95% Confidence Interval for Mean		Minimum	Maximum
					Lower Bound	Upper Bound		
WT	4	.9873	.02531	.01266	.9471	1.0276	.95	1.00
PV	4	.8079	.11643	.05821	.6226	.9931	.66	.93
mdx	4	.9195	.18680	.09340	.6223	1.2168	.81	1.20
mdx/PV	4	.7451	.35198	.17599	.1851	1.3052	.42	1.15
Total	16	.8650	.20996	.05249	.7531	.9768	.42	1.20

Test of Homogeneity of Variances

SERCA1

Levene Statistic	df1	df2	Sig.
10.633	3	12	.001

ANOVA

SERCA1

	Sum of Squares	df	Mean Square	F	Sig.
Between Groups	.142	3	.047	1.097	.388
Within Groups	.519	12	.043		
Total	.661	15			

Multiple Comparisons

Dependent Variable: SERCA1

(I) Genotype	(J) Genotype	Mean Difference (I-J)	Std. Error	Sig.	95% Confidence Interval	
					Lower Bound	Upper Bound
WT	PV	.17948	.14705	.246	-.1409	.4999
	mdx	.06782	.14705	.653	-.2526	.3882
	mdx/PV	.24221	.14705	.125	-.0782	.5626
PV	WT	-.17948	.14705	.246	-.4999	.1409
	mdx	-.11165	.14705	.462	-.4320	.2087
	mdx/PV	.06273	.14705	.677	-.2577	.3831
mdx	WT	-.06782	.14705	.653	-.3882	.2526
	PV	.11165	.14705	.462	-.2087	.4320
	mdx/PV	.17438	.14705	.259	-.1460	.4948
mdx/PV	WT	-.24221	.14705	.125	-.5626	.0782
	PV	-.06273	.14705	.677	-.3831	.2577
	mdx	-.17438	.14705	.259	-.4948	.1460

5) SERCA2 levels in PV models:

Descriptives

SERCA2

	N	Mean	Std. Deviation	Std. Error	95% Confidence Interval for Mean		Minimum	Maximum
					Lower Bound	Upper Bound		
WT	4	1.2974	.38869	.19434	.6790	1.9159	1.00	1.82
PV	4	1.2902	.40498	.20249	.6458	1.9346	.86	1.69
mdx	4	.7905	.04704	.02352	.7156	.8653	.74	.84
mdx/PV	4	.9930	.48135	.24067	.2271	1.7589	.62	1.70
Total	16	1.0928	.39797	.09949	.8807	1.3048	.62	1.82

Test of Homogeneity of Variances

SERCA2

Levene Statistic	df1	df2	Sig.
3.320	3	12	.057

180

ANOVA

SERCA2

	Sum of Squares	df	Mean Square	F	Sig.
Between Groups	.729	3	.243	1.770	.206
Within Groups	1.647	12	.137		
Total	2.376	15			

Multiple Comparisons

Dependent Variable: SERCA2

(I) Genotype	(J) Genotype	Mean Difference (I-J)	Std. Error	Sig.	95% Confidence Interval	
					Lower Bound	Upper Bound
WT	PV	.00726	.26196	.978	-.5635	.5780
	mdx	.50695	.26196	.077	-.0638	1.0777
	mdx/PV	.30444	.26196	.268	-.2663	.8752
PV	WT	-.00726	.26196	.978	-.5780	.5635
	mdx	.49969	.26196	.081	-.0711	1.0705
	mdx/PV	.29718	.26196	.279	-.2736	.8679
mdx	WT	-.50695	.26196	.077	-1.0777	.0638
	PV	-.49969	.26196	.081	-1.0705	.0711
	mdx/PV	-.20251	.26196	.454	-.7733	.3683
mdx/PV	WT	-.30444	.26196	.268	-.8752	.2663
	PV	-.29718	.26196	.279	-.8679	.2736
	mdx	.20251	.26196	.454	-.3683	.7733

6) Total utrophin levels in CnA* models:

t-Test: Two-Sample Assuming Equal Variances

	Variable mdx	Variable mdx/CnA*
Mean	0.842697	1.636483
Variance	0.081017	0.138693
Observations	3	3
Pooled Variance	0.109855	
Hypothesized Mean Difference	0	
df	4	
t Stat	-2.93318	

P(T<=t) one-tail	0.021339	
t Critical one-tail	2.131847	
P(T<=t) two-tail	0.042678	
t Critical two-tail	2.776445	

7) HSP70 levels in CnA* models:

t-Test: Two-Sample Assuming Equal Variances

	Variable mdx	Variable mdx/CnA*
Mean	0.833651	0.870902
Variance	0.042237	0.04419
Observations	3	3
Pooled Variance	0.043213	
Hypothesized Mean Difference	0	
Df	4	
t Stat	-0.21947	
P(T<=t) one-tail	0.418514	
t Critical one-tail	2.131847	
P(T<=t) two-tail	0.837028	
t Critical two-tail	2.776445	

8) Total utrophin levels in CaMBP models:

Note: The four sets of utrophin were done on separate gels. CaMBP, mdx and mdx/CaMBP were normalized to WT in each set and WT was standardized to 1.

t-Test: Two-Sample Assuming Equal Variances

	Variable mdx	Variable mdx/CaMBP
Mean	1	0.374818
Variance	0	0.064136
Observations	3	3
Pooled Variance	0.032068	
Hypothesized Mean Difference	0	
Df	4	
t Stat	4.275776	
P(T<=t) one-tail	0.006445	
t Critical one-tail	2.131847	

P(T<=t) two-tail	0.012891
t Critical two-tail	2.776445

9) HSP70 levels in CaMBP models:

t-Test: Two-Sample Assuming Equal Variances

	Variable mdx	Variable mdx/CaMBP
Mean	0.998953	0.755409
Variance	0.078827	0.192775
Observations	3	3
Pooled Variance	0.135801	
Hypothesized Mean Difference	0	
Df	4	
t Stat	0.809416	
P(T<=t) one-tail	0.231837	
t Critical one-tail	2.131847	
P(T<=t) two-tail	0.463674	
t Critical two-tail	2.776445	

Histology

1) NFATc1 nuclear localization in PV models:

Descriptives

NFATc1 nuclear localization

	N	Mean	Std. Deviation	Std. Error	95% Confidence Interval for Mean		Minimum	Maximum
					Lower Bound	Upper Bound		
WT	3	32.5795	7.23009	4.17429	14.6189	50.5400	24.24	36.99
PV	3	9.9939	.84413	.48736	7.8970	12.0908	9.02	10.53
mdx	3	16.2044	1.40801	.81292	12.7067	19.7021	14.91	17.70
mdx/PV	3	5.5476	1.86867	1.07888	.9055	10.1896	3.39	6.63
Total	12	16.0813	11.19084	3.23052	8.9710	23.1917	3.39	36.99

Test of Homogeneity of Variances

NFATc1 nuclear localization

Levene Statistic	df1	df2	Sig.
9.233	3	8	.006

ANOVA

NFATc1 nuclear localization

	Sum of Squares	df	Mean Square	F	Sig.
Between Groups	1260.662	3	420.221	28.752	.000
Within Groups	116.922	8	14.615		
Total	1377.584	11			

Multiple Comparisons

Dependent Variable: NFATc1 nuclear localization

(I) Genotype	(J) Genotype	Mean Difference (I-J)	Std. Error	Sig.	95% Confidence Interval	
					Lower Bound	Upper Bound
WT	PV	22.58558*	3.12146	.000	15.3875	29.7837
	mdx	16.37510*	3.12146	.001	9.1770	23.5732
	mdx/PV	27.03189*	3.12146	.000	19.8338	34.2300
PV	WT	-22.58558*	3.12146	.000	-29.7837	-15.3875
	mdx	-6.21047	3.12146	.082	-13.4086	.9876
	mdx/PV	4.44632	3.12146	.192	-2.7518	11.6444
mdx	WT	-16.37510*	3.12146	.001	-23.5732	-9.1770
	PV	6.21047	3.12146	.082	-.9876	13.4086
	mdx/PV	10.65679*	3.12146	.009	3.4587	17.8549
mdx/PV	WT	-27.03189*	3.12146	.000	-34.2300	-19.8338
	PV	-4.44632	3.12146	.192	-11.6444	2.7518
	mdx	-10.65679*	3.12146	.009	-17.8549	-3.4587

*. The mean difference is significant at the 0.05 level.

2) Fiber-type proportions in PV models:

Note: student t-test was done to compare each MyHC type in mdx compared to mdx/PV

t-Test: Two-Sample Assuming Equal Variances
(MyHC I)

	Variable mdx	Variable mdx/PV
Mean	41.04335	44.20607
Variance	221.0337	50.77086
Observations	4	4
Pooled Variance	135.9023	
Hypothesized Mean Difference	0	
Df	6	
t Stat	-0.38367	
P(T<=t) one-tail	0.357224	
t Critical one-tail	1.94318	
P(T<=t) two-tail	0.714448	
t Critical two-tail	2.446912	

t-Test: Two-Sample Assuming Equal Variances
(MyHC IIa)

	Variable mdx	Variable mdx/PV
Mean	50.24074	48.83463
Variance	282.5569	32.8443
Observations	4	4
Pooled Variance	157.7006	
Hypothesized Mean Difference	0	
Df	6	
t Stat	0.15835	
P(T<=t) one-tail	0.439688	
t Critical one-tail	1.94318	
P(T<=t) two-tail	0.879376	
t Critical two-tail	2.446912	

t-Test: Two-Sample Assuming Equal Variances
(MyHC I/IIa co-expression)

	Variable mdx	Variable mdx/PV
Mean	5.861323	3.74982
Variance	2.881379	4.278988

185

Observations	4	4
Pooled Variance	3.580183	
Hypothesized Mean Difference	0	
df	6	
t Stat	1.578171	
P(T<=t) one-tail	0.082801	
t Critical one-tail	1.94318	
P(T<=t) two-tail	0.165603	
t Critical two-tail	2.446912	

3) H&E central nucleation in PV models:

t-Test: Two-Sample Assuming Equal Variances

	Variable mdx	Variable mdx/PV
Mean	100	120.1314
Variance	0	15.93319
Observations	4	4
Pooled Variance	7.966596	
Hypothesized Mean Difference	0	
df	6	
t Stat	-10.0868	
P(T<=t) one-tail	2.76E-05	
t Critical one-tail	1.94318	
P(T<=t) two-tail	5.51E-05	
t Critical two-tail	2.446912	

4) H&E size variability in PV models:

t-Test: Two-Sample Assuming Equal Variances

	Variable mdx	Variable mdx/PV
Mean	100	144.0923
Variance	0	757.4866
Observations	4	4
Pooled Variance	378.7433	
Hypothesized Mean Difference	0	
Df	6	

t Stat	-3.2041
P(T<=t) one-tail	0.009252
t Critical one-tail	1.943181
P(T<=t) two-tail	0.018504
t Critical two-tail	2.446914

5) Evan's blue intensity in PV models:

t-Test: Two-Sample Assuming Equal Variances

	Variable mdx	Variable mdx/PV
Mean	20.72271	75.96756
Variance	112.6333	752.357
Observations	3	3
Pooled Variance	432.4952	
Hypothesized Mean Difference	0	
Df	4	
t Stat	-3.25347	
P(T<=t) one-tail	0.015637	
t Critical one-tail	2.131847	
P(T<=t) two-tail	0.031273	
t Critical two-tail	2.776445	

6) MyHC I central nucleation in PV models:

Descriptives

Central nucleation

	N	Mean	Std. Deviation	Std. Error	95% Confidence Interval for Mean		Minimum	Maximum
					Lower Bound	Upper Bound		
mdx-TypeI +ve	4	10.4374	2.67827	1.33913	6.1757	14.6991	6.47	12.30
mdx/PV-Type I +ve	3	32.8799	8.14085	4.70012	12.6569	53.1029	25.00	41.26
mdx-Type I -ve	4	37.6226	9.35807	4.67904	22.7319	52.5134	25.18	47.06
mdx/PV-Type I -ve	3	43.9219	8.89645	5.13637	21.8219	66.0219	34.27	51.79
Total	14	30.1890	15.04895	4.02200	21.5000	38.8780	6.47	51.79

Test of Homogeneity of Variances

Central nucleation

Levene Statistic	df1	df2	Sig.
1.210	3	10	.356

ANOVA

Central nucleation

	Sum of Squares	df	Mean Square	F	Sig.
Between Groups	2369.042	3	789.681	13.732	.001
Within Groups	575.080	10	57.508		
Total	2944.122	13			

Multiple Comparisons

Dependent Variable: Central nucleation

(I) Genotype	(J) Genotype	Mean Difference (I-J)	Std. Error	Sig.	95% Confidence Interval	
					Lower Bound	Upper Bound
mdx-Type I +ve	mdx/PV-Type I +ve	-22.44251*	5.79192	.003	-35.3477	-9.5373
	mdx-Type I -ve	-27.18525*	5.36228	.000	-39.1331	-15.2373
	mdx/PV-Type I -ve	-33.48452*	5.79192	.000	-46.3897	-20.5793
mdx/PV-Type I +ve	mdx-TypeI +ve	22.44251*	5.79192	.003	9.5373	35.3477
	mdx-Type I -ve	-4.74274	5.79192	.432	-17.6479	8.1625
	mdx/PV-Type I -ve	-11.04201	6.19182	.105	-24.8383	2.7542
mdx-Type I -ve	mdx-TypeI +ve	27.18525*	5.36228	.000	15.2373	39.1331
	mdx/PV-Type I +ve	4.74274	5.79192	.432	-8.1625	17.6479
	mdx/PV-Type I -ve	-6.29927	5.79192	.302	-19.2045	6.6059
mdx/PV-Type I -ve	mdx-TypeI +ve	33.48452*	5.79192	.000	20.5793	46.3897
	mdx/PV-Type I +ve	11.04201	6.19182	.105	-2.7542	24.8383
	mdx-Type I -ve	6.29927	5.79192	.302	-6.6059	19.2045

*. The mean difference is significant at the 0.05 level.

Appendix II: Chapter 3- Statistical Analyses

QPCR

1) RCAN1.4 levels in soleus muscles of PV models:

Descriptives

RCAN1.4

	N	Mean	Std. Deviation	Std. Error	95% Confidence Interval for Mean		Minimum	Maximum
					Lower Bound	Upper Bound		
WT	4	1.3785	.37520	.18760	.7815	1.9755	1.00	1.87
PV	4	3.5689	1.02850	.51425	1.9323	5.2055	2.57	4.87
mdx	4	3.4565	1.58098	.79049	.9408	5.9722	1.99	5.25
mdx/PV	4	6.9215	3.32524	1.66262	1.6303	12.2127	4.10	11.74
Total	16	3.8314	2.67540	.66885	2.4057	5.2570	1.00	11.74

Test of Homogeneity of Variances

RCAN1.4

Levene Statistic	df1	df2	Sig.
3.569	3	12	.047

ANOVA

RCAN1.4

	Sum of Squares	df	Mean Square	F	Sig.
Between Groups	63.100	3	21.033	5.702	.012
Within Groups	44.266	12	3.689		
Total	107.366	15			

Multiple Comparisons

Dependent Variable: RCAN1.4

(I) Genotype	(J) Genotype	Mean Difference (I-J)	Std. Error	Sig.	95% Confidence Interval	
					Lower Bound	Upper Bound
WT	PV	-2.19041	1.35809	.133	-5.1494	.7686
	mdx	-2.07802	1.35809	.152	-5.0371	.8810
	mdx/PV	-5.54303[*]	1.35809	.002	-8.5021	-2.5840

PV	WT	2.19041	1.35809	.133	-.7686	5.1494
	mdx	.11238	1.35809	.935	-2.8466	3.0714
	mdx/PV	-3.35263*	1.35809	.030	-6.3117	-.3936
mdx	WT	2.07802	1.35809	.152	-.8810	5.0371
	PV	-.11238	1.35809	.935	-3.0714	2.8466
	mdx/PV	-3.46501*	1.35809	.025	-6.4240	-.5060
mdx/PV	WT	5.54303*	1.35809	.002	2.5840	8.5021
	PV	3.35263*	1.35809	.030	.3936	6.3117
	mdx	3.46501*	1.35809	.025	.5060	6.4240

*. The mean difference is significant at the 0.05 level.

2) RCAN1.4 levels in EDL muscles of PV models: Kriskal Wallis non-parametric test:

	N	Mean	Std. Deviation
WT	3	3.2623	.87256
PV	3	1.4077	.50373
mdx	3	5.7770	1.93515
mdx/PV	3	4.3927	2.80839
Total	12	3.7099	2.25656

Hypothesis Test Summary

	Null Hypothesis	Test	Sig.	Decision
1	The distribution of RCAN is the same across categories of Genotype.	Independent-Samples Kruskal-Wallis Test	.066	Retain the null hypothesis.

Asymptotic significances are displayed. The significance level is .05.

3) Calsarcin-1 levels in soleus muscles of PV models:

Descriptives

Calsarcin-1

	N	Mean	Std. Deviation	Std. Error	95% Confidence Interval for Mean		Minimum	Maximum
					Lower Bound	Upper Bound		
WT	4	4.3679	3.89354	1.94677	-1.8276	10.5634	1.00	9.98
PV	4	8.8391	4.17848	2.08924	2.1902	15.4880	5.80	15.02
mdx	4	28.7825	26.67746	13.33873	-13.6673	71.2323	3.92	51.88
mdx/PV	4	35.3554	21.32983	10.66492	1.4149	69.2959	10.92	58.22
Total	16	19.3362	20.52341	5.13085	8.4001	30.2724	1.00	58.22

Test of Homogeneity of Variances

Calsarcin-1

Levene Statistic	df1	df2	Sig.
25.599	3	12	.000

ANOVA

Calsarcin-1

	Sum of Squares	df	Mean Square	F	Sig.
Between Groups	2720.352	3	906.784	3.024	.071
Within Groups	3597.804	12	299.817		
Total	6318.156	15			

Multiple Comparisons

Dependent Variable: Calsarcin-1

(I) Genotype	(J) Genotype	Mean Difference (I-J)	Std. Error	Sig.	95% Confidence Interval	
					Lower Bound	Upper Bound
WT	PV	-4.47127	12.24371	.721	-31.1480	22.2055
	mdx	-24.41467	12.24371	.069	-51.0914	2.2621
	mdx/PV	-30.98756*	12.24371	.026	-57.6643	-4.3108
PV	WT	4.47127	12.24371	.721	-22.2055	31.1480
	mdx	-19.94340	12.24371	.129	-46.6202	6.7334
	mdx/PV	-26.51629	12.24371	.051	-53.1930	.1605

	WT	24.41467	12.24371	.069	-2.2621	51.0914
mdx	PV	19.94340	12.24371	.129	-6.7334	46.6202
	mdx/PV	-6.57289	12.24371	.601	-33.2496	20.1039
	WT	30.98756*	12.24371	.026	4.3108	57.6643
mdx/PV	PV	26.51629	12.24371	.051	-.1605	53.1930
	mdx	6.57289	12.24371	.601	-20.1039	33.2496

*. The mean difference is significant at the 0.05 level.

4) Calsarcin-1 levels in EDL muscles of PV models:

Descriptives

Calsarcin-1

	N	Mean	Std. Deviation	Std. Error	95% Confidence Interval for Mean		Minimum	Maximum
					Lower Bound	Upper Bound		
WT	3	3.8617	3.48453	2.01180	-4.7943	12.5178	1.00	7.74
PV	3	2.6053	1.22637	.70805	-.4412	5.6518	1.86	4.02
mdx	3	8.6736	9.70529	5.60335	-15.4357	32.7829	2.76	19.87
mdx/PV	3	6.5238	5.56433	3.21256	-7.2988	20.3463	2.24	12.81
Total	12	5.4161	5.59274	1.61448	1.8626	8.9696	1.00	19.87

Test of Homogeneity of Variances

Calsarcin-1

Levene Statistic	df1	df2	Sig.
5.337	3	8	.026

ANOVA

Calsarcin-1

	Sum of Squares	df	Mean Square	F	Sig.
Between Groups	66.465	3	22.155	.638	.611
Within Groups	277.601	8	34.700		
Total	344.066	11			

Multiple Comparisons

Dependent Variable: Calsarcin-1

(I) Genotype	(J) Genotype	Mean Difference (I-J)	Std. Error	Sig.	95% Confidence Interval	
					Lower Bound	Upper Bound
WT	PV	1.25641	4.80972	.801	-9.8348	12.3476
	mdx	-4.81190	4.80972	.346	-15.9031	6.2793
	mdx/PV	-2.66205	4.80972	.595	-13.7533	8.4292
PV	WT	-1.25641	4.80972	.801	-12.3476	9.8348
	mdx	-6.06831	4.80972	.243	-17.1595	5.0229
	mdx/PV	-3.91845	4.80972	.439	-15.0097	7.1728
mdx	WT	4.81190	4.80972	.346	-6.2793	15.9031
	PV	6.06831	4.80972	.243	-5.0229	17.1595
	mdx/PV	2.14985	4.80972	.667	-8.9414	13.2411
mdx/PV	WT	2.66205	4.80972	.595	-8.4292	13.7533
	PV	3.91845	4.80972	.439	-7.1728	15.0097
	mdx	-2.14985	4.80972	.667	-13.2411	8.9414

5) MLP levels in soleus muscles of PV models:

Descriptives

MLP

	N	Mean	Std. Deviation	Std. Error	95% Confidence Interval for Mean		Minimum	Maximum
					Lower Bound	Upper Bound		
WT	4	8.5681	3.16846	1.58423	3.5264	13.6098	5.84	12.26
PV	4	11.2472	2.85125	1.42563	6.7102	15.7842	7.96	14.88
mdx	4	6.5623	4.81832	2.40916	-1.1047	14.2293	1.00	12.61
mdx/PV	4	6.6709	4.21651	2.10825	-.0385	13.3803	1.98	11.49
Total	16	8.2621	3.95975	.98994	6.1521	10.3721	1.00	14.88

Test of Homogeneity of Variances

MLP

Levene Statistic	df1	df2	Sig.
.559	3	12	.652

193

ANOVA

MLP

	Sum of Squares	df	Mean Square	F	Sig.
Between Groups	57.703	3	19.234	1.300	.319
Within Groups	177.492	12	14.791		
Total	235.195	15			

Multiple Comparisons

Dependent Variable: MLP

(I) Genotype	(J) Genotype	Mean Difference (I-J)	Std. Error	Sig.	95% Confidence Interval	
					Lower Bound	Upper Bound
WT	PV	-2.67910	2.71946	.344	-8.6043	3.2461
	mdx	2.00580	2.71946	.475	-3.9194	7.9310
	mdx/PV	1.89722	2.71946	.499	-4.0280	7.8224
PV	WT	2.67910	2.71946	.344	-3.2461	8.6043
	mdx	4.68490	2.71946	.111	-1.2403	10.6101
	mdx/PV	4.57632	2.71946	.118	-1.3489	10.5015
mdx	WT	-2.00580	2.71946	.475	-7.9310	3.9194
	PV	-4.68490	2.71946	.111	-10.6101	1.2403
	mdx/PV	-.10857	2.71946	.969	-6.0338	5.8166
mdx/PV	WT	-1.89722	2.71946	.499	-7.8224	4.0280
	PV	-4.57632	2.71946	.118	-10.5015	1.3489
	mdx	.10857	2.71946	.969	-5.8166	6.0338

6) MLP levels in EDL muscles of PV models:

Descriptives

MLP

	N	Mean	Std. Deviation	Std. Error	95% Confidence Interval for Mean		Minimum	Maximum
					Lower Bound	Upper Bound		
WT	3	2.0069	.99790	.57614	-.4720	4.4858	1.25	3.14
PV	3	1.9808	1.01490	.58595	-.5403	4.5020	1.00	3.03
mdx	3	5.4481	2.35989	1.36248	-.4142	11.3104	3.52	8.08

194

mdx/PV	3	2.9308	2.71433	1.56712	-3.8120	9.6736	1.20	6.06
Total	12	3.0917	2.21345	.63897	1.6853	4.4980	1.00	8.08

Test of Homogeneity of Variances

MLP

Levene Statistic	df1	df2	Sig.
2.654	3	8	.120

ANOVA

MLP

	Sum of Squares	df	Mean Square	F	Sig.
Between Groups	23.968	3	7.989	2.136	.174
Within Groups	29.925	8	3.741		
Total	53.893	11			

Multiple Comparisons

Dependent Variable: MLP

(I) Genotype	(J) Genotype	Mean Difference (I-J)	Std. Error	Sig.	95% Confidence Interval	
					Lower Bound	Upper Bound
WT	PV	.02605	1.57916	.987	-3.6155	3.6676
	mdx	-3.44122	1.57916	.061	-7.0828	.2003
	mdx/PV	-.92394	1.57916	.575	-4.5655	2.7176
PV	WT	-.02605	1.57916	.987	-3.6676	3.6155
	mdx	-3.46727	1.57916	.059	-7.1088	.1743
	mdx/PV	-.94999	1.57916	.564	-4.5915	2.6916
mdx	WT	3.44122	1.57916	.061	-.2003	7.0828
	PV	3.46727	1.57916	.059	-.1743	7.1088
	mdx/PV	2.51728	1.57916	.150	-1.1243	6.1588
mdx/PV	WT	.92394	1.57916	.575	-2.7176	4.5655
	PV	.94999	1.57916	.564	-2.6916	4.5915
	mdx	-2.51728	1.57916	.150	-6.1588	1.1243

7) RCAN1.4 levels in EDL muscles of CnA* models:

Descriptives

RCAN1.4

	N	Mean	Std. Deviation	Std. Error	95% Confidence Interval for Mean		Minimum	Maximum
					Lower Bound	Upper Bound		
WT	3	6.7756	4.19668	2.42295	-3.6496	17.2007	3.59	11.53
CnA	3	7.3028	4.81259	2.77855	-4.6523	19.2579	4.42	12.86
Mdx	3	2.1684	1.01298	.58484	-.3479	4.6848	1.00	2.80
mdx/CnA	3	2.3387	.66428	.38352	.6885	3.9888	1.65	2.98
Total	12	4.6464	3.73738	1.07889	2.2717	7.0210	1.00	12.86

Test of Homogeneity of Variances

RCAN1.4

Levene Statistic	df1	df2	Sig.
6.068	3	8	.019

ANOVA

RCAN1.4

	Sum of Squares	df	Mean Square	F	Sig.
Between Groups	69.167	3	23.056	2.183	.168
Within Groups	84.481	8	10.560		
Total	153.648	11			

Multiple Comparisons

Dependent Variable: RCAN1.4

(I) Genotype	(J) Genotype	Mean Difference (I-J)	Std. Error	Sig.	95% Confidence Interval	
					Lower Bound	Upper Bound
WT	CnA	-.52724	2.65332	.847	-6.6458	5.5913
	mdx	4.60711	2.65332	.121	-1.5115	10.7257
	mdx/CnA	4.43689	2.65332	.133	-1.6817	10.5555
CnA	WT	.52724	2.65332	.847	-5.5913	6.6458
	mdx	5.13435	2.65332	.089	-.9842	11.2529
	mdx/CnA	4.96413	2.65332	.098	-1.1544	11.0827
Mdx	WT	-4.60711	2.65332	.121	-10.7257	1.5115
	CnA	-5.13435	2.65332	.089	-11.2529	.9842

	mdx/CnA	-.17022	2.65332	.950	-6.2888	5.9483
	WT	-4.43689	2.65332	.133	-10.5555	1.6817
mdx/CnA	CnA	-4.96413	2.65332	.098	-11.0827	1.1544
	mdx	.17022	2.65332	.950	-5.9483	6.2888

8) Calsarcin-2 levels in EDL muscles of CnA* models:

Descriptives

Calsarcin-2

	N	Mean	Std. Deviation	Std. Error	95% Confidence Interval for Mean		Minimum	Maximum
					Lower Bound	Upper Bound		
WT	3	5.4847	.28371	.16380	4.7799	6.1895	5.16	5.65
CnA	3	7.2099	2.65420	1.53240	.6165	13.8033	4.18	9.12
Mdx	3	6.3149	1.97651	1.14114	1.4050	11.2248	5.09	8.59
mdx/CnA	3	4.0088	3.67884	2.12398	-5.1299	13.1475	1.00	8.11
Total	12	5.7546	2.44557	.70598	4.2007	7.3084	1.00	9.12

Test of Homogeneity of Variances

Calsarcin-2

Levene Statistic	df1	df2	Sig.
3.660	3	8	.063

ANOVA

Calsarcin-2

	Sum of Squares	df	Mean Square	F	Sig.
Between Groups	16.658	3	5.553	.904	.481
Within Groups	49.131	8	6.141		
Total	65.789	11			

Multiple Comparisons

Dependent Variable: Calsarcin-2

(I) Genotype	(J) Genotype	Mean Difference (I-J)	Std. Error	Sig.	95% Confidence Interval	
					Lower Bound	Upper Bound
WT	CnA	-1.72522	2.02343	.419	-6.3913	2.9408
	mdx	-.83020	2.02343	.692	-5.4962	3.8358
	mdx/CnA	1.47590	2.02343	.487	-3.1901	6.1419
CnA	WT	1.72522	2.02343	.419	-2.9408	6.3913
	mdx	.89502	2.02343	.670	-3.7710	5.5611
	mdx/CnA	3.20112	2.02343	.152	-1.4649	7.8672
Mdx	WT	.83020	2.02343	.692	-3.8358	5.4962
	CnA	-.89502	2.02343	.670	-5.5611	3.7710
	mdx/CnA	2.30610	2.02343	.287	-2.3599	6.9721
mdx/CnA	WT	-1.47590	2.02343	.487	-6.1419	3.1901
	CnA	-3.20112	2.02343	.152	-7.8672	1.4649
	mdx	-2.30610	2.02343	.287	-6.9721	2.3599

9) MLP levels in EDL muscles of CnA* models:

Descriptives

MLP

	N	Mean	Std. Deviation	Std. Error	95% Confidence Interval for Mean		Minimum	Maximum
					Lower Bound	Upper Bound		
WT	3	7.1036	5.04364	2.91195	-5.4255	19.6327	2.83	12.67
CnA	3	8.5211	6.04437	3.48972	-6.4939	23.5362	2.91	14.92
Mdx	3	1.6426	.37522	.21663	.7105	2.5747	1.28	2.03
mdx/CnA	3	3.0761	2.35078	1.35722	-2.7635	8.9158	1.00	5.63
Total	12	5.0859	4.57841	1.32167	2.1769	7.9948	1.00	14.92

Test of Homogeneity of Variances

MLP

Levene Statistic	df1	df2	Sig.
2.695	3	8	.117

ANOVA

MLP

	Sum of Squares	df	Mean Square	F	Sig.
Between Groups	95.301	3	31.767	1.879	.212
Within Groups	135.279	8	16.910		
Total	230.580	11			

Multiple Comparisons

Dependent Variable: MLP

(I) Genotype	(J) Genotype	Mean Difference (I-J)	Std. Error	Sig.	95% Confidence Interval	
					Lower Bound	Upper Bound
WT	CnA	-1.41753	3.35757	.684	-9.1601	6.3250
	mdx	5.46094	3.35757	.143	-2.2816	13.2035
	mdx/CnA	4.02746	3.35757	.265	-3.7151	11.7700
CnA	WT	1.41753	3.35757	.684	-6.3250	9.1601
	mdx	6.87847	3.35757	.075	-.8641	14.6210
	mdx/CnA	5.44499	3.35757	.144	-2.2976	13.1876
Mdx	WT	-5.46094	3.35757	.143	-13.2035	2.2816
	CnA	-6.87847	3.35757	.075	-14.6210	.8641
	mdx/CnA	-1.43347	3.35757	.681	-9.1760	6.3091
mdx/CnA	WT	-4.02746	3.35757	.265	-11.7700	3.7151
	CnA	-5.44499	3.35757	.144	-13.1876	2.2976
	mdx	1.43347	3.35757	.681	-6.3091	9.1760

Immunoblotting

1) RCAN1 levels in PV models:

Descriptives

RCAN1

	N	Mean	Std. Deviation	Std. Error	95% Confidence Interval for Mean		Minimum	Maximum
					Lower Bound	Upper Bound		

WT	3	1.0531	.09205	.05314	.8245	1.2818	1.00	1.16
PV	3	1.2222	.64067	.36989	-.3693	2.8138	.81	1.96
Mdx	3	1.4098	.29933	.17282	.6662	2.1534	1.22	1.76
mdx/PV	3	.9412	.13483	.07784	.6063	1.2761	.80	1.07
Total	12	1.1566	.36056	.10408	.9275	1.3857	.80	1.96

Test of Homogeneity of Variances

RCAN1

Levene Statistic	df1	df2	Sig.
7.035	3	8	.012

ANOVA

RCAN1

	Sum of Squares	df	Mean Square	F	Sig.
Between Groups	.377	3	.126	.953	.460
Within Groups	1.053	8	.132		
Total	1.430	11			

Multiple Comparisons

Dependent Variable: RCAN1

(I) Genotype	(J) Genotype	Mean Difference (I-J)	Std. Error	Sig.	95% Confidence Interval	
					Lower Bound	Upper Bound
WT	PV	-.16911	.29629	.584	-.8523	.5141
	mdx	-.35667	.29629	.263	-1.0399	.3266
	mdx/PV	.11195	.29629	.715	-.5713	.7952
PV	WT	.16911	.29629	.584	-.5141	.8523
	mdx	-.18756	.29629	.544	-.8708	.4957
	mdx/PV	.28106	.29629	.371	-.4022	.9643
Mdx	WT	.35667	.29629	.263	-.3266	1.0399
	PV	.18756	.29629	.544	-.4957	.8708
	mdx/PV	.46862	.29629	.152	-.2146	1.1519
mdx/PV	WT	-.11195	.29629	.715	-.7952	.5713
	PV	-.28106	.29629	.371	-.9643	.4022
	mdx	-.46862	.29629	.152	-1.1519	.2146

2) Calsarcin-1 levels in PV models:

Descriptives

Calsarcin-1

	N	Mean	Std. Deviation	Std. Error	95% Confidence Interval for Mean		Minimum	Maximum
					Lower Bound	Upper Bound		
WT	3	.8144	.32140	.18556	.0160	1.6128	.44	1.00
PV	3	.6534	.25840	.14919	.0115	1.2953	.43	.94
Mdx	3	.4972	.20399	.11777	-.0095	1.0039	.36	.73
mdx/PV	3	.5588	.05656	.03265	.4183	.6993	.51	.62
Total	12	.6310	.23384	.06751	.4824	.7795	.36	1.00

Test of Homogeneity of Variances

Calsarcin-1

Levene Statistic	df1	df2	Sig.
2.979	3	8	.096

ANOVA

Calsarcin-1

	Sum of Squares	df	Mean Square	F	Sig.
Between Groups	.172	3	.057	1.066	.416
Within Groups	.430	8	.054		
Total	.602	11			

Multiple Comparisons

Dependent Variable: Calsarcin-1

(I) Genotype	(J) Genotype	Mean Difference (I-J)	Std. Error	Sig.	95% Confidence Interval	
					Lower Bound	Upper Bound
WT	PV	.16105	.18924	.419	-.2753	.5974
	mdx	.31722	.18924	.132	-.1192	.7536
	mdx/PV	.25560	.18924	.214	-.1808	.6920
PV	WT	-.16105	.18924	.419	-.5974	.2753
	mdx	.15617	.18924	.433	-.2802	.5926
	mdx/PV	.09455	.18924	.631	-.3418	.5309

Mdx	WT	-.31722	.18924	.132	-.7536	.1192
	PV	-.15617	.18924	.433	-.5926	.2802
	mdx/PV	-.06162	.18924	.753	-.4980	.3748
mdx/PV	WT	-.25560	.18924	.214	-.6920	.1808
	PV	-.09455	.18924	.631	-.5309	.3418
	mdx	.06162	.18924	.753	-.3748	.4980

3) MLP levels in PV models:

Descriptives

MLP

	N	Mean	Std. Deviation	Std. Error	95% Confidence Interval for Mean		Minimum	Maximum
					Lower Bound	Upper Bound		
WT	3	.7881	.36708	.21193	-.1238	1.6999	.36	1.00
PV	3	.6549	.16122	.09308	.2544	1.0554	.47	.75
Mdx	3	.7028	.35915	.20736	-.1894	1.5950	.33	1.05
mdx/PV	3	.6885	.45505	.26272	-.4419	1.8189	.17	1.00
Total	12	.7086	.30489	.08801	.5148	.9023	.17	1.05

Test of Homogeneity of Variances

MLP

Levene Statistic	df1	df2	Sig.
1.329	3	8	.331

ANOVA

MLP

	Sum of Squares	df	Mean Square	F	Sig.
Between Groups	.029	3	.010	.078	.970
Within Groups	.994	8	.124		
Total	1.023	11			

Multiple Comparisons

Dependent Variable: MLP

(I) Genotype	(J) Genotype	Mean Difference (I-J)	Std. Error	Sig.	95% Confidence Interval	
					Lower Bound	Upper Bound
WT	PV	.13318	.28775	.656	-.5304	.7967
	mdx	.08526	.28775	.775	-.5783	.7488
	mdx/PV	.09958	.28775	.738	-.5640	.7631
PV	WT	-.13318	.28775	.656	-.7967	.5304
	mdx	-.04791	.28775	.872	-.7115	.6156
	mdx/PV	-.03359	.28775	.910	-.6971	.6300
Mdx	WT	-.08526	.28775	.775	-.7488	.5783
	PV	.04791	.28775	.872	-.6156	.7115
	mdx/PV	.01432	.28775	.962	-.6492	.6779
mdx/PV	WT	-.09958	.28775	.738	-.7631	.5640
	PV	.03359	.28775	.910	-.6300	.6971
	mdx	-.01432	.28775	.962	-.6779	.6492

4) RCAN1 levels in CnA* models:

Descriptives

RCAN1

	N	Mean	Std. Deviation	Std. Error	95% Confidence Interval for Mean		Minimum	Maximum
					Lower Bound	Upper Bound		
WT	3	1.0690	.11956	.06903	.7720	1.3660	1.00	1.21
CnA	3	1.4339	.69304	.40013	-.2877	3.1555	.76	2.14
mdx	3	1.0275	.53294	.30769	-.2965	2.3514	.60	1.62
mdx/CnA	3	.7691	.24667	.14241	.1564	1.3819	.59	1.05
Total	12	1.0749	.46251	.13351	.7810	1.3687	.59	2.14

Test of Homogeneity of Variances

RCAN1

Levene Statistic	df1	df2	Sig.
1.851	3	8	.216

ANOVA

RCAN1

	Sum of Squares	df	Mean Square	F	Sig.
Between Groups	.674	3	.225	1.071	.414
Within Groups	1.679	8	.210		
Total	2.353	11			

Multiple Comparisons

Dependent Variable: RCAN1

(I) Genotype	(J) Genotype	Mean Difference (I-J)	Std. Error	Sig.	95% Confidence Interval	
					Lower Bound	Upper Bound
WT	CnA	-.36490	.37405	.358	-1.2275	.4977
	mdx	.04158	.37405	.914	-.8210	.9041
	mdx/CnA	.29992	.37405	.446	-.5626	1.1625
CnA	WT	.36490	.37405	.358	-.4977	1.2275
	mdx	.40647	.37405	.309	-.4561	1.2690
	mdx/CnA	.66481	.37405	.113	-.1977	1.5274
mdx	WT	-.04158	.37405	.914	-.9041	.8210
	CnA	-.40647	.37405	.309	-1.2690	.4561
	mdx/CnA	.25834	.37405	.509	-.6042	1.1209
mdx/CnA	WT	-.29992	.37405	.446	-1.1625	.5626
	CnA	-.66481	.37405	.113	-1.5274	.1977
	mdx	-.25834	.37405	.509	-1.1209	.6042

5) Calsarcin-2 levels in CnA* models:

Descriptives

Calsarcin-2

	N	Mean	Std. Deviation	Std. Error	95% Confidence Interval for Mean		Minimum	Maximum
					Lower Bound	Upper Bound		
WT	3	1.1512	.26183	.15117	.5007	1.8016	1.00	1.45
CnA	3	1.4186	.16594	.09581	1.0064	1.8308	1.25	1.58

mdx	3	1.2481	.24137	.13936	.6485	1.8477	1.06	1.52
mdx/CnA	3	.9326	.13565	.07832	.5957	1.2696	.81	1.08
Total	12	1.1876	.25505	.07363	1.0256	1.3497	.81	1.58

Test of Homogeneity of Variances

Calsarcin-2

Levene Statistic	df1	df2	Sig.
1.069	3	8	.415

ANOVA

Calsarcin-2

	Sum of Squares	df	Mean Square	F	Sig.
Between Groups	.370	3	.123	2.856	.105
Within Groups	.346	8	.043		
Total	.716	11			

Multiple Comparisons

Dependent Variable: Calsarcin-2

(I) Genotype	(J) Genotype	Mean Difference (I-J)	Std. Error	Sig.	95% Confidence Interval	
					Lower Bound	Upper Bound
WT	CnA	-.26742	.16968	.154	-.6587	.1239
	mdx	-.09692	.16968	.584	-.4882	.2944
	mdx/CnA	.21853	.16968	.234	-.1728	.6098
CnA	WT	.26742	.16968	.154	-.1239	.6587
	mdx	.17050	.16968	.344	-.2208	.5618
	mdx/CnA	.48595*	.16968	.021	.0947	.8772
mdx	WT	.09692	.16968	.584	-.2944	.4882
	CnA	-.17050	.16968	.344	-.5618	.2208
	mdx/CnA	.31545	.16968	.100	-.0758	.7067
mdx/CnA	WT	-.21853	.16968	.234	-.6098	.1728
	CnA	-.48595*	.16968	.021	-.8772	-.0947
	mdx	-.31545	.16968	.100	-.7067	.0758

*. The mean difference is significant at the 0.05 level

6) MLP levels in CnA* models:

Descriptives

MLP

	N	Mean	Std. Deviation	Std. Error	95% Confidence Interval for Mean		Minimum	Maximum
					Lower Bound	Upper Bound		
WT	3	1.2190	.37931	.21899	.2767	2.1612	1.00	1.66
CnA	3	1.1699	.36113	.20850	.2728	2.0670	.90	1.58
mdx	3	.7720	.02296	.01326	.7150	.8290	.75	.79
mdx/CnA	3	.7076	.01391	.00803	.6731	.7422	.69	.72
Total	12	.9671	.32751	.09454	.7590	1.1752	.69	1.66

Test of Homogeneity of Variances

MLP

Levene Statistic	df1	df2	Sig.
8.481	3	8	.007

ANOVA

MLP

	Sum of Squares	df	Mean Square	F	Sig.
Between Groups	.630	3	.210	3.054	.092
Within Groups	.550	8	.069		
Total	1.180	11			

Multiple Comparisons

Dependent Variable: MLP

(I) Genotype	(J) Genotype	Mean Difference (I-J)	Std. Error	Sig.	95% Confidence Interval	
					Lower Bound	Upper Bound
WT	CnA	.04912	.21409	.824	-.4446	.5428
	mdx	.44699	.21409	.070	-.0467	.9407
	mdx/CnA	.51136*	.21409	.044	.0177	1.0051
CnA	WT	-.04912	.21409	.824	-.5428	.4446
	mdx	.39787	.21409	.100	-.0958	.8916
	mdx/CnA	.46224	.21409	.063	-.0314	.9559
mdx	WT	-.44699	.21409	.070	-.9407	.0467

	CnA	-.39787	.21409	.100	-.8916	.0958
	mdx/CnA	.06437	.21409	.771	-.4293	.5581
mdx/CnA	WT	-.51136[*]	.21409	.044	-1.0051	-.0177
	CnA	-.46224	.21409	.063	-.9559	.0314
	mdx	-.06437	.21409	.771	-.5581	.4293

*. The mean difference is significant at the 0.05 level.

Appendix III: Chapter 4- Statistical Analyses

Semi-quantitative PCR

1) β-MyHC levels in normotensive and 14 day stimulated hearts:

Descriptives

β-MyHC

	N	Mean	Std. Deviation	Std. Error	95% Confidence Interval for Mean		Minimum	Maximum
					Lower Bound	Upper Bound		
WT -VE	3	.4679	.16859	.09734	.0491	.8867	.34	.66
WT +VE 14 days	3	.8566	.16214	.09361	.4538	1.2594	.67	.96
KO -VE	3	.3856	.11942	.06894	.0889	.6822	.26	.49
KO +VE 14 days	3	1.2670	.17642	.10186	.8288	1.7053	1.13	1.46
Total	12	.7443	.38998	.11258	.4965	.9921	.26	1.46

Test of Homogeneity of Variances

β-MyHC

Levene Statistic	df1	df2	Sig.
.346	3	8	.793

ANOVA

β-MyHC

	Sum of Squares	df	Mean Square	F	Sig.
Between Groups	1.473	3	.491	19.617	.000
Within Groups	.200	8	.025		
Total	1.673	11			

Multiple Comparisons

Dependent Variable: β-MyHC

(I) Genotype	(J) Genotype	Mean Difference (I-J)	Std. Error	Sig.	95% Confidence Interval	
					Lower Bound	Upper Bound
WT -VE	WT +VE 14 days	-.38868*	.12916	.017	-.6865	-.0908
	KO -VE	.08237	.12916	.541	-.2155	.3802
	KO +VE 14 days	-.79908*	.12916	.000	-1.0969	-.5012
WT +VE 14 days	WT -VE	.38868*	.12916	.017	.0908	.6865
	KO -VE	.47105*	.12916	.007	.1732	.7689
	KO +VE 14 days	-.41040*	.12916	.013	-.7083	-.1126
KO -VE	WT -VE	-.08237	.12916	.541	-.3802	.2155
	WT +VE 14 days	-.47105*	.12916	.007	-.7689	-.1732
	KO +VE 14 days	-.88146*	.12916	.000	-1.1793	-.5836
KO +VE 14 days	WT -VE	.79908*	.12916	.000	.5012	1.0969
	WT +VE 14 days	.41040*	.12916	.013	.1126	.7083
	KO -VE	.88146*	.12916	.000	.5836	1.1793

*. The mean difference is significant at the 0.05 level.

2) ANP levels in normotensive and 14 day stimulated hearts:

Descriptives

ANP

	N	Mean	Std. Deviation	Std. Error	95% Confidence Interval for Mean		Minimum	Maximum
					Lower Bound	Upper Bound		
WT -VE	3	.2186	.04780	.02760	.0999	.3374	.16	.25
WT +VE 14 days	3	.4755	.08816	.05090	.2564	.6945	.38	.55
KO -VE	3	.2643	.09525	.05499	.0277	.5009	.16	.34
KO +VE 14 days	3	.5260	.01685	.00973	.4841	.5678	.51	.54
Total	12	.3711	.14998	.04329	.2758	.4664	.16	.55

Test of Homogeneity of Variances

ANP

Levene Statistic	df1	df2	Sig.
3.200	3	8	.084

ANOVA

ANP

	Sum of Squares	df	Mean Square	F	Sig.
Between Groups	.209	3	.070	14.325	.001
Within Groups	.039	8	.005		
Total	.247	11			

Multiple Comparisons

Dependent Variable: ANP

(I) Genotype	(J) Genotype	Mean Difference (I-J)	Std. Error	Sig.	95% Confidence Interval	
					Lower Bound	Upper Bound
WT -VE	WT +VE 14 days	-.25685*	.05688	.002	-.3880	-.1257
	KO -VE	-.04567	.05688	.445	-.1768	.0855
	KO +VE 14 days	-.30734*	.05688	.001	-.4385	-.1762
WT +VE 14 days	WT -VE	.25685*	.05688	.002	.1257	.3880
	KO -VE	.21118*	.05688	.006	.0800	.3424
	KO +VE 14 days	-.05049	.05688	.401	-.1817	.0807
KO -VE	WT -VE	.04567	.05688	.445	-.0855	.1768
	WT +VE 14 days	-.21118*	.05688	.006	-.3424	-.0800
	KO +VE 14 days	-.26167*	.05688	.002	-.3928	-.1305
KO +VE 14 days	WT -VE	.30734*	.05688	.001	.1762	.4385
	WT +VE 14 days	.05049	.05688	.401	-.0807	.1817
	KO -VE	.26167*	.05688	.002	.1305	.3928

*. The mean difference is significant at the 0.05 level.

3) BNP levels in normotensive and 14 day stimulated hearts:

Descriptives

BNP

	N	Mean	Std. Deviation	Std. Error	95% Confidence Interval for Mean		Minimum	Maximum
					Lower Bound	Upper Bound		
WT -VE	3	.0808	.03937	.02273	-.0170	.1786	.04	.12
WT +VE 14 days	3	.2160	.00928	.00536	.1930	.2391	.21	.23
KO -VE	3	.1319	.04276	.02469	.0257	.2381	.10	.18
KO +VE 14 days	3	.1715	.02038	.01177	.1209	.2221	.15	.19
Total	12	.1500	.05845	.01687	.1129	.1872	.04	.23

Test of Homogeneity of Variances

BNP

Levene Statistic	df1	df2	Sig.
1.808	3	8	.224

ANOVA

BNP

	Sum of Squares	df	Mean Square	F	Sig.
Between Groups	.030	3	.010	10.251	.004
Within Groups	.008	8	.001		
Total	.038	11			

Multiple Comparisons

Dependent Variable: BNP

(I) Genotype	(J) Genotype	Mean Difference (I-J)	Std. Error	Sig.	95% Confidence Interval	
					Lower Bound	Upper Bound
WT -VE	WT +VE 14 days	-.13524*	.02543	.001	-.1939	-.0766
	KO -VE	-.05108	.02543	.079	-.1097	.0076
	KO +VE 14 days	-.09071*	.02543	.007	-.1493	-.0321
WT +VE 14 days	WT -VE	.13524*	.02543	.001	.0766	.1939
	KO -VE	.08416*	.02543	.011	.0255	.1428
	KO +VE 14 days	.04454	.02543	.118	-.0141	.1032

KO -VE	WT -VE	.05108	.02543	.079	-.0076	.1097
	WT +VE 14 days	-.08416*	.02543	.011	-.1428	-.0255
	KO +VE 14 days	-.03962	.02543	.158	-.0983	.0190
KO +VE 14 days	WT -VE	.09071*	.02543	.007	.0321	.1493
	WT +VE 14 days	-.04454	.02543	.118	-.1032	.0141
	KO -VE	.03962	.02543	.158	-.0190	.0983

*. The mean difference is significant at the 0.05 level.

QPCR

1) Calsarcin-1 levels in normotensive and 14 day stimulated hearts:

Descriptives

Calsarcin-1

	N	Mean	Std. Deviation	Std. Error	95% Confidence Interval for Mean		Minimum	Maximum
					Lower Bound	Upper Bound		
WT -VE	3	1.5822	.63267	.36527	.0105	3.1538	1.00	2.26
WT +VE 14 days	3	5.7069	.70142	.40497	3.9645	7.4493	4.90	6.12
KO -VE	3	2.4209	1.30922	.75588	-.8314	5.6732	1.24	3.83
KO +VE 14 days	3	4.8697	2.62680	1.51658	-1.6556	11.3951	1.88	6.80
Total	12	3.6449	2.20594	.63680	2.2433	5.0465	1.00	6.80

Test of Homogeneity of Variances

Calsarcin-1

Levene Statistic	df1	df2	Sig.
4.065	3	8	.050

ANOVA

Calsarcin-1

	Sum of Squares	df	Mean Square	F	Sig.
Between Groups	34.515	3	11.505	4.841	.033
Within Groups	19.013	8	2.377		
Total	53.528	11			

Multiple Comparisons

Dependent Variable: Calsarcin-1

(I) Genotype	(J) Genotype	Mean Difference (I-J)	Std. Error	Sig.	95% Confidence Interval	
					Lower Bound	Upper Bound
WT -VE	WT +VE 14 days	-4.12470*	1.25873	.011	-7.0273	-1.2221
	KO -VE	-.83868	1.25873	.524	-3.7413	2.0640
	KO +VE 14 days	-3.28755*	1.25873	.031	-6.1902	-.3849
WT +VE 14 days	WT -VE	4.12470*	1.25873	.011	1.2221	7.0273
	KO -VE	3.28602*	1.25873	.031	.3834	6.1887
	KO +VE 14 days	.83715	1.25873	.525	-2.0655	3.7398
KO -VE	WT -VE	.83868	1.25873	.524	-2.0640	3.7413
	WT +VE 14 days	-3.28602*	1.25873	.031	-6.1887	-.3834
	KO +VE 14 days	-2.44886	1.25873	.088	-5.3515	.4538
KO +VE 14 days	WT -VE	3.28755*	1.25873	.031	.3849	6.1902
	WT +VE 14 days	-.83715	1.25873	.525	-3.7398	2.0655
	KO -VE	2.44886	1.25873	.088	-.4538	5.3515

*. The mean difference is significant at the 0.05 level.

2) CnAβ1 levels in normotensive and 14 day stimulated hearts:

Descriptives

CnAβ1

	N	Mean	Std. Deviation	Std. Error	95% Confidence Interval for Mean		Minimum	Maximum
					Lower Bound	Upper Bound		
WT -VE	3	2.4564	1.14438	.66071	-.3864	5.2992	1.37	3.65
WT +VE 14 days	3	4.1993	.19155	.11059	3.7235	4.6752	4.00	4.38
KO -VE	3	2.5813	.99899	.57677	.0997	5.0630	1.90	3.73
KO +VE 14 days	3	2.0881	1.14892	.66333	-.7660	4.9422	1.00	3.29
Total	12	2.8313	1.17587	.33944	2.0842	3.5784	1.00	4.38

213

Test of Homogeneity of Variances

CnAβ1

Levene Statistic	df1	df2	Sig.
1.511	3	8	.284

ANOVA

CnAβ1

	Sum of Squares	df	Mean Square	F	Sig.
Between Groups	7.881	3	2.627	2.868	.104
Within Groups	7.329	8	.916		
Total	15.209	11			

Multiple Comparisons

Dependent Variable: CnAβ1

(I) Genotype	(J) Genotype	Mean Difference (I-J)	Std. Error	Sig.	95% Confidence Interval	
					Lower Bound	Upper Bound
WT -VE	WT +VE 14 days	-1.74294	.78148	.056	-3.5450	.0592
	KO -VE	-.12494	.78148	.877	-1.9270	1.6772
	KO +VE 14 days	.36830	.78148	.650	-1.4338	2.1704
WT +VE 14 days	WT -VE	1.74294	.78148	.056	-.0592	3.5450
	KO -VE	1.61800	.78148	.072	-.1841	3.4201
	KO +VE 14 days	2.11124*	.78148	.027	.3091	3.9133
KO -VE	WT -VE	.12494	.78148	.877	-1.6772	1.9270
	WT +VE 14 days	-1.61800	.78148	.072	-3.4201	.1841
	KO +VE 14 days	.49324	.78148	.546	-1.3089	2.2953
KO +VE 14 days	WT -VE	-.36830	.78148	.650	-2.1704	1.4338
	WT +VE 14 days	-2.11124*	.78148	.027	-3.9133	-.3091
	KO -VE	-.49324	.78148	.546	-2.2953	1.3089

*. The mean difference is significant at the 0.05 level.

3) ATF4 levels in normotensive and 14 day stimulated hearts:

Descriptives

ATF4

	N	Mean	Std. Deviation	Std. Error	95% Confidence Interval for Mean		Minimum	Maximum
					Lower Bound	Upper Bound		
WT -VE	4	5.9883	4.75434	2.37717	-1.5769	13.5535	1.00	12.44
WT +VE 14 days	4	14.4966	8.35622	4.17811	1.2000	27.7933	5.18	24.43
KO -VE	4	8.1644	4.08719	2.04359	1.6608	14.6681	3.44	12.80
KO +VE 14 days	4	12.1799	7.90211	3.95106	-.3941	24.7540	3.51	21.67
Total	16	10.2073	6.79112	1.69778	6.5886	13.8260	1.00	24.43

Test of Homogeneity of Variances

ATF4

Levene Statistic	df1	df2	Sig.
1.479	3	12	.270

ANOVA

ATF4

	Sum of Squares	df	Mean Square	F	Sig.
Between Groups	177.053	3	59.018	1.376	.297
Within Groups	514.736	12	42.895		
Total	691.789	15			

Multiple Comparisons

Dependent Variable: ATF4

(I) Genotype	(J) Genotype	Mean Difference (I-J)	Std. Error	Sig.	95% Confidence Interval	
					Lower Bound	Upper Bound
WT -VE	WT +VE 14 days	-8.50837	4.63113	.091	-18.5987	1.5820
	KO -VE	-2.17616	4.63113	.647	-12.2665	7.9142
	KO +VE 14 days	-6.19166	4.63113	.206	-16.2820	3.8987
WT +VE 14 days	WT -VE	8.50837	4.63113	.091	-1.5820	18.5987
	KO -VE	6.33221	4.63113	.197	-3.7581	16.4226
	KO +VE 14 days	2.31671	4.63113	.626	-7.7737	12.4071
KO -VE	WT -VE	2.17616	4.63113	.647	-7.9142	12.2665
	WT +VE 14 days	-6.33221	4.63113	.197	-16.4226	3.7581

215

	KO +VE 14 days	-4.01550	4.63113	.403	-14.1059	6.0749
	WT -VE	6.19166	4.63113	.206	-3.8987	16.2820
KO +VE 14 days	WT +VE 14 days	-2.31671	4.63113	.626	-12.4071	7.7737
	KO -VE	4.01550	4.63113	.403	-6.0749	14.1059

4) Foxo3a levels in normotensive and 14 day stimulated hearts:

Descriptives

Foxo3a

	N	Mean	Std. Deviation	Std. Error	95% Confidence Interval for Mean		Minimum	Maximum
					Lower Bound	Upper Bound		
WT -VE	3	1.3641	.40548	.23410	.3569	2.3714	1.00	1.80
WT +VE 14 days	3	1.9699	.54447	.31435	.6174	3.3225	1.64	2.60
KO -VE	3	1.5112	.13952	.08055	1.1646	1.8578	1.42	1.67
KO +VE 14 days	3	2.6801	.96190	.55535	.2906	5.0696	1.65	3.55
Total	12	1.8813	.73623	.21253	1.4135	2.3491	1.00	3.55

Test of Homogeneity of Variances

Foxo3a

Levene Statistic	df1	df2	Sig.
2.522	3	8	.131

ANOVA

Foxo3a

	Sum of Squares	df	Mean Square	F	Sig.
Between Groups	3.151	3	1.050	2.989	.096
Within Groups	2.811	8	.351		
Total	5.962	11			

Multiple Comparisons

Dependent Variable: Foxo3a

(I) Genotype	(J) Genotype	Mean Difference (I-J)	Std. Error	Sig.	95% Confidence Interval Lower Bound	95% Confidence Interval Upper Bound
WT -VE	WT +VE 14 days	-.60580	.48401	.246	-1.7219	.5103
	KO -VE	-.14703	.48401	.769	-1.2631	.9691
	KO +VE 14 days	-1.31596*	.48401	.026	-2.4321	-.1998
WT +VE 14 days	WT -VE	.60580	.48401	.246	-.5103	1.7219
	KO -VE	.45877	.48401	.371	-.6573	1.5749
	KO +VE 14 days	-.71016	.48401	.180	-1.8263	.4060
KO -VE	WT -VE	.14703	.48401	.769	-.9691	1.2631
	WT +VE 14 days	-.45877	.48401	.371	-1.5749	.6573
	KO +VE 14 days	-1.16893*	.48401	.042	-2.2851	-.0528
KO +VE 14 days	WT -VE	1.31596*	.48401	.026	.1998	2.4321
	WT +VE 14 days	.71016	.48401	.180	-.4060	1.8263
	KO -VE	1.16893*	.48401	.042	.0528	2.2851

*. The mean difference is significant at the 0.05 level.

5) Myostatin levels in normotensive and 14 day stimulated hearts:

Descriptives

Myostatin

	N	Mean	Std. Deviation	Std. Error	95% Confidence Interval for Mean Lower Bound	95% Confidence Interval for Mean Upper Bound	Minimum	Maximum
WT -VE	4	5.9163	4.89668	2.44834	-1.8754	13.7080	1.19	12.37
WT +VE 14 days	4	3.6115	1.95252	.97626	.5046	6.7184	1.59	5.96
KO -VE	4	9.2726	9.43216	4.71608	-5.7361	24.2813	1.00	22.63
KO +VE 14 days	4	43.2075	39.99396	19.99698	-20.4318	106.8468	5.93	99.95
Total	16	15.5020	24.90983	6.22746	2.2285	28.7755	1.00	99.95

Test of Homogeneity of Variances

Myostatin

Levene Statistic	df1	df2	Sig.
4.357	3	12	.027

ANOVA

Myostatin

	Sum of Squares	df	Mean Square	F	Sig.
Between Groups	4158.677	3	1386.226	3.231	.061
Within Groups	5148.818	12	429.068		
Total	9307.495	15			

Multiple Comparisons

Dependent Variable: Myostatin

(I) Genotype	(J) Genotype	Mean Difference (I-J)	Std. Error	Sig.	95% Confidence Interval	
					Lower Bound	Upper Bound
WT -VE	WT +VE 14 days	2.30486	14.64698	.878	-29.6082	34.2179
	KO -VE	-3.35627	14.64698	.823	-35.2693	28.5568
	KO +VE 14 days	-37.29116*	14.64698	.026	-69.2042	-5.3781
WT +VE 14 days	WT -VE	-2.30486	14.64698	.878	-34.2179	29.6082
	KO -VE	-5.66113	14.64698	.706	-37.5742	26.2519
	KO +VE 14 days	-39.59602*	14.64698	.019	-71.5090	-7.6830
KO -VE	WT -VE	3.35627	14.64698	.823	-28.5568	35.2693
	WT +VE 14 days	5.66113	14.64698	.706	-26.2519	37.5742
	KO +VE 14 days	-33.93489*	14.64698	.039	-65.8479	-2.0219
KO +VE 14 days	WT -VE	37.29116*	14.64698	.026	5.3781	69.2042
	WT +VE 14 days	39.59602*	14.64698	.019	7.6830	71.5090
	KO -VE	33.93489*	14.64698	.039	2.0219	65.8479

*. The mean difference is significant at the 0.05 level.

Immunoblotting

1) GATA4 whole protein levels in NFATc2+/+ and NFATc2-/- hearts:

t-Test: Two-Sample Assuming Equal Variances

	Variable NFATc2+/+	Variable NFATc2-/-
Mean	1	3.108567
Variance	0	0.566065
Observations	3	3
Pooled Variance	0.283032	
Hypothesized Mean Difference	0	
Df	4	
t Stat	-4.85417	
P(T<=t) one-tail	0.004157	
t Critical one-tail	2.131847	
P(T<=t) two-tail	0.008314	
t Critical two-tail	2.776445	

2) GATA4 cytoplasmic protein levels in NFATc2+/+ and NFATc2-/- hearts:

t-Test: Two-Sample Assuming Equal Variances

	Variable NFATc2+/+	Variable NFATc2-/-
Mean	1	0.974108
Variance	0	0.172746
Observations	3	3
Pooled Variance	0.086373	
Hypothesized Mean Difference	0	
df	4	
t Stat	0.107902	
P(T<=t) one-tail	0.459635	
t Critical one-tail	2.131846	
P(T<=t) two-tail	0.919269	
t Critical two-tail	2.776451	

3) GATA4 nuclear protein levels in NFATc2+/+ and NFATc2-/- hearts:

t-Test: Two-Sample Assuming Equal Variances

	Variable NFATc2+/+	Variable NFATc2-/-
Mean	1	1.697305
Variance	0	0.017893
Observations	3	3
Pooled Variance	0.008946	
Hypothesized Mean Difference	0	
df	4	
t Stat	-9.02909	
P(T<=t) one-tail	0.000417	
t Critical one-tail	2.131846	
P(T<=t) two-tail	0.000833	
t Critical two-tail	2.776451	

4) pAkt Ser 473 protein levels in normotensive and 14 day stimulated hearts:

Descriptives

pAkt Ser 473

	N	Mean	Std. Deviation	Std. Error	95% Confidence Interval for Mean		Minimum	Maximum
					Lower Bound	Upper Bound		
WT -VE	4	1.1732	.34647	.17324	.6219	1.7245	1.00	1.69
WT +VE 14 days	4	1.8466	.60999	.30500	.8760	2.8173	1.03	2.50
KO -VE	4	1.2184	.18837	.09418	.9186	1.5181	.94	1.35
KO +VE 14 days	4	1.6098	.28669	.14334	1.1536	2.0660	1.36	1.97
Total	16	1.4620	.45310	.11327	1.2206	1.7034	.94	2.50

Test of Homogeneity of Variances

pAkt Ser 473

Levene Statistic	df1	df2	Sig.
.993	3	12	.429

ANOVA

pAkt Ser 473

	Sum of Squares	df	Mean Square	F	Sig.
Between Groups	1.250	3	.417	2.733	.090
Within Groups	1.829	12	.152		
Total	3.079	15			

Multiple Comparisons

Dependent Variable: pAkt Ser 473

(I) Genotype	(J) Genotype	Mean Difference (I-J)	Std. Error	Sig.	95% Confidence Interval	
					Lower Bound	Upper Bound
WT -VE	WT +VE 14 days	-.67339[*]	.27609	.031	-1.2749	-.0718
	KO -VE	-.04514	.27609	.873	-.6467	.5564
	KO +VE 14 days	-.43655	.27609	.140	-1.0381	.1650
WT +VE 14 days	WT -VE	.67339[*]	.27609	.031	.0718	1.2749
	KO -VE	.62824[*]	.27609	.042	.0267	1.2298
	KO +VE 14 days	.23684	.27609	.408	-.3647	.8384
KO -VE	WT -VE	.04514	.27609	.873	-.5564	.6467
	WT +VE 14 days	-.62824[*]	.27609	.042	-1.2298	-.0267
	KO +VE 14 days	-.39141	.27609	.182	-.9930	.2101
KO +VE 14 days	WT -VE	.43655	.27609	.140	-.1650	1.0381
	WT +VE 14 days	-.23684	.27609	.408	-.8384	.3647
	KO -VE	.39141	.27609	.182	-.2101	.9930

*. The mean difference is significant at the 0.05 level.

5) α-SMA protein levels in normotensive and 14 day stimulated hearts:

Note: Each set of α-SMA was carried out on a separate gel, quantified and normalized to WT, which is standardized to 1. Therefore multiple student-t-tests were performed.

t-Test: Two-Sample Assuming Equal Variances

	Variable NFATc2+/+ Ang II -ve	*Variable NFATc2+/+ Ang II +ve*
Mean	1	1.738549
Variance	0	0.638017

Observations	4	4
Pooled Variance	0.319009	
Hypothesized Mean Difference	0	
Df	6	
t Stat	-1.84924	
P(T<=t) one-tail	0.056955	
t Critical one-tail	1.94318	
P(T<=t) two-tail	0.11391	
t Critical two-tail	2.446912	

t-Test: Two-Sample Assuming Equal Variances

	Variable NFATc2+/+ Ang II -ve	*Variable NFATc2-/- Ang II -ve*
Mean	1	0.909822
Variance	0	0.134441
Observations	4	4
Pooled Variance	0.067221	
Hypothesized Mean Difference	0	
df	6	
t Stat	0.491887	
P(T<=t) one-tail	0.320138	
t Critical one-tail	1.94318	
P(T<=t) two-tail	0.640276	
t Critical two-tail	2.446912	

t-Test: Two-Sample Assuming Equal Variances

	Variable NFATc2+/+ Ang II +ve	*Variable NFATc2-/- Ang II +ve*
Mean	1.738549	1.958736
Variance	0.638017	1.422662
Observations	4	4
Pooled Variance	1.03034	
Hypothesized Mean Difference	0	
df	6	
t Stat	-0.30677	
P(T<=t) one-tail	0.384692	
t Critical one-tail	1.94318	
P(T<=t) two-tail	0.769385	

	t Critical two-tail	2.446912

t-Test: Two-Sample Assuming Equal Variances

	Variable NFATc2-/- Ang II -ve	*Variable NFATc2-/- Ang II +ve*
Mean	0.909822	1.958736
Variance	0.134441	1.422662
Observations	4	4
Pooled Variance	0.778552	
Hypothesized Mean Difference	0	
df	6	
t Stat	-1.68117	
P(T<=t) one-tail	0.071863	
t Critical one-tail	1.94318	
P(T<=t) two-tail	0.143727	
t Critical two-tail	2.446912	

6) pFoxo3a Ser 253 protein levels in normotensive and 14 day stimulated hearts:

Descriptives

pFoxo3a Ser 253

	N	Mean	Std. Deviation	Std. Error	95% Confidence Interval for Mean		Minimum	Maximum
					Lower Bound	Upper Bound		
WT -VE	4	.9164	.40502	.20251	.2720	1.5609	.35	1.31
WT +VE 14 days	4	.9370	.37434	.18717	.3413	1.5327	.57	1.46
KO -VE	4	1.0469	.31270	.15635	.5494	1.5445	.74	1.35
KO +VE 14 days	4	1.0462	.52232	.26116	.2150	1.8773	.55	1.73
Total	16	.9866	.37261	.09315	.7881	1.1852	.35	1.73

Test of Homogeneity of Variances

pFoxo3a Ser 253

Levene Statistic	df1	df2	Sig.
.399	3	12	.757

223

ANOVA

pFoxo3a Ser 253

	Sum of Squares	df	Mean Square	F	Sig.
Between Groups	.058	3	.019	.115	.950
Within Groups	2.024	12	.169		
Total	2.083	15			

Multiple Comparisons

Dependent Variable: pFoxo3a Ser 253

(I) Genotype	(J) Genotype	Mean Difference (I-J)	Std. Error	Sig.	95% Confidence Interval	
					Lower Bound	Upper Bound
WT -VE	WT +VE 14 days	-.02056	.29042	.945	-.6533	.6122
	KO -VE	-.13051	.29042	.661	-.7633	.5023
	KO +VE 14 days	-.12972	.29042	.663	-.7625	.5031
WT +VE 14 days	WT -VE	.02056	.29042	.945	-.6122	.6533
	KO -VE	-.10994	.29042	.712	-.7427	.5228
	KO +VE 14 days	-.10916	.29042	.714	-.7419	.5236
KO -VE	WT -VE	.13051	.29042	.661	-.5023	.7633
	WT +VE 14 days	.10994	.29042	.712	-.5228	.7427
	KO +VE 14 days	.00079	.29042	.998	-.6320	.6336
KO +VE 14 days	WT -VE	.12972	.29042	.663	-.5031	.7625
	WT +VE 14 days	.10916	.29042	.714	-.5236	.7419
	KO -VE	-.00079	.29042	.998	-.6336	.6320

7) Vimentin protein levels in normotensive and 14 day stimulated hearts:

Descriptives

Vimentin

	N	Mean	Std. Deviation	Std. Error	95% Confidence Interval for Mean		Minimum	Maximum
					Lower Bound	Upper Bound		
WT -VE	4	.9419	.25013	.12506	.5439	1.3399	.59	1.18
WT +VE 14 days	4	1.1188	.10512	.05256	.9515	1.2861	1.01	1.26
KO -VE	4	.9706	.14524	.07262	.7395	1.2017	.86	1.17

KO +VE 14 days	4	.8841	.14826	.07413	.6481	1.1200	.68	.99
Total	16	.9788	.17703	.04426	.8845	1.0732	.59	1.26

Test of Homogeneity of Variances

Vimentin

Levene Statistic	df1	df2	Sig.
.820	3	12	.507

ANOVA

Vimentin

	Sum of Squares	df	Mean Square	F	Sig.
Between Groups	.120	3	.040	1.371	.299
Within Groups	.350	12	.029		
Total	.470	15			

Multiple Comparisons

Dependent Variable: Vimentin

(I) Genotype	(J) Genotype	Mean Difference (I-J)	Std. Error	Sig.	95% Confidence Interval	
					Lower Bound	Upper Bound
WT -VE	WT +VE 14 days	-.17689	.12077	.169	-.4400	.0863
	KO -VE	-.02866	.12077	.816	-.2918	.2345
	KO +VE 14 days	.05786	.12077	.641	-.2053	.3210
WT +VE 14 days	WT -VE	.17689	.12077	.169	-.0863	.4400
	KO -VE	.14823	.12077	.243	-.1149	.4114
	KO +VE 14 days	.23475	.12077	.076	-.0284	.4979
KO -VE	WT -VE	.02866	.12077	.816	-.2345	.2918
	WT +VE 14 days	-.14823	.12077	.243	-.4114	.1149
	KO +VE 14 days	.08652	.12077	.487	-.1766	.3497
KO +VE 14 days	WT -VE	-.05786	.12077	.641	-.3210	.2053
	WT +VE 14 days	-.23475	.12077	.076	-.4979	.0284
	KO -VE	-.08652	.12077	.487	-.3497	.1766

8) CnAβ protein levels in normotensive and 14 day stimulated hearts:

Descriptives

CnAβ

	N	Mean	Std. Deviation	Std. Error	95% Confidence Interval for Mean		Minimum	Maximum
					Lower Bound	Upper Bound		
WT -VE	4	.9412	.08517	.04258	.8057	1.0768	.82	1.00
WT +VE 14 days	4	.8757	.10636	.05318	.7064	1.0449	.75	.99
KO -VE	4	.9958	.10367	.05183	.8309	1.1608	.87	1.12
KO +VE 14 days	4	.7428	.17940	.08970	.4573	1.0283	.52	.96
Total	16	.8889	.14771	.03693	.8102	.9676	.52	1.12

Test of Homogeneity of Variances

CnAβ

Levene Statistic	df1	df2	Sig.
.704	3	12	.568

ANOVA

CnAβ

	Sum of Squares	df	Mean Square	F	Sig.
Between Groups	.143	3	.048	3.096	.068
Within Groups	.184	12	.015		
Total	.327	15			

Multiple Comparisons

Dependent Variable: CnAβ

(I) Genotype	(J) Genotype	Mean Difference (I-J)	Std. Error	Sig.	95% Confidence Interval	
					Lower Bound	Upper Bound
WT -VE	WT +VE 14 days	.06555	.08768	.469	-.1255	.2566
	KO -VE	-.05460	.08768	.545	-.2456	.1364

	KO +VE 14 days	.19844*	.08768	.043	.0074	.3895
WT +VE 14 days	WT -VE	-.06555	.08768	.469	-.2566	.1255
	KO -VE	-.12015	.08768	.196	-.3112	.0709
	KO +VE 14 days	.13289	.08768	.155	-.0581	.3239
KO -VE	WT -VE	.05460	.08768	.545	-.1364	.2456
	WT +VE 14 days	.12015	.08768	.196	-.0709	.3112
	KO +VE 14 days	.25304*	.08768	.014	.0620	.4441
KO +VE 14 days	WT -VE	-.19844*	.08768	.043	-.3895	-.0074
	WT +VE 14 days	-.13289	.08768	.155	-.3239	.0581
	KO -VE	-.25304*	.08768	.014	-.4441	-.0620

*. The mean difference is significant at the 0.05 level.

9) pAkt Ser 473 protein levels in normotensive and 28 day stimulated hearts:

Descriptives

pAkt Ser 473

	N	Mean	Std. Deviation	Std. Error	95% Confidence Interval for Mean		Minimum	Maximum
					Lower Bound	Upper Bound		
WT -VE	3	.9637	.06288	.03631	.8075	1.1199	.89	1.00
WT +VE 28 days	3	1.2035	.88883	.51317	-1.0045	3.4115	.65	2.23
KO -VE	3	.9035	.17538	.10125	.4678	1.3392	.79	1.11
KO +VE 28 days	3	1.9697	.98267	.56734	-.4714	4.4108	1.00	2.97
Total	12	1.2601	.72274	.20864	.8009	1.7193	.65	2.97

Test of Homogeneity of Variances

pAkt Ser 473

Levene Statistic	df1	df2	Sig.
3.445	3	8	.072

ANOVA

pAkt Ser 473

	Sum of Squares	df	Mean Square	F	Sig.
Between Groups	2.165	3	.722	1.612	.262
Within Groups	3.581	8	.448		
Total	5.746	11			

Multiple Comparisons

Dependent Variable: pAkt Ser 473

(I) Genotype	(J) Genotype	Mean Difference (I-J)	Std. Error	Sig.	95% Confidence Interval	
					Lower Bound	Upper Bound
WT -VE	WT +VE 28 days	-.23981	.54625	.672	-1.4995	1.0198
	KO -VE	.06019	.54625	.915	-1.1995	1.3199
	KO +VE 28 days	-1.00600	.54625	.103	-2.2657	.2537
WT +VE 28 days	WT -VE	.23981	.54625	.672	-1.0198	1.4995
	KO -VE	.30000	.54625	.598	-.9597	1.5597
	KO +VE 28 days	-.76618	.54625	.198	-2.0258	.4935
KO -VE	WT -VE	-.06019	.54625	.915	-1.3199	1.1995
	WT +VE 28 days	-.30000	.54625	.598	-1.5597	.9597
	KO +VE 28 days	-1.06618	.54625	.087	-2.3258	.1935
KO +VE 28 days	WT -VE	1.00600	.54625	.103	-.2537	2.2657
	WT +VE 28 days	.76618	.54625	.198	-.4935	2.0258
	KO -VE	1.06618	.54625	.087	-.1935	2.3258

10) pFoxo3a Ser 253 protein levels in normotensive and 28 day stimulated hearts:

Descriptives

pFoxo3a Ser 253

	N	Mean	Std. Deviation	Std. Error	95% Confidence Interval for Mean		Minimum	Maximum
					Lower Bound	Upper Bound		
WT -VE	3	1.0593	.10270	.05930	.8042	1.3144	1.00	1.18
WT +VE 28 days	3	1.3651	.06523	.03766	1.2031	1.5271	1.29	1.42
KO -VE	3	1.3827	.61963	.35775	-.1566	2.9219	.79	2.03
KO +VE 28 days	3	1.6639	.68462	.39527	-.0368	3.3646	.95	2.32

Total	12	1.3678	.45569	.13155	1.0782	1.6573	.79	2.32

Test of Homogeneity of Variances

pFoxo3a Ser 253

Levene Statistic	df1	df2	Sig.
2.535	3	8	.130

ANOVA

pFoxo3a Ser 253

	Sum of Squares	df	Mean Square	F	Sig.
Between Groups	.549	3	.183	.844	.507
Within Groups	1.735	8	.217		
Total	2.284	11			

Multiple Comparisons

Dependent Variable: pFoxo3a Ser 253

(I) Genotype	(J) Genotype	Mean Difference (I-J)	Std. Error	Sig.	95% Confidence Interval	
					Lower Bound	Upper Bound
WT -VE	WT +VE 28 days	-.30581	.38023	.444	-1.1826	.5710
	KO -VE	-.32340	.38023	.420	-1.2002	.5534
	KO +VE 28 days	-.60465	.38023	.150	-1.4815	.2722
WT +VE 28 days	WT -VE	.30581	.38023	.444	-.5710	1.1826
	KO -VE	-.01758	.38023	.964	-.8944	.8592
	KO +VE 28 days	-.29884	.38023	.455	-1.1757	.5780
KO -VE	WT -VE	.32340	.38023	.420	-.5534	1.2002
	WT +VE 28 days	.01758	.38023	.964	-.8592	.8944
	KO +VE 28 days	-.28125	.38023	.481	-1.1581	.5956
KO +VE 28 days	WT -VE	.60465	.38023	.150	-.2722	1.4815
	WT +VE 28 days	.29884	.38023	.455	-.5780	1.1757
	KO -VE	.28125	.38023	.481	-.5956	1.1581

11) Vimentin protein levels in normotensive and 28 day stimulated hearts:

Descriptives

Vimentin

	N	Mean	Std. Deviation	Std. Error	95% Confidence Interval for Mean		Minimum	Maximum
					Lower Bound	Upper Bound		
WT -VE	3	1.0433	.07504	.04332	.8569	1.2297	1.00	1.13
WT +VE 28 days	3	1.1546	.21383	.12346	.6234	1.6858	.96	1.38
KO -VE	3	1.2340	.21624	.12485	.6969	1.7712	1.07	1.48
KO +VE 28 days	3	1.3625	.37953	.21912	.4197	2.3053	.93	1.62
Total	12	1.1986	.24248	.07000	1.0445	1.3527	.93	1.62

Test of Homogeneity of Variances

Vimentin

Levene Statistic	df1	df2	Sig.
3.031	3	8	.093

ANOVA

Vimentin

	Sum of Squares	df	Mean Square	F	Sig.
Between Groups	.162	3	.054	.895	.485
Within Groups	.484	8	.061		
Total	.647	11			

Multiple Comparisons

Dependent Variable: Vimentin

(I) Genotype	(J) Genotype	Mean Difference (I-J)	Std. Error	Sig.	95% Confidence Interval	
					Lower Bound	Upper Bound
WT -VE	WT +VE 28 days	-.11127	.20090	.595	-.5745	.3520
	KO -VE	-.19070	.20090	.370	-.6540	.2726
	KO +VE 28 days	-.31914	.20090	.151	-.7824	.1441
WT +VE 28 days	WT -VE	.11127	.20090	.595	-.3520	.5745
	KO -VE	-.07943	.20090	.703	-.5427	.3838
	KO +VE 28 days	-.20787	.20090	.331	-.6711	.2554

230

KO -VE	WT -VE	.19070	.20090	.370	-.2726	.6540
	WT +VE 28 days	.07943	.20090	.703	-.3838	.5427
	KO +VE 28 days	-.12845	.20090	.540	-.5917	.3348
KO +VE 28 days	WT -VE	.31914	.20090	.151	-.1441	.7824
	WT +VE 28 days	.20787	.20090	.331	-.2554	.6711
	KO -VE	.12845	.20090	.540	-.3348	.5917

12) α-SMA protein levels in normotensive and 28 day stimulated hearts:

Descriptives

α-SMA

	N	Mean	Std. Deviation	Std. Error	95% Confidence Interval for Mean		Minimum	Maximum
					Lower Bound	Upper Bound		
WT -VE	3	1.0496	.08583	.04955	.8363	1.2628	1.00	1.15
WT +VE 28 days	3	2.9670	.21094	.12179	2.4430	3.4911	2.74	3.15
KO -VE	3	1.0185	.22951	.13251	.4483	1.5886	.78	1.24
KO +VE 28 days	3	2.5772	.44401	.25635	1.4742	3.6802	2.15	3.04
Total	12	1.9031	.94848	.27380	1.3004	2.5057	.78	3.15

Test of Homogeneity of Variances

α-SMA

Levene Statistic	df1	df2	Sig.
1.446	3	8	.300

ANOVA

α-SMA

	Sum of Squares	df	Mean Square	F	Sig.
Between Groups	9.292	3	3.097	41.069	.000
Within Groups	.603	8	.075		
Total	9.896	11			

Multiple Comparisons

Dependent Variable: α-SMA

(I) Genotype	(J) Genotype	Mean Difference (I-J)	Std. Error	Sig.	95% Confidence Interval	
					Lower Bound	Upper Bound
WT -VE	WT +VE 28 days	-1.91749*	.22423	.000	-2.4346	-1.4004
	KO -VE	.03108	.22423	.893	-.4860	.5482
	KO +VE 28 days	-1.52763*	.22423	.000	-2.0447	-1.0105
WT +VE 28 days	WT -VE	1.91749*	.22423	.000	1.4004	2.4346
	KO -VE	1.94857*	.22423	.000	1.4315	2.4657
	KO +VE 28 days	.38985	.22423	.120	-.1272	.9069
KO -VE	WT -VE	-.03108	.22423	.893	-.5482	.4860
	WT +VE 28 days	-1.94857*	.22423	.000	-2.4657	-1.4315
	KO +VE 28 days	-1.55872*	.22423	.000	-2.0758	-1.0416
KO +VE 28 days	WT -VE	1.52763*	.22423	.000	1.0105	2.0447
	WT +VE 28 days	-.38985	.22423	.120	-.9069	.1272
	KO -VE	1.55872*	.22423	.000	1.0416	2.0758

*. The mean difference is significant at the 0.05 level.

13) Calsarcin-1 protein levels in normotensive and 28 day stimulated hearts:

Descriptives

Calsarcin-1

	N	Mean	Std. Deviation	Std. Error	95% Confidence Interval for Mean		Minimum	Maximum
					Lower Bound	Upper Bound		
WT -VE	3	1.0240	.04153	.02397	.9208	1.1271	1.00	1.07
WT +VE 28 days	3	.3904	.02677	.01546	.3239	.4569	.36	.41
KO -VE	3	1.2490	.34750	.20063	.3858	2.1123	.86	1.54
KO +VE 28 days	3	.4412	.25662	.14816	-.1962	1.0787	.28	.74
Total	12	.7761	.42812	.12359	.5041	1.0482	.28	1.54

Test of Homogeneity of Variances

Calsarcin-1

Levene Statistic	df1	df2	Sig.
5.642	3	8	.023

232

ANOVA

Calsarcin-1

	Sum of Squares	df	Mean Square	F	Sig.
Between Groups	1.638	3	.546	11.552	.003
Within Groups	.378	8	.047		
Total	2.016	11			

Multiple Comparisons

Dependent Variable: Calsarcin-1

(I) Genotype	(J) Genotype	Mean Difference (I-J)	Std. Error	Sig.	95% Confidence Interval	
					Lower Bound	Upper Bound
WT -VE	WT +VE 28 days	.63361*	.17751	.007	.2243	1.0429
	KO -VE	-.22503	.17751	.241	-.6344	.1843
	KO +VE 28 days	.58274*	.17751	.011	.1734	.9921
WT +VE 28 days	WT -VE	-.63361*	.17751	.007	-1.0429	-.2243
	KO -VE	-.85864*	.17751	.001	-1.2680	-.4493
	KO +VE 28 days	-.05087	.17751	.782	-.4602	.3585
KO -VE	WT -VE	.22503	.17751	.241	-.1843	.6344
	WT +VE 28 days	.85864*	.17751	.001	.4493	1.2680
	KO +VE 28 days	.80777*	.17751	.002	.3984	1.2171
KO +VE 28 days	WT -VE	-.58274*	.17751	.011	-.9921	-.1734
	WT +VE 28 days	.05087	.17751	.782	-.3585	.4602
	KO -VE	-.80777*	.17751	.002	-1.2171	-.3984

*. The mean difference is significant at the 0.05 level.

14) CnAβ protein levels in normotensive and 28 day stimulated hearts:

Descriptives

CnAβ

	N	Mean	Std. Deviation	Std. Error	95% Confidence Interval for Mean		Minimum	Maximum
					Lower Bound	Upper Bound		

WT -VE	3	1.0618	.10700	.06178	.7960	1.3276	1.00	1.19
WT +VE 28 days	3	1.2472	.48079	.27758	.0529	2.4415	.72	1.67
KO -VE	3	1.3794	.40255	.23241	.3794	2.3793	1.07	1.83
KO +VE 28 days	3	.9959	.19514	.11266	.5112	1.4807	.86	1.22
Total	12	1.1711	.32486	.09378	.9647	1.3775	.72	1.83

Test of Homogeneity of Variances

CnAβ

Levene Statistic	df1	df2	Sig.
2.480	3	8	.135

ANOVA

CnAβ

	Sum of Squares	df	Mean Square	F	Sig.
Between Groups	.275	3	.092	.829	.514
Within Groups	.885	8	.111		
Total	1.161	11			

Multiple Comparisons

Dependent Variable: CnAβ

(I) Genotype	(J) Genotype	Mean Difference (I-J)	Std. Error	Sig.	95% Confidence Interval	
					Lower Bound	Upper Bound
WT -VE	WT +VE 28 days	-.18543	.27164	.514	-.8118	.4410
	KO -VE	-.31758	.27164	.276	-.9440	.3088
	KO +VE 28 days	.06585	.27164	.815	-.5606	.6922
WT +VE 28 days	WT -VE	.18543	.27164	.514	-.4410	.8118
	KO -VE	-.13215	.27164	.640	-.7586	.4942
	KO +VE 28 days	.25127	.27164	.382	-.3751	.8777
KO -VE	WT -VE	.31758	.27164	.276	-.3088	.9440
	WT +VE 28 days	.13215	.27164	.640	-.4942	.7586
	KO +VE 28 days	.38343	.27164	.196	-.2430	1.0098
KO +VE 28 days	WT -VE	-.06585	.27164	.815	-.6922	.5606
	WT +VE 28 days	-.25127	.27164	.382	-.8777	.3751
	KO -VE	-.38343	.27164	.196	-1.0098	.2430

Histology

1) Relative HW/BW in normotensive NFATc2+/+ and NFATc2-/- hearts:

t-Test: Two-Sample Assuming Equal Variances

	Variable NFATc2+/+	Variable NFATc2-/-
Mean	5.018853	4.756885
Variance	0.600745	0.206136
Observations	7	7
Pooled Variance	0.40344	
Hypothesized Mean Difference	0	
df	12	
t Stat	0.771602	
P(T<=t) one-tail	0.227638	
t Critical one-tail	1.782288	
P(T<=t) two-tail	0.455277	
t Critical two-tail	2.178813	

2) Relative HW/BW in normotensive and 14 day stimulated NFATc2+/+ and NFATc2-/- hearts:

Descriptives

HW

	N	Mean	Std. Deviation	Std. Error	95% Confidence Interval for Mean		Minimum	Maximum
					Lower Bound	Upper Bound		
WT -VE	7	5.0189	.77508	.29295	4.3020	5.7357	4.48	6.56
WT +VE 14 days	7	6.0967	.82406	.31146	5.3345	6.8588	5.13	7.74
KO -VE	7	4.7569	.45402	.17160	4.3370	5.1768	4.35	5.70
KO +VE 14 days	7	5.9283	.92318	.34893	5.0745	6.7821	4.61	7.26
Total	28	5.4502	.92740	.17526	5.0906	5.8098	4.35	7.74

Test of Homogeneity of Variances

HW

Levene Statistic	df1	df2	Sig.
.899	3	24	.456

ANOVA

HW

	Sum of Squares	df	Mean Square	F	Sig.
Between Groups	9.193	3	3.064	5.242	.006
Within Groups	14.029	24	.585		
Total	23.222	27			

Multiple Comparisons

Dependent Variable: HW

(I) Genotype	(J) Genotype	Mean Difference (I-J)	Std. Error	Sig.	95% Confidence Interval	
					Lower Bound	Upper Bound
WT -VE	WT +VE 14 days	-1.07780*	.40868	.014	-1.9213	-.2343
	KO-VE	.26197	.40868	.528	-.5815	1.1054
	KO +VE 14 days	-.90943*	.40868	.036	-1.7529	-.0660
WT +VE 14 days	WT -VE	1.07780*	.40868	.014	.2343	1.9213
	KO -VE	1.33977*	.40868	.003	.4963	2.1832
	KO +VE 14 days	.16837	.40868	.684	-.6751	1.0118
KO -VE	WT -VE	-.26197	.40868	.528	-1.1054	.5815
	WT +VE 14 days	-1.33977*	.40868	.003	-2.1832	-.4963
	KO +VE 14 days	-1.17140*	.40868	.009	-2.0149	-.3279
KO +VE 14 days	WT -VE	.90943*	.40868	.036	.0660	1.7529
	WT +VE 14 days	-.16837	.40868	.684	-1.0118	.6751
	KO -VE	1.17140*	.40868	.009	.3279	2.0149

*. The mean difference is significant at the 0.05 level.

3) Left ventricle inner chamber diameter: Total heart diameter in NFATc2+/+ and NFATc2-/-
hearts:

t-Test: Two-Sample Assuming Equal Variances

	Variable 1 NFATc2+/+	Variable 2 NFATc2-/-
Mean	0.457415	0.586696
Variance	0.00228	0.001459
Observations	3	3
Pooled Variance	0.001869	
Hypothesized Mean Difference	0	
df	4	
t Stat	-3.66221	
P(T<=t) one-tail	0.010769	

t Critical one-tail	2.131847
P(T<=t) two-tail	0.021538
t Critical two-tail	2.776445

4) Right ventricular wall diameter: Total heart diameter in NFATc2+/+ and NFATc2-/- hearts:

t-Test: Two-Sample Assuming Equal Variances

	Variable 1 *NFATc2+/+*	*Variable 2* *NFATc2-/-*
Mean	0.114921	0.086165
Variance	0.001145	0.000353
Observations	3	3
Pooled Variance	0.000749	
Hypothesized Mean Difference	0	
df	4	
t Stat	1.286941	
P(T<=t) one-tail	0.13377	
t Critical one-tail	2.131847	
P(T<=t) two-tail	0.26754	
t Critical two-tail	2.776445	

5) NFAT nuclear localization in NFATc2+/+ and NFATc2-/- hearts:

t-Test: Two-Sample Assuming Equal Variances

NFATc1	*Variable 1* *NFATc2+/+*	*Variable 2* *NFATc2-/-*
Mean	14.36666667	22
Variance	0.253333333	0.67
Observations	3	3
Pooled Variance	0.461666667	
Hypothesized Mean Difference	0	
df	4	
t Stat	-13.75927649	
P(T<=t) one-tail	8.08348E-05	
t Critical one-tail	2.131846486	
P(T<=t) two-tail	0.00016167	
t Critical two-tail	2.776450856	

t-Test: Two-Sample Assuming Equal Variances

NFATc2	*Variable 1* *NFATc2+/+*	*Variable 2* *NFATc2-/-*
Mean	8.14	4.26
Variance	0.7284	1.7553
Observations	3	3

Pooled Variance	1.24185
Hypothesized Mean Difference	0
df	4
t Stat	4.264251239
P(T<=t) one-tail	0.006504748
t Critical one-tail	2.131846486
P(T<=t) two-tail	0.013009496
t Critical two-tail	2.776450856

t-Test: Two-Sample Assuming Equal Variances

NFATc3	Variable 1 NFATc2+/+	Variable 2 NFATc2-/-
Mean	10.12	9.776667
Variance	0.3292	6.892433
Observations	3	3
Pooled Variance	3.610816667	
Hypothesized Mean Difference	0	
df	4	
t Stat	0.221288518	
P(T<=t) one-tail	0.417852642	
t Critical one-tail	2.131846486	
P(T<=t) two-tail	0.835705284	
t Critical two-tail	2.776450856	

-Test: Two-Sample Assuming Equal Variances

NFATc4	Variable 1 NFATc2+/+	Variable 2 NFATc2-/-
Mean	10.64333	10.56
Variance	5.754633	8.5783
Observations	3	3
Pooled Variance	7.166467	
Hypothesized Mean Difference	0	
df	4	
t Stat	0.038125	
P(T<=t) one-tail	0.485707	
t Critical one-tail	2.131846	
P(T<=t) two-tail	0.971415	
t Critical two-tail	2.776451	

6) NFAT nuclear localization in normotensive and 14 day stimulated NFATc2+/+ and NFATc2-/- hearts:

Descriptives

NFATc1 nuclear localization

	N	Mean	Std. Deviation	Std. Error	95% Confidence Interval for Mean		Minimum	Maximum
					Lower Bound	Upper Bound		
WT -VE	3	8.8480	1.08445	.62611	6.1541	11.5419	7.64	9.74
WT +VE 14 days	3	14.6195	4.14565	2.39349	4.3211	24.9179	10.64	18.91
KO -VE	3	18.0189	3.67902	2.12408	8.8797	27.1581	13.82	20.68
KO +VE 14 days	3	22.5326	6.53823	3.77485	6.2907	38.7745	16.13	29.20
Total	12	16.0048	6.38688	1.84373	11.9467	20.0628	7.64	29.20

Test of Homogeneity of Variances

NFATc1 nuclear localization

Levene Statistic	df1	df2	Sig.
1.336	3	8	.329

ANOVA

NFATc1 nuclear localization

|	Sum of Squares	df	Mean Square	F	Sig.
Between Groups	299.423	3	99.808	5.348	.026
Within Groups	149.292	8	18.662		
Total	448.715	11			

Multiple Comparisons

Dependent Variable: NFATc1 nuclear localization

(I) Genotype	(J) Genotype	Mean Difference (I-J)	Std. Error	Sig.	95% Confidence Interval	
					Lower Bound	Upper Bound
	WT +VE 14 days	-5.77148	3.52718	.140	-13.9052	2.3622
WT -VE	KO-VE	-9.17091*	3.52718	.032	-17.3046	-1.0372
	KO +VE 14 days	-13.68460*	3.52718	.005	-21.8183	-5.5509

WT +VE 14 days	WT -VE	5.77148	3.52718	.140	-2.3622	13.9052
	KO -VE	-3.39943	3.52718	.363	-11.5331	4.7343
	KO +VE 14 days	-7.91311	3.52718	.055	-16.0468	.2206
KO -VE	WT -VE	9.17091[*]	3.52718	.032	1.0372	17.3046
	WT +VE 14 days	3.39943	3.52718	.363	-4.7343	11.5331
	KO +VE 14 days	-4.51369	3.52718	.237	-12.6474	3.6200
KO +VE 14 days	WT -VE	13.68460[*]	3.52718	.005	5.5509	21.8183
	WT +VE 14 days	7.91311	3.52718	.055	-.2206	16.0468
	KO -VE	4.51369	3.52718	.237	-3.6200	12.6474

*. The mean difference is significant at the 0.05 level.

Appendix IV: Chapter 4-Additional Figures
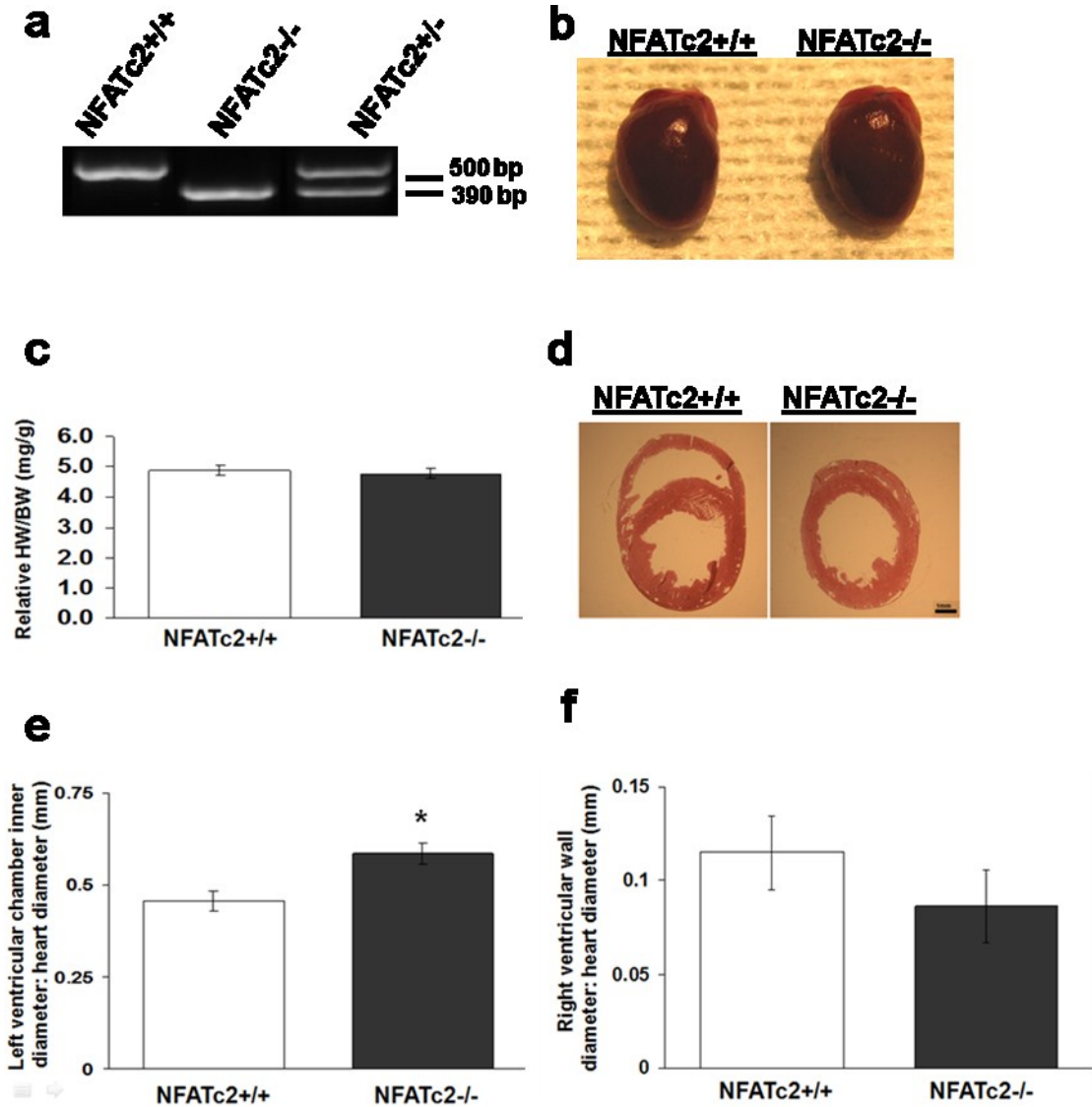
Figure 1: *NFATc2-/-* **mice have similar relative heart weights but different morphological characteristics to those of** *NFATc2+/+* **mice**

 (**a**) Representative photomicrographs of ethidium bromide-stained agarose gels depicting DNA products of the Wild-Type (*NFATc2+/+*), *NFATc2* knockout (*NFATc2-/-*) and heterozygous genotypes (*NFATc2+/-*); *NFATc2+/+* bands are shown at 500 bp and *NFATc2-/-* bands are shown at 390 bp. (**b**) Freshly extracted mice hearts. (**c**) Quantification of the relative HW/BW for *NFATc2+/+* and *NFATc2-/-* (n=7) mice. (**d**) Representative photomicrographs of cross sections from *NFATc2+/+* and *NFATc2-/-* hearts processed for hematoxylin and eosin staining and

quantification of the left ventricular chamber inner wall diameter (**e**) and right ventricular wall diameter (**f**) normalized to total heart diameter (n=3; P<0.05). *compared to *NFATc2*+/+. Scale bars, 1mm. Means ± SEM are shown. (Figure 1 is taken from Patrick Sin-Chan, MSc thesis, 2011).
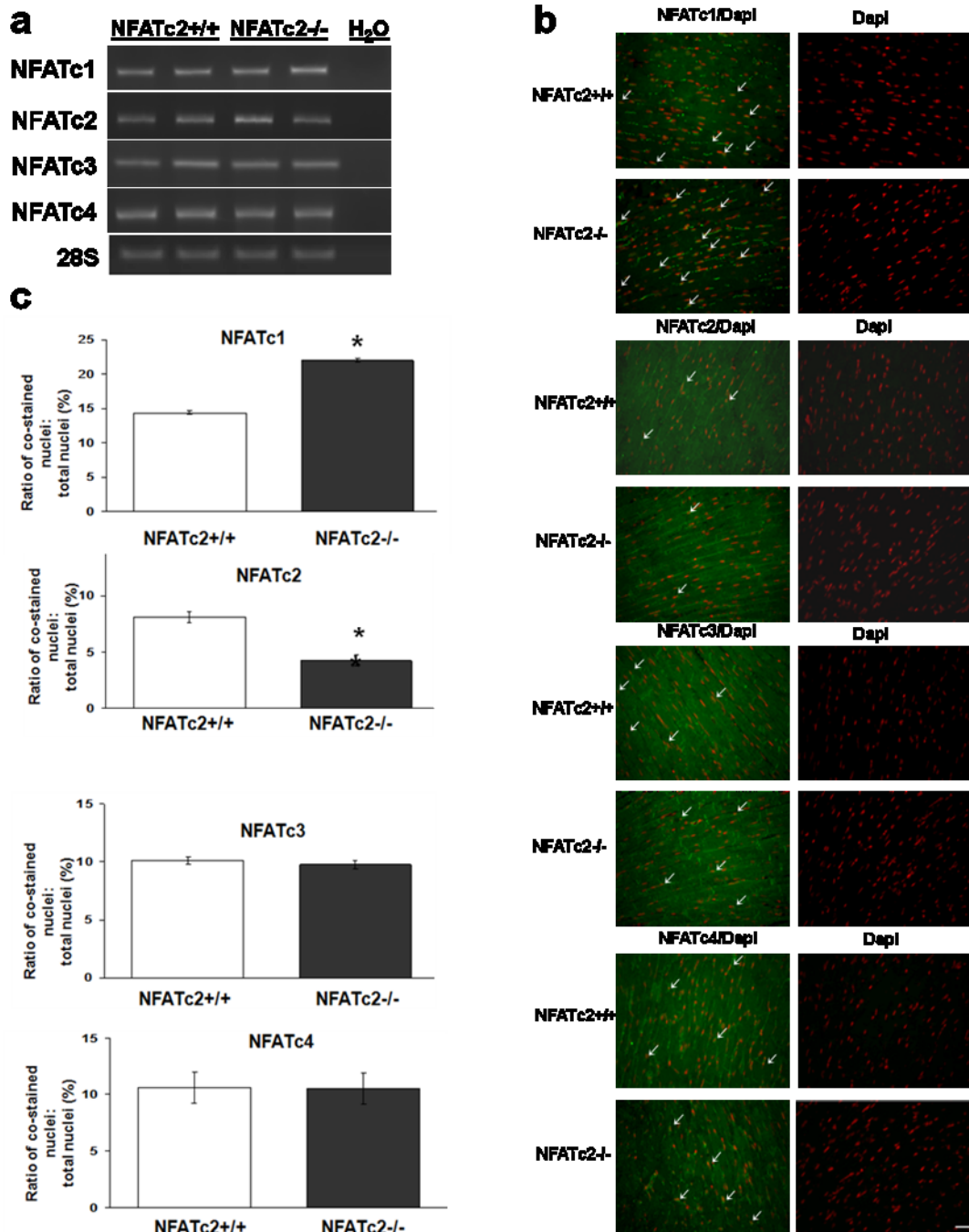
Figure 2: NFATc1 nuclear localization in the hearts of *NFATc2*+/+ and *NFATc2*-/- mice

(**a**) Representative photomicrographs of ethidium bromide-stained agarose gels depicting PCR products for NFATc1-c4 showing no significant differences between *NFATc2*+/+ and *NFATc2*-/- hearts (n=3). (**b**) Representative photomicrographs depicting nuclear localization of NFAT isoforms in the heart. Arrows indicate nuclei positively stained for NFATc1-4 isoforms. To control for unspecific secondary antibody staining, the Dapi images have only the secondary antibody conjugated to the fluorophore Alexa 488 added, without a primary antibody. Scale bars,

20μm. (**c**) Quantification of the percentage of myonuclei stained for NFATc1-4 reveals significant increase in NFATc1 nuclear localization of *NFATc2*-/- hearts compared to *NFATc2*+/+ hearts (n=3; p<0.05). *compared to *NFATc2*+/+. Means ± SEM are shown. (Figure 2 is taken from Patrick Sin-Chan, MSc thesis, 2011).
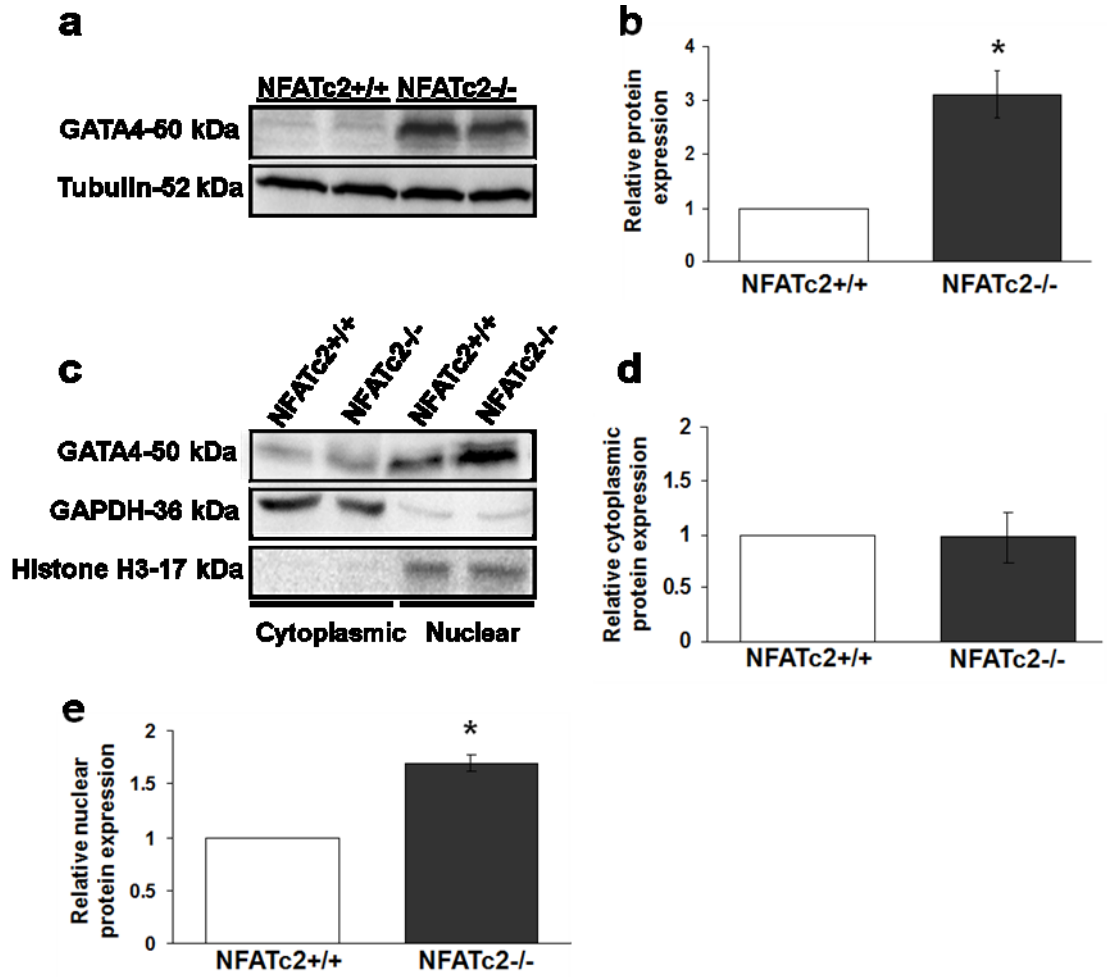
Figure 3: GATA4 has higher nuclear expression in the hearts of *NFATc2*-/- mice

(**a-b**) Representative immunoblot of GATA4 expression in whole heart protein homogenate and its quantification normalized to α-tubulin expression (n=3; P<0.05). (**c-e**) Representative immunoblot and respective quantifications of hearts fractionated in cytoplasmic and nuclear protein extracts. A double band is visualized in the nuclear fraction possibly due to additional phosphorylated sites on GATA4 (n=3; P<0.05). *compared to *NFATc2*+/+. Means ± SEM are shown. (Figure 3 is taken from Patrick Sin-Chan, MSc thesis, 2011).
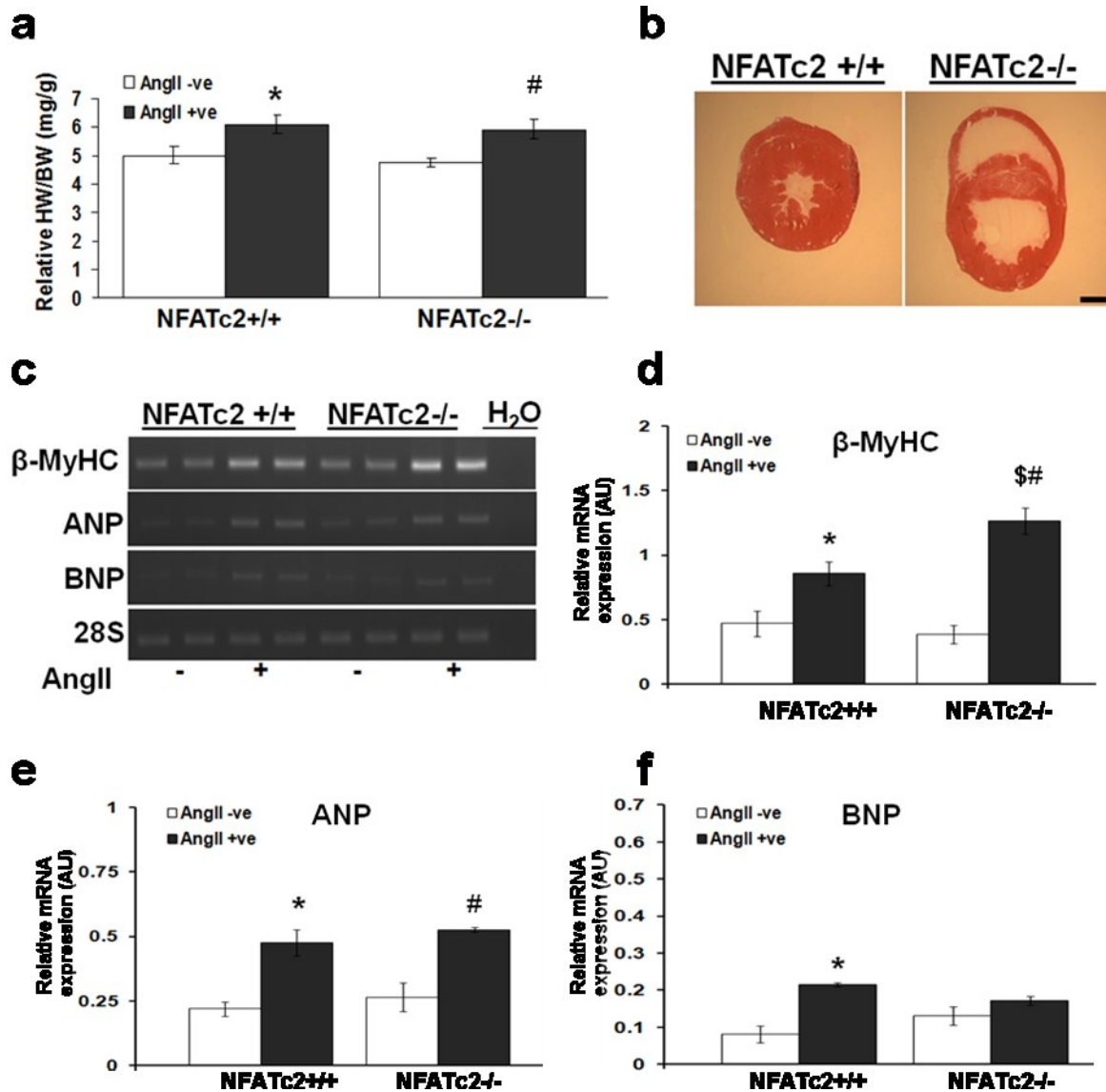
Figure 4: The 14 day Ang II-stimulated mice display more severe heart pathology

(**a**) HW/BW ratio of normotensive and Ang II-stimulated adult *NFATc2+/+* and *NFATc2-/-* mice (n=7; P<0.05). (**b**) Representative photomicrographs of cross sections from 14 day Ang II-stimulated *NFATc2+/+* and *NFATc2-/-* hearts processed for hematoxylin and eosin staining. Scale bars, 1mm. (**c**) Representative photomicrographs of ethidium bromide-stained agarose gels depicting PCR products for *β-MyHC*, *ANP* and *BNP*. (**d-f**) Quantifications of *β-MyHC*, *ANP* and *BNP* transcript levels normalized to 28S housekeeping gene (n=3; P<0.05). AU represents Arbitrary Units. *compared to normotensive *NFATc2+/+*, $compared to stimulated *NFATc2+/+* and #compared to normotensive *NFATc2-/-*. Means ± SEM are shown. (Figure 4 except 4a, is taken from Patrick Sin-Chan, MSc thesis, 2011).